Theses and Dissertations

12-2016

Membrane Chromatography for Bioseparations: Ligand Design and Optimization

Zizhao Liu
University of Arkansas, Fayetteville

Follow this and additional works at: http://scholarworks.uark.edu/etd

Part of the Biochemical and Biomolecular Engineering Commons, and the Biochemistry Commons

Membrane Chromatography for Bioseparations: Ligand Design and Optimization

A dissertation submitted in partial fulfillment
of the requirements for the degree of
Doctor of Philosophy in Chemical Engineering

by

Zizhao Liu
China Pharmaceutical University
Bachelor of Science in Bioengineering, 2011

December 2016
University of Arkansas

This dissertation is approved for recommendation to the Graduate Council.

_____
Dr. Xianghong Qian
Dissertation Director

_____   _____
Dr. Ranil Wickramasinghe   Dr. Jeff Wolchok
Committee Member   Committee Member

_____   _____
Dr. Peter Czermak   Dr. Steve Cramer
Committee Member   Committee Member

Abstract

Membrane chromatography, or membrane adsorber, represents an attractive alternative to conventional packed bed chromatography used in downstream processing. Membrane chromatography has many advantages, including high productivity, low buffer consumption and ease to scale up. This doctoral dissertation focuses on developing novel polymeric ligands for protein separations using membrane chromatography. Atom transfer radical polymerization (ATRP), known as a controlled radical polymerization technique, has been used to control the architecture of grafted polymeric ligands. The center theme of this dissertation is to develop new polymeric ligands and investigate how the polymer's property (e.g. flexibility, hydrophobicity) and architecture (e.g. chain density, chain length) affect the protein separation performances.

In chapter 2, a synthetic polymeric ligand has been developed for affinity membrane chromatography. It is the first time that bisphosphonate-type monomers with high affinity to arginine have been successfully polymerized and grafted from membrane surfaces with ATRP. Binding capacity for lysozyme (an arginine-rich protein) reaches 12 mg/mL and 4 mg/mL for static binding and dynamic binding (recovery 90%), respectively. Our results show binding capacity increases with the amount of copolymerized affinity monomer and the importance of introducing the hydrophilic spacer monomer for effective binding of lysozyme.

Chapter 3 and 4 involve developing responsive membranes for hydrophobic interaction chromatography (HIC). The responsive HIC ligand can switch between hydrophobic to hydrophilic state depending on salt concentrations and salt types. In chapter

3, in order to provide more understanding of the responsive HIC membrane system, we have mainly investigated how the binding conditions (varied pHs, salts and proteins) influence the binding performances.

Finally, comb-like copolymeric ligands were designed for our responsive HIC membranes (chapter 4). The effects of backbone density, backbone length and PVCL density were investigated by dynamic binding studies. Our results show the BSA binding capacity and recovery strongly depend on the structure of grafted comb-like ligands. In chapter 5, we have shown the effect of copolymerization with different monomers on binding capacity and recovery. Preliminary data shows possibilities of developing ph-and-salt responsive membrane adsorbers for bioseparations.

Acknowledgement

First of all, I would like to express my sincere gratitude to my supervisor Xianghong Qian for her motivation, patience and support for my Ph.D. study. Her guidance helps me in my research and propels me to try my best for not only experiments but also my presentation and writing. I could not thank enough for her insightful comments and encouragements for making me grow from an undergraduate student to an independent researcher. Thank you and Prof. Ranil Wickramasinghe for bringing me into the membrane research field.

Besides my advisor, I would like to thank my dissertation committee: Prof. Ranil Wickramasinghe (co-advisor), Prof. Jeff Wolchok, Prof. Peter Czermak and Prof. Steve Cramer. Thanks for your time to attend my defense, especially for Prof. Peter Czermak and Prof. Steve Cramer from outside of university. Also thanks for your inputs that broaden and deepen my research from many perspectives.

My thank also goes to Dr. Schwark from Prof. Ulbricht's group who gave me great help for monomer synthesis, Dr. Lester and Dr. Shein who helped to test my NMR samples, Dr. Yang and Dr. Lei who taught me ATRP and UV-initiated polymerization and Dr. Du who collaborated with me on the affinity membrane work. I want to thank all the other group members who helped me in my research. Financial support from the Arkansas Biosciences Institute and University of Arkansas are gratefully acknowledged.

Last but not the least, I would like to thank my family for supporting me in the U.S., especially on cooking and other general living skills. Your love always keeps me moving forward.

Table of Contents

List of Figures

List of Tables

List of Published Papers

Liu, Z., Wickramasinghe, S. R., Qian, X. "Membrane Chromatography for Protein Purifications from Ligand Design to Functionalization", Separation Science and Technology, 2016 (accepted, chapter 1)

Liu, Z.; Du, H.; Wickramasinghe, S.R.; Qian, X. (2014) Membrane Surface Engineering for Protein Separations: Experiments and Simulations. Langmuir, 30(35): 10651-10660. (published, chapter 2)

Liu, Z.; Wickramasinghe, S.R.; Qian, X. The Effects of Salt Ions on Responsive Hydrophobic Interaction Membrane Chromatography. To be submitted, chapter 3

Liu, Z.; Wickramasinghe, S.R.; Qian, X. The Effects of Polymer Architecture on Responsive Hydrophobic Interaction Membrane Chromatography. To be submitted, chapter 4

Chapter 1 Introduction: Membrane Chromatography for Protein Purifications from

Ligand Design to Functionalization

*This chapter is based on an accepted manuscript: Liu, Z., Wickramasinghe, S. R., Qian, X. "Membrane Chromatography for Protein Purifications from Ligand Design to Functionalization" accepted, Separation Science and Technology, 2016

Abstract

Protein-based therapeutics, in particular monoclonal antibodies (mAbs) are in high demand for treating a variety of conditions. Here membrane chromatography for protein purifications is reviewed. In particular, current status and development for various capture and polishing steps including protein A, ion exchange and hydrophobic interaction chromatography are discussed. In addition, new developments in ligand design and membrane functionalization for membrane chromatography are discussed. In-depth discussions on polymeric ligands with UV-initiated polymerization or atom transfer radical polymerization (ATRP) are included. Finally in silico simulations to help design new ligands and elucidate the binding interactions are also briefly reviewed.

1.1 Therapeutic Monoclonal Antibody: Current Market and Manufacturing Challenges

A therapeutic monoclonal antibody (mAb), or immunoglobulin G (IgG), is capable of binding a targeted molecule specifically by its fragment-antigen binding (Fab) region. Through this specific binding, it can trigger cell apoptosis or changes in signaling pathways. This binding specificity greatly reduces the drug side effects and enables mAbs to be used in cancer and autoimmune disease treatment with a significant advantage over other non-

specific therapies such as radiotherapy and chemotherapy. Up till 2015, 47 mAb products have been approved in US and Europe with more than 300 mAb candidates in development [1]. The total sale of mAb products reached $75 billion in 2013, which was an increase of 90% compared to the total sale in 2008 [1], indicating a rapid growth of the mAb market.

The large demand for mAb products places a great challenge on the manufacturing process. The drastic improvement in the upstream process has led to a more than ten-fold increase of cell titers, which shifts the bottleneck of the manufacturing process to the downstream [2, 3, 4]. The total cost for downstream process accounts for up to 80% of the total manufacturing cost [5]. Therefore, there is a large driving force to reduce the cost by developing new downstream processing technologies.

1.2 Current Chromatographic Materials: An Overview of Ligands

A common mAb manufacturing process is shown schematically in Figure 1.1. After fermentation, mAb products are first clarified by the removal of solids and cell debris through depth filtrations or centrifugations. Then, the clarified mAb filtrate or supernatant is processed through 2-3 stages of chromatographic unit operations to remove impurities, including host cell proteins (HCPs), DNAs, media components, endotoxins, viruses and aggregates. These chromatographic steps include protein A chromatography, ion-exchange chromatography (IEX), hydrophobic interaction chromatography (HIC) and multi-modal chromatography (MMC). The mechanism, mode of operation and limitations for these four different chromatographic steps are summarized in Table 1.1. Each of the chromatographic steps will be discussed in the following sections. After the downstream processing, the HCP

and DNA impurity levels are required to be below 100 ppm and 10 ppb respectively [6]. Virus

particles need to be less than 1 per 10^6 does, which translates to 12-18 $\log_{10}$ removal for

endogenous retroviruses and 6 $\log_{10}$ removal for adventitious viruses when Chinese Hamster

Ovaries (CHO) is used as the cell line [7].

Table 1.1 Comparison of four chromatographic steps in the downstream process.

Chromatography	Mechanism	Running Mode	Elution Strategy	Limitations
Protein A Chromatography	Affinity Interaction	Bind and elute	Low pH (4-5 [6])	Expensive, ligand leaching and denature, product aggregation due to low pH elution
IEC	Electrostatic interaction	Flow through /Bind and Elute (CEX)	High salt conc. (>150 mM)	Large buffer usage due to low conductivity required for binding
HIC	Hydrophobic interaction	Flow through	Low salt conc.	Low binding capacity, salt disposal cost, protein solubility limitation under high salt conc.
Multi-modal	Multi-type interactions (electrostatic interaction, hydrophobic interaction and hydrogen bonding interaction)	Flow through	Condition from DOE	Still under development: lack of deep understanding
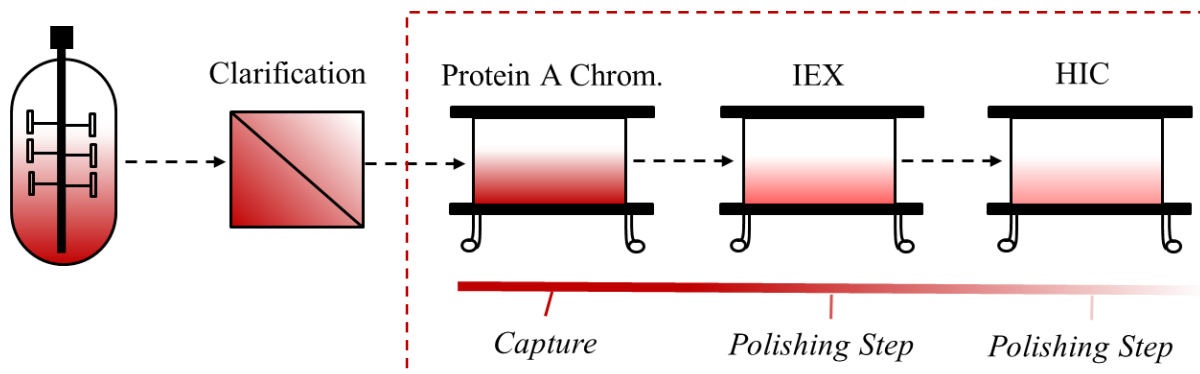
Figure 1.1 Major chromatographic steps for mAb purifications after clarification. Chromatographic processes normally start with a capture step utilizing protein-A chromatography, followed by two polishing steps involving IEX and HIC.

1.2.1 Protein A Chromatography

The first step during chromatographic purification begins with protein A chromatography, which is the workhorse among all the chromatographic unit operations. Protein A is a 42 kDa protein from the cell wall of *S. aureus (SpA)* [8, 9]. The high affinity of protein A to the fragment crystallizable (Fc) region of IgG enables it to capture mAb products directly from harvested cell culture fluid (HCCF) effectively. The specific interactions between protein A and mAbs involve the formation of hydrogen bonds and two salt bridges [10]. The binding strength appears to be pH dependent. The strong binding interaction occurs at close to pH 7. Protein A chromatography runs in a bind and elute mode, where mAbs bind at the neutral condition and elute at the acidic condition. Most impurities are washed away during the binding and wash steps, rendering a final purity of mAb products to be over 95% [11]. Elution is normally conducted at lower pH condition (4-5) and the yield is generally above 90%.

Even though protein A chromatography has been widely used in industry, the high material cost and ligand stability issue are the two main challenges that propel the

development of alternative mAb capture step. Currently with the recombinant DNA technology, protein A is expressed in *Escherichia coli (E.coli)* as the host cell, which makes manufacturing cost very high. As a result, protein A resin material cost can go up to $9,000–12,000 per liter, which is about 30 times higher than the other non-affinity media [12], including IEX and HIC. Therefore, there is a great demand for designing new cheaper affinity ligand. In addition, the denaturation of protein A due to the harsh regeneration condition is a major concern. As protein A column is expensive, it is usually used for many cycles with NaOH as a cleaning reagent for regeneration. After several regeneration steps, the caustic condition tends to denature protein A and reduces its binding capacity. Significant efforts have been devoted to mutate protein A in order to improve its stability under alkali condition. For example, alkali-tolerant rProtein A ligand has been developed by GE Healthcare as the "MabSelect SuRe" resin. In addition, protein A leaching is another serious concern. Protein A is immune-toxic and has to be removed by the subsequent ion exchange chromatography steps. GE Healthcare has developed "Mabselect" series of resins to reduce the leaching by engineering a C-terminal cysteine into protein A to form a thio-ether linkage with the epoxide spacer arm to the base matrix. In addition, mutated protein A is under development to increase the elution pH in order to reduce mAb aggregation [13].

1.2.2 Ion Exchange Chromatography

Ion exchange chromatography (IEC) is commonly used afterward the protein A capture step to further remove remaining HCPs, viruses, leached protein As and endotoxins. Based on the charges on mAbs and impurities as shown in Figure 1.2, cation exchange

chromatography (CEX) and anion exchange chromatography (AEX) are used accordingly in

a flow-through mode. Compared to protein A chromatography, IEC has a much lower

material cost, higher resistance to alkaline cleaning buffer and relatively high binding

capacity. In recently years, high capacity CEX has been developed as an alternative to protein

A chromatography [14, 15, 16, 17]. Membrane adsorbers have found the niche application in IEC

due to its high-throughput binding, low operating pressure and ease of scale up. Since the

impurity amount is actually very low after protein A step, membrane adsorbers have enough

binding capacity to achieve the separation goal by binding the impurities in a flow-through

mode.
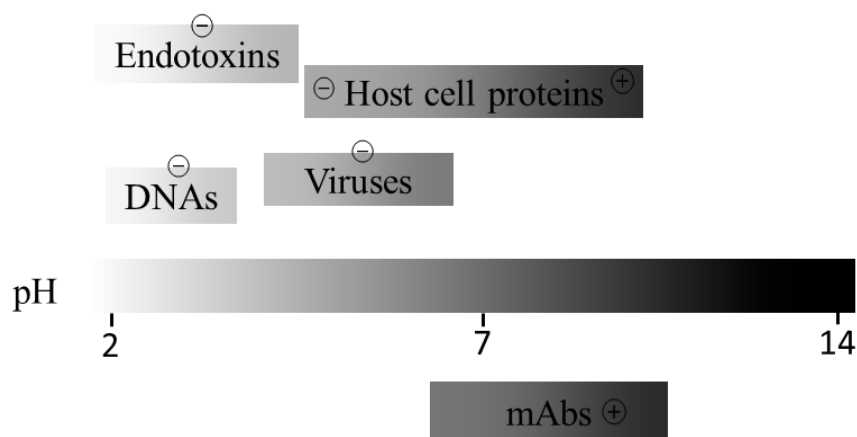
Figure 1.2 Charges of impurities and mAbs (pI >7.5) in ion-exchange chromatography step. (166). At pH 7-8, negatively charged impurities including viruses, endotoxins, DNAs and part of negatively charged HCPs can be removed by AEX in the flow-through mode.

A major advance for anion exchange chromatography (AEX) development is the

usage of primary amine as the salt tolerant ligand [18, 19, 20]. Compare to strong the quaternary

amine (Q ligand), The electrostatic interaction and hydrogen bonding interaction enable the

primary amine to bind protein under relatively high conductivity (up to 200 mM NaCl) [21, 22,

23]. This salt tolerance feature makes it possible for AEX to be directly loaded from the elution

pool of CEX (~15 mS/cm) without dilution. More discussion on the development of salt

tolerant AEX membranes will be presented below.

1.2.3 Hydrophobic Interaction Chromatography

The last polishing step is normally carried out using hydrophobic interaction

chromatography (HIC). HIC has been widely used as the second polishing step, following the

IEC step. It has been used extensively in a flow-through mode to remove aggregates and

HCPs which are more hydrophobic comparing to the mAb products. At high salt

concentration, the aqueous surface tension increases leading to the more favorable

hydrophobic interaction. In addition, enhanced charge screening at high salt concentration

leads to the reduced electrostatic interaction and further promotes the hydrophobic

interaction. N-alkyl (C_1-C_8) and aryl (phenyl) are the two most common ligand types for HIC

as shown in Figure 1.3.

$$-O\text{—} \qquad -O(CH_2)nCH_3$$
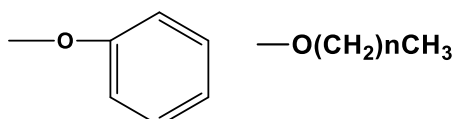
Figure 1.3 Two general types of traditional HIC ligands (aliphatic and aromatic HIC
ligands).

Compared to reverse phase chromatography, HIC ligands are considered to be mildly

hydrophobic, which ensures the eluted proteins to be biologically active instead of being

denatured. The ammonium sulfate concentration reported to be used in the existing HIC flow-

through process is ranged from 200 mM to 650 mM $(NH_4)_2SO_4$ [24].

Compared to reverse phase chromatography, HIC ligands are considered to be mildly

hydrophobic, which ensures the eluted proteins to be biologically active instead of being

denatured. Ammonium sulfate $(NH_4)_2SO_4$ is effective and gentle as a salt medium. The concentrations reported to be used in the existing HIC flow-through processes range from 200 mM to 650 mM [24].

Recently there is a growing interest in developing HIC membrane adsorbers for protein separations [25, 26, 27, 28, 29, 30, 31]. These HIC membrane adsorbers possess the advantages of membrane chromatography and perform the purification based on the HIC principles. Sartobind® Phenyl membranes (Sartorius AG) were the first commercialized HIC membrane adsorbers that are marketed for protein capture (20 mg IgG/mL) or polishing step to remove impurities such as aggregates and HCPs. HIC membranes have been also developed for protein fractionations [26, 32, 33, 34, 35] and preparative protein purifications [27, 28, 29, 36]. The disadvantages of traditional HIC chromatography are its low capacity, low recovery and high concentration of salt required during the process. The capacity for these HIC ligands is generally below 40 mg/mL [24], which is significantly lower than the capacity of protein A, ion-exchange, and mixed mode based resins (> 100 mg/mL). Conventional hydrophobic ligands tend to denature protein leading to irreversible binding of the protein as well as protein aggregation. New efforts are dedicated to developing more gentle thermo-responsive HIC ligands for protein separations [37]. Chapter 3 and 4 are presenting a thermo-responsive polymer used as the HIC ligand for protein separations. Compared to traditional non-responsive HIC ligands, thermo-responsive polymers possessing both hydrophobic and hydrophilic residues are only moderately hydrophobic. The hydrophobic-to-hydrophilic transition can be switched by reducing the temperature and/or salt concentration. Since the

binding and elution of the proteins are based on the conformational and hydrophobicity switching of the thermo-responsive ligands, high resolution and high recovery of the protein separations can be achieved [28, 38, 39, 40, 41].

1.2.4 Multi-modal Chromatography

Multi-modal chromatography (MMC) binds proteins based on more than one type of interactions, which includes van der Waals, electrostatic and hydrogen bonding interactions. The interactions can come from the ligand, spacer or matrix. MMC has been developed for separating mAbs [42, 43, 44], glycosylated proteins [45] and vaccines [46]. The earliest MMC was reported almost at the same time when HIC was first developed [47]. In early 1990, Kasche et.al developed pH-induced multimodal chromatography with phenylbutyl amine as the ligand. Penicillin amidase was adsorbed via the hydrophobic interaction and eluted at lower pH due to electrostatic repulsion. Burton and Harding developed hydrophobic charge induction chromatography (HCIC) with pyridyl and imidazolyl ligands in 1998 [48]. It was found that at high ligand density, protein adsorption is almost salt independent. The pyridiyl ligand (4-mercaptoethylpyridine) was subsequently commercialized by Pall Corporation as the MEP Hypercel MMC sorbent. Besides hydrophobic interaction, the S atom on the ligand can selectively interact with IgG via thio-philic interaction [43, 49]. Capto^{TM} adhere is marketed as an alternative to conventional IEX and HIC. It is a strong anion-exchange type MMC. Quaternary amine, hydroxyl and phenyl groups provide electrostatic, hydrogen bonding and hydrophobic interactions respectively. Another ligand 2-benzamido-4-mercaptobutanoic acid developed by Li and co-workers [50] has been commercialized by GE Healthcare with a brand

named Capto MMC. A similar cation exchange hydrophobic ligand has been commercialized

by Bio-Rad (Nuvia cPrime). The structures of these commercialized ligands are shown in

Figure 1.4.

a.MEP Hypercel **b.Capto™** **c.Capto™** **d.Nuvia cPrime**
 adhere **MMC**
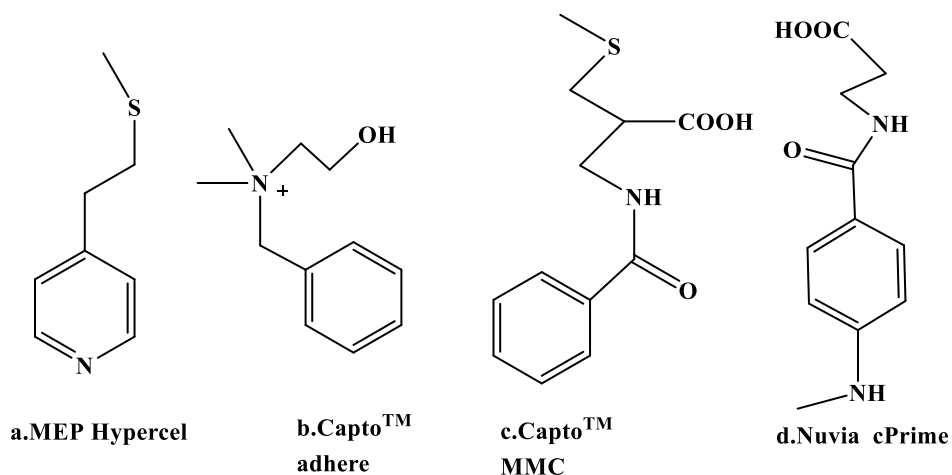
Figure 1.4 Commercialized MMC ligands by Pall Corporation (a), GE Healthcare (b,c) and Bio-Rad (d).

Recently, a phenylboronic acid ligand is developed as a synthetic ligand for direct

capture of mAbs from serum-free CHO cell cultures. Boronic acid group can offer an affinity

interaction with the oligosaccharide on the Fc domain besides the hydrophobic interaction [51].

A new HCIC ligand has been developed by Tong and co-workers [44]. The new HCIC ligand

contains a tryptophan moiety which has an affinity to Fc and 5-amino-benzimidazole for

facile elution with pH change. The same ligand has been used for human serum albumin

(HSA) capture from culture broth [52]. The capacity reaches 141.33 mg/g at pH 5, which is two

times higher than the commercialized MX-Trp-650m resin manufactured by TOSOH.

There are many advantages of using MMC over the conventional ion-exchange and

hydrophobic interaction chromatography. First, it has been shown that proteins can be bound

to MMC at a wide range of ionic strength [48, 53, 54]. As a result, MMC is salt-tolerant (up to 300

mM NaCl). In addition, it can maintain the high capacity for targeted proteins at much lower

salt concentrations compared to the conventional HIC. In addition, a wider operation window

means that more conditions (pH and salt concentration) can be selected. Secondly, by

carefully balancing the electrostatic and hydrophobic interactions, it is possible to achieve

highly selective separations. Cramer's group recently studied the selectivity of MMC with

different Fabs and related variants [55] and two MMC resins (Capto MMC and Nuvia cPrime)

to investigate the ligand geometric re-arrangement effects [56]. Their results show the spatial

organization of MMC ligands plays very important roles in binding the complementarity-

determining region (CDR) on the Fabs, which is hypothesized to be the critical binding site

for MMC. Their results further show that Nuvia cPrime and some other MMC prototype

ligands have higher selectivity over Capto MMC. Quantitative structure–activity relationship

(QSAR) models were used to predict the protein retention to evaluate the effects of ligand

structure. Overall, the exposure, shape and density of hydrophobic moiety in MMC ligand

can affect the selectivity between aliphatic and aromatic residues on proteins. Different

mobile phase modulators [57, 58, 59] (urea, arginine, ethylene glycol etc.) and controlled pH

gradient elution methods [60] have also been investigated for increasing the selectivity of

MMC.

1.3 Membrane Chromatography: An Alternative to Packed Bed Chromatography

Packed bed column chromatography has been widely used in downstream processing for

purification of proteins, DNAs and other pharmaceutical products. However, one major

drawback of the packed bed column chromatography is the slow pore-diffusion which

severely restricts its efficiency for separation (shown in Figure 1.5). The diffusion of targeted

products to the ligands on the chromatography is a slow process leading to the dramatic drop

of binding capacity as the feed flow rate increases. Besides diffusion limitation, the packed

bed chromatography also suffers from large buffer consumption as well as extra costs for

packing and testing.
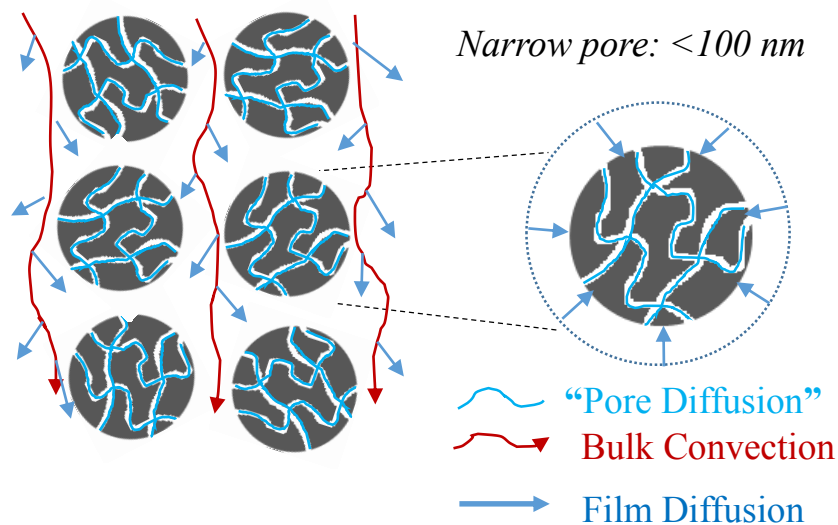
Figure 1.5 Transport mechanism of packed bed chromatography.

An alternative is to use adsorptive membrane chromatography during downstream

processing [61, 62]. Adsorptive membranes, known as membrane adsorbers, are a type of

macroporous membranes functionalized by ligands attached on the membrane pore surface

(Figure 1.6). Membrane adsorbers represent a type of liquid-solid membrane contactor and

have been used extensively in the flow-through mode [23] to remove containments, such as

aggregates [63], virus [22, 64] and DNA [64, 65]. In recent years, with the enhanced capacity, there has

been an increased interest in using adsorptive membranes in a bind and elute mode for

protein separations [66, 67, 68, 69, 70, 71, 72].

Compared to the resin-based chromatography, the pore diffusion limitation is eliminated in membrane adsorbers during the transport process where convection becomes the dominated transport mechanism as illustrated in Figure 1.6. Consequently, several studies show that the binding capacity is independent of a wide range of flow rate [71, 72, 73]. Moreover, the operation can be performed at relatively low pressure, which reduces protein denaturation and aggregation. Buffer usage of membranes is lower than resin due to a lower void volume. Membranes have captured more attentions in recent years because of the "single-use" (disposable) application in many downstream processes. Due to the low material cost of membranes, single-use membrane processes, such as mAb purification (flow through) and virus filtration, greatly reduce the cost of re-validation. Finally, the membrane system is easier to scale up and the cost of packing and testing is subsequently reduced significantly. Traditionally, membrane-based purification is always limited by its low capacity. However, with the improvement of the matrix for higher surface area [74] or introducing polymeric ligands [54, 71, 75], high capacity membranes have been developed to compete with protein A resins. Recently, a new membrane laterally-fed device has been designed for a large scale membrane-based bind-and-elute mAb purification process [76]. Traditional stacked-disc and radial flow devices suffer from low binding efficiency due to the large dead volume and dispersion caused by the flow-path variability. Using the laterally-fed membrane device, the elution peak becomes significantly sharper and more symmetrical. Their protein fractionation results show a clear advantage of using this laterally-fed device with an improved resolving power.
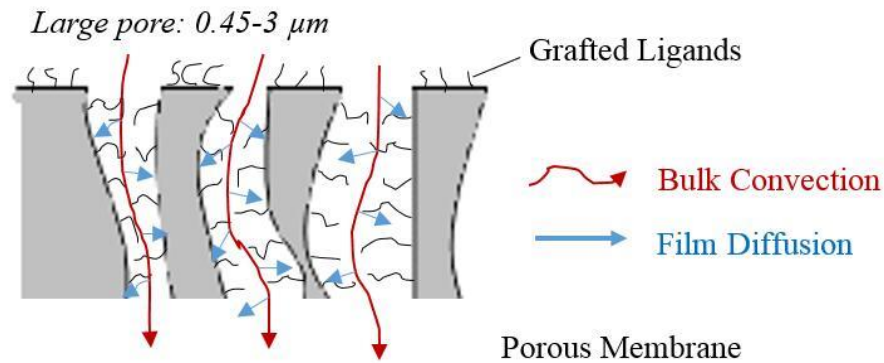
Figure 1.6 Transport mechanism of membrane chromatography. Compared to packed bed chromatography, the pore diffusion process is basically eliminated due to the macroporous structure of membranes.

The commercialized membrane adsorbers are summarized in Tables 1.2 and 1.3 based on the membrane type, ligand and binding capacity. As described in the Tables, the microporous membranes are used with pore size ranging from 0.65 μm to 3 μm. Polyethylene, polyethersulfone (PES) and regenerated cellulose membranes are commonly used as membrane substrates. Most membrane adsorbers are stacked-disks, but hollow fiber membrane adsorbers have also been commercialized. Hydrophilic membrane substrate is preferred because of its good biocompatibility and low non-specific protein binding. It is important to note that the base membrane is normally bio-insert so that fouling or non-specific binding is reduced and ligand selectivity is enhanced [77]. The base membrane is also important for IEX, which is known as the mix-mode effect [78]. Similarly, any electrostatic interaction between base membrane and protein will affect HIC. Leonard provided a detailed review on the packing materials for protein chromatography [79]. Lenhoff also reviewed different adsorbent structures for ion-exchange chromatography [80]. Major membrane adsorbers are cation or anion exchange type. The anion exchange ligands include quaternary

amine (Q), diethylamine (D) and primary amine. Traditionally, quaternary amine was widely used as the strong anion exchange ligand. However, it was found that the virus clearance drops dramatically at moderate salt concentrations. When salt concentration increased to 50 - 150 mM NaCl, virus clearance of MMV or ΦX 174 could decrease from 5-6 log removal value (LRV) to only 1 LRV [64]. The HCP clearance also becomes less than 1 LRV in 50 mM NaCl [64]. As a result, Q ligand-based anion exchange purification step requires a large amount of buffer to dilute the loading product in order to maintain its binding capacity. Primary amine was then developed as a salt tolerant ligand by introducing the secondary hydrogen bonding interaction in addition to the electrostatic interaction. The primary amine ligand was first designed and selected by Riordan et.al [18, 81] for virus removal and then developed and commercialized, e.g. "ChromaSorb" by MilliporeSigma [20]. This primary amine based AEX can have a 5 LRV for ΦX 174 under 150 mM NaCl condition, whereas Q based AEX has zero clearance [18]. Sulfonic and carboxylic acid groups have been used in the cation exchange membranes. Sartorius AG launched HIC membrane using phenyl as the ligand. Phenyl groups are first used in HIC membrane by Kubota et.al in 1995 [82] and developed later by Faber et.al from Sartorius Stedim Biotech GmbH [29]. HIC phenyl membrane has been scaled up to 5 L marketed for both capture and polishing steps. Sartorius AG also has affinity membranes with protein A as ligands. However, this affinity membrane is only commercialized in a lab-scale with a small bed volume (2 mL) for mg level IgG purification. Another affinity membrane developed by Sartorius AG is the metal chelate adsorbers. This membrane is based on immobilized metal affinity chromatography (IMAC), where

genetically expressed protein with His-6-tag can bind to Ni^{2+}, Co^{2+}, Zn^{2+} or Cu^{2+} ions which are pre-loaded on membranes grafted with iminodiacetic acid (IDA) ligands.

Table 1.2 Summary of commercialized membrane adsorbers used in downstream polish steps.

Company	Membrane Adsorber	Type	Application
Asahi Kasei Medical	QYUSPEED D	AEX	Removal of HCP, virus, DNA etc.
MilliporeSigma	ChromaSorb™	AEX	Removal of HCP, virus, DNA etc.
Pall Corporation	Mustang® Q	AEX	Removal of DNA, HCP, virus etc.
	Mustang® E	AEX	Removal of endotoxin
	Mustang® S	CEX	IgG, Factor VIII, removal of HCP(+)
Sartorius AG	Sartobind®S	CEX	Removal of positive charge HCP
	Sartobind®C	CEX	
	Sartobind®Q	AEX	Removal of virus, DNA, HCP(-),endotoxin
	Sartobind®D	AEX	
	Sartobind®STIC	AEX	
	Protein A	Affinity	IgG purification(mg level)
	IDA-Ni^{2+} or Co^{2+}	Affinity	His-tag proteins purification
	Sartobind®Phenyl	HIC	Aggregates removal
Natrix Separations, Inc.	NatriFlo® HD-Q	AEX	HCP removal, DNA removal and Viral Clearance
	Natrix HD-Sb	Multi-modal	mAb capture and aggregates removal

Table 1.3 Detailed information on ligands and binding capacities of commercialized membrane adsorbers.

Membrane	Impurity removal	Membrane substrate and Ligand	Additional information
QYUSPEED D	BSA: >40 mg/ml (DBC 10%), DNA: >25 mg/ml, Porcine Parvovirus: > 5 LRV	Polyethylene membrane with Diethylamino group	First AEX hollow fiber membrane adsorbers
ChromaSorb™	Virus (MMV)>4 LRV, DNA>3 LRV, Endotoxin>3 LRV	Polyethylene membrane (0.65 μm) with poly allylamine ligand	Salt tolerant (>150 mM NaCl, 30 mS/cm in buffer when remove MMV),Scales up from 0.08 ml to 50 ml
Mustang® Q	DNA: 30 mg/ml, BSA: 70 mg/ml	PES membrane 0.8μm with quaternary amines ligands	Strong anion-exchange membrane
Sartorius® Q	DNA>2 LRV, Endotoxin>2.8, HCP:1.9 LRV, BSA: 29 mg/ml	Regenerated cellulose membrane(>3μm pore size) with quaternary amines ligand	Strong anion-exchange membrane, Scale up from 0.08 to 1620 ml
Sartorius® D	BSA: 22 mg/ml	Regenerated cellulose membrane with diethylamine as ligand	Weak anion-exchange membrane
Sartorius salt tolerant AEX	BSA: 36 mg/ml in 200 mM NaCl compare to 3.6 mg/l(Sartorius Q) at the same condition, DNA: 22 mg/ml, LRV for MMV: >4.96	Primary amine as ligand	Weak anion-exchange membrane
NatriFlo® HD-Q	3D hydrogel matrix, BSA: >200 mg/ml, DNA: > 20 mg/ml, xMuLV:>4.8 LRV, HCP: up to 4 kg/L	Quaternary amine as ligand	Strong anion-exchange membrane
Natrix® HD-Sb	mAb:> 90 mg/ml (10% breakthrough),HCP: >1.4LR,Aggregates: up to 12% removal	Sulfonic acid and t-butyl	Multi-modal membrane
Mustang® S	60 mg/ml human IgG, 47 mg/ml for lysozyme	0.8 μm pore size membrane+ Sulfonic acid (S)	Used for Baculoviruses capture
Sartorius® S	Lysozyme: >29 mg/ml	Regenerated cellulose membrane (>3μm pore size)with sulfonic acid as ligand	Strong cation-exchange membrane
Sartorius® C	Lysozyme: 22 mg/ml	Regenerated cellulose membrane with carboxylic acid as ligand	Weak cation-exchange membrane
Sartobind® Phenyl membrane	14.6 mg/ml(globulin, at 0.9M (NH4)2SO4)	Regenerated cellulose membrane with phenyl as ligand	First commercialized HIC membrane,0.08 mL to 5 L
Sartobind® Protein A membrane	10-15 mg/unit polyclonal IgG	Regenerated cellulose membrane with protein A as ligand	Only available in 2mL bed volume

1.4 Membrane Functionalization

Membrane functionalization is an effective way to change the property of membrane drastically without altering too much of the membrane bulk structure [83]. Functional groups can be introduced to control the interaction of different species within the membrane surface region for various applications such as anti-fouling [84, 85, 86], metal ions removal [87, 88] and protein separations [37, 70, 75, 89, 90]. Besides controlling surface interaction during separations, new properties can be introduced through membrane functionalization such as catalytic membranes designed for cellulose hydrolysis [91] and responsive membranes for many applications [30, 37, 92, 93, 94]. Physical coating [95, 96], chemical treatment [97], plasma treatment [98], self-assembly (self-assembled monolayers [99] and layer-by-layer assembly [100, 101, 102, 103]) and polymer-grafting method [67, 89, 90] are common methods to modify membrane surfaces.

Polymer-grafting method has many advantages compared to other surface modification techniques for developing membrane adsorbers. First, it is a chemical modification method with polymers covalently attached to the membrane surfaces. Therefore, the stability of grafted polymers is much higher than physical coating and self-assembly methods. This is especially important when developing membrane adsorbers to prevent ligand leakage particularly during bioseparations. Secondly, instead of introducing simple functional groups such as hydroxyl or amine groups by chemical or plasma treatment, complex polymer structures can be utilized for realizing sophisticated protein separations. The surface properties of the membranes can be tailored easily and dramatically by selecting

specific monomers. Furthermore, by varying polymerization time and initiation condition, it is possible to control the polymer chain length and density in a decoupled way. The architecture of grafted polymeric ligands has been shown to have a critical impact on the performance of the membrane adsorbers [31, 68, 71, 90, 104]. Therefore, polymer-grafting method is superior to other surface modification techniques for preparing membrane adsorbers used in downstream bioseparations.

"Grafting to" and "grafting from" are the two most common strategies for grafting polymers on the membrane surfaces [83]. The "grafting to" method involves conjugation of pre-synthesized polymers with reactive anchor groups onto the membrane. On the other hand, polymerization can be initiated from the membrane surface via "grafting from" method. "Grafting to" method has a better knowledge of grafted polymer properties, such as the polymer molecular weight and polydispersity. However, the grafting density is usually lower than polymers grafted by "grafting from" method [105]. The 'grafting from' method will be discussed in more detail below.

1.4.1 "Grafting From" Method

Three different initiation processes are commonly used in the "grafting from" method. The first approach starts the initiation of polymerization on membrane surface by plasma treatment [106, 107, 108], UV irradiation [109, 110], high-energy radiation [111] (γ-ray irradiation) to create radicals from the membrane substrate. The second approach is to use a photo-initiator [68, 70, 89] grafted on the membrane substrate. The third one is to immobilize a radical initiator for living polymerization [54, 112, 113, 114]. In this section, we focus on UV-initiated

polymerization (with and without photo-initiator) and surface-initiated atom transfer radical

polymerization (SI-ATRP) as a living polymerization technique.

1.4.2 UV-induced Polymerization

UV-initiated polymerization has been widely used in membrane surface modification

for many applications, such as protein separations [68, 70, 89, 104, 115, 116, 117, 118], surface

hydrophilicity enhancement [119, 120, 121], anti-fouling [85, 110, 122, 123, 124, 125], catalysis of reaction [91],

responsive membranes [126, 127, 128], nanofiltration [129] and metal ion removal [130]. Polymerization

initiation starts by abstracting a hydrogen atom on the membrane surface from the radicals

induced by UV light. For example, the carbonyl group can be excited to the triplet state to

form a reactive free radical as shown in Figure 1.7a. If the membrane itself is photosensitive,

then the free radicals can be generated on the membrane backbone as shown in Figure 1.7b.

Polysulfone (PS) or poly (ethersulfone) (PES) membranes are sensitive to the UV light in the

range from 200 to 320 nanometer (nm) [131].
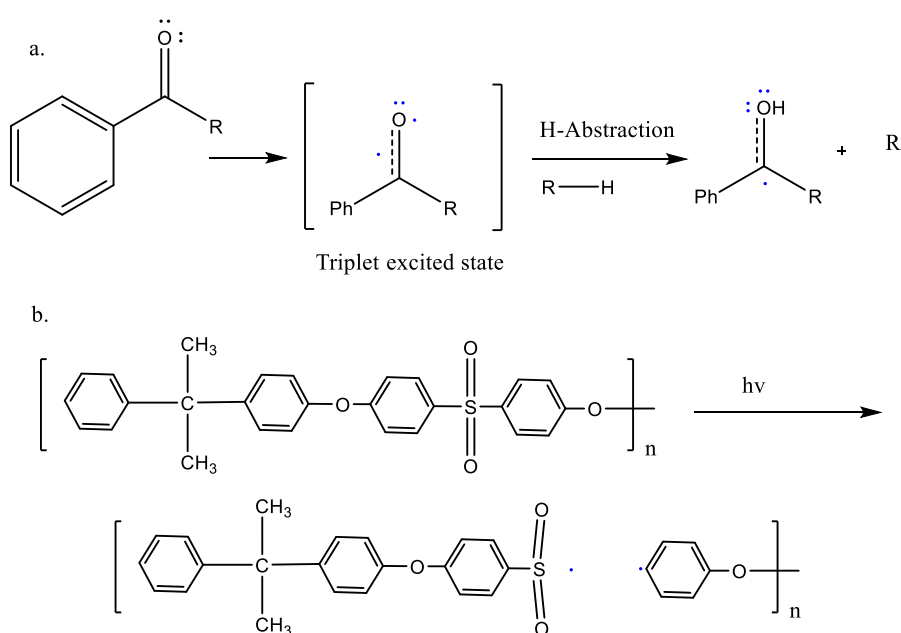
Figure 1.7 Mechanism of UV-induced polymerization with type II photo-initiator (a) and without photo-initiator (b, PES membrane).

Compared to other polymer-grafting methods, UV-initiated polymerization has many advantages in terms of cost and efficiency. Firstly, the modification is much simpler and cheaper than other methods such as SI-ATRP. The UV-initiated polymerization can be carried out in air, whereas typical SI-ATRP requires an oxygen-free environment during polymerization. It is also cheaper than plasma-initiated polymerization due to the lower energy required. Secondly, the UV-initiated polymerization process is quite clean where only monomers, solvent and UV light are required whereas catalyst removal for ATRP remains to be one of the major challenges. Thirdly, the polymerization rate and degree of polymerization are generally much higher for UV-initiated polymerization than for ATRP resulting in higher modification efficiency.

1.4.2.1 UV-induced Polymerization without Photo-initiator

As described before, PS and PES membranes are photo-sensitive and polymers can be grafted on the membrane backbone. Many monomers have been grafted by this method with PES or PS membranes, including hydroxyethylmethacrylate (HEMA) [109], glycidyl methacrylate (GMA) [109] and methyl methacrylate (MAA) [109], N-vinyl-2-pyrrolidinone (NVP) [132, 133]. As a result, hydroxyl, epoxy and carboxylic groups can be easily introduced for post-modification. UV-initiated polymerization on PES membranes has studied extensively [109, 110, 132, 133, 134, 135]. It was found that polymers on membrane backbone were cleaved initially generating radicals followed by polymerization with the monomers [109]. It was further found that the polymerization occurred deeply inside the ultrafiltration (UF) PES membranes [109].

The main advantage of this method is that the modification procedure is rather simple without any need of pre-treatment. PES or PS membranes can be immersed inside the monomer solution while polymerization starts from the radicals formed at the membrane backbones as shown in Figure 1.7b. It was also found that PES membranes are more susceptible to UV initiated polymerization than PS membranes using the same monomers [132].

1.4.2.2 UV-induced Polymerization with Photo-initiator

Currently there exist two photo-initiator types used for membrane surface modification. Type I initiator has been developed and used in industry to hydrophilize polyvinylidene fluoride (PVDF) [136] and polyethylene (PP) [137] membranes. The initiation of type I initiator is the free radical generation from the cleavage of initiator itself under UV irradiation. The radicals formed on membrane surface abstract hydrogen atoms on membrane substrate thus transferring radicals to the membrane. Benzoin derivatives, peroxides and azo compounds are commonly used type I photo-initiators. For example, benzoin ethyl ether (BEE) derivative has been used for membrane imprinting by cross-linking via UV-initiated polymerization [138]. Interestingly, the BEE initiators could be covalently immobilized on the membrane surface prior to UV irradiation through the carbodiimide coupling [68, 91, 139]. After UV irradiation of BEE, highly reactive radicals are generated from the immobilized BEE initiator whereas radicals formed in the bulk solution have very low reactivity as shown in Figure 1.8 [139].
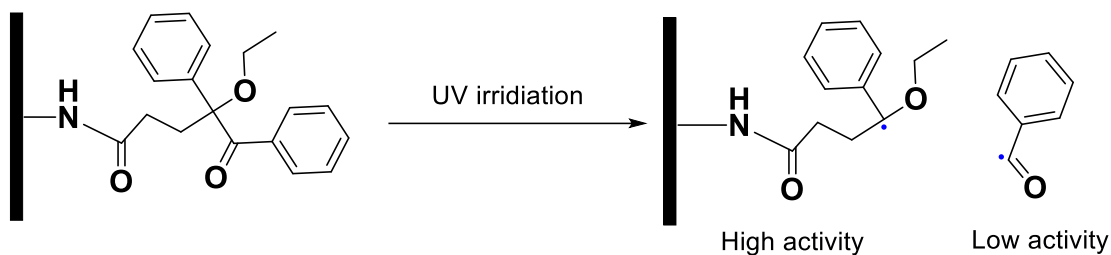
Figure 1.8 Initiation mechanism of immobilized type I BEE initiator. The high activity radical is formed on the immobilized BEE initiator side. Low activity radical is formed in the bulk solution.

Type II initiators, such as benzophenone (BP) or its derivatives have been widely studied and used for the modification of polyethylene terephthalate (PET) [140, 141, 142, 143, 144], polypropylene [89, 119, 145, 146], polyacrylonitrile (PAN) [126, 147, 148], PVDF [149] and regenerated cellulose membranes [104]. The enhanced polymerization on surfaces comes from radical generation via H abstraction from the substrate polymers leading to higher grafting densities. Many protocols have been developed using BP initiator to improve the initiation efficiency. *Simultaneous* and *two-step* polymerizations are the two common approaches to conduct UV-initiated polymerizations. *Simultaneous* method involves grafting process in a solution containing both monomers and BP initiator [142, 143, 150, 151]. The grafting density obtained by this method is relatively low with significant amount of polymerization occurring in the bulk solution. In addition, this approach is limited by the solvents that can be used since BP initiators are not soluble in water. In addition, only some solvents will be effective for the hydrogen abstraction reaction. For the two-step polymerization method, local BP concentration can been increased by pre-coating the initiator on the membrane surface prior to UV irradiation. The polymerization reaction can be conducted in a different solvent so that monomers can be easily dissolved. This approach greatly extends the application of BP

initiators. This protocol works quite well with the hydrophobic membranes and monomers that have high solubility in water. BP initiators adsorbed on the membrane surface have a low solubility in water leading to the reduced bulk solution phase polymerization. Ma and co-workers developed sequential UV irradiation steps with BP initiator covalently attached on PP membrane first [145]. The grafting degree has increased 4 times compared to the simultaneous method. More importantly, the grafting density can be controlled to some degree through the initiator immobilization step. Many other attempts have been made to improve the immobilization efficiency of BP initiators in order to have a better control of the grafting density. Geismann and Ulbricht have immobilized a charged BP derivative initiator on PET membrane through electrostatic interaction [144]. Ulbricht and Yang have introduced a new "entrapping method" for BP initiator immobilization. PP membrane was first pre-swelled in heptane with the BP initiators. The membrane was then washed with non-swelling solvent to remove the surface adsorbed initiators. Finally, polymerization on the membrane substrate was performed using a non-swelling monomer solution. The entrapping method has many advantages over BP surface adsorption method. Firstly, after BP initiators are entrapped inside the membrane substrate, other non-aqueous solvents can be used for polymerization without the concern of BP dissolving in the bulk solution leading to bulk solution phase polymerization. Secondly, grafting density can be controlled to some degree by varying the initial BP concentration during the pre-swelling step. Wang et.al has modified regenerated cellulose (RC) membranes with poly (acrylic acid) for protein separations. Heptane was used as a non-polar solvent to coat the BP initiators on the RC membrane

surface which is considered polar. The heptane solvent prevents the entrapment of the BP initiators into the bulk cellulose substrate [104]. Hu and co-worker reported using $FeCl_3$ with the BP initiators to improve the degree of grafting of 2-hydroxyethyl methacrylate on PP membranes. It is believed that there is a synergistic effect between Fe^{3+} and BP initiator. Their results showed that there was 2.5 times increase in grafting degree compared to the direct BP adsorption method. Similar synergist effect was also reported by He et.al for the PET membrane modification when tertiary amine groups were present [140, 152]. There is a better control for both the grafting density and polymer chain length in the presence of tertiary amines compared to the non-aminolysed PET membranes [152].

1.4.2.3 Membrane Adsorbers Prepared by UV-initiated Polymerization

Various types of ligands have been grafted on membrane substrates via UV-initiated polymerization reactions. These ligands include protein streptavidin [117], polymer brushes [89, 104, 140], responsive hydrogels [30, 41, 118] and molecularly imprinted polymers. Affinity [115, 116, 117, 140], ion-exchange [89, 104] and HIC membranes [30, 41, 118] were developed for protein separations and purifications.

Borcherding et al. prepared an affinity membrane by immobilizing proteins as ligands. The affinity comes from the specific interactions between streptavidin and biotin. Epoxy groups were first grafted on membranes via UV-initiated polymerization followed by coupling with affinity protein ligand streptavidin. BP initiators were coated on PP membranes (0.4 μm pore size) for 18 h followed by grafting of poly (glycidylmethacrylate (GMA)) in a monomer solution containing BP, $NaIO_4$, GMA and water (10% v/v methanol). Streptavidin

was then covalently immobilized reacting with the epoxy groups on the membrane. The binding capacity is comparable to commercialized streptavidin immobilized particles.

Affinity membranes have also been developed by He et al [140] using synthetic copolymer brushes as ligands for the first time. This protein-selective copolymer ligand contains bisphosphonato-m-xylylene methacrylamide monomer that has a high affinity to arginine. It is possible to separate cytochrome C (lysine rich) from lysozyme (arginine rich) with similar pIs and sizes since these two proteins have a different number of arginine residues. The adsorption isotherm shows the binding constant with the copolymer ligand is 15 times higher for lysozyme than for cytochrome C. Selective binding of lysozyme in a 1:1 lysozyme and cytochrome C mixture was also successful. This work demonstrates for the first time that synthetic polymer brushes can be used as high performance affinity ligands to achieve high-resolution protein separations.

Poly (vinylcaprolactam) (PVCL) hydrogel has been coated with cellulose filter papers [118] and PVDF membranes [41] by a simultaneous UV-initiated polymerization using BP initiators. PVCL is a thermo-responsive polymer which is also salt responsive since its LCST is salt concentration and salt type dependent. Protein binds to the ligands under high salt concentration when PVCL is hydrophobic and elution is promoted under low salt concentration when PVCL changes to hydrophilic state. Recently, Wu et.al designed a branched poly (N-isopropyl acrylamide (NIPAM)-co-butyl acrylate) ligands coated on cellulose filter by simultaneous UV-initiated polymerization [30]. The bind and elute studies were supposed to be conducted in a salt-free environment by varying the temperature

between 41°C and 10°C for bind and elute respectively. However, they found out that 1.75 M (NH$_4$)$_2$SO$_4$ is still needed for IgG to bind to the ligands at 41°C.

Ulbricht and Yang have modified PP membranes with copolymer cation-exchange ligands comprised of acrylic acid (AA), acryl amide (AAm) monomers and cross-linker methylene bisacrylamide (MBAA) [89]. Binding capacity and recovery were compared for poly (AA) brushes, poly (AA-co-AAm) and cross-linked poly (AA-co-MBAA) modified membranes. Both the adsorption and entrapping methods for coating BP were used. The modified membranes showed a pH-dependent water permeability as well as reversible lysozyme binding. Results from binding capacity indicate that membranes modified via BP entrapping method have twice as higher a capacity than those modified via BP adsorption method. The cross-linked poly (AA-co-MBAA) modified membranes have a lower pH responsiveness but higher lysozyme binding capacity than the non cross-linked PAA modified membranes. It is also interesting to see that poly (AA-co-AAm) modified membranes also have higher binding capacity than poly (AA) modified membranes. Poly (AA) brushes have also been grafted on regenerated cellulose membranes by Wang et al. [104]. Again, the 10% breakthrough binding capacity increased about 70% after incorporating a cross-linked PAA compared to the linear PAA ligands. The highest dynamic binding capacity was obtained on a membrane substrate with uniform pore sizes functionalized with cross-linked PAA ligands. At 10 ml/min flow rate, the binding capacity reached 38 mg/ml for lysozyme and 36 mg/ml for IgG.

More sophisticated molecularly imprinted polymer (MIP) ligands were developed by UV-initiated polymerization [115]. IgG was used as a template protein to first bind to PET membrane modified with poly (methacrylic acid) via ATRP as the scaffold. Then, a MIP hydrogel layer is synthesized in the presence of bound IgG by UV-initiated polymerization of acrylamide and with MBAA as a cross-linker. IgG was successfully separated from HSA (human serum albumin) by this MIP ligands. Their results show that the scaffold length, hydrogel layer thickness and degree of cross-linking are all crucial parameters for the binding capacity and protein selectivity. The slow mass transfer rate of IgG in the MIP polymer matrix is one of the major barriers for the application. A responsive MIP ligand was also developed [116]. The hydrogel layer consists of poly (N-isopropylacrylamide) (PNIPAM). A pronounced de-swelling occurred when proteins bound to the MIP hydrogel ligands.

1.4.3 Atom Transfer Radical Polymerization (ATRP)

1.4.3.1 ATRP Fundamentals

The control of polymer architecture and composition has long been a great challenge for making well-defined and uniform polymer materials. The rapid uncontrollable polymerization including UV- or thermo-initiated polymerization leads to a board molecular weight (MW) distribution. ATRP has emerged as one of the most effective and commonly used controllable radical polymerization technique since it was first reported by Matyjaszewski in 1995 [153]. The narrow MW distribution, first-order polymerization kinetics, ease of control and versatile end-group functionality make ATRP a superior polymerization method compared to other conventional radical polymerization methods. As shown in Figure

1.9, ATRP process is established by an equilibrium between the activation and deactivation

reactions, where a transition metal complex serves as the catalyst. R-X is the dormant species

(cannot polymerize) with a halogen group whereas R˙ represents the active radical.
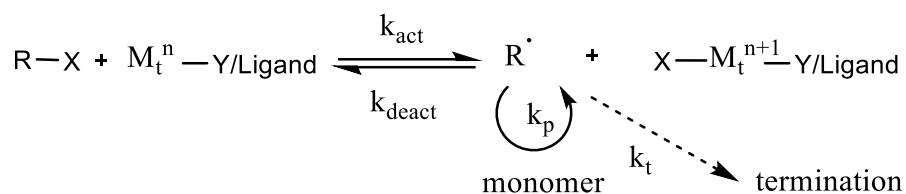
$$\text{Rp} = \text{kp} \cdot [M] \cdot [P^*] = kp \cdot Keq \cdot [M] \cdot [I_0] \cdot [Cu^I]/[Cu^{II}] \text{ (Eq.1)}$$

Figure 1.9 Scheme of ATRP catalyzed by transition metal complex system (X, M and Y represents halogen atom, metal and another halogen atom, respectively. k_{act}, k_{deact}, k_p and k_t are rate constants for activation, deactivation, polymerization and termination reactions, respectively. For kinetics Eq.1, [P*] is the radical concentration. K_{eq} is the equilibrium constant. [I_0], [Cu^I] and [Cu^{II}] are concentration of initial initiator, Cu^I and Cu^{II}, respectively.

In contrast to the uncontrollable radical polymerization, the radical concentration with

ATRP is much lower leading to low probability of termination (1-10%) [154]. Based on the

kinetics as described by Eq.1 [155], the polymerization rate (Rp) can be controlled by the

monomer and initiator concentrations, and the ratio between Cu^I and Cu^{II}. The reactivity (k_p)

and equilibrium constant (K_{eq}) depend on monomer type, catalyst used as well as the solvent

media. Ideally, the radical concentration remains constant with first-order kinetics to

monomer concentration [155]. However, in reality, due to radical termination or catalyst

oxidization, the Cu^{II} concentration will build up leading to a decrease in polymerization rate.

1.4.3.2 Selection of Appropriate Polymerization Conditions

Based on the monomer reactivity, it is critical to select an appropriate ligand, the

initiator, the catalyst Cu^I/Cu^{II} ratio, the solvent medium as well as the temperature for ATRP

reaction. In particular, an appropriate ratio of the Cu^I/Cu^{II} is critical for a reasonable

polymerization rate with minimum chain termination. Usually, there is a tradeoff between the rate of polymerization and amount of chain termination. Typically for a well-controlled ATRP, less than 5% of the chains are terminated at the initial stage and more than 90% of the chains continue to grow [155]. It has been shown that adding more Cu^{II} can effectively reduce the termination at the initial stage of polymerization. Therefore, Cu^{II} is usually added at the beginning to slow down the polymerization. If there is not sufficient concentration of Cu^{II} at the beginning, more Cu^{II} ions will be generated during the ATRP reactions irreversibly due to radical termination (each termination event will generate two equal moles of Cu^{II}).

The reactivity of radical polymerization is largely intrinsic to the monomer. The general order of monomer reactivity follows acrylonitrile > methacrylates > acrylates$\approx$ styrene > acrylamides [154]. Halide reactivity follows I > Br > Cl, which affects the selection of appropriate initiator and catalyst. For example, CuBr will be catalytically more active than CuCl. For the same halide end group, the reactivity order follows $3^o > 2^o > 1^o$.

One of the most efficient ways to modulate polymerization rate is to select an appropriate ligand that complexes with the transition metal catalyst. The equilibrium constant K_{eq} or K_{ATRP} can vary from 10^{-2} to 10^{-11} for different ligands. With regard to the solvent medium, both the catalyst and monomer need to be dissolved or at least in one phase of the solvent. Various aqueous, water mixtures and organic solvents have been successful for ATRP. Moreover, the rate of ATRP polymerization is strongly influenced by the solvent polarity [156].

1.4.3.3 Surface-initiated ATRP (SI-ATRP)

SI-ATRP plays an important and unique role in surface modification of polymer chains. Poly- dispersity of the modified polymer chains affects membrane transport, binding and antifouling properties. SI-ATRP provides a unique polymerization scheme to control independently the polymer chain length and chain density.

Generally, the membrane modification procedure involves initiator immobilization and polymerization steps. Unlike solution ATRP, the initiator needs to be first immobilized on the surface as schematically shown in Figure 1.13 followed by polymerization at the liquid/solid interface. The strategies to immobilize ATRP initiators on membrane substrates are summarized in Table 1.4. The initiation efficiency is generally hard to predict. The surface curvature seems to have an impact on the immobilization efficiency. The reported initiation efficiency is higher for particles (80%) than for flat surfaces (10%) and convex surfaces (30%) [157].
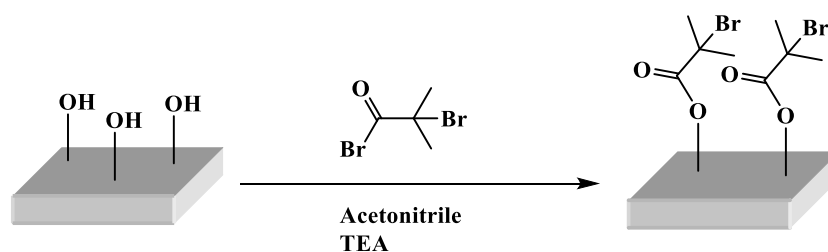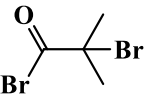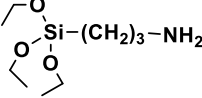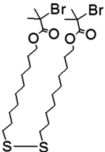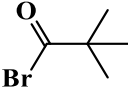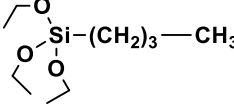
Figure 1.10 Scheme of initiator immobilization on the substrate with abundant hydroxyl groups.

Table 1.4 Initiator immobilization strategy based on various surface functional groups.

		Cellulose/Polyamide Membrane	Silicon/Ceramic	Metal (oxide)
Functional Group	Surface	-OH or -NH₂	-OH after pretreatment with piranha solution	e.g. Gold
	Initiator	(2-bromoisobutyryl bromide structure)	(EtO)₃Si−(CH₂)₃−NH₂	(disulfide initiator with Br groups)
Non-initiator (density regulator)		(2,2-dimethyl acyl bromide structure)	(EtO)₃Si−(CH₂)₃−CH₃	(thiol with OH group)

The main advantage of SI-ATRP comes from its ability to control the grafting density and chain length of polymer chains independently. There are a number of different commercialized initiators suitable for different substrates. In addition, the "living" polymerization feature of ATRP makes it possible to graft block, gradient and statistical copolymers from surfaces, which is hard to achieve using other radical polymerization methods. Different polymeric shapes can also be synthesized including comb, star, or dendritic conformations. Moreover, the halide end group enables post-modification by nucleophilic substitution to introduce other functional groups.

The propagation and termination of SI-ATRP on a flat substrate could be quite different from the reactions occurred solution. It is possible that when the grafting density is high, the radicals at the polymer ends will combine and terminate. The assumption that polymers grown in solution and on substrates have similar properties is still an open question,

especially at high grafting densities [157]. Quantification of grafted polymer chain density and chain length is another major challenge.

1.4.3.4 Membrane Adsorbers Prepared by ATRP
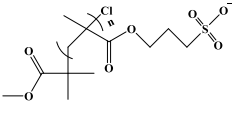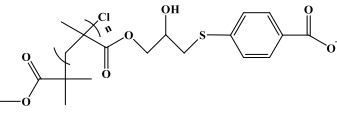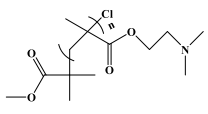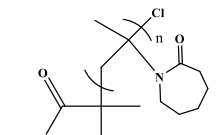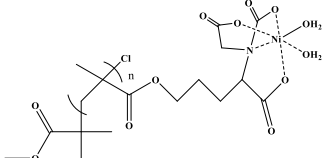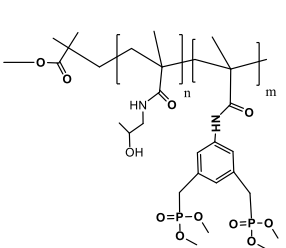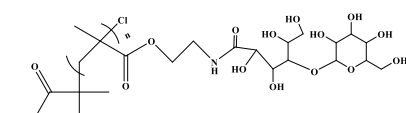
ATRP has been successfully applied to develop membrane adsorbers for protein separations. High capacity membrane adsorbers with cation-exchange ligands grafted via ATRP were first reported in 2008 [112]. PAA was grafted from 1 µm pore size regenerated cellulose membrane substrate. The binding capacities for lysozyme reached 98.5 mg/mL and 71.2 mg/mL for static and dynamic binding studies respectively. It is higher than 21.8 mg/mL from the Sartobind C membranes' dynamic binding capacity at the time. They found that the effective pore size is reduced to around 100 nm after modification but the pore morphology remains more or less the same. The polymer chain length on binding was investigated by varying the ATRP time. The binding capacity reached the maximum value at ATRP 1 h and decreases with longer ATRP times. High capacity anion-exchange membrane adsorbers have also been developed using poly (2-dimethylaminoethyl methacrylate) (poly (DMAEMA)) as ligands [75]. BSA binding capacity increases with chain length and reaches the maximum of 66.3 mg/mL for the static binding capacity after 12 h ATRP. Significant flux reduction was observed for longer ATRP times. Anthrax protective antigen (PA) protein was purified from Escherichia coli lysate using the same anion exchange membrane adsorbers with poly (DMAEMA) ligands [113]. The BSA dynamic binding capacity reached 80 mg/mL, compared to 20 mg/mL from Sartobind D and 20-60 mg/mL from HiTrap^{TM} DEAE FF resin. Sulfonic groups have been polymerized from the membranes with 0.2, 0.45 and 1 µm pore sizes.

Again, high binding capacities were achieved but the effects of pore size effect on capacity are not conclusive. Finally, high capacity multimodal (MM) membrane adsorbers have been developed using ATRP [54]. Poly (4-mercaptobenzoic acid) was modified on membranes by epoxy conjugation after ATRP of the epoxy monomer. IgG static binding capacity reached 180 mg/mL and 60 mg/mL for 10% dynamic binding capacity [158], which is higher than the commercialized Capto MMC resins (60-70 mg/mL). The MM membranes show salt-tolerant binding (up to 300 mM ionic strength, SBC remains 120 mg/mL). The kinetic studies showed the major limitation step of protein adsorption is the binding process between proteins and ligands other than the transport process.

Besides the high capacity ion-exchange membranes, HIC [37] and affinity membranes [31, 69, 90, 114] have been developed by SI-ATRP as well. PVCL has been grafted as HIC ligands on RC membranes by SI-ATRP [37]. The PVCL modified membranes show a higher binding capacity than the hydrophilized PVDF membrane used as HIC membranes [118]. Overall, the binding capacity is comparable to Sartobind®phenyl membranes. High protein recovery (>97%) was achieved in a bind-and-elute mode with BSA. The recovery of BSA decreases evidently with high PVCL grafting density (> 5 h initiation reaction time). Salt effects on binding capacity and recovery were systematically investigated and correlated to the hydrophobicity change of PVCL. In addition, monomers with a high affinity to arginine have been modified on RC membrane as synthetic affinity ligands. Lysozyme binding capacity reached 12 mg/mL, which is six times higher than what achieved before with UV-initiated polymerization for grafting the same type of ligands. It is likely that ATRP leads to more

uniform brushes as well as high grafting degrees compared to UV-initiated polymerization, resulting in improvement in binding capacity. Moreover, it shows that the binding capacity increases with the amount of copolymerized affinity monomers. The results also demonstrate that copolymerization of a hydrophilic spacer monomer, which increases the flexibility of polymeric ligand, is critical to have a high lysozyme binding capacity. The complementary molecular dynamics simulation results show that the affinity between the copolymer ligand to lysozyme comes from multiple interactions, including hydrogen bonding, electrostatic and cation-π interactions. A summary of different polymeric ligand structures, membrane adsorber types and binding capacities are shown in Table 1.5.

Table 1.5 Summary of membrane adsorbers prepared by ATRP.

Membrane Adsorber	Ligand and Sturcture		Binding Capacity
Cation Exchange membrane	poly(sulfonic acid)		Static: 70 mg lysozyme/mL Dynamic: 50 mg lysozyme/mL
	poly(acrylic acid)		Static: 98.5 mg lysozyme /mL Dynamic: 71.2 mg lysozyme/mL
Multimodal membrane	poly(4-mercaptobenzoic acid)		Static: 180 mg IgG /mL
Anion Exchange membrane	poly(2-dimethylaminoethyl methacrylate)		Static:80 mg BSA/mL
HIC membrane	poly(vinyl)caprol actam		Static: 14 mg BSA/mL Dynamic: 5.5 mg BSA/mL
Affinity membrane	poly(nitrilotriacet ate (NTA)-Ni2+)		Dynamic: 85 mg HisU/mL
	poly(5-(methacryloylam ino)-m-xylylene bisphosphonic acid tetramethylester)-co-poly(N-(2-hydroxypropyl) methacrylamide)		Static: 12 mg lysozyme/mL Dynamic: 4 mg lysozyme/mL
	polysaccharides		Dynamic: 23.6 mg Peanut agglutinin /mL

1.5 Membrane Surface Characterization

Membrane surface characterization is important to correlate the performance of modified membranes and provide guidance to optimize the modification condition for better performances. Here, we focus on four categories of characterization techniques on membrane properties of the composition, morphology, wettability and surface zeta potential. Those properties are crucial characterize in order to provide a deep understanding of membrane performances. This section provides a brief introduction to the techniques used for polymeric membrane surface characterization. Attenuated total reflectance fourier transform infrared (ATR-FTIR) spectroscopy and X-ray photoelectron spectroscopy (XPS) will be presented as techniques for chemical composition characterization of membranes. Scanning electron microscopy (SEM) and atomic force microscopy (AFM) are techniques used for membrane morphology characterization. Contact angle measurements are used for testing the wettability of membranes. Surface zeta potential of membranes can also be measured in our lab.

Membrane surface characterization is different from common surface analysis. First, sample preparation becomes extremely critical for preservation of membrane's structure and prevention of contamination from outside. Any process causing property change of membranes should be conducted carefully to minimize the artifacts. For example, membrane washing and drying processes may have large impacts on the many characterization results. Inappropriate washing or drying can cause a drastic change of membrane properties like pore collapsing, swelling, degradation, surface reconstruction [159] etc. Secondly, there is a limitation on the analysis of membrane surface in term of depth. Generally, ATR-FTIR can

detect functional groups on membrane surface with a depth of 0.1 to 10 μm whereas the

analysis depth for XPS is only about 10 nm. Thirdly, it is important to note that the

characterization environment might be completely different from the membrane's

performance environment. Overall, results of non-invasive, in-situ and real-time

characterization with minimum sample preparation are always more representative for

elucidating the membrane performances.

1.5.1 Chemical Composition

ATR-FTIR and XPS are frequently used for analyzing the chemical composition of

membranes after surface modification. functional groups presented on the membrane can be

detected by ATR-FTIR and the state and type of elements are usually measured by XPS.

ATR-FTIR is a technique designed for surface characterization based on FTIR

principles. The transmittance peaks in FTIR results indicate IR light (4000 to 400 cm^{-1}) is

absorbed at frequencies that match energy required for molecular vibrations in certain modes.

Because different functional groups have their unique molecular vibration modes which can

only absorb certain frequencies of IR light, therefore it is possible to distinguish each

functional group based on the position of the FTIR peaks. For surface analysis, an ATR

accessory is needed for a total internal reflection between the membrane surface and an

internal reflection element (IRE). IRE is usually made of crystals (ZnSe or Germanium etc.)

that have a high reflective index than most membranes. Eventually, an evanescent wave is

formed when the reflected IR light penetrates a short depth (dp) into the membrane surface

(Figure 1.14).
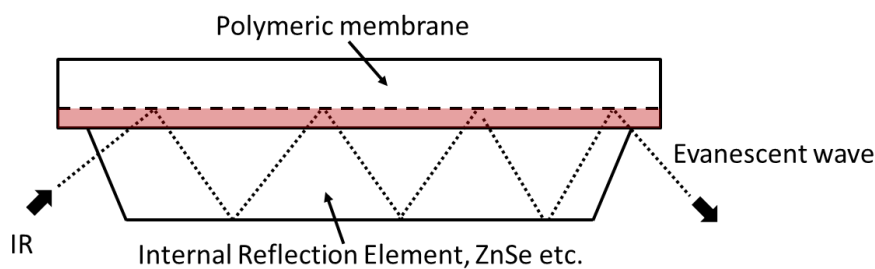
Figure 1.11 ATR-FTIR measurement for polymeric membrane surface.

Therefore, the ATR-FTIR peaks represent the interaction between the evanescent IR wave and functional group on the membrane surface. The penetration depth (dp) is proportional to IR wavelength. In other words, ATR-FTIR spectrum intensities at longer wavelength tend to be higher since it has a larger penetration depth [105]. Overall, the ATR-FTIR peak position and shape are similar to FTIR spectrum except at long wavelength region [160]. One of the challenges associated with ATR-FTIR is the contact problem between membrane and IRE crystal. When the membrane is stiff or non-deformable, it is tricky to make sure a good contact even with the sample clamp to apply pressure. The poor contact will affect more on the short wavelengths region due to its short penetration depth. There is also a chance of scratching the IRE crystal surface if membranes were pressed too hard on the surface. It also imposes difficulty on quantitative analysis of ATR-FTIR spectrum when the contact area is different for each measurement.

Compared to ATR-FTIR, XPS is far more surface sensitive. It is possible for XPS to have ppm level detection. The spatial resolution can reach about 10 μm [161]. XPS can provide information on the functional groups presented on membrane surfaces. The penetration depth of XPS is between 1 nm to 10 nm, depending on the detector angle. XPS is based on a

process when electrons emit from atoms under the excitation of X-ray (photons). Einstein equation describes the relation of energy terms related to the process:

$$E_B = h\nu - E_K - \Phi, \qquad (Eq.1.1)$$

Where E_B is the binding energy of the electron. E_K is the kinetic energy of electron depending on X-ray energy and Φ is a constant represented the work function of the detector. Since $h\nu$, E_K and Φ are measurable or known, E_B is calculated based on the Einstein equation (Eq.1.1). Not only each element has different binding energy, but different oxidation states of the same element also have different values of binding energy. In a typical XPS spectrum, the peak represents electrons excited and escaped without energy loss at a certain binding energy. Therefore, the XPS spectrum presents an accurate electronic structure of an element since all electrons with a binding energy less than X-ray energy contribute peaks in the spectrum. Usually, a wide scan is first conducted to cover a range of 0-1000 eV for the detection of all elements except hydrogen and helium. Then, a high-resolution scan can be carried out for interested peaks. The chemical bond can be characterized as well because the binding energy will be shifted by the electron density change induced by the neighboring atoms. For example, when C_{1s} has more O around (C-O or -O-C=O), the binding energy will shift up to 4 eV higher. It is the same reason why different oxidation states of metals can be detected because of the binding energy change. The high-resolution peak can therefore be decoupled into various single peaks which represent each type of binding energy peak based on different neighboring groups. Angle-resolved XPS is another powerful tool to analyze membrane surfaces if gradient chemical composition existed after surface modification.

$$I=I_0\exp(-d/(\lambda\cos\Theta)) \quad (\text{Eq 1.2})$$

Where I is the intensity of electrons emitted from all depths greater than d form a 90° detector

angle (normal to the surface). I_0 represents intensity from an infinitely thick substrate. Θ is

the detector angle, which is the angle to the normal direction of the surface. Λ is known as the

attenuation length of the electrons. Normally, for collecting 95% of the signal, the XPS

analysis depth is defined as 3λ. By changing the detection angle Θ from 90°, the analysis

depth is reduced by $\cos\Theta$ (Eq 1.2). So, by comparing the spectrum at different detection

angles, a composition profile can be constructed corresponding to different depths.

1.5.2 Membrane Morphology

Membrane morphology is often characterized by pore structures (pore size and pore

size distribution), porosity, roughness, thickness etc.. Membrane morphology is critical for

membrane performances. For example, the pore size distribution (especially the largest pore)

is extremely important for virus filtration membrane since any virus leakage should be

prevented during the filtration. SEM and AFM are two common microscopy techniques for

membrane morphology characterization. Compared to conventional optical microscopes,

SEM and AFM have much higher resolution. The wavelength of a 50 keV electron beam is

0.0055 nm, which will be able to resolve 0.0024 nm theoretically[105]. Modern AFM can reach

atom level resolution with single molecule attached on the tip. There are many differences

between SEM and AFM. First, SEM usually requires an ultra-high vacuum environment

whereas AFM can work in atmospheric pressure. AFM in our lab can even scan surfaces

placed in liquid. Secondly, for SEM, polymeric membranes often need a metal coating

(several nm) to increase the conductivity of the surface but AFM does not any pre-coating.

Thirdly, SEM can easily scan much larger and rougher surfaces than AFM. For very rough or porous surfaces, the scanning rate becomes very slow for AFM if the scanning area is large at the same time. The maximum scan size of Bruker Dimension Icon AFM in our lab is 80 μm under the tapping mode. Furthermore, AFM results are naturally three-dimensional (3D) so that roughness can be calculated easily while SEM needs a reconstruction process to restore the 3D image.

The interactions of the electron beam with specimen can generate many signals, which includes backscattered electrons, secondary electrons, adsorbed electrons, transmitted electrons and characteristic X-rays. Secondary electron detectors are the standard detector for SEM. Cold field emission filament has been widely used as the electron gun for SEM, which is also named field emission SEM (FESEM). High electric field is used in FESEM so that electrons can be emitted at low temperature with a narrow 10 nm crossover size. Other electron guns like thermionic emission W-filament have much larger μm range beam size. A high vacuum is needed for the electron gun and sample chamber to avoid the foreign atom interference. A typical setup of SEM is shown in Figure 1.15. The resolution of SEM can be optimized by adjusting beam current, accelerating voltage and working distance. Usually, the resolution will be higher under conditions of low beam current, high accelerating voltage and short working distance (mm range). However, there is a trade-off between resolution and noise level.
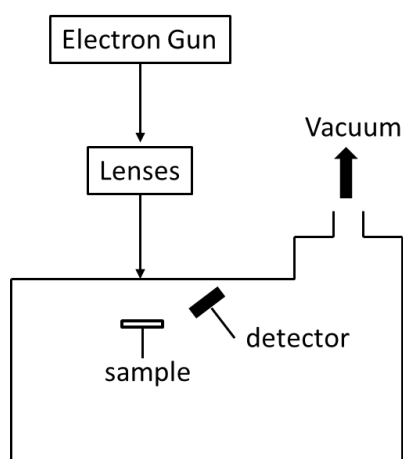
Figure 1.12 A simplified scheme of SEM instrument (electron gun, lenses, sample, detector and sample chamber).

SEM has been used for membrane surface characterization for many purposes, including membrane surface fouling studies [162, 163, 164], observing pore structures after surface modifications [31, 66, 74, 165], observing membrane cross-section structures [164, 166, 167], etc.. Membrane sample preparation is very important to have SEM imagines reflecting the true surface morphology of membranes. For example, direct drying from high surface tension solvent like water may cause dramatic structure change. Freeze-drying and critical point drying are common methods used for drying membranes to keep the original structure. Critical point drying starts with a gradient solvent changing process from high surface tension solvent (water) to low surface tension solvent (ethanol). Then, the solvent is replaced by liquid CO_2 and finally the membrane is dried by removal of liquid CO_2 by rising temperature. The cross-section of a membrane is normally prepared by a freeze-fracturing method, where the membrane is immersed into liquid nitrogen and fractured to expose the cross-section. Another sample preparation required is metal coating because most polymeric membranes are

not conductive. Charging artifacts are always the concern when electrons accumulate on the membrane surface when the surface coating is not enough.

AFM has become increasingly popular for membrane surface characterization over the years. The principle of AFM relies on the force between the tip and sample (Figure 1.16 (b)). The tip movement is tracked by a laser system. Based on the sample-tip separation distance, AFM can be run in the contact mode, tapping mode or non-contact mode. Most polymeric membranes are using tapping mode for characterization. The surface tracking with the AFM tip relies on a program of a feed-back loop that has a "setpoint" of tip-sample separation distance or force in contact mode, or the probe oscillation amplitude in the tapping mode. The computer will compare the current status of the tip with the "setpoint" and move the tip towards the "setpoint" by changing the shape of probe base which is made of voltage sensitive piezoelectric material. Thus, at each horizontal scanning direction (x and y), the movements of the tip in the vertical direction (z) are recorded by the laser system and plotted as height AFM image. The laser system can provide a resolution of less than 1 nm for the tip vertical movement, which is good enough for most membrane surface characterization.
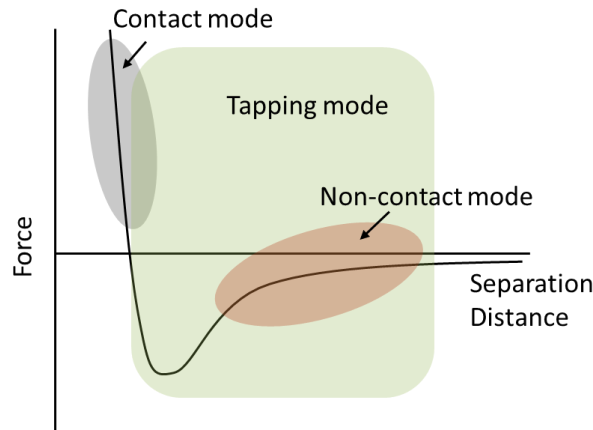
Figure 1.13 Scheme of AFM instrument (a) and operation modes based on the force-distance curve (b).

Compared with SEM, membrane surface can be characterized by AFM in its natural state without coating. AFM can even characterize a membrane immersed in the liquid which is close to its working state and without drying. The roughness of membrane is always obtained by AFM. Recently, AFM colloidal probe has been developed for studying the interaction between the membrane and other molecules such as foulants or other biomolecules [138, 149, 168, 169, 170]. The AFM force-distance curve provides a powerful tool to study the affinity between a modified AFM tip and a modified surface. Furthermore, nano-mechanical properties, such as modulus, deformation and adhesion, can also be measured by AFM with a calibrated tip.

1.5.3 Wettability: Contact Angle Measurement

The wettability of membrane surfaces can be measured by contact angles. Contact angles indicate the wettability of the surface for a certain type of testing liquid. For a flat and homogenous surface (Figure 1.17), contact angles can be correlated with surface tension by Young's equation (Eq. 1.3).

$$\cos\theta = \frac{\gamma SG - \gamma SL}{\gamma LG} \qquad \text{Eq. 1.3}$$

$\gamma SG, \gamma SL$ and γLG represent surface tension between solid(S), liquid (L) and gas (G),

respectively.
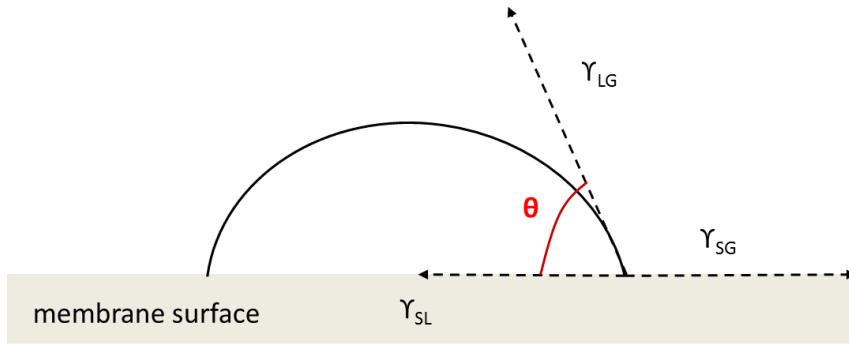
Figure 1.14 Scheme of the contact angle of an ideal surface (homogenous, flat and smooth).

Generally, for a certain type of liquid, the lower the contact angle, the higher

wettability of the liquid for the membrane surface. However, for a polymeric membrane,

contact angle results are more complex to interpret. Many other factors will have impacts on

the contact angle results such as roughness and surface heterogeneity due to the porous

structure of the membrane. Wenzel's model (Eq. 1.4) and Cassie's model (Eq. 1.5) are two

models that have applied to the membrane surfaces successfully.

$$\cos\theta' = \sigma\cos\theta_Y \qquad \text{Eq. 1.4}$$

$$\cos\theta'' = f\cos\theta_Y + f - 1 \qquad \text{Eq. 1.5}$$

σ is the correction factor for the contact length change caused by roughness. f is the fraction

of area for solid surface. θ_Y is Young's contact angle for an idea surface. In this dissertation,

contact angle is used for characterizing the hydrophobicity of a responsive HIC membrane.

Sessile drop method and captive bubble method are commonly used for membrane surface. For sessile drop method, a liquid drop is placed on the surface exposed in air. In the captive bubble method, a membrane is immersed in liquid and an air bubble is attached on the membrane surface. Both methods can give results of static or dynamic contact angle. For a dynamic contact angle measurement, advancing and receding angles are obtained by expanding and retracting the drop size. When the interface of gas, liquid and solid breaks during the size expanding/retracting process monitored by the contact length change, the contact angle is recorded as advancing (expanding) and receding (retracting) angle. The difference between advancing and receding angle is called hysteresis which indicates the surface heterogeneity. Baek and co-workers have shown that captive bubble method is more repeatable than sessile drop method for reverse osmosis (RO) membranes [171]. Sessile drop method is more sensitive to membrane sample preparation and testing environment such as humidity. In addition, since captive bubble method is conducted in liquid, it eliminates the difference of results caused by the membrane drying process. Hydrophilic membranes like regenerated cellulose membrane are very sensitive to moisture. As a result, based on different drying processes, the results given by sessile drop method may be varied in different literatures for the same membrane [171].

1.5.4 Surface Zeta Potential

The surface charge of polymeric membranes can be described by surface zeta potentials. Ions will be attracted to membrane surface with the opposite charge to form a stern layer with strong interaction and a diffusion region for less attracted ions. This structure of

ion layers is called "electrical double layer". The surface zeta potential can be measured by electrophoretic light scattering. Probing particles are added to the electrical field for movement. It is tracked by the frequency shift of a laser light because the frequency shift is proportional to the speed of the particles (Laser Doppler Method). The electroosmotic flow is generated due to the surface charge of surfaces. Figure 1.18 shows an asymmetric electroosmotic profile due to the charge difference between the sample surface and cell surface.
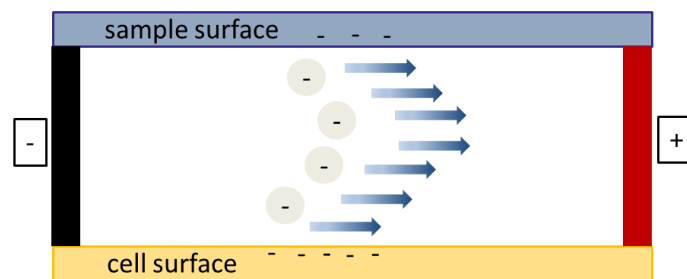
Figure 1.15 Zeta potential measurement Device and principle for surface zeta measurement.

The velocity of electroosmotic flow (W_1) at upper (sample) surface is determined by Eq.1.6

$$w_1 = v_0 + \frac{\Delta v_0}{2} \qquad (Eq.1.6)$$

v_0 is the average of electroosmotic flow at upper and lower surfaces of the cell ($v_0=(w_1+w_0)/2$), Δv_0 is the difference of electroosmotic flow between upper (w_1) and lower surfaces (w_0) of the cell ($\Delta v_0=w_1+w_0$). v_0 and Δv_0 are calculated from least square fitting from apparent particle mobility measured from different vertical position (z direction). Surface zeta potential is then calculated by Smolochowski equation (Eq.1.7):

$$Z = \frac{\eta}{\varepsilon_0 \varepsilon_r} w_1 \qquad (Eq.1.7)$$

η is the solution viscosity. ε_0 and ε_r are dielectric constants in the vacuum and solvent, respectively.

Membrane zeta potential is an important property to provide information on the electrostatic interaction between the outside particles and surface. The zeta potential change of membrane has been studied frequently since it is closely correlated to the membrane performance, such as flux [172], rejection of charged species [173, 174, 175] and tendency of fouling [176, 177, 178, 179, 180, 181]

1.6 Future Outlooks

1.6.1 Downstream Process Development

The advancement of downstream processing is mainly driven by the manufacturing cost and timeline. The new disruptive bioprocesses are seeking for more efficient manufacturing of therapeutic proteins while maintaining the high quality and consistency of products. However, downstream processing is highly regulated and changes are likely to be slow due to the high cost of validation. It is important to note that current resin-based purification platform is quite mature for mAb purifications. New advances for mAb purifications lie mainly in improving the efficiency and understanding of the current platform. Continuous bioprocessing and single-use technology are the two most important disruptive technologies under development. High-throughput technology based on the design of experiment (DoE) has greatly shortened the process development timeline. New advances are focusing on scale down instruments such as Robocolumn® for resin high-throughput screening. It further reduces the cost of process development by minimizing the usage of resin volume and speeding up the process optimization. However, the ability of those mini-columns to predict a large-scale purification is still under investigation case by case. Besides

efficiency improvement, other fundamental studies are focusing on improving the understanding of protein/ligand interaction with single molecule microscopy, optimization of chromatography performance by mechanistic modeling and fouling studies on resins. In particular, fouling mechanism of protein A resin for repeated usage is still being investigated.

There is also a growing interest in developing new purification platform for non-mAb products including vaccines, drug conjugates, gene therapy vectors and antibody fragments. Capto^{TM} L is resin developed by GE Healthcare for purifications of a wide range of antibody fragments, such as Fabs, single-chain variable fragments (scFv), domain antibodies (Dabs). Protein L is used as the ligand since it has an affinity to the kappa light chain of the antibody. Recently, polypeptides have received a lot of attention as affinity ligands for non-mAb product purifications. However, more understandings are needed for the rational design and screening of the polypeptide-based affinity ligands to achieve high affinity and to find a suitable condition to elute. Avitide, Inc. is the first company manufacturing polypeptide-based affinity resins for non-mAb products purifications. However, the elution and regeneration of polypeptide-based affinity resins remain challenging. Another purification challenge is the separation of bispecific antibody since protein A chromatography has limited resolving power between the original unreacted antibodies and bispecific antibodies.

Besides ion-exchange and hydrophobic interaction chromatography, multi-modal chromatography is currently under intensive investigation due to its superior properties including salt-tolerance, high capacity, wide operational window and unique selectivity. However, it was studied mainly with the flow-through mode. The optimal conditions for

binding and elution rely on trial and error as well as DoE. A better understanding of MMC is necessary in order to design better and more economically viable ligands. Currently applying multi-modal chromatography for virus purification is also under intense investigation.

1.6.2 Membrane Chromatography

Membrane-based chromatography for protein purifications has tremendous potential for improving the efficiency of downstream processing and reducing the cost in terms of processing time and buffer consumption. However, it is important to note that most flow-through polishing steps still use packed bed columns, even though membrane adsorbers offer a clear advantage. In recent years, the major breakthrough of membrane chromatography comes from its dramatically increased binding capacity which was a limiting factor before. Compared to traditional membrane adsorbers, the next generation base matrix of membranes renders a higher specific area, higher ligand density as well as optimized 3D binding environment. Hydrogel used by Natrix Separations company and nanofibers utilized by Puridify company are the two most successful base matrixes for high-capacity membrane adsorbers. The capacity of Natrix-HD-Q reaches 270 mg/mL, which surpasses most Q resins and traditional Q membrane adsorbers. The emergence of high capacity multi-modal membranes provides new opportunities for membrane adsorbers that can compete with protein A chromatography in a bind-and-elute mode. In addition, new protein A membranes developed by Natrix Separation show promising results for HCP removal. Compared to protein A resin, protein A membrane demonstrates higher productivity, comparable but more consistent yields for different mAb products.

Using membranes for continuous bioprocessing is also attractive because of its high-throughput and ease of scaling up. Electrospun nanofiber membranes have been developed for a continuous simulated moving bed (SMB) process. The high specific area of nanofibers ($10 \text{ m}^2/\text{g}$) compared to traditional membrane adsorbers ($2 \text{ m}^2/\text{g}$) increases the capacity while maintains the same high-throughput. Other areas of interest for the new adsorptive membrane-based process are also currently under investigation including employing adsorptive membranes during the clarification step before protein A chromatography, virus removal with AEX membrane adsorbers and membrane based large bio-molecule (vaccine, drug conjugates etc.) separations. Using membranes to separate non-mAb products remains attractive with improved binding capacity and productivity.

1.6.3 Ligand Design for Downstream Process

Ligand design is critical to downstream processing because it has a direct impact on the performances of various chromatography steps. For affinity ligands used in mAb capture step, new ligands are under development. However, they are difficult to compete with protein A in terms of selectivity (binding directly from harvest cell culture fluid), capacity (>100 mg/mL) and effective elution/regeneration (repeated usage at least 80 times without losing capacity). Therefore, new advances for affinity ligands are mainly focusing on new opportunities with non-mAb products such as vaccines, drug conjugates and antibody fragments. Polypeptides are one of promising affinity ligands for providing a platform to separate non-mAb products. Theoretically, it can separate any products with an appropriate arrangement of amino acids. However, because the affinity interaction is rather complex, the

rational design of polypeptides is extremely difficult as the possible amino acid sequences increase dramatically when the number of amino acid increases. Another challenge associated with polypeptide ligands is the elution as well as their regeneration. It is difficult to find a ligand that has a strong affinity yet facile elution/regeneration at the same time.

Currently, the pharmaceutical industry is in the process of adopting multi-modal chromatography. Relying on the high-throughput technology, developing multi-modal chromatography has been greatly shortened even though the mechanism is not yet fully understood. Besides salt-tolerance and wide operational window, more studies are now exploring its unique selectivity for protein separations. Again, a better understanding of the binding mechanism will be critical to further optimize the ligands.

Synthetic polymeric ligands are becoming attractive due to its low manufacturing cost, high stability, and the possibility for introducing new functionalities such as salt or pH responsiveness. "Grafting from" method based on free radical polymerization is the common technique used for functionalizing membranes with synthetic polymeric ligands. Controlled radical polymerization represents the future with a much better control over the grafting chain density and polymer length. However, it remains challenge to quantify the chain length and chain density of the polymeric ligands grafted. Therefore, techniques to cleave those grafted polymeric ligands are in high demands. . In addition, it is also attractive to modify the chain-end functionality through click chemistry which is highly efficient and specific [182]. The click reaction between azide and alkyne has been widely used as it has a high yield (>95%) and moderate temperature (25ºC-70ºC) [183, 184]. Combination of ATRP or reversible addition

fragmentation techniques (RAFT) with this type of click reactions has also been reported for high-yield grafting of polymers via "Grafting to" method [185, 186, 187]. Another important future direction for synthetic ligands is to use copolymers instead of homopolymers for better performance. Copolymer ligands have been adopted in commercial cation exchanger Capto^{TM} S ImpAct involving random copolymerization of pyrrolidone and monomers containing a sulfonate group. Our study also shows that for an affinity ligand, the spacer monomer plays an important role in achieving high capacity [31]. Recently, we are looking at salt-responsive HIC copolymer ligands to improve binding capacity and functionality. Overall, a better understanding of the effects of polymer architecture on binding and eluting mechanisms is needed in order to improve and optimize the performances of these ligands.

1.6.4 In Silico Ligand Design and Elucidation of Binding Mechanism

The significant strides made in both software and hardware technologies enable the molecular simulations to play an increasingly important role in designing novel ligands, optimizing ligand performance and elucidating the mechanisms for binding interactions. In particular, all atomistic molecular dynamics (MD) simulations can be employed to understand the structure, conformation and hydration properties of the ligands as well as their interactions with proteins or products of interest [31, 188, 189, 190, 191, 192]. Earlier [188, 189, 190] classical MD simulations have been conducted to investigate the hydrophobic-to-hydrophilic transition of thermal and salt responsive ligands PNIPAM and its copolymers in various salt solutions and the effects of salt ions on the hydration of the polymers and LCST transition dynamics. MD simulations [31] have also been used to elucidate the binding mechanisms of arginine

selective affinity ligands with arginine-rich proteins such as lysozyme. Currently significant

efforts are also being dedicated to design and optimize polypeptide ligands for protein

binding and purifications. Needless to say, modeling and simulations will play a more

important role in membrane chromatography development.

Acknowledgement

Reference

1.   Ecker, D. M.; Jones, S. D.; Levine, H. L. The therapeutic monoclonal antibody market. *mAbs* **2015,** *7* (1), 9-14.

2.   Cramer, S. M.; Holstein, M. A. Downstream bioprocessing: recent advances and future promise. *Curr. Opin. Chem. Eng.* **2011,** *1* (1), 27-37.

3.   Guiochon, G.; Beaver, L. A. Separation science is the key to successful biopharmaceuticals. *J. Chromatogr. A* **2011,** *1218* (49), 8836-8858.

4.   Freitag, R. Chromatographic Techniques in the Downstream Processing of Proteins in Biotechnology. In *Animal Cell Biotechnology*, Pörtner, R., Ed.; Humana Press, 2014; Vol. 1104, pp 419-458.

5.   Gottschalk, U. Downstream Processing of Monoclonal Antibodies: from High Dilution to High Purity. *Biopharm. Int.* **2005,** *18*, 42-58.

6.   Chollangi, S.; Parker, R.; Singh, N.; Li, Y.; Borys, M.; Li, Z. Development of robust antibody purification by optimizing protein-A chromatography in combination with precipitation methodologies. *Biotechnol. Bioeng.* **2015,** *112* (11), 2292-2304.

7.   Mani Krishnan; Kern, G. Virus Removal by Filtration: Points to Consider. *BioPharm International* **2006,** *19* (10).

8.   Lindmark, R.; Thorén-Tolling, K.; Sjöquist, J. Binding of immunoglobulins to protein A and immunoglobulin levels in mammalian sera. *Journal of Immunological Methods* **1983,** *62* (1), 1-13.

9.   Gouda, H.; Shiraishi, M.; Takahashi, H.; Kato, K.; Torigoe, H.; Arata, Y.; Shimada, I. NMR Study of the Interaction between the B Domain of Staphylococcal Protein A and the Fc Portion of Immunoglobulin G. *Biochemistry* **1998,** *37* (1), 129-136.

10.   Lain, B. Protein A. *Bioprocess International*, 2013.

11.   Gronemeyer, P.; Ditz, R.; Strube, J. Trends in Upstream and Downstream Process Development for Antibody Manufacturing. *Bioengineering* **2014,** *1* (4), 188.

12.   Follman, D. K.; Fahrner, R. L. Factorial screening of antibody purification processes using three chromatography steps without protein A. *J. Chromatogr. A* **2004,** *1024* (1–2), 79-85.

13.   Pabst, T. M.; Palmgren, R.; Forss, A.; Vasic, J.; Fonseca, M.; Thompson, C.; Wang, W. K.; Wang, X.; Hunter, A. K. Engineering of novel Staphylococcal Protein A ligands to enable milder elution pH and high dynamic binding capacity. *J. Chromatogr. A* **2014,** *1362*, 180-185.

14.   Miesegaes, G. R.; Lute, S.; Strauss, D. M.; Read, E. K.; Venkiteshwaran, A.; Kreuzman, A.; Shah, R.; Shamlou, P.; Chen, D.; Brorson, K. Monoclonal antibody capture and viral clearance by cation exchange chromatography. *Biotechnol. Bioeng.* **2012,** *109* (8), 2048-2058.

15.   Lain B, C. M., Zarbis-Papastoitsis G. Development of a high-capacity mab capture step based on cation-exchange chromatography. *BioProcess International.* **2009**.

16.   A., A. Implementing cost reduction strategies for humAb manufacturing processes. *BioProcess International.* **2009**.

17.   Urmann, M.; Graalfs, H.; Joehnck, M.; Jacob, L. R.; Frech, C. Cation-exchange chromatography of monoclonal antibodies: Characterization of a novel stationary phase designed for production-scale purification. *mAbs* **2010,** *2* (4), 395-404.

18.   Riordan, W.; Heilmann, S.; Brorson, K.; Seshadri, K.; He, Y.; Etzel, M. Design of salt-tolerant membrane adsorbers for viral clearance. *Biotechnology and Bioengineering* **2009,** *103* (5), 920-929.

19.   Champagne, J.; Balluet, G.; Gantier, R.; Toueille, M. "Salt tolerant" anion exchange chromatography for direct capture of an acidic protein from CHO cell culture. *Protein Expression and Purif.* **2013,** *89* (2), 117-123.

20.   Woo, M.; Khan, N. Z.; Royce, J.; Mehta, U.; Gagnon, B.; Ramaswamy, S.; Soice, N.; Morelli, M.; Cheng, K.-S. A novel primary amine-based anion exchange membrane adsorber. *J. Chromatogr. A* **2011,** *1218* (32), 5386-5392.

21.   Johansson, B.-L.; Belew, M.; Eriksson, S.; Glad, G.; Lind, O.; Maloisel, J.-L.; Norrman, N. Preparation and characterization of prototypes for multi-modal separation media aimed for

capture of negatively charged biomolecules at high salt conditions. *J. Chromatogr. A* **2003,** *1016* (1), 21-33.

22.   Weaver, J.; Husson, S. M.; Murphy, L.; Wickramasinghe, S. R. Anion exchange membrane adsorbers for flow-through polishing steps: Part I. clearance of minute virus of mice. *Biotechnol. Bioeng.* **2013,** *110* (2), 491-499.

23.   Weaver, J.; Husson, S. M.; Murphy, L.; Wickramasinghe, S. R. Anion exchange membrane adsorbers for flow-through polishing steps: Part II. Virus, host cell protein, DNA clearance, and antibody recovery. *Biotechnol. Bioeng.* **2013,** *110* (2), 500-510.

24.   Ghose, S.; Tao, Y.; Conley, L.; Cecchini, D. Purification of monoclonal antibodies by hydrophobic interaction chromatography under no-salt conditions. *mAbs* **2013,** *5* (5), 795-800.

25.   Kuczewski, M.; Fraud, N.; Faber, R.; Zarbis-Papastoitsis, G. Development of a polishing step using a hydrophobic interaction membrane adsorber with a PER.C6®-derived recombinant antibody. *Biotechnol. Bioeng.* **2010,** *105* (2), 296-305.

26.   Saufi, S. M.; Fee, C. J. Mixed matrix membrane chromatography based on hydrophobic interaction for whey protein fractionation. *Journal of Membrane Science* **2013,** *444* (0), 157-163.

27.   Puthirasigamany, M.; Wirges, M.; Zeiner, T. Membrane chromatography for the purification of laccase from the supernatant of Pleurotus sapidus. *Biochemical Engineering Journal* **2013,** *70* (0), 180-187.

28.   Mah, K. Z.; Ghosh, R. Paper-based composite lyotropic salt-responsive membranes for chromatographic separation of proteins. *Journal of Membrane Science* **2010,** *360* (1–2), 149-154.

29.   Kosior, A.; Antošová, M.; Faber, R.; Villain, L.; Polakovič, M. Single-component adsorption of proteins on a cellulose membrane with the phenyl ligand for hydrophobic interaction chromatography. *J. Membr. Sci.* **2013,** *442* (0), 216-224.

30.   Wu, Q.; Wang, R.; Chen, X.; Ghosh, R. Temperature-responsive membrane for hydrophobic interaction based chromatographic separation of proteins in bind-and-elute mode. *Journal of Membrane Science* **2014,** *471* (0), 56-64.

31.   Liu, Z.; Du, H.; Wickramasinghe, S. R.; Qian, X. Membrane Surface Engineering for Protein Separations: Experiments and Simulations. *Langmuir* **2014,** *30* (35), 10651-10660.

32.   Yu, D. Q.; Shang, X. J.; Ghosh, R. Fractionation of different PEGylated forms of a protein by chromatography using environment-responsive membranes. *J. Chromatogr. A* **2010,** *1217* (35), 5595-5601.

33.   Wang, L.; Ghosh, R. Feasibility Study for the Fractionation of the Major Human Immunoglobulin G Subclasses Using Hydrophobic Interaction Membrane Chromatography. *Anal. Chem.* **2010,** *82* (1), 452-455.

34.   Ghosh, R. Fractionation of human plasma proteins by hydrophobic interaction membrane chromatography. *J. Membr. Sci.* **2005,** *260* (1-2), 112-118.

35.   Wang, L.; Ghosh, R. Fractionation of monoclonal antibody aggregates using membrane chromatography. *J. Membr. Sci.* **2008,** *318* (1-2), 311-316.

36.   Ghosh, R.; Wang, L. Purification of humanized monoclonal antibody by hydrophobic interaction membrane chromatography. *J. Chromatogr. A* **2006,** *1107* (1-2), 104-109.

37.   Himstedt, H. H.; Qian, X.; Weaver, J. R.; Wickramasinghe, S. R. Responsive membranes for hydrophobic interaction chromatography. *J. Membr. Sci.* **2013,** *447* (0), 335-344.

38.   Zhang, R.; Yang, G.; Xin, P.; Qi, L.; Chen, Y. Preparation of poly(N-isopropylacrylamide)-grafted polymer monolith for hydrophobic interaction chromatography of proteins. *Journal of Chromatography A* **2009,** *1216* (12), 2404-2411.

39.   Yu, D.; Chen, X.; Pelton, R.; Ghosh, R. Paper-PEG-based membranes for hydrophobic interaction chromatography: Purification of monoclonal antibody. *Biotechnol. Bioeng.* **2008,** *99* (6), 1434-1442.

40.   Huang, R.; Mah, K. Z.; Malta, M.; Kostanski, L. K.; Filipe, C. D. M.; Ghosh, R. Chromatographic separation of proteins using hydrophobic membrane shielded with an environment-responsive hydrogel. *J. Membr. Sci.* **2009,** *345* (1-2), 177-182.

41.   Huang, R.; Kostanski, L. K.; Filipe, C. D. M.; Ghosh, R. Environment-responsive hydrogel-based ultrafiltration membranes for protein bioseparation. *J. Membr. Sci.* **2009,** *336* (1-2), 42-49.

42.   Chen, J.; Tetrault, J.; Zhang, Y.; Wasserman, A.; Conley, G.; DiLeo, M.; Haimes, E.; Nixon, A. E.; Ley, A. The distinctive separation attributes of mixed-mode resins and their application in monoclonal antibody downstream purification process. *J. Chromatogr. A* **2010,** *1217* (2), 216-224.

43.   Boschetti, E. Antibody separation by hydrophobic charge induction chromatography. *Trends Biotechnol.* **2002,** *20* (8), 333-337.

44.   Tong, H.-F.; Lin, D.-Q.; Chu, W.-N.; Zhang, Q.-L.; Gao, D.; Wang, R.-Z.; Yao, S.-J. Multimodal charge-induction chromatography for antibody purification. *J. Chromatogr. A* **2016,** *1429*, 258-264.

45.   Kallberg, K.; Becker, K.; Bülow, L. Application of a pH responsive multimodal hydrophobic interaction chromatography medium for the analysis of glycosylated proteins. *Journal of Chromatography A* **2011,** *1218* (5), 678-683.

46.   Paul, J.; Jensen, S.; Dukart, A.; Cornelissen, G. Optimization of a preparative multimodal ion exchange step for purification of a potential malaria vaccine. *J. Chromatogr. A* **2014,** *1366*, 38-44.

47.   Zhao, G.; Dong, X.-Y.; Sun, Y. Ligands for mixed-mode protein chromatography: Principles, characteristics and design. *J. Biotechnol.* **2009,** *144* (1), 3-11.

48.   Burton, S. C.; Harding, D. R. K. Hydrophobic charge induction chromatography: salt independent protein adsorption and facile elution with aqueous buffers. *J. Chromatogr. A* **1998,** *814* (1–2), 71-81.

49.   Boschetti, E. The use of thiophilic chromatography for antibody purification: a review. *J. Biochem. Bioph. Methods* **2001,** *49* (1–3), 361-389.

50.   Li, P.; Xiu, G.; Mata, V. G.; Grande, C. A.; Rodrigues, A. E. Expanded bed adsorption/desorption of proteins with Streamline Direct CST I adsorbent. *Biotechnol. Bioeng.* **2006,** *94* (6), 1155-1163.

51.   dos Santos, R.; Rosa, S. A. S. L.; Aires-Barros, M. R.; Tover, A.; Azevedo, A. M. Phenylboronic acid as a multi-modal ligand for the capture of monoclonal antibodies: Development and optimization of a washing step. *J. Chromatogr. A* **2014,** *1355*, 115-124.

52.   Wu, Q.-C.; Lin, D.-Q.; Shi, W.; Zhang, Q.-L.; Yao, S.-J. A mixed-mode resin with tryptamine ligand for human serum albumin separation. *J. Chromatogr. A* **2016,** *1431*, 145-153.

53.   Burton, S. C.; Haggarty, N. W.; Harding, D. R. K. One step purification of chymosin by mixed mode chromatography. *Biotechnology and Bioengineering* **1997,** *56* (1), 45-55.

54.   Wang, J.; Sproul, R. T.; Anderson, L. S.; Husson, S. M. Development of multimodal membrane adsorbers for antibody purification using atom transfer radical polymerization. *Polymer* **2014,** *55* (6), 1404-1411.

55.   Karkov, H. S.; Woo, J.; Krogh, B. O.; Ahmadian, H.; Cramer, S. M. Evaluation of selectivity in homologous multimodal chromatographic systems using in silico designed antibody fragment libraries. *J. Chromatogr. A* **2015,** *1426*, 102-109.

56.   Woo, J.; Parimal, S.; Brown, M. R.; Heden, R.; Cramer, S. M. The effect of geometrical presentation of multimodal cation-exchange ligands on selective recognition of hydrophobic regions on protein surfaces. *J. Chromatogr. A* **2015,** *1412*, 33-42.

57.   Wolfe, L. S.; Barringer, C. P.; Mostafa, S. S.; Shukla, A. A. Multimodal chromatography: Characterization of protein binding and selectivity enhancement through mobile phase modulators. *J. Chromatogr. A* **2014,** *1340*, 151-156.

58.   Sheth, R. D.; Morrison, C. J.; Cramer, S. M. Selective displacement chromatography in multimodal cation exchange systems. *Journal of Chromatography A* **2011,** *1218* (51), 9250-9259.

59.   Hou, Y.; Cramer, S. M. Evaluation of selectivity in multimodal anion exchange systems: A priori prediction of protein retention and examination of mobile phase modifier effects. *J. Chromatogr. A* **2011,** *1218* (43), 7813-7820.

60.   Holstein, M. A.; Nikfetrat, A. A. M.; Gage, M.; Hirsh, A. G.; Cramer, S. M. Improving selectivity in multimodal chromatography using controlled pH gradient elution. *J. Chromatogr. A* **2012,** *1233*, 152-155.

61.   Roper, D. K.; Lightfoot, E. N. Separation of biomolecules using adsorptive membranes. *J. Chromatogr. A* **1995,** *702* (1–2), 3-26.

62.   Ghosh, R. Protein separation using membrane chromatography: opportunities and challenges. *J. Chromatogr. A* **2002,** *952* (1-2), 13-27.

63.   Yoo, S. M.; Ghosh, R. Simultaneous removal of leached protein-A and aggregates from monoclonal antibody using hydrophobic interaction membrane chromatography. *J. Membr. Sci.* **2012,** *390*, 263-269.

64.   Phillips, M.; Cormier, J.; Ferrence, J.; Dowd, C.; Kiss, R.; Lutz, H.; Carter, J. Performance of a membrane adsorber for trace impurity removal in biotechnology manufacturing. *Journal of Chromatography A* **2005,** *1078* (1–2), 74-82.

65.   Bhut, B. V.; Weaver, J.; Carter, A. R.; Wickramasinghe, S. R.; Husson, S. M. The role of polymer nanolayer architecture on the separation performance of anion-exchange membrane adsorbers: Part II. DNA and virus separations. *Biotechnol. Bioeng.* **2011,** *108* (11), 2654-2660.

66.   Wei, Y.; Ma, J.; Wang, C. Preparation of high-capacity strong cation exchange membrane for protein adsorption via surface-initiated atom transfer radical polymerization. *J. Membr. Sci.* **2013,** *427* (0), 197-206.

67.   Singh, N.; Wang, J.; Ulbricht, M.; Wickramasinghe, S. R.; Husson, S. M. Surface-initiated atom transfer radical polymerization: A new method for preparation of polymeric membrane adsorbers. *J. Membr. Sci.* **2008,** *309* (1–2), 64-72.

68.   Schwark, S.; Ulbricht, M. Toward protein-selective membrane adsorbers: A novel surface-selective photo-grafting method. *Eur. Polym. J.* **2012,** *48* (11), 1914-1922.

69.   Jain, P.; Vyas, M. K.; Geiger, J. H.; Baker, G. L.; Bruening, M. L. Protein Purification with Polymeric Affinity Membranes Containing Functionalized Poly(acid) Brushes. *Biomacromolecules* **2010,** *11* (4), 1019-1026.

70.   He, D.; Sun, W.; Schrader, T.; Ulbricht, M. Protein adsorbers from surface-grafted copolymers with selective binding sites. *J. Mater. Chem.* **2009,** *19* (2), 253-260.

71.   Chenette, H. C. S.; Robinson, J. R.; Hobley, E.; Husson, S. M. Development of high-productivity, strong cation-exchange adsorbers for protein capture by graft polymerization from membranes with different pore sizes. *J. Membr. Sci.* **2012,** *423–424* (0), 43-52.

72.   Bhut, B. V.; Husson, S. M. Dramatic performance improvement of weak anion-exchange membranes for chromatographic bioseparations. *J. Membr. Sci.* **2009,** *337* (1–2), 215-223.

73.   Ghosh, R. Separation of proteins using hydrophobic interaction membrane chromatography. *J. Chromatogr. A* **2001,** *923* (1–2), 59-64.

74.   Dods, S. R.; Hardick, O.; Stevens, B.; Bracewell, D. G. Fabricating electrospun cellulose nanofibre adsorbents for ion-exchange chromatography. *J. Chromatogr. A* **2015,** *1376*, 74-83.

75.   Bhut, B. V.; Wickramasinghe, S. R.; Husson, S. M. Preparation of high-capacity, weak anion-exchange membranes for protein separations using surface-initiated atom transfer radical polymerization. *J. Membr. Sci.* **2008,** *325* (1), 176-183.

76.   Madadkar, P.; Ghosh, R. High-resolution protein separation using a laterally-fed membrane chromatography device. *J. Membr. Sci.* **2016,** *499*, 126-133.

77.   Kumar, A.; Heaton, J. C.; McCalley, D. V. Practical investigation of the factors that affect the selectivity in hydrophilic interaction chromatography. *J. Chromatogr. A* **2013,** *1276*, 33-46.

78.   Kopaciewicz, W.; Rounds, M. A.; Regnier, F. E. Stationary phase contributions to retention in high-performance anion-exchange protein chromatography: ligand density and mixed mode effects. *J. Chromatogr. A* **1985,** *318*, 157-172.

79.   Leonard, M. New packing materials for protein chromatography. *Journal of Chromatography B: Biomedical Sciences and Applications* **1997,** *699* (1), 3-27.

80.   Lenhoff, A. M. Protein adsorption and transport in polymer-functionalized ion-exchangers. *J. Chromatogr. A* **2011,** *1218* (49), 8748-8759.

81.   Riordan, W. T.; Heilmann, S. M.; Brorson, K.; Seshadri, K.; Etzel, M. R. Salt tolerant membrane adsorbers for robust impurity clearance. *Biotechnol. Progr.* **2009,** *25* (6), 1695-1702.

82.   Kubota, N.; Kounosu, M.; Saito, K.; Sugita, K.; Watanabe, K.; Sugo, T. Preparation of a hydrophobic porous membrane containing phenyl groups and its protein adsorption performance. *Journal of Chromatography A* **1995,** *718* (1), 27-34.

83.   Ulbricht, M. Advanced functional polymer membranes. *Polymer* **2006,** *47* (7), 2217-2262.

84.   Yang, Q.; Kaul, C.; Ulbricht, M. Anti-nonspecific Protein Adsorption Properties of Biomimetic Glycocalyx-like Glycopolymer Layers: Effects of Glycopolymer Chain Density and Protein Size. *Langmuir* **2010,** *26* (8), 5746-5752.

85.   Yang, Q.; Strathmann, M.; Rumpf, A.; Schaule, G.; Ulbricht, M. Grafted Glycopolymer-Based Receptor Mimics on Polymer Support for Selective Adhesion of Bacteria. *ACS Appl. Mat. Interfaces* **2010,** *2* (12), 3555-3562.

86.   Himstedt, H. H.; Yang, Q.; Dasi, L. P.; Qian, X.; Wickramasinghe, S. R.; Ulbricht, M. Magnetically Activated Micromixers for Separation Membranes. *Langmuir* **2011,** *27* (9), 5574-5581.

87.   Ritchie, S. M. C.; Bachas, L. G.; Olin, T.; Sikdar, S. K.; Bhattacharyya, D. Surface Modification of Silica- and Cellulose-Based Microfiltration Membranes with Functional Polyamino Acids for Heavy Metal Sorption. *Langmuir* **1999,** *15* (19), 6346-6357.

88.   Gui, M.; Papp, J. K.; Colburn, A. S.; Meeks, N. D.; Weaver, B.; Wilf, I.; Bhattacharyya, D. Engineered iron/iron oxide functionalized membranes for selenium and other toxic metal removal from power plant scrubber water. *J. Membr. Sci.* **2015,** *488*, 79-91.

89.   Ulbricht, M.; Yang, H. Porous Polypropylene Membranes with Different Carboxyl Polymer Brush Layers for Reversible Protein Binding via Surface-Initiated Graft Copolymerization. *Chem. Mater.* **2005,** *17* (10), 2622-2631.

90.   Yang, Q.; Ulbricht, M. Cylindrical Membrane Pores with Well-Defined Grafted Linear and Comblike Glycopolymer Layers for Lectin Binding. *Macromolecules* **2011,** *44* (6), 1303-1310.

91.   Qian, X.; Lei, J.; Wickramasinghe, S. R. Novel polymeric solid acid catalysts for cellulose hydrolysis. *RSC Adv.* **2013,** *3* (46), 24280-24287.

92.   Xiao, L.; Isner, A.; Waldrop, K.; Saad, A.; Takigawa, D.; Bhattacharyya, D. Development of bench and full-scale temperature and pH responsive functionalized PVDF membranes with tunable properties. *J. Membr. Sci.* **2014,** *457* (0), 39-49.

93.   Zhou, S.; Xue, A.; Zhang, Y.; Li, M.; Wang, J.; Zhao, Y.; Xing, W. Fabrication of temperature-responsive ZrO2 tubular membranes, grafted with poly (N-isopropylacrylamide) brush chains, for protein removal and easy cleaning. *J. Membr. Sci.* **2014,** *450* (0), 351-361.

94.   Sinha, M. K.; Purkait, M. K. Preparation and characterization of stimuli-responsive hydrophilic polysulfone membrane modified with poly (N-vinylcaprolactam-co-acrylic acid). *Desalination* **2014,** *348* (0), 16-25.

95.   Jaroslav, M. Coatings and surface modification technologies: a finite element bibliography (1995–2005). *Modell. Simul. Mater. Sci. Eng.* **2005,** *13* (6), 935.

96.   Dickson, J. M.; Childs, R. F.; McCarry, B. E.; Gagnon, D. R. Development of a coating technique for the internal structure of polypropylene microfiltration membranes. *J. Membr. Sci.* **1998,** *148* (1), 25-36.

97.   Lu, A.-H.; Li, W.-C.; Muratova, N.; Spliethoff, B.; Schuth, F. Evidence for C-C bond cleavage by H2O2 in a mesoporous CMK-5 type carbon at room temperature. *Chem. Commun.* **2005,** (41), 5184-5186.

98.   Förch, R.; Zhang, Z.; Knoll, W. Soft Plasma Treated Surfaces: Tailoring of Structure and Properties for Biomaterial Applications. *Plasma Processes Polym.* **2005,** *2* (5), 351-372.

99.   Ruckenstein, E.; Li, Z. F. Surface modification and functionalization through the self-assembled monolayer and graft polymerization. *Adv. Colloid Interface Sci.* **2005,** *113* (1), 43-63.

100.   Lvov, Y.; Decher, G.; Moehwald, H. Assembly, structural characterization, and thermal behavior of layer-by-layer deposited ultrathin films of poly(vinyl sulfate) and poly(allylamine). *Langmuir* **1993,** *9* (2), 481-486.

101.   Joseph, N.; Ahmadiannamini, P.; Hoogenboom, R.; Vankelecom, I. F. J. Layer-by-layer preparation of polyelectrolyte multilayer membranes for separation. *Polymer Chemistry* **2014,** *5* (6), 1817-1831.

102.   Ahmadiannamini, P.; Li, X.; Goyens, W.; Joseph, N.; Meesschaert, B.; Vankelecom, I. F. J. Multilayered polyelectrolyte complex based solvent resistant nanofiltration membranes prepared from weak polyacids. *J. Membr. Sci.* **2012,** *394–395*, 98-106.

103.   Vaterrodt, A.; Thallinger, B.; Daumann, K.; Koch, D.; Guebitz, G. M.; Ulbricht, M. Antifouling and Antibacterial Multifunctional Polyzwitterion/Enzyme Coating on Silicone Catheter Material Prepared by Electrostatic Layer-by-Layer Assembly. *Langmuir* **2016,** *32* (5), 1347-1359.

104.   Wang, J.; Faber, R.; Ulbricht, M. Influence of pore structure and architecture of photo-grafted functional layers on separation performance of cellulose-based macroporous membrane adsorbers. *J. Chromatogr. A* **2009,** *1216* (37), 6490-6501.

105.   Xu, Z., Wan, L, Huang, X. *Surface Engineering of Polymer Membranes*; Springer: Advanced Topics in Science and Technology in China, 2009.

106.   Moses, K. J.; Cohen, Y. Wettability of terminally anchored polymer brush layers on a polyamide surface. *J. Colloid Interface Sci.* **2014,** *436*, 286-295.

107.   Ma, Z.; Ramakrishna, S. Ce(IV)-induced graft copolymerization of methacrylic acid on electrospun polysulphone nonwoven fiber membrane. *J. Appl. Polym. Sci.* **2006,** *101* (6), 3835-3841.

108.   Gancarz, I.; Poźniak, G.; Bryjak, M.; Frankiewicz, A. Modification of polysulfone membranes. 2. Plasma grafting and plasma polymerization of acrylic acid. *Acta Polym.* **1999,** *50* (9), 317-326.

109.   Yamagishi, H.; Crivello, J. V.; Belfort, G. Development of a novel photochemical technique for modifying poly (arylsulfone) ultrafiltration membranes. *Journal of Membrane Science* **1995,** *105* (3), 237-247.

110.   Taniguchi, M.; Belfort, G. Low protein fouling synthetic membranes by UV-assisted surface grafting modification: varying monomer type. *Journal of Membrane Science* **2004,** *231* (1–2), 147-157.

111.   Nasef, M. M.; Hegazy, E.-S. A. Preparation and applications of ion exchange membranes by radiation-induced graft copolymerization of polar monomers onto non-polar films. *Prog. Polym. Sci.* **2004,** *29* (6), 499-561.

112.   Singh, N.; Wang, J.; Ulbricht, M.; Wickramasinghe, S. R.; Husson, S. M. Surface-initiated atom transfer radical polymerization: A new method for preparation of polymeric membrane adsorbers. *J. Membr. Sci.* **2008,** *309* (1-2), 64-72.

113.   Bhut, B. V.; Christensen, K. A.; Husson, S. M. Membrane chromatography: Protein purification from E. coil lysate using newly designed and commercial anion-exchange stationary phases. *J. Chromatogr. A* **2010,** *1217* (30), 4946-4957.

114.   Chenette, H. C. S.; Husson, S. M. Membrane adsorbers comprising grafted glycopolymers for targeted lectin binding. *J. Appl. Polym. Sci.* **2015,** *132* (21), n/a-n/a.

115.   Yin, D.; Ulbricht, M. Antibody-Imprinted Membrane Adsorber via Two-Step Surface Grafting. *Biomacromolecules* **2013,** *14* (12), 4489-4496.

116.   Adrus, N.; Ulbricht, M. Molecularly imprinted stimuli-responsive hydrogels for protein recognition. *Polymer* **2012,** *53* (20), 4359-4366.

117.   Borcherding, H.; Hicke, H.-G.; Jorcke, D.; Ulbricht, M. Affinity Membranes as a Tool for Life Science Applications. *Ann. N.Y. Acad. Sci.* **2003,** *984* (1), 470-479.

118.   Mah, K. Z.; Ghosh, R. Paper-based composite lyotropic salt-responsive membranes for chromatographic separation of proteins. *J. Membr. Sci.* **2010,** *360* (1-2), 149-154.

119.   Hu, M.-X.; Yang, Q.; Xu, Z.-K. Enhancing the hydrophilicity of polypropylene microporous membranes by the grafting of 2-hydroxyethyl methacrylate via a synergistic effect of photoinitiators. *Journal of Membrane Science* **2006,** *285* (1–2), 196-205.

120.   Ulbricht, M.; Matuschewski, H.; Oechel, A.; Hicke, H.-G. Photo-induced graft polymerization surface modifications for the preparation of hydrophilic and low-proten-adsorbing ultrafiltration membranes. *J. Membr. Sci.* **1996,** *115* (1), 31-47.

121.   Bernstein, R.; Antón, E.; Ulbricht, M. Tuning the nanofiltration performance of thin film strong polyelectrolyte hydrogel composite membranes by photo-grafting conditions. *J. Membr. Sci.* **2013,** *427*, 129-138.

122.   Lei, J.; Ulbricht, M. Macroinitiator-mediated photoreactive coating of membrane surfaces with antifouling hydrogel layers. *J. Membr. Sci.* **2014,** *455*, 207-218.

123.   Quilitzsch, M.; Ulbricht, M. Low-Fouling UF Membranes for Water Treatment by Surface Modification with Hydrogel Layers via a New Macro-Initiator. *Procedia Engineering* **2012,** *44*, 1521-1522.

124.   Bahners, T.; Klingelhöller, K.; Ulbricht, M.; Wego, A.; Schollmeyer, E. Photo-chemical Surface Modification for the Control of Protein Adsorption on Textile Substrates. *J. Adhes. Sci. Technol.* **2011,** *25* (17), 2219-2238.

125.   Peeva, P. D.; Pieper, T.; Ulbricht, M. Tuning the ultrafiltration properties of anti-fouling thin-layer hydrogel polyethersulfone composite membranes by suited crosslinker monomers and photo-grafting conditions. *J. Membr. Sci.* **2010,** *362* (1–2), 560-568.

126.   Ulbricht, M. Photograft-polymer-modified microporous membranes with environment-sensitive permeabilities. *Reactive and Functional Polymers* **1996,** *31* (2), 165-177.

127.   Birkner, M.; Ulbricht, M. Ultrafiltration membranes with markedly different pH- and ion-responsivity by photografted zwitterionic polysulfobetain or polycarbobetain. *J. Membr. Sci.* **2015,** *494*, 57-67.

128.   Geismann, C.; Tomicki, F.; Ulbricht, M. Block Copolymer Photo-Grafted Poly(Ethylene Terephthalate) Capillary Pore Membranes Distinctly Switchable by Two Different Stimuli. *Sep. Sci. Technol.* **2009,** *44* (14), 3312-3329.

129.   Bernstein, R.; Antón, E.; Ulbricht, M. UV-Photo Graft Functionalization of Polyethersulfone Membrane with Strong Polyelectrolyte Hydrogel and Its Application for Nanofiltration. *ACS Appl. Mat. Interfaces* **2012,** *4* (7), 3438-3446.

130.   Farjadian, F.; Schwark, S.; Ulbricht, M. Novel functionalization of porous polypropylene microfiltration membranes: via grafted poly(aminoethyl methacrylate)

anchored Schiff bases toward membrane adsorbers for metal ions. *Polymer Chemistry* **2015,** *6* (9), 1584-1593.

131.   Kuroda, S.-i.; Mita, I.; Obata, K.; Tanaka, S. Degradation of aromatic polymers: Part IV—Effect of temperature and light intensity on the photodegradation of polyethersulfone. *Polym. Degrad. Stab.* **1990,** *27* (3), 257-270.

132.   Kaeselev, B.; Pieracci, J.; Belfort, G. Photoinduced grafting of ultrafiltration membranes: comparison of poly(ether sulfone) and poly(sulfone). *Journal of Membrane Science* **2001,** *194* (2), 245-261.

133.   Pieracci, J.; Crivello, J. V.; Belfort, G. Photochemical modification of 10 kDa polyethersulfone ultrafiltration membranes for reduction of biofouling. *J. Membr. Sci.* **1999,** *156* (2), 223-240.

134.   Yamagishi, H.; Crivello, J. V.; Belfort, G. Evaluation of photochemically modified poly (arylsulfone) ultrafiltration membranes. *J. Membr. Sci.* **1995,** *105* (3), 249-259.

135.   Pieracci, J.; Crivello, J. V.; Belfort, G. Increasing membrane permeability of UV-modified poly(ether sulfone) ultrafiltration membranes. *J. Membr. Sci.* **2002,** *202* (1–2), 1-16.

136.   J., S. M. US Patent US 4618533 A Porous membrane having hydrophilic surface and process1986.

137.   Hopin Hu, Z. C. US Patent US5209849 A Hydrophilic microporous polyolefin membrane1993.

138.   Hilal, N.; Kochkodan, V. Surface modified microfiltration membranes with molecularly recognising properties. *J. Membr. Sci.* **2003,** *213* (1–2), 97-113.

139.   He, D.; Susanto, H.; Ulbricht, M. Photo-irradiation for preparation, modification and stimulation of polymeric membranes. *Prog. Polym. Sci.* **2009,** *34* (1), 62-98.

140.   Lin, Z.; Yang, F.; He, X.; Zhao, X.; Zhang, Y. Preparation and evaluation of a macroporous molecularly imprinted hybrid silica monolithic column for recognition of proteins by high performance liquid chromatography. *J Chromatogr A* **2009,** *1216* (49), 8612-22.

141.   Hicke, H.-G.; Ulbricht, M.; Becker, M.; Radosta, S.; Heyer, A. G. Novel enzyme-membrane reactor for polysaccharide synthesis. *J. Membr. Sci.* **1999,** *161* (1–2), 239-245.

142.   Yang, B.; Yang, W. Thermo-sensitive switching membranes regulated by pore-covering polymer brushes. *J. Membr. Sci.* **2003,** *218* (1–2), 247-255.

143.   Yang, B.; Yang, W. Novel pore-covering membrane as a full open/close valve. *J. Membr. Sci.* **2005,** *258* (1–2), 133-139.

144. Geismann, C.; Ulbricht, M. Photoreactive Functionalization of Poly(ethylene terephthalate) Track-Etched Pore Surfaces with "Smart" Polymer Systems. *Macromol. Chem. Phys.* **2005,** *206* (2), 268-281.

145. Ma, H.; Davis, R. H.; Bowman, C. N. A Novel Sequential Photoinduced Living Graft Polymerization. *Macromolecules* **2000,** *33* (2), 331-335.

146. Bondar, Y.; Kim, H. J.; Yoon, S. H.; Lim, Y. J. Synthesis of cation-exchange adsorbent for anchoring metal ions by modification of poly(glycidyl methacrylate) chains grafted onto polypropylene fabric. *React. Funct. Polym.* **2004,** *58* (1), 43-51.

147. Ulbricht, M.; Schwarz, H.-H. Novel high performance photo-graft composite membranes for separation of organic liquids by pervaporation. *J. Membr. Sci.* **1997,** *136* (1–2), 25-33.

148. Nayak, A.; Liu, H.; Belfort, G. An Optically Reversible Switching Membrane Surface. *Angew. Chem. Int. Ed.* **2006,** *45* (25), 4094-4098.

149. Hilal, N.; Kochkodan, V.; Al-Khatib, L.; Levadna, T. Surface modified polymeric membranes to reduce (bio)fouling: a microbiological study using E. coli. *Desalination* **2004,** *167*, 293-300.

150. Tazuke, S.; Kimura, H. Surface photografting, 2. Modification of polypropylene film surface by graft polymerization of acrylamide. *Die Makromolekulare Chemie* **1978,** *179* (11), 2603-2612.

151. Wu, G.; Li, Y.; Han, M.; Liu, X. Novel thermo-sensitive membranes prepared by rapid bulk photo-grafting polymerization of N,N-diethylacrylamide onto the microfiltration membranes Nylon. *J. Membr. Sci.* **2006,** *283* (1–2), 13-20.

152. He, D.; Ulbricht, M. Surface-selective photo-grafting on porous polymer membranes via a synergist immobilization method. *J. Mater. Chem.* **2006,** *16* (19), 1860-1868.

153. Wang, J.-S.; Matyjaszewski, K. Controlled/"living" radical polymerization. atom transfer radical polymerization in the presence of transition-metal complexes. *J. Am. Chem. Soc.* **1995,** *117* (20), 5614-5615.

154. Matyjaszewski, K. Atom Transfer Radical Polymerization (ATRP): Current Status and Future Perspectives. *Macromolecules* **2012,** *45* (10), 4015-4039.

155. Matyjaszewski, K.; Xia, J. Atom Transfer Radical Polymerization. *Chem. Rev.* **2001,** *101* (9), 2921-2990.

156. Braunecker, W. A.; Tsarevsky, N. V.; Gennaro, A.; Matyjaszewski, K. Thermodynamic Components of the Atom Transfer Radical Polymerization Equilibrium: Quantifying Solvent Effects. *Macromolecules* **2009,** *42* (17), 6348-6360.

157.   Khabibullin, A. Surface-Initiated Atom Transfer Radical Polymerization. In *Controlled Radical Polymerization at and from Solid Surfaces*, Vana, P., Ed.; Springer International Publishing, 2016.

158.   Wang, J.; Jenkins, E. W.; Robinson, J. R.; Wilson, A.; Husson, S. M. A new multimodal membrane adsorber for monoclonal antibody purifications. *Journal of Membrane Science* **2015,** *492*, 137-146.

159.   Chen, W.; McCarthy, T. J. Adsorption/Migration of a Perfluorohexylated Fullerene from the Bulk to the Polymer/Air Interface. *Macromolecules* **1999,** *32* (7), 2342-2347.

160.   Koulis CV, R. J., Bibby AM. Comparison of Transmission and Internal Reflection Infrared Spectra of Cocaine. *Journal of Forensic Sciences* **2001,** *46* (4), 822-829.

161.   Adamsons, K. Chemical surface characterization and depth profiling of automotive coating systems. *Prog. Polym. Sci.* **2000,** *25* (9), 1363-1409.

162.   Behzad, A.; Hooghan, K.; Aubry, C.; Khan, M.; Croue, J. SEM-FIB Characterization of Reverse Osmosis Membrane Fouling. *Microsc. Microanal.* **2011,** *17* (Supplement S2), 1768-1769.

163.   Lim, A. L.; Bai, R. Membrane fouling and cleaning in microfiltration of activated sludge wastewater. *J. Membr. Sci.* **2003,** *216* (1–2), 279-290.

164.   Chede, S.; Escobar, I. C. Fouling control using temperature responsive N-isopropylacrylamide (NIPAAm) membranes. *Environmental Progress & Sustainable Energy* **2015**, n/a-n/a.

165.   Feng, Q.; Hou, D.; Zhao, Y.; Xu, T.; Menkhaus, T. J.; Fong, H. Electrospun Regenerated Cellulose Nanofibrous Membranes Surface-Grafted with Polymer Chains/Brushes via the Atom Transfer Radical Polymerization Method for Catalase Immobilization. *ACS Appl. Mat. Interfaces* **2014,** *6* (23), 20958-20967.

166.   Ferlita, R. R.; Phipps, D.; Safarik, J.; Yeh, D. H. Cryo-snap: A simple modified freeze-fracture method for SEM imaging of membrane cross-sections. *Environ. Prog.* **2008,** *27* (2), 204-209.

167.   Livazovic, S.; Li, Z.; Behzad, A. R.; Peinemann, K. V.; Nunes, S. P. Cellulose multilayer membranes manufacture with ionic liquid. *J. Membr. Sci.* **2015,** *490*, 282-293.

168.   Bowen, W. R.; Hilal, N.; Lovitt, R. W.; Wright, C. J. A new technique for membrane characterisation: direct measurement of the force of adhesion of a single particle using an atomic force microscope. *J. Membr. Sci.* **1998,** *139* (2), 269-274.

169. Richard Bowen, W.; Hilal, N.; Lovitt, R. W.; Wright, C. J. Characterisation of membrane surfaces: direct measurement of biological adhesion using an atomic force microscope. *J. Membr. Sci.* **1999,** *154* (2), 205-212.

170. Ang, W. S.; Elimelech, M. Fatty acid fouling of reverse osmosis membranes: Implications for wastewater reclamation. *Water Res.* **2008,** *42* (16), 4393-4403.

171. Baek, Y.; Kang, J.; Theato, P.; Yoon, J. Measuring hydrophilicity of RO membranes by contact angles via sessile drop and captive bubble method: A comparative study. *Desalination* **2012,** *303*, 23-28.

172. Huisman, I. H.; Vellenga, E.; Trägårdh, G.; Trägårdh, C. The influence of the membrane zeta potential on the critical flux for crossflow microfiltration of particle suspensions. *J. Membr. Sci.* **1999,** *156* (1), 153-158.

173. Bellona, C.; Drewes, J. E. The role of membrane surface charge and solute physico-chemical properties in the rejection of organic acids by NF membranes. *J. Membr. Sci.* **2005,** *249* (1–2), 227-234.

174. Oo, M. H.; Ong, S. L. Implication of zeta potential at different salinities on boron removal by RO membranes. *J. Membr. Sci.* **2010,** *352* (1–2), 1-6.

175. Skluzacek, J. M.; Tejedor, M. I.; Anderson, M. A. NaCl rejection by an inorganic nanofiltration membrane in relation to its central pore potential. *J. Membr. Sci.* **2007,** *289* (1–2), 32-39.

176. Nabe, A.; Staude, E.; Belfort, G. Surface modification of polysulfone ultrafiltration membranes and fouling by BSA solutions. *J. Membr. Sci.* **1997,** *133* (1), 57-72.

177. Burns, D. B.; Zydney, A. L. Buffer effects on the zeta potential of ultrafiltration membranes. *J. Membr. Sci.* **2000,** *172* (1–2), 39-48.

178. Al-Amoudi, A.; Williams, P.; Mandale, S.; Lovitt, R. W. Cleaning results of new and fouled nanofiltration membrane characterized by zeta potential and permeability. *Sep. Purif. Technol.* **2007,** *54* (2), 234-240.

179. Nakamura, K.; Orime, T.; Matsumoto, K. Response of zeta potential to cake formation and pore blocking during the microfiltration of latex particles. *J. Membr. Sci.* **2012,** *401–402*, 274-281.

180. Hurwitz, G.; Guillen, G. R.; Hoek, E. M. V. Probing polyamide membrane surface charge, zeta potential, wettability, and hydrophilicity with contact angle measurements. *J. Membr. Sci.* **2010,** *349* (1–2), 349-357.

181. Bouzid, H.; Rabiller-Baudry, M.; Paugam, L.; Rousseau, F.; Derriche, Z.; Bettahar, N. E. Impact of zeta potential and size of caseins as precursors of fouling deposit on limiting and

critical fluxes in spiral ultrafiltration of modified skim milks. *J. Membr. Sci.* **2008,** *314* (1–2), 67-75.

182.   Golas, P. L.; Matyjaszewski, K. Marrying click chemistry with polymerization: expanding the scope of polymeric materials. *Chem. Soc. Rev.* **2010,** *39* (4), 1338-1354.

183.   Jung, N.; Bräse, S. Click Reactions: Azide-Alkyne Cycloaddition. In *Kirk-Othmer Encyclopedia of Chemical Technology*; John Wiley & Sons, Inc., 2000.

184.   Yang, Q.; Mi, B. Nanomaterials for Membrane Fouling Control: Accomplishments and Challenges. *Advances in Chronic Kidney Disease* **2013,** *20* (6), 536-555.

185.   Ranjan, R.; Brittain, W. J. Combination of Living Radical Polymerization and Click Chemistry for Surface Modification. *Macromolecules* **2007,** *40* (17), 6217-6223.

186.   Zheng, S.; Yang, Q.; Mi, B. Novel antifouling surface with improved hemocompatibility by immobilization of polyzwitterions onto silicon via click chemistry. *Appl. Surf. Sci.* **2016,** *363*, 619-626.

187.   Demirci, G.; Tasdelen, M. A. Synthesis and characterization of graft copolymers by photoinduced CuAAC click chemistry. *Eur. Polym. J.* **2015,** *66*, 282-289.

188.   Du, H. B.; Wickramasinghe, R.; Qian, X. H. Effects of Salt on the Lower Critical Solution Temperature of Poly (N-Isopropylacrylamide). *Journal of Physical Chemistry B* **2010,** *114* (49), 16594-16604.

189.   Du, H. B.; Qian, X. H. Molecular Dynamics Simulations of PNIPAM-co-PEGMA Copolymer Hydrophilic to Hydrophobic Transition in NaCl Solution. *Journal of Polymer Science Part B-Polymer Physics* **2011,** *49* (15), 1112-1122.

190.   Du, H.; Wickramasinghe, S. R.; Qian, X. Specificity in Cationic Interaction with Poly(N-isopropylacrylamide). *The Journal of Physical Chemistry B* **2013,** *117* (17), 5090-5101.

191.   Du, H.; Qian, X. The hydration properties of carboxybetaine zwitterion brushes. *Journal of computational chemistry* **2016,** *37* (10), 877-885.

192.   Himstedt, H. H.; Du, H.; Marshall, K. M.; Wickramasinghe, S. R.; Qian, X. pH Responsive Nanofiltration Membranes for Sugar Separations. *Industrial & Engineering Chemistry Research* **2013,** *52* (26), 9259-9269.

Chapter 2 Membrane Surface Engineering for Protein Separations: Experiments and Simulations

* This chapter is adapted from a published paper by Liu, Z.; Du, H.; Wickramasinghe, S. R.; Qian, X. Membrane Surface Engineering for Protein Separations: Experiments and Simulations. Langmuir 2014, 30 (35), 10651-10660.

Abstract

A bisphosphonate derived ligand was successfully synthesized and grafted from the surface of regenerated cellulose membrane using atom transfer radical polymerization (ATRP) for protein separations. This ligand has a remarkable affinity for arginine (Arg) residues on protein surface. Hydrophilic residues N-(2-hydroxypropyl) methacrylamide (HPMA) was copolymerized to enhance the flexibility of the copolymer ligand and further improve specific protein adsorption. The polymerization of bisphosphonate derivatives was successful for the first time using ATRP. Static and dynamic binding capacities were determined for binding and elution of Arg rich lysozyme. The interaction mechanism between the copolymer ligand and lysozyme was elucidated using classical molecular dynamics (MD) simulations.

2.1 Introduction

Biopharmaceuticals, represent an increasingly large fraction of the overall pharmaceutical market. Since downstream purification costs can account for up to 80% of the manufacturing cost[1] there is a tremendous need for new technologies that reduce the overall manufacturing cost. In addition, as more efficient upstream process steps lead to higher cell titers, higher product protein concentrations are being observed during the purification steps. This is leading to new challenges during purification. Membrane chromatography or membrane adsorption, where a macroporous membrane is used as a support material and the ligands are bound to the pore surface, offers significant advantages over traditional packed bed

chromatography[2]. Membrane chromatography can be run at much lower pressure drops and are easy to scale up. Importantly, since the feed is pumped through the membrane pores, transport of the solute to the binding sites occurs mainly by fast convective flow. Consequently, the dynamic capacity is independent of flow rate over a much larger range of flow rates compared to packed beds[2, 3]. Nevertheless the major perceived disadvantage is that the capacity is likely lower than for porous resin particles. Increasing the capacity of membrane adsorbers is critical if membrane chromatography is to be widely used commercially.

Specific protein-ligand recognition is critical for developing high affinity chromatography for protein purifications. It provides an effective strategy to separate different proteins that have similar size and charge but different amino acid residues on surface. Applying this molecular recognition strategy to surface modification of membranes is promising to generate high performance membrane chromatography for protein purifications. Bisphosphonate and its derivative have been studied[4, 5] recently as molecular tweezers for specific protein separations due to their high affinity for lysine and arginine. One of these synthetic tweezers exhibiting high affinity for lysine possesses two anionic phosphonate arms and a rigid non-polar cavity. The tweezer with m-xylene bisphosphonate recognition motif as shown in Figure 2.1(*a*) was incorporated in the first synthetic receptor for Arg-Gly-Asp (RGD) sequence[6]. However, the binding affinity between the molecular tweezers and these amino acids become rather weak in aqueous solution for all the cases investigated. Thus, significant efforts[5, 7, 8, 9, 10, 11] have been devoted to turning a single relatively weak binding site into multivalent binding sites by forming bisphosphonate dendrimers or linear copolymers. The dendrimers incorporate the m-xylene bisphosphonate functional group at the branch ends[7]. Binding for Lys and Arg residues on protein surface in aqueous solution is enhanced

72

significantly due to multivalent interactions leading to an increase in binding constant K_a from around 10 M^{-1} to 10^6 M^{-1}.
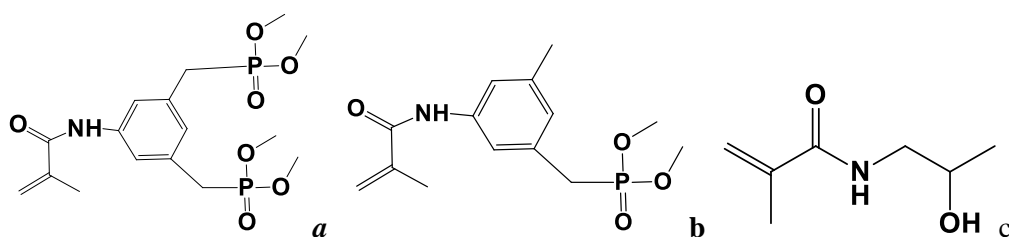
Figure 2.1 Monomers in the various synthesized copolymer ligands for specific protein separations: 5-(methacryloylamino)-m-xylylene bisphosphonic acid tetramethylester (Bis-P, *a*), 5-(methacryloylamino)-m-xylylene monophosphonic acid tetramethylester (Mono-P, *b*) and N-(2-hydroxypropyl) methacrylamide (HPMA, *c*)

Various linear copolymers incorporating m-xylene bisphosphonate recognition motif were synthesized via free radical polymerization under heat[8] or UV-initiated radical polymerization[11] reactions that are difficult to control. Copolymers of bisphosphonate motif (neutral or anionic) and another alcohol monomer (methacryloylamino-2-hydroxypropane) has also been grafted on poly (ethylene terephthalate) track-etched membrane surfaces using UV-initiated radical polymerization[9]. The neutral copolymer modified membrane has selectivity for lysozyme but that modified with anionic copolymer does not. Moreover, binding constants for membranes grafted with the neutral bisphosphonate ligands are about 15 times higher for lysozyme than for cytochrome C. These results confirm that the copolymers incorporated with neutral bisphosphonate functional group have a higher binding capacity as well as a better selectivity for Arg-rich proteins than those incorporated with derivatives of anionic bisphosphonate. Membranes grafted with anionic copolymers exhibit similar binding characteristics to conventional ion exchange resins.

So far none of the radical polymerization processes was conducted in a controllable manner, which is important for grafting a uniform layer of bisphosphonate polymers at the desirable chain length and chain density on membrane surfaces for optimal protein binding.

Recently, Tominey and co-workers[10] used reversible addition-fragmentation chain transfer (RAFT) polymerization to synthesize copolymers of bisphosphonate in aqueous solution. The copolymer of anionic bisphosphonate and N-isopropylacrylamide (PNIPAM) is capable of precipitating positively charged histidine (His) rich proteins[10]. Previous work on polymerization from methacrylamide and its derivatives are almost all initiated by UV [12, 13, 14, 15] or more recently via RAFT polymerization[16, 17, 18, 19, 20]. Only a few more recent studies[21, 22, 23, 24] have reported successful synthesis of polymers from methacrylamide and its derivatives using atom-transfer radical polymerization (ATRP). As far as we are aware, our work is the first to copolymerize methacrylamide derivative involving the crucial binding site m-xylene bisphosphonate (Bis-P) via ATRP. Slow growth of polymer chain via ATRP is common for this type of monomers because of their low reactivity as well as their tendency to form complexes with copper catalyst used for ATRP reactions[25, 26].

Since the binding capacity for protein is likely to depend strongly on the chain length and chain density of the polymeric layers grafted, the controllable ATRP polymerization reaction clearly has an advantage over other polymerization reactions for developing high affinity, high capacity polymeric ligands. Unlike UV-initiated polymerization, ATRP synthesized polymers generally have low poly-dispersity. Further ATRP allows good control of the chain length and chain density of grafted polymer layer. Therefore, optimizing ATRP reaction conditions for Bis-P monomer is crucial to have a well-defined polymeric ligand layer on membrane surface. Additionally, a well-characterized polymer structure can be crucial in elucidating the binding mechanism between protein and ligand.

Membrane chromatography formed by grafting protein affinity ligands on microporous membrane substrates demonstrates several advantages over conventional packed-bed column. The large porous structure enables separation to conduct at much lower pressure drop. Additionally, unlike resins, protein separation is not limited by diffusion when

pumping the feed solution through the membrane pores. The open porous nature of membrane chromatography makes it easier for proteins to reach the polymeric ligands grafted on membrane surfaces. As a result, the dynamic binding capacity of membrane chromatography becomes independent of flow rate over a large range of operating conditions leading to much higher productivity than the corresponding resin column[27, 28].

2.2 Materials

2-Bromo-2-methylpropionyl bromide (BIB, 98%), 4-(dimethylamino) pyridine (≥99%), copper (I) chloride (≥99.995%), copper (II) chloride (≥99.995%) and *N,N,N′,N″,N″*-pentamethyldiethylenetriamine (PMDETA, 99%) were purchased from Sigma Aldrich (St. Louis, MO). 4-(2-hydroxyethyl)-1-piperazineethanesulfonic acid (HEPES, 99%) and triethylamine (TEA, ≥99%) were obtained from Alfa Aesar (Ward Hill, MA). Chloroform-d (99.9 atom % D) was obtained from Acros Organics (Pittsburgh, PA). Methanol (99.8%) and acetonitrile (99.8%) were obtained from EMD Chemicals (Billerica, MA). Boric anhydride was purchased from Avantor Performance Materials (Center Valley, PA). Anhydrous acetonitrile was obtained by distilling acetonitrile with boric anhydride. N-(2-hydroxypropyl) methacrylamide (HPMA) was purchased from Polysciences, Inc (Warrington, PA). Sodium hydroxide (98%) was obtained from J. T. Baker (Center Valley, PA). Sodium chloride (99%) was bought from Macron™ Chemicals (Center Valley, PA). Lysozyme, from egg white was purchased from OmniPur® (Gibbstown, NJ). Regenerated cellulose membranes (0.45μm pore size, RC55, 47mm diameter) were purchased from Whatman Ltd (Pittsburgh, PA). 5-(Methacryloylamino)-m-xylylene bisphosphonic acid tetrame-thylester were synthesized following the procedure reported in literature before[9].

2.3 Experimental

2.3.1 Synthesis of 5-(methacryloylamino)-m-xylylenebisphosphonic acid

tetramethylester

Briefly, synthesis started from the bromination reaction of 5-Nitro-m-xylene. After the bromides were added on the methyl groups, trimethylphosphite was used for Arbuzov reaction to introduce the phosphonate groups. Then, the nitro-group was reduced to the amine-group by hydrogenation reaction. Finally, methacryloyl chloride was conjugated to form a methylacrylamide type monomer. The details on its synthesis and characterization are included in the appendix 1.

2.3.2 ATRP Initiator Immobilization

All new regenerated cellulose (RC) membranes (0.45 μm in pore diameter) were washed with methanol overnight before use. Thereafter methanol was removed in vacuum oven at 35 ℃ overnight. RC membranes were incubated in anhydrous acetonitrile solution (25 mL) containing 2-bromoisobutyryl bromide (2-BIB, 40 mM), triethylamine (TEA, 5 mM) and 4-dimethylaminopyridine (DMAP, 0.25 mM) for 3 h. After the reaction, the membranes were taken out and rinsed with acetonitrile several times and then washed with DI water overnight. All the membranes were then dried in vacuum oven at 35 ℃ overnight.

2.3.3 Polymerization

The polymerization solution comprised Bis-P monomer or monomer mixture; catalyst, copper (I) chloride; copper (II) chloride; ligand N,N,N′,N″,N″-pentamethyldiethylenetriamine (PMDETA); and solvent, methanol/water mixture (4:1,v/v). The ratio among monomer: CuCl: CuCl$_2$: PMDETA is 50:1:0.1:1.2. Prior to polymerization reaction, flasks were de-oxygenated by vacuum and argon back-filling process three times. After the predetermined time of ATRP, membranes were first washed with methanol and

water mixture (1:1, v/v) and then DI water. Finally all membranes were dried in vacuum oven and weight change before and after ATRP were recorded. The degree of grafting (DG, $\mu g/cm^2$) was calculated according to the following equation:

$$DG = \frac{W_1 - W_0}{W_0 \times Spec}\qquad(1)$$

where W_0 is the mass of the membrane after initiator immobilization and W_1 is the mass of the membrane after ATRP and vacuum drying. *Spec* represents the specific area of the membrane ($6.3\ m^2/g$ was used in this study based on the recommendation by manufacturer).

2.3.4 Protein Binding Test

Static Binding All membranes were first equilibrated with buffer *A* (25 mM HEPES buffer, pH=7.1) for 1 h. Then various concentrations of lysozyme solutions were prepared using buffer *A*. Then the equilibrated membranes were incubated with lysozyme solution for 20 h at room temperature with shaking. At the same time, 5 different concentrations of lysozyme solutions in buffer *A* without membranes were prepared in order to generate the standard curve. After equilibration, the concentrations of protein solutions were determined with UV absorbance at 280 nm. Membranes were regenerated by 2 M sodium chloride overnight. The binding capacity of each membrane was determined based on the standard curve generated. The binding capacity *q* in mg/mL for each protein concentration was calculated according to the following equation:

$$q = \frac{\text{amount of protein bound to membrane (mg)}}{\text{membrane volume (mL)}}\qquad(2)$$

Dynamic Binding Membranes were soaked in buffer *A* for 1 h before use. For loading, solution containing 0.1 mg /mL lysozyme in buffer *A* (25 mM HEPES buffer, pH=7.1) was used. One membrane (bed volume 0.02 mL) was loaded into a stainless steel flow cell (Mustang Coin ® module, Pall Corporation) with two flow distributers to ensure a uniform flow across the whole membrane. All runs were conducted using ÄKTA FPLC from GE Healthcare Bio-Sciences Corp. (Piscataway, NJ, USA). A procedure described below was developed using Unicorn software v. 5.31[29] to automate the lysozyme binding and elution experiments. First, each membrane was wetted with buffer *B* (25mM HEPES buffer with 1 M NaCl, pH=7.1) in the reverse flow configuration over 5 minutes by increasing the flow rate from 0.2 mL/min to 1.0 mL/min in 0.2 mL/min increment. The membrane was then equilibrated in the forward flow configuration in the buffer *A* at 1 mL/min for 10 minutes. Afterwards, 0.1 mg/mL lysozyme solution was loaded onto the membrane at a flow rate of 2 mL/min for 5 minutes. Unbound protein was then washed from the membrane using the feed buffer for 10 minutes at 1 mL/min, followed by a step change to run buffer *B* through the membrane at 2 mL/min. The run was complete when the UV absorbance at 280 nm became constant. Washing fraction (includes loading fraction) and elution fraction were collected and their respective volumes were determined. Protein concentrations in the sample solution, washing and elution fractions were determined with UV absorbance at 280 nm. Lysozyme dynamic binding capacity and recovery were determined following the same procedure as before[29]. The amount of protein bound was calculated by subtracting the washed out protein from the amount loaded. Recovery was calculated by dividing the amount of protein eluted by the total amount of protein bound.

2.3.5 Surface Analysis

Scanning Electron Microscopy (SEM) SEM was used to characterize the surface morphology of unmodified membrane and Bis-P/Mono-P modified membranes. The images were obtained in the FEI Nova Nanolab 200 Duo-Beam Workstation. Samples were coated with gold and scanned using a 15 kV electron beam.

X-ray Photoelectron Spectroscopy (XPS) Unmodified, initiator immobilized, Bis-P and Bis-P-co-HPMA modified membranes with varying ATRP times were analyzed using XPS (phi versa probe XPS). The spectra with broad energy range were obtained using a pass energy of 112 eV at 1 eV interval. High-resolution scans were conducted using a pass energy of 23.5 eV at 0.2 eV interval.

Classical Molecular Dynamics (MD) Simulations Classical molecular dynamics (MD) simulation has become a very useful tool for obtaining molecular level insights in many chemical and biochemical processes. We have successfully employed MD simulations to investigate thermo-responsive polymers in solutions[30, 31, 32] as well as separation of sugar molecules using nanofiltration membranes[33]. In order to elucidate the binding mechanism between the copolymer ligand Bis-co-HPMA and lysozyme, all-atom molecular dynamics (MD) simulations were conducted in aqueous solution containing one lysozyme and one copolymer chain. The 8 positive charges on lysozyme surface were balanced with 8 Cl^- anions in the unit cell to maintain charge neutrality. The copolymer chain contains 14 Bis-P and 56 HPMA residues with each Bis-P residue separated by 4 HPMA residues. The protein and the copolymer were solvated by 35000 water molecules. The simulations were conducted at 300 K for a total of 940 nanoseconds (ns). The highly efficient and well parallelized NAMD code[34] was used for the simulations. The atomic charges of the Bis-P and HPMA

residues were calculated at the HF/6-31G* level using Gaussian09[35] according to the RESP protocol[36]. The structures of Bis-P and HPMA linear trimers were optimized in gas phase at the B3LYP/6-31G* level for the subsequent charge calculations. The atomic charges of the end residues of the trimmers were used for the corresponding end residues in the copolymer. The atomic charges of the mid-residues of the trimers were used for the corresponding mid-residues in the copolymer. The general AMBER force field (GAFF)[37] was used for the copolymer and AMBER force field ff10[38] was used for the lysozyme protein. The initial copolymer structures containing Bis-P and HPMA residues were constructed by LEaP module in AMBERTOOLS[39]. This was followed by MD simulations in vacuum for about 100 picosecond (ps) at 300 K. The copolymer conformation thus obtained was used as the starting structure for the subsequent MD simulations in aqueous solution. The atomic structure of lysozyme was obtained from the X-ray crystallography HEWL (1DPX) data available from RCSB PDB[40]. The initial separation distance between the mass centers of the polymer chain and lysozyme was about 52 Å. The TIP3P[41] model was used for the water molecules. The force field parameters for Cl$^-$ ion compatible with TIP3P water model were obtained from Salt Ion version 08[42] available in the AMBERTOOLS package[39]. The simulations were conducted under constant temperature and constant pressure (NPT) at 1 atm using Langevin-Hoover scheme[43, 44]. Periodic boundary condition (PBC) was applied. The initial unit cell has a dimension of 105 x 105 x 105 Å^3. A 12 Å cut off was used for the short-range electrostatic interaction as well as for the *van der Waals* interaction. Long-range electrostatic interaction was determined using Particle Mesh Ewald (PME) method[45, 46]. A 2 femtosecond (fs) time step was used. The rigid bonds of water were constrained using the SETTLE algorithm[47]. The electrostatic and *van der Waals* interaction energies between the copolymer and lysozyme were determined for the systems as a function of simulation time. The number of hydrogen bonds formed between the protein and polymer was also

determined. A hydrogen bond is formed if the distance between the two heavy atoms A and B is less than 3.5 Å and the angle A—H $\cdots$ B is greater than 150°. The pair correlation functions between functional groups on the copolymer and surface residues on protein were calculated during various simulation periods.

2.4 Results and Discussion

2.4.1 Polymer Syntheses and Characterization
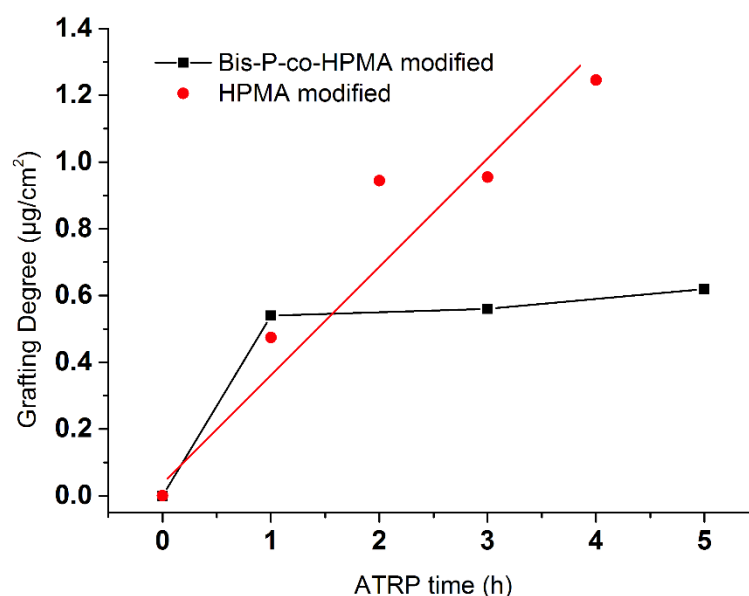
Figure 2.2 Degree of grafting (DG) as a function of polymerization time for both poly (HPMA) and poly (Bis-P-co-HPMA) grown on regenerated cellulose membranes.

Figure 2.2 shows the DG value as a function of polymerization time for both poly (HPMA) and poly (Bis-P-co-HPMA) grafted on regenerated cellulose membrane substrates. Polymerization of HPMA is rather fast and DG value increases almost linearly with ATRP time. On the other hand, copolymerization of HPMA and Bis-P appears to be rather complex. During the first hour of ATRP reaction, the copolymer DG value increases at the same rate as that of homopolymer HPMA. However, during the subsequent ATRP times, the DG value increases only very slightly. This is probably due to the rather slow incorporation of Bis-P into the copolymer. Also, regenerated cellulose membranes are very sensitive to the moisture level in air due to its rather hydrophilic nature. There is always some uncertainty in weight

81

measurement when the DG value is low as is in this case even though the same procedure was used for all the measurements. It can be seen that poly (HPMA) growth is much faster than poly (Bis-P-co-HPMA). During the first hour, the DG values are almost the same for both polymers indicating that the copolymer is probably dominated by HPMA. The rather slow polymerization of Bis-P is due probably to its bulky structure and the stability of conjugated-π system. For the subsequent ATRP times, poly (HPMA) continues to grow at the same rate as before whereas the growth of poly (Bis-P-co-HPMA) slows down significantly. This is probably due to the increased incorporation of the Bis-P monomers in the copolymer as the concentration of HPMA decreases. This is confirmed by XPS data as shown in Figure 2.3 and is reflected in its binding capacity that will be discussed in more detail later. Since the DG values are in the ug/cm^2 range, the thicknesses of the grafted polymer layer are likely in the nanometer scale and were not determined. The degree of polymerization (DP) values were not estimated either. We will characterize the thickness of the grafted polymer layer and determine its DP value in our future investigations.

The XPS data are shown in Figure 2.3 for the unmodified and initiator immobilized membranes as well as for membranes grafted with poly (Bis-P) homo-polymer, poly (Bis-P-co-HPMA) copolymer after 1, 3 and 5 h of ATRP reactions. It can be seen that after initiator immobilization, small bromide Br_{3p}, Br_{3d} peaks appear at binding energies at around 70 and 175 eV respectively. The existence of these two peaks indicates that ATRP initiators are successfully immobilized on membrane surfaces.
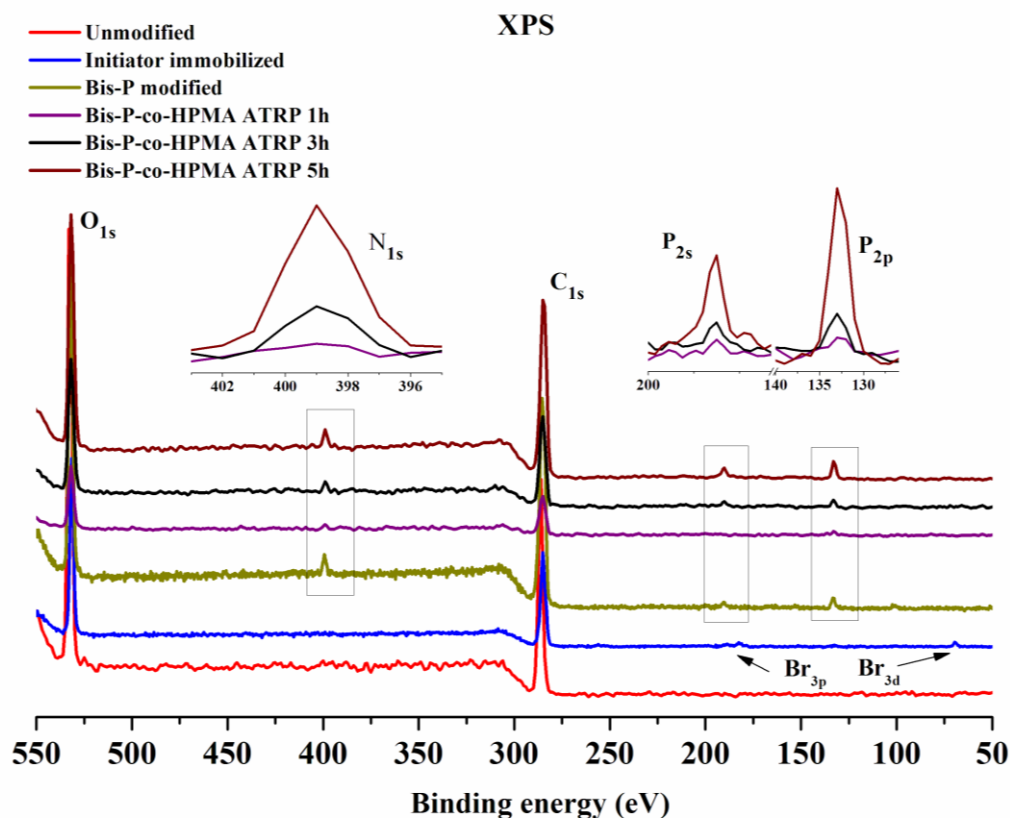
Figure 2.3 XPS spectra for the unmodified, initiator immobilized, Bis-P and Bis-P-co-HPMA modified membranes.

After ATRP reaction, new peaks representing N_{1s} (~ 400 eV), P_{2s} (~180 eV) and P_{2p} (~125 eV) appear. The N_{1s} peak comes from the amide bond in Bis-P or in HPMA whereas both the P_{2s} and P_{2p} peaks come from the phosphonate ester group in Bis-P only. Additionally, for the Bis-P-co-HPMA modified membranes, the N_{1s}, P_{2s} and P_{2p} peak intensities increase with ATRP reaction time. In particular, the P_{2s} and P_{2p} peaks in the copolymer are barely visible for the 1 h ATRP time in agreement with our hypothesis that the initial growth of the copolymer is dominated by polymerization of HPMA. After 3 h of ATRP, these two peaks become much more prominent indicating increased incorporation of Bis-P in the copolymer. Their peak intensities increase significantly from 3 to 5 h ATRP time suggesting more copolymerization of Bis-P. These XPS results indicate that the copolymers of Bis-P and HPMA are successfully grafted on the membrane surface and that their growth and incorporation vary with ATRP time. The SEM images of unmodified, Mono-P-co-

HPMA and Bis-P-co-HPMA modified membranes are shown in Figure 2.4. Membrane

modification was conducted using ATRP for 3 h and 5 h under the same conditions as before.

From Figure 2.4, it can be seen that membrane pore sizes remain more or less the same

before and after surface modification. This is in agreement with the low DGs after surface

modification shown in Figure 2.2.
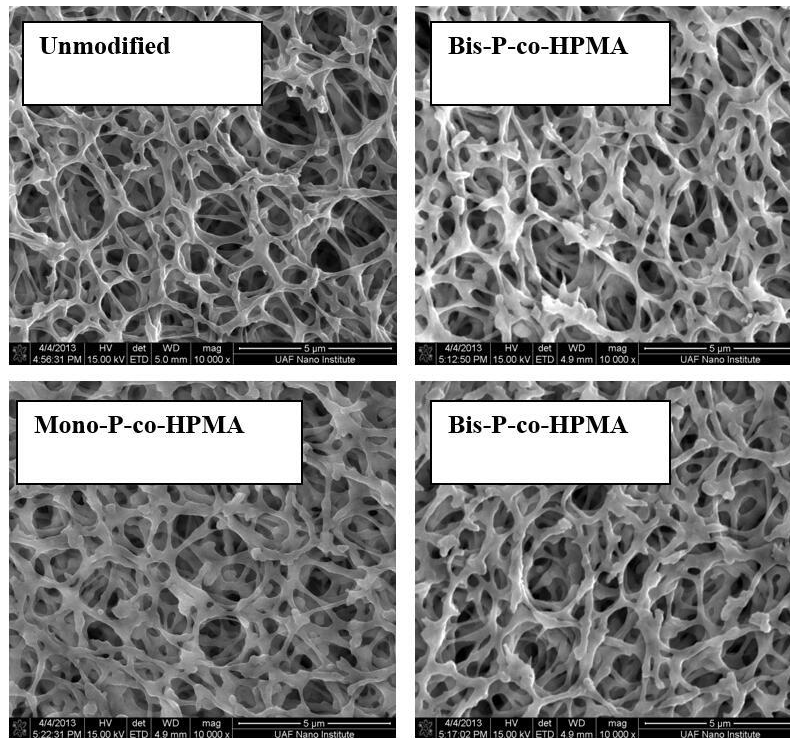
Figure 2.4 SEM images for unmodified, Mono-P-co-HPMA modified after ATRP 5 h, and
Bis-P-co-HPMA modified after ATRP 3h and 5 h membranes.

2.4.2 Static Binding Results

Based on the Langmuir isotherm

$$q = q_{max} \frac{Kc}{1+Kc} \qquad (3)$$

where q and q_{max} represent the binding capacity and maximum binding capacity respectively,

K is the equilibrium constant and c is the protein concentration, Figure 2.5a plots the static

binding capacity q in mg/mL membrane volume as a function of lysozyme concentration C_{eq}

in mg/mL solution for HPMA modified as well as 1, 3 and 5 h ATRP modified Bis-P-co-

HPMA membranes. Figure 2.5b plots c/q vs. c based on the corresponding Langmuir linear regression as shown in equation (4)

$$\frac{c}{q} = \frac{c}{q_{max}} + \frac{1}{Kq_{max}} \qquad (4)$$

to obtain the maximum binding capacities q_{max} and binding constants K for the three Bis-P-co-HPMA modified membranes. All data points are the average of two runs with ± 0.3 mg/mL for the error bar. By comparison, at 0.1mg/mL lysozyme concentration, the unmodified membrane has a binding capacity of 3.8 ± 0.4 mg/mL.

It can be seen from Figure 2.5a that poly (HPMA) modified membrane, which represents the control here, has very low binding affinity for lysozyme compared to those of copolymer ligand modified membranes. Langmuir model fits well for lysozyme adsorption on Bis-P-co-HPMA modified membranes. Table 2.1 shows the maximum binding capacities, the binding equilibrium constants and associated free energies for lysozyme binding to copolymer modified membrane substrates from Langmuir linear regression shown in Figure 2.5b.
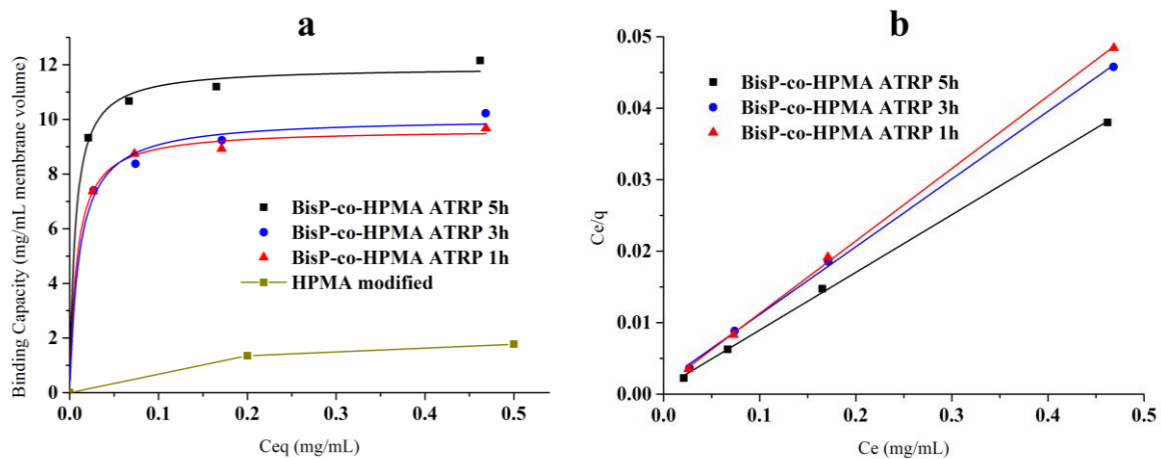
Figure 2.5 Langmuir isotherm curves (a) for ATRP 1, 3 and 5 h Bis-P-co-HPMA modified membranes as well as HPMA modified membrane for comparison. Langmuir linear regression (b) for ATRP 1, 3 and 5 h Bis-P-co-HPMA modified membranes.

The maximum binding capacities obtained are about 9.9, 10.6 and 12.4 mg/mL for

ATRP 1, 3 and 5 h Bis-P-co-HPMA modified membranes respectively indicating longer polymer chains possessing higher capacity for lysozyme binding. This also agrees with our XPS data with higher P_{2s} and P_{2p} peaks observed at longer ATRP times indicating more Bis-P residues being incorporated. As a result, the longer copolymer chains synthesized have more binding sites for lysozyme thus higher capacity. However, it seems that the difference in binding capacities between ATRP 1 and 3 h is smaller than that between ATRP 3 and 5 h. This is in agreement with the DG values and XPS peak intensities at various ATRP times. As mentioned earlier, this is probably due to that fact that the ratio of Bis-P over HPMA monomers increases as a function of ATRP time. The initial polymer growth is likely to be dominated by the polymerization of HPMA as Bis-P is more difficult to polymerize[11]. As time goes on, the reduced HPMA concentration leads to more availability of Bis-P for polymerization resulting in more incorporation of Bis-P in the polymer towards longer polymerization time.

Table 2.1 The fitting parameters obtained based on Langmuir linear regression for lysozyme binding to three different Bis-P-co-HPMA modified membranes.

	ATRP-1 h	ATRP-3 h	ATRP-5 h
Binding Capacity q_{max} (mg/mL)	9.9	10.6	12.4
Binding Constant K (M^{-1})	1.3×10^6	0.8×10^6	1.3×10^6
Binding Free Energy ΔG (kJ/mol)	-35	-34	-35

The binding constants for ATRP 1 h, 3 h and 5 h modified samples are in the order of $\sim 10^6$ (M^{-1}), similar to previous results[9] using UV initiated free radical polymerization reaction. This indicates that the binding mechanism for lysozyme interaction with Bis-P-co-HPMA ligands immobilized on membrane substrate is similar irrespective whether the polymer is synthesized via ATRP or UV-initiated polymerization. The binding capacities

obtained are in the range between 10-12 mg/mL for the three ATRP times investigated. The

longer the ATRP time is, the higher the capacity becomes. This seems to indicate that the

longer polymer ligands which incorporate more Bis-P residues have more binding sites for

the protein. The binding capacities obtained here are much higher than the ones for the

copolymer ligands grafted on PET membranes using UV polymerization reaction, which are

all around 2 mg/mL. This 5-fold increase in binding capacity is significant and can be due to

several possible reasons. Firstly, the regenerated cellulose MF membranes have a higher

porosity than the PET membranes. Therefore more surface areas are available for grafting

copolymer ligands leading to more binding sites for lysozyme protein. However, the

estimated DG values ($\sim$2 ug/cm^2) for PET membranes are larger than the corresponding DG

values ($\sim$0.5 ug/cm^2) obtained here for poly (Bis-P-co-HPMA) modified membranes. More

recent work by Schwark and coworkers[11, 48] for various Bis-P copolymers grafted on

regenerated cellulose membranes using UV initiated polymerization indicate that DG values

are at around 0.2 ug/cm^2 only. Their maximum binding capacity is roughly about 2 mg/mL

similar to their PET membranes. Therefore the significant increase in binding capacity using

ATRP polymerization is probably not due to the more available surface area in the cellulose

membranes. This points to another more probable reason that ATRP is more efficient in

incorporating Bis-P leading to more binding sites available on each copolymer ligand. This

becomes more evident when comparing the DG values and binding capacities for ATRP and

UV initiated polymerization reactions on regenerated cellulose membrane substrate. For

ATRP, DG value of around 0.6 μg/cm^2 can be reached at 5 h ATRP time whereas it can only

reach 0.2 μg/cm^2 for poly (Bis-P-co-HPMA) with UV polymerization. Moreover, the

maximum lysozyme binding capacity reaches 10 mg/mL with ATRP whereas only 2 mg/mL

was obtained for UV. The superior binding capacity obtained using ATRP is not unexpected

since ATRP reaction is much slower than UV that allows free radicals requiring higher

barriers to create to be incorporated. On the other hand, the fast UV polymerization will favor polymerization of lower barrier free radicals. Evidently, ATRP polymerization is a preferred scheme to achieve higher binding capacity for grafting poly (Bis-P-co-HPMA) on surfaces with potential application as membrane chromatography.

In addition, we are able to synthesize poly (Bis-P), poly (Mono-P) homopolymers as well as poly (Mono-P-co-HPMA) using ATRP at the same condition for synthesizing poly (Bis-P-co-HPMA). However, the binding capacity for poly (Bis-P) is extremely low (result not shown here) even though there are plenty of binding sites available on the polymer chain. The binding capacities for poly (Mono-P) as well as poly (Mono-P-co-HPMA) are also low, even though the DG reaches 1.61 ug/cm^2 for poly (Mono-P) modified membrane (ATRP 6 h, two times higher initiator concentration used) and 0.77 μg/cm^2 for poly (Mono-P-co-HPMA) (ATRP 4 h, the same initiator concentration used as before).

Our results indicate that the presence of HPMA residue (or potentially other residues as well) is necessary for the effective binding between lysozyme and polymer ligand. This is probably due to the fact that Bis-P has a conjugated ring structure thus more rigid making it difficult to topologically fit the protein surface without the more flexible spacer monomer. The incorporation of HPMA makes the copolymer more flexible and binds more effectively with the protein surfaces. In addition, it seems that both phosphonate groups on the Bis-P monomer are also needed in order to have strong affinity with lysozyme. Our classical MD simulation results indicate that H-bonds are formed not only between the amino acids on lysozyme surface and Bis-P, but also between amino acids and HPMA residues indicating the important role HPMA plays in protein-ligand interaction here. Our MD simulations further demonstrate that H-bonds form and break at ps time scale. The presence of both phosphonate arms enables the formation of at least one H-bond between Bis-P and Arg or some other

amino acid residues on lysozyme surface at all times. More on binding mechanism will be discussed in the MD simulations section.

2.4.3 Dynamic Binding Results

Table 2.2 Dynamic binding capacity, recovery and mass balance for unmodified and poly (Bis-P-co-HPMA) modified membranes at lysozyme concentration 0.1 mg/mL and flow rate 2 mg/ml. The mean values and standard deviations are determined with three measurements.

Membrane Condition	Binding Capacity (mg/mL)	Recovery	Mass Balance
Unmodified Membrane	1.78 ±0.08	89.9 ±2.7%	99.1 ±0.2%
Poly (Bis-P-co-HPMA) modified at ATRP 1 h	4.00 ±0.10	88.8 ±3.6%	98.9 ±0.9%
Poly (Bis-P-co-HPMA) modified at ATRP 3 h	3.32 ±0.06	84.5 ±4.8%	98.8 ±0.2%
Poly (Bis-P-co-HPMA) modified at ATRP 5 h	3.95 ±0.23	91.9 ±2.1%	98.1 ±0.7%

Table 2.2 shows lysozyme dynamic binding data for unmodified and poly (Bis-P-co-HPMA) modified membranes. In contrast to static binding results, it is interesting to see that the dynamic binding capacity of ATRP 1 h modified membrane has a slightly higher binding capacity than ATRP 5 h modified membranes at 4.0 mg/mL. Static binding can be considered an equilibrium process so that the total number of binding sites correlated to the incorporated Bis-P residues in the copolymer ligand determines the maximum binding capacity. However, in the dynamic mode, besides the total number of binding sites, the composition and conformation of the ligand are also critical. The driving force for the static binding is the thermodynamics of the protein-ligand interaction free energy. On the other hand, dynamic binding is also strongly affected by the kinetics and the barrier to reach the binding sites. As a result, the locations of the binding sites affect significantly the dynamic binding capacity. The easily accessible sites will contribute to the binding whereas those less exposed sites will be

difficult for lysozyme to reach and not contribute to the dynamic binding capacity. For the ATRP 1 h modified membrane, the Bis-P residues are likely located at or near the surface, and therefore they are readily available for lysozyme binding. However, as the ATRP time increases, those sites are likely buried deeper and deeper and the barrier becomes higher to reach those sites. Besides the location of the binding sites, the composition and flexibility of the copolymer ligands may also play an important role in the dynamics binding interactions. Interestingly, the ATRP 3 h modified membrane has a slightly lower binding constant than the ATRP 1 h and 5 h modified membranes as shown in the static binding results, this membrane also shows a slight lower dynamics binding capacity and earlier breakthrough as shown in Figure 2.6a. The elution curves are also shown in Figure 2.6b. The breakthrough time is very similar for ATRP 1 h and 5 h modified samples but ATRP 3 h modified membrane has an early breakthrough. Thus elution peak showing the eluted amount of lysozyme follows the order: ATRP 5 h > ATRP 1 h > ATRP 3 h. The recovery of the bound lysozyme is around 84%-90%, which indicates that binding interaction is mostly reversible. Both the static and dynamic binding results show that ATRP 3 h modified membrane has consistent lower binding constant, lower dynamic binding capacity and lower recovery compared to the other two membranes. It seems that the monomer composition and conformation of the copolymer ligand affects strongly the binding affinity as well as the dynamics binding behavior.
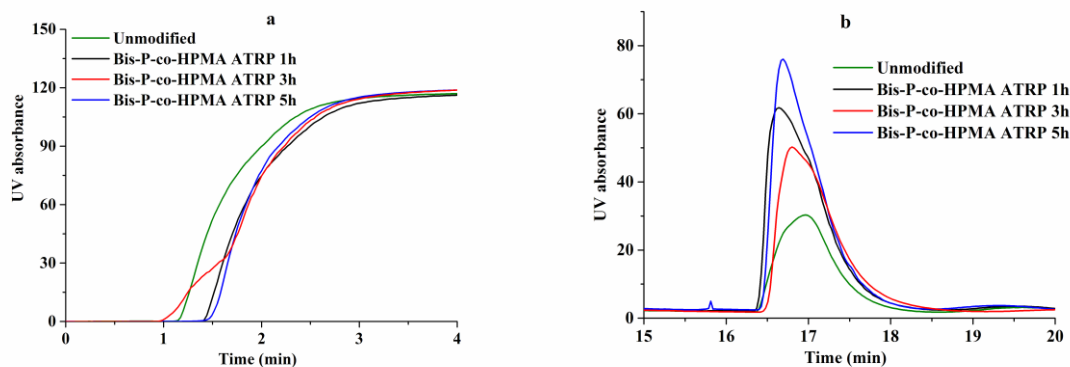
Figure 2.6 Breakthrough (a) and elution curves (b) at lysozyme loading and elution rate 2 mL/min for unmodified membranes, poly (Bis-P-co-HPMA) modified membranes at ATRP time 1, 3 and 5 h respectively.

2.4.4 Binding Interactions from Classical MD Simulations

In order to elucidate the interaction mechanism between lysozyme and poly (Bis-P-co-HPMA) and further optimize binding capacity, all atom classical MD simulations were conducted for one lysozyme interacting with a copolymer ligand consisting of 14 monomers of Bis-P and 56 monomers of HPMA. Each Bis-P residue is evenly spaced and separated by 4 HPMA residues. A total of over 900 ns simulations were conducted at neutral pH and room temperature under NPT. Figure 2.7 shows the interaction energies between lysozyme and the copolymer ligand during the simulation period. A dielectric constant of 4[49] was used to determine the electrostatic interaction energy. Earlier studies[50, 51] indicate dielectric constant is different for different materials and 4 is appropriate for protein interactions in aqueous solution. It can be seen that both electrostatic and *van der Waals* interaction energies become more negative as simulation time increases indicating that the interaction becomes stronger as time goes on. It can also be seen that both electrostatic and *van der Waals* interaction energies follow the same trend since both are sensitive to the separation distances between lysozyme and the copolymer ligand. It is also clear that *van der Waals* interaction contributes critically to the binding energy. This indicates that matching in topology that results in maximized *van der Waals* contact is indeed critically important in protein-ligand interactions.
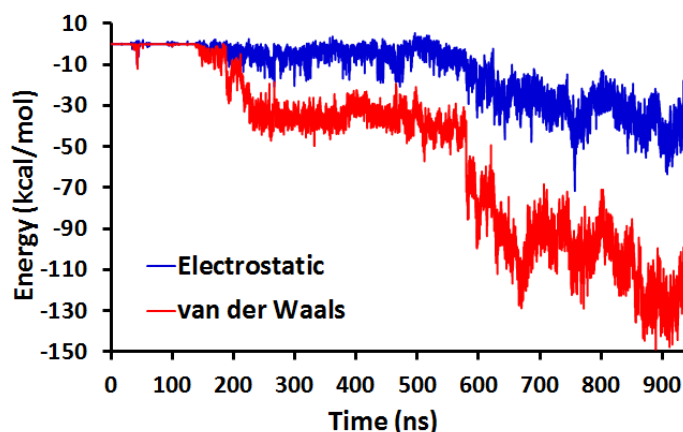
Figure 2.7 The Interaction energies between lysozyme and the copolymer in aqueous solution during the 940 ns simulation time.

In order to develop an effective membrane chromatography for protein separations, specific binding interaction between protein and ligand is necessary. It is known that *van der Waals* and electrostatic interactions are not specific thus not applicable for specific affinity separations. In order to achieve specific protein separations, specific binding interactions are required. Thus more specific interactions involving cation-π and the H-bond interactions are necessary. Figure 2.8(a-d) shows the conformational structures of the protein-copolymer ligand complex at 4 different simulation times. The light yellow shaded areas indicate H-bond interaction whereas the gray area in Figure 2.8(a) indicates cation-π interaction. Figure 2.8(a) exhibits the protein-coplymer ligand complex at around 625 ns. H-bonds between Bis-P and Arg, between Bis-P and Ser as well as between HPMA and Lys were observed. In addition, the positively charged Arg residue was found to interact with the aromatic Bis-P via cation-π interaction. During the simulation period, it was found that the H-bonds form and break at ps time scale continuously. Only occasional cation-π interaction was observed suggesting that it is not the dominant interaction mechanism. Figure 2.8(b-d) shows the protein-ligand complex at around 760, 809 and 915 ns respectively demonstrating multiple H-bond interactions. At longer simulation time, it appears that more H-bonds are being

formed. This agrees with the *van der Waals* and electrostatic interaction energy results suggesting that the protein-copolymer ligand complex is more tightly bound towards the end of the simulation time. In addition, it was found that only one of the phosphonate groups on Bis-P residue maintains H-bond interaction with one of the Arg residues on lysozyme surface persistently. However, our binding studies indicate that poly (Mono-P-co-HPMA) has only weak affinity towards lysozyme indicating that both phosphonate groups in Bis-P residues are necessary for high affinity binding. This is probably due to the enhanced binding interaction when H-bonds are continuously being formed in the case of poly (Bis-P-co-HPMA) ligand whereas H-bonds are intermittently formed in poly (Mono-P-co-HPMA) ligand. In addition, the presence of both phosphonate groups on Bis-P increases the hydrophilicity of the ligand rendering it more effective in binding to the hydrophilic residues on protein surface.
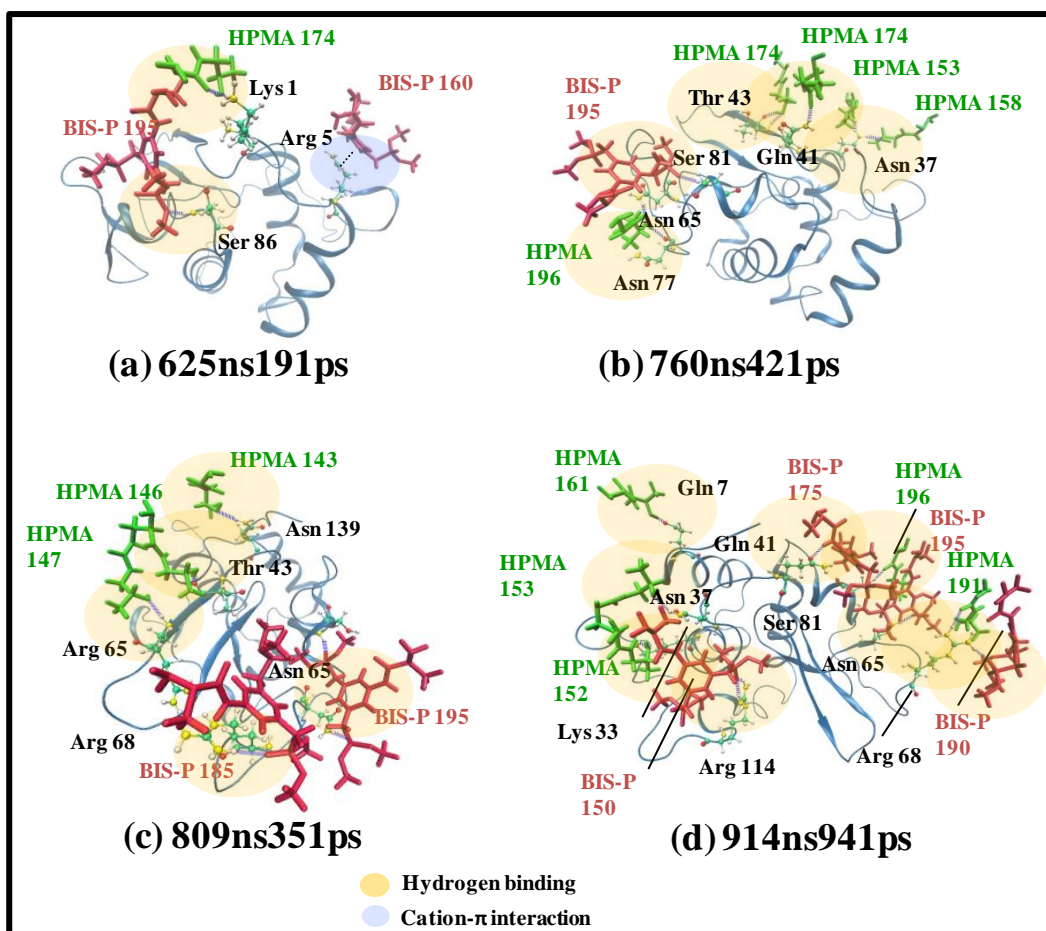
Figure 2.8 The protein-copolymer ligand complex at four different simulation times demonstrating the topological matching as well as more specific cation-   and hydrogen bonding interactions between lysozyme and copolymer ligand.

Figure 2.9a shows the average number of H-bonds formed between Bis-P and various amino acid residues on protein surface at 580-700 ns, 700-820 ns and 820-940 ns simulation period respectively. Different amino acid residues are represented by different colors in the legend. The corresponding color in the bar represents the average number of H-bonds formed between this amino acid type and the Bis-P residues in the copolymer. It can be seen that Arg and Asn have persistent H-bond interactions with Bis-P. However, besides Arg and Asn, other amino acid residues are also involved in the H-bond interaction with Bis-P and the frequency of the H-bond formation varies from time period to time period. At the last time period, Arg residues clearly dominate the H-bond interaction with Bis-P. Gln, which does not interact strongly with Bis-P during the first two time periods, appears to have

increased its interaction with Bis-P during the last simulation period. Nevertheless, it is clear that Bis-P selectively binds to positively charge Arg residues via H-bond. It is known that H-bond is significantly stronger when H donor is positively charged. The pair correlation functions between the O atoms in the phosphonate groups on Bis-P and the C atoms in the guadnium group on Arg during three simulation periods show that the interaction strength between Bis-P and the Arg increases as the simulation time increases. (See Appendix I)
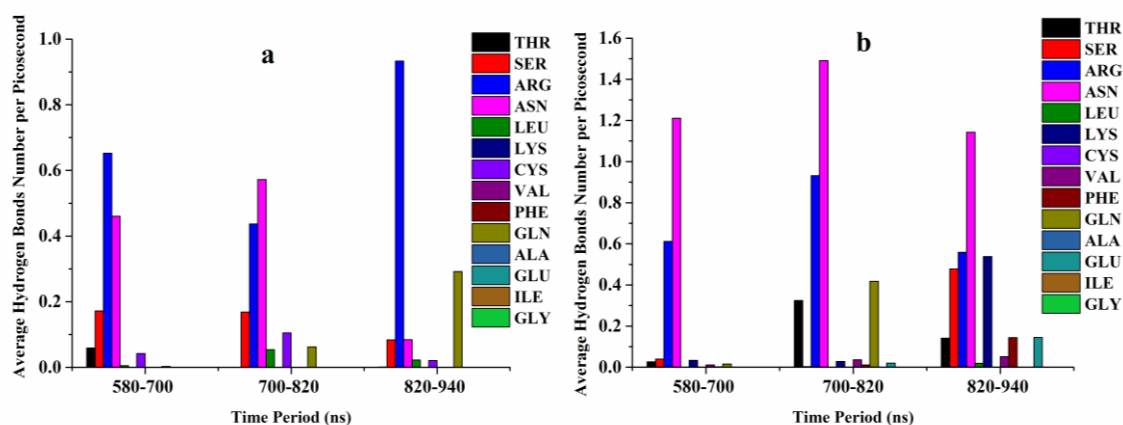
Figure 2.9 The average number of H-bonds formed between Bis-P residues (a) / HPMA (b) and various amino acids on lysozyme during three simulation periods at 580-700, 700-820 and 820-940 ns respectively.

Figure 2.9b shows the average H-bond numbers between HPMA residues on the copolymer and various amino acids on lysozyme during the same three simulation periods. It seems that both Arg and Asn residues form persistent H-bonds with HPMA similar to Bis-P with Asn dominating the interaction. The total number of H-bonds formed is higher with HPMA than with Bis-P since 4 times more HPMA residues are present in the copolymer. It also seems that HPMA only forms H-bond selectively with Arg and Asn during the first time period, but interacts with a number of other amino acids as the copolymer bound more tightly to the protein. This appears opposite to Bis-P where it more selectively binds to Arg residues largely.

2.5 Conclusions

Our work demonstrates that it is possible to graft synthetic polymeric ligands on UF membrane surfaces to selectively bind to the Arg rich proteins. Further we are able to show for the first time that these poly (Bis-P-co-HPMA) ligands can be synthesized using controlled ATRP reaction varying polymer chain length. Moreover, our results show that the more Bis-P monomers incorporated into the copolymer ligands, the higher the static binding capacity. Compared to the ligands previously grafted on PET membranes using UV initiated polymerization reactions, the capacity of our affinity membrane reaches 12 mg/mL, significantly higher than 2 mg/mL achieved before. Our dynamic binding results indicate that over 90% recovery can be achieved. The mechanism for poly (Bis-P-co-HPMA) binding to lysozyme protein was elucidated using classical MD simulations. H-bonding, *van der Waals*, electrostatic, as well as cation-π interactions all contributed to the specific binding interactions between lysozyme and the copolymer ligand. In particular our results show that the presence of both phosphonate groups as well HPMA are essential for achieving strong binding interactions.

Supporting Information Available: This material is available free of charge via the Internet at http://pubs.acs.org.

References

1.   Gottschalk, U. Downstream Processing of Monoclonal Antibodies: from High Dilution to High Purity. *Biopharm Int.* **2005,** *18*, 42-58.

2.   Specht, R.; Han, B.; Wickramasinghe, S. R.; Carlson, J. O.; Czermak, P.; Wolf, A.; Reif, O.-W. Densonucleosis virus purification by ion exchange membranes. *Biotechnol. Bioeng.* **2004,** *88* (4), 465-473.

3.   John Curling, U. G. Process Chromatography: Five Decades of Innovation. *BioPharm Int.* **2007,** *20* (10), 70-94.

4.   Fokkens, M.; Schrader, T.; Kläner, F.-G. A molecular tweezer for lysine and arginine. *J. Am. Chem. Soc.* **2005,** *127* (41), 14415-14421.

5.   Renner, C.; Piehler, J.; Schrader, T. Arginine- and lysine-specific polymers for protein recognition and immobilization. *J. Am. Chem. Soc.* **2005,** *128* (2), 620-628.

6.   Rensing, S.; Schrader, T. The first synthetic receptor for the RGD sequence. *Org. Lett.* **2002,** *4* (13), 2161-2164.

7.   Arendt, M.; Sun, W.; Thomann, J.; Xie, X.; Schrader, T. Dendrimeric bisphosphonates for multivalent protein surface binding. *Chem.Asian J.* **2006,** *1* (4), 544-554.

8.   Koch, S. J.; Renner, C.; Xie, X.; Schrader, T. Tuning linear copolymers into protein-specific hosts. *Angew. Chem. Int. Ed.* **2006,** *45* (38), 6352-6355.

9.   He, D.; Sun, W.; Schrader, T.; Ulbricht, M. Protein adsorbers from surface-grafted copolymers with selective binding sites. *J. Mater. Chem.* **2009,** *19* (2), 253-260.

10.   Tominey, A. F.; Liese, J.; Wei, S.; Kowski, K.; Schrader, T.; Kraft, A. RAFT polymers for protein recognition. *Beilstein J. Org. Chem.* **2010,** *6*, 66.

11.   Schwark, S.; Ulbricht, M. Toward protein-selective membrane adsorbers: A novel surface-selective photo-grafting method. *Eur. Polym. J.* **2012,** *48* (11), 1914-1922.

12.   Soga, O.; van Nostrum, C. F.; Hennink, W. E. Poly(N-(2-hydroxypropyl) methacrylamide mono/dii lactate): A new class of biodegradable polymers with tuneable thermosensitivity. *Biomacromolecules* **2004,** *5* (3), 818-821.

13.   Zheng, Z.-B.; Zhu, G.; Tak, H.; Joseph, E.; Eiseman, J. L.; Creighton, D. J. N-(2-hydroxypropyl)methacrylamide copolymers of a glutathione (GSH)-activated glyoxalase I inhibitor and DNA alkylating agent: synthesis, reaction kinetics with GSH, and in vitro antitumor activities. *Bioconjugate Chem.* **2005,** *16* (3), 598-607.

14.   Sudre, G.; Hourdet, D.; Cousin, F.; Creton, C.; Tran, Y. Structure of surfaces and interfaces of poly(N,N-dimethylacrylamide) hydrogels. *Langmuir* **2012,** *28* (33), 12282-12287.

15.   Chen, R.; Benicewicz, B. C. Preparation and properties of poly(methacrylamide)s containing oligoaniline side chains. *Macromolecules* **2003,** *36* (17), 6333-6339.

16.   Scales, C. W.; Vasilieva, Y. A.; Convertine, A. J.; Lowe, A. B.; McCormick, C. L. Direct, controlled synthesis of the nonimmunogenic, hydrophilic Polymer, poly(N-(2-hydroxypropyl)methacrylamide) via RAFT in aqueous media. *Biomacromolecules* **2005,** *6* (4), 1846-1850.

17.   Apostolovic, B.; Klok, H.-A. Copolymerization behavior of N-(2-hydroxypropyl)methacrylamide and a methacrylated coiled-coil peptide derivative. *Biomacromolecules* **2010,** *11* (7), 1891-1895.

18.   Luo, K.; Yang, J.; Kopečková, P.; Kopeček, J. i. Biodegradable multiblock poly[N-(2-hydroxypropyl)methacrylamide] via reversible addition−fragmentation chain transfer polymerization and click chemistry. *Macromolecules* **2011,** *44* (8), 2481-2488.

19.   Treat, N. J.; Smith, D.; Teng, C.; Flores, J. D.; Abel, B. A.; York, A. W.; Huang, F.; McCormick, C. L. Guanidine-containing methacrylamide (co)polymers via RAFT: toward a cell-penetrating peptide mimic. *ACS Macro Letters* **2011,** *1* (1), 100-104.

20.   Qin, Z.; Liu, W.; Li, L.; Guo, L.; Yao, C.; Li, X. Galactosylated N-2-hydroxypropyl methacrylamide-b-N-3-guanidinopropyl methacrylamide block copolymers as hepatocyte-targeting gene carriers. *Bioconjugate Chem.* **2011,** *22* (8), 1503-1512.

21.   Pan, K.; Zhang, X.; Ren, R.; Cao, B. Double stimuli-responsive membranes grafted with block copolymer by ATRP method. *J. Membr. Sci.* **2010,** *356* (1–2), 133-137.

22.   Gao, G.; Yu, K.; Kindrachuk, J.; Brooks, D. E.; Hancock, R. E. W.; Kizhakkedathu, J. N. Antibacterial surfaces based on polymer brushes: investigation on the influence of brush properties on antimicrobial peptide immobilization and antimicrobial activity. *Biomacromolecules* **2011,** *12* (10), 3715-3727.

23.   Wever, D. A. Z.; Raffa, P.; Picchioni, F.; Broekhuis, A. A. Acrylamide homopolymers and acrylamide–N-isopropylacrylamide block copolymers by atomic transfer radical polymerization in water. *Macromolecules* **2012,** *45* (10), 4040-4045.

24.   Kim, K.; Choi, S.-y.; Jeon, H.; Lee, J.; Choo, D.; Kim, J.; Kang, Y.; Yoo, H.-O. Synthesis of new pH-sensitive amphiphilic block copolymers and study for the micellization using a fluorescence probe. *Macromol. Res.* **2008,** *16* (2), 169-177.

25.   Teodorescu, M.; Matyjaszewski, K. atom transfer radical polymerization of (meth)acrylamides. *Macromolecules* **1999,** *32* (15), 4826-4831.

26.   Teodorescu, M.; Matyjaszewski*, K. Controlled polymerization of (meth)acrylamides by atom transfer radical polymerization. *Macromol. Rapid Commun.* **2000,** *21* (4), 190-194.

27.   Chenette, H. C. S.; Robinson, J. R.; Hobley, E.; Husson, S. M. Development of high-productivity, strong cation-exchange adsorbers for protein capture by graft polymerization from membranes with different pore sizes. *J. Membr. Sci.* **2012,** *423–424* (0), 43-52.

28.   Bhut, B. V.; Husson, S. M. Dramatic performance improvement of weak anion-exchange membranes for chromatographic bioseparations. *J. Membr. Sci.* **2009,** *337* (1–2), 215-223.

29.   Himstedt, H. H.; Qian, X.; Weaver, J. R.; Wickramasinghe, S. R. Responsive membranes for hydrophobic interaction chromatography. *J. Membr. Sci.* **2013,** *447* (0), 335-344.

30.   Du, H. B.; Wickramasinghe, R.; Qian, X. H. Effects of Salt on the Lower Critical Solution Temperature of Poly (N-Isopropylacrylamide). *J. Phys. Chem. B* **2010,** *114* (49), 16594-16604.

31.   Du, H. B.; Qian, X. H. Molecular Dynamics Simulations of PNIPAM-co-PEGMA Copolymer Hydrophilic to Hydrophobic Transition in NaCl Solution. *J. Polym. Sci., Part B: Polym. Phys.* **2011,** *49* (15), 1112-1122.

32.   Du, H.; Wickramasinghe, S. R.; Qian, X. Specificity in Cationic Interaction with Poly(N-isopropylacrylamide). *J. Phys. Chem. B* **2013,** *117* (17), 5090-5101.

33.   Himstedt, H. H.; Du, H.; Marshall, K. M.; Wickramasinghe, S. R.; Qian, X. pH Responsive Nanofiltration Membranes for Sugar Separations. *Ind. Eng. Chem. Res.* **2013,** *52* (26), 9259-9269.

34.   Phillips, J. C.; Braun, R.; Wang, W.; Gumbart, J.; Tajkhorshid, E.; Villa, E.; Chipot, C.; Skeel, R. D.; Kale, L.; Schulten, K. Scalable molecular dynamics with NAMD. *J. Comput. Chem.* **2005,** *26* (16), 1781-1802.

35.   Frisch, M. J.; Trucks, G. W.; Schlegel, H. B.; Scuseria, G. E. Gaussian 09, Revision C.01, Gaussian, Inc., Wallingford CT, 2010.

36.   Wang, J. M.; Cieplak, P.; Kollman, P. A. How well does a restrained electrostatic potential (resp) model perform in calculating conformational energies of organic and biological molecules? *J. Comput. Chem.* **2000,** *21* (12), 1049-1074.

37.   Wang, J. M.; Wolf, R. M.; Caldwell, J. W.; Kollman, P. A.; Case, D. A. Development and testing of a general amber force field. *J. Comput. Chem.* **2004,** *25* (9), 1157-1174.

38.   AMBER tools 12 manual. Available at: http://ambermd.org/doc12/AmberTools12.pdf.

39.   Case, D. A.; Cheatham, T. E.; Darden, T.; Gohlke, H.; Luo, R.; Merz, K. M.; Onufriev, A.; Simmerling, C.; Wang, B.; Woods, R. J. The Amber biomolecular simulation programs. *J. Comput. Chem.* **2005,** *26* (16), 1668-1688.

40.   Weiss, M. S.; Palm, G. J.; Hilgenfeld, R. Crystallization, structure solution and refinement of Hen Egg-White Lysozyme at pH 8.0 in the presence of MPD. *Acta Crystallogr., Sect D: Biol. Crystallogr.* **2000,** *56*, 952-958.

41.   Jorgensen, W. L.; Chandrasekhar, J.; Madura, J. D.; Impey, R. W.; Klein, M. L. Comparison of simple potential functions for simulating liquid water. *J. Chem. Phys.* **1983,** *79* (2), 926-935.

42.   Joung, I. S.; Cheatham, T. E., III. Determination of alkali and halide monovalent ion parameters for use in explicitly solvated biomolecular simulations. *J. Phys. Chem. B* **2008,** *112* (30), 9020-9041.

43.   Martyna, G. J.; Tobias, D. J.; Klein, M. L. Constant pressure molecular dynamics algorithms. *J. Chem. Phys.* **1994,** *101* (5), 4177-4189.

44.   Feller, S. E.; Zhang, Y. H.; Pastor, R. W.; Brooks, B. R. Constant pressure molecular dynamics simulation: the Langevin piston method. *J. Chem. Phys.* **1995,** *103* (11), 4613-4621.

45.   Darden, T.; York, D.; Pedersen, L. Particle mesh Ewald: An N-log(N) method for Ewald sums in large systems. *J. Chem. Phys.* **1993,** *98* (12), 10089-10092.

46.   Essmann, U.; Perera, L.; Berkowitz, M. L.; Darden, T.; Lee, H.; Pedersen, L. G. A smooth particle mesh Ewald method. *J. Chem. Phys.* **1995,** *103* (19), 8577-8593.

47.   Miyamoto, S.; Kollman, P. A. Settle: An analytical version of the SHAKE and RATTLE algorithm for rigid water models. *J. Comput. Chem.* **1992,** *13* (8), 952-962.

48.   Schwark, S. Antikörper-selektive materialien für die produkt aufreinigung: gepfropfte PET- und cellulose-basierte makroporöse membranadsorber. *Dissertation* **2013**.

49.   Li, L.; Li, C.; Zhang, Z.; Alexov, E. On the Dielectric "constant" of proteins: smooth dielectric function for macromolecular modeling and its implementation in DelPhi. *J. Chem. Theory Comput.* **2013,** *9* (4), 2126-2136.

50.   Pohl, H. A. Giant polarization in high polymers. *J. Electron. Mater.* **1986,** *15* (4), 201-203.

51.   Maier, G. Low dielectric constant polymers for microelectronics. *Prog. Polym. Sci.* **2001,** *26* (1), 3-65.

Chapter 3 The Effects of Salt Ions on Responsive Hydrophobic Interaction Membrane

Chromatography

This chapter is based on a submitted manuscript: Liu, Z.; Du, H.; Wickramasinghe, S.R.; Qian, X. The Effects of Salt Ions on Responsive Hydrophobic Interaction Membrane Chromatography. Langmuir, in review, 2016

Abstract

The lower critical solution temperature (LCST) of poly (vinylcaprolactam) (PVCL) is dependent on the salt type and salt concentration. PVCL grafted on the regenerated cellulose membranes has been used as a responsive hydrophobic interaction membrane (HIC) chromatography for protein separations in a bind-and-elute mode. Here systematic investigations were conducted to understand the effects of salt on the chromatographic behavior of this novel HIC responsive membrane system. Dynamic binding capacities and recoveries of two proteins (IgG_4 and BSA) were determined at different pH, salt type and salt concentration at room temperature. In addition, the cationic effects on static binding were investigated with monovalent (Na^+, NH_4^+), divalent (Zn^{2+}) and trivalent (Al^{3+}) sulfate salt solutions. Variation of hydrophobicity for the PVCL modified membrane with Na_2SO_4 concentration measured by contact angle correlates well with the binding capacity and the performance of HIC.

3.1 Introduction

The past decade has seen the rapid development of upstream technology for biopharmaceuticals. As a consequence, the concentration of recombinant protein products has markedly increased from milligram per liter (mg/L) to grams per liter (g/L)[1]. At the same time, the regulatory agencies demand high purity of products, which greatly heightens the need for the dramatic improvement of efficiency in the downstream processing and

purification. The bottleneck has shifted from bio-processing to downstream purification of products[1, 2, 3]. To date, estimated cost for downstream processing can go as high as 50%-80% of the total manufacturing cost[2]. Therefore, one of the main objectives associated with the downstream processing is to reduce its cost while maintaining the high quality of the products.

Packed bed column chromatography has been widely used in downstream processing for purification of proteins, DNAs and other pharmaceutical products. However, one major drawback of the packed bed column chromatography is the slow pore diffusion which severely restricts its efficiency for separation. The diffusion of targeted products to the ligands on the chromatography is a slow process leading to the dramatic drop of binding capacity as the feed flow rate increases. Besides diffusion limitation, the packed bed chromatography also suffers from the requirement of large buffer consumption as well as extra packing and testing costs. An alternative is to use adsorptive membrane chromatography during downstream processing[4, 5]. Adsorptive membranes, known as membrane adsorbers, are macroporous membranes functionalized by specific ligands attached on the membrane pore surface. Membrane adsorbers represent a class of liquid-solid membrane contactor and have been used extensively in a flow-through mode[6] to remove containments such as aggregates[7], viruses[8, 9] and DNAs[9, 10]. In recent years, there has been an increased interest in using adsorptive membranes in a bind-and-elute mode for protein separation[11, 12, 13, 14, 15, 16, 17]. In contrast to column-based chromatography, the convective flow dominates the transport of targeted products to the ligands due to the open pore structure of the membranes. Consequently, studies show that the membrane binding capacity is independent of a wide range of flow rate[16, 17, 18]. Moreover, the operation can be performed at relatively low pressure, which reduces protein denaturation and aggregation. Finally, the

membrane system is easier to scale up and the cost of packing and testing is subsequently reduced significantly.

Hydrophobic interaction chromatography (HIC) plays an import role in downstream processing. The targeted proteins bind to hydrophobic ligands under high salt concentration buffers and elute at low salt concentration buffers. At high salt concentrations, aqueous surface tension increases leading to the more favorable hydrophobic interaction. Moreover, enhanced charge screening at high salt concentration leads to the reduced electrostatic interaction further promoting hydrophobic interaction. On the contrary, low salt concentration reduces surface tension thus weakens hydrophobic interaction leading to the dissociation of the protein and ligand. This unique high-salt binding and low-salt elution enables HIC to be used in the intermediate purification steps, following salt-precipitation, ion-exchange or affinity-based adsorption purification steps. N-alkyl (C_1-C_8) and aryl (phenyl) are the two most common ligand types for HIC. Compared to reverse phase chromatography, HIC ligands are considered to be mildly hydrophobic, which ensures the eluted proteins to be biologically active. The factors that affect HIC behavior have been extensively studied with different salt buffer type and concentration[19, 20, 21, 22, 23, 24]. Hofmeister series refers to the specific ion interactions with proteins and polymer[25, 26, 27, 28]. Theoretical models based on solvophobic theory or preferential interaction theory were developed to quantitatively explain and predict the salt concentration effects on the chromatographic behaviors[29, 30, 31, 32, 33, 34, 35, 36]. Ion specificity remains to be a theoretical challenge in understanding the interactions between the salt ions and proteins or polymers. However, these models were used to explain the effects of salt on conventional hydrophobic interactions. Here our focus is on the effects of salt ions on the hydrophobic interaction based on thermo-responsive polymeric ligands.

Thermo-responsive polymer exhibits a lower critical solution temperature (LCST), above which the polymer adopts a collapsed hydrophobic conformation. However, at a temperature

below its LCST, the polymer adopts an extended coil-like hydrophilic conformation. The presence of the salt tends to reduce the transition temperature. The reduction of LCST is found to be strongly dependent on the salt type and salt concentration. The higher the concentration is, the larger the reduction is. It is also ion specific with cations and anions each following a different order depending on the ionic charge and size. Our earlier studies[37, 38, 39] investigating the specific interactions of ions with poly (N-isopropylacrylamide) (PNIPAM) show that the cations interact directly with the amide O and anionic interaction the polymer is mediated by the cations even though larger size anions form hydrophobic interaction with the isopropyl group. The LCST of PNIPAM is about 32°C in water and about 20°C in 1 M NaCl. It only depends slightly on the molecular weight of the polymer chain. Besides PNIPAM, poly (N-vinylcaprolactam) (PVCL) is also a thermo-responsive polymer. However, the LCST of PVCL depends strongly on the polymer molecular weight and concentration. For very dilute PVCL concentrations, the LCST of PVCL varies from about 32°C for long polymer chains to over 50°C for short chains. Both polymers are biocompatible and are being investigated for a variety of biomedical applications e.g. drug delivery.

Recently there is a growing interest in developing HIC membrane adsorbers for protein separations[40, 41, 42, 43, 44, 45, 46]. These HIC membrane adsorbers possess the advantages of membrane chromatography and perform protein purification based on the HIC principles. Sartobind® Phenyl membrane adsorbers (*Sartorius Stedim Biotech*) were the first commercialized HIC membrane adsorbers that can be used in the protein capture and polishing step to remove denatured protein aggregates. HIC membranes have been also developed for protein fractionation[41, 47, 48, 49, 50] and preparative protein purification[42, 43, 44, 51]. The disadvantages of traditional HIC membrane chromatography are its low capacity and low recovery. The capacity for these HIC ligands is only around 10-15 mg/mL significantly lower than the over 100 mg/mL capacity for the ion-exchange based ligands. Conventional

hydrophobic ligands tend to denature protein leading to irreversible binding the proteins as well as protein aggregation. On the other hand, thermo-responsive polymers possessing both hydrophobic and hydrophilic residues are only moderately hydrophobic. The hydrophobic-to-hydrophilic transition can be switched by reducing the temperature and/or salt concentration. Since the binding and elution of the proteins are based on the conformational switching of the thermo-responsive ligands, relative high recovery of the proteins is expected. Among these HIC membrane adsorbers, high recovery and high resolution for protein purification are achieved. [43, 52, 53, 54, 55] In order to further develop responsive HIC membrane chromatography for biotechnological applications, maximizing its capacity and investigating the effects of salt ions on its binding and elution are crucially important.

In addition to salt concentration, salt ion type also plays a critical role in HIC. The microcalorimetric studies show the binding process involves the dehydration of both protein and ligand, structural change of protein and rearrangement of excluded water in the bulk solution[56]. Salt ion type effect on HIC has been studied extensively by protein retention experiments[19, 20, 21, 22, 23, 24]. It has been shown that the effects of different ions on protein binding correlate with the Hofmeister series[24, 30]. Hofmeister series refers to the different ability of different ions to denature protein[25]. Cations and anions have their respective orders. The direct Hofmeister series for the anions follows the order $PO_4^{3-}> SO_4^{2-}> CH_3COO^->$ $Cl^-> Br^-> NO^{3-}> I^-> ClO^{4-}> SCN^-$. For the cations, the order follows $NH_4^+> K^+> Na^+> Li^+>$ $Mg^{2+}> Ca^{2+}$ [26, 27, 57]. Ions on the left side generally have greater ability to decrease the solubility of hydrocarbon (salting-out), promote hydrophobic interaction as well as stabilize proteins. However, inverse Hofmeister effects have also been observed[58, 59]. It was thought that the ion order depends on both the surface hydrophobicity and surface polarity[60]. So far, the exact nature of ion specificity on physical and biological phenomena remains unexplained and under considerable debate. It is not sure whether it is caused by the changes in the bulk

water structure in different salt solutions or by the direct ion-protein interactions. Based on the Hofmeister effect, Cramer et.al has successfully modeled the HIC adsorption isotherm[22], investigated the protein selectivity in HIC[61], HIC retention behaviors[62, 63] and pH effects in HIC[64].

Hofmeister series has been related to the LCST decrease of thermo-responsive polymers as well[37, 65]. As mentioned, our earlier studies[37, 38, 39] on the effects of salt ions on PNIPAM using classical molecular (MD) simulations demonstrate that the presence of ions and their hydration tend to decrease the LCST whereas the direct cation–amide O binding tends to increase the LCST. The strength of the cation–amide O interaction is dictated by the competition between the electrostatic and the hydration forces. For the singly charged alkali cations (Li^+, Na^+, K^+ and Rb^+), electrostatic interactions dominate. The larger the cation is, the weaker the binding interaction with the amide O. For the doubly charged cations (Mg^{2+} and $Ca^{2+)}$, the strong hydration of these divalent ions overcomes the electrostatic attraction leading to the very weak binding between the cations and the amide O. Moreover, our simulation results show that the LCST transition dynamics and the degree of hydration/dehydration are ion specific. Experimentally, responsive HIC membrane chromatography using PNIPAM and its copolymers as ligands shows relatively low capacity and recovery. The PVCL ligands grafted on the regenerated cellulose membranes using atom-transfer radical polymerization exhibit both higher capacity and higher recovery than the PNIPAM ligands. Our results show effective binding of BSA and IgG_4 in the high salt buffer (1.8 M $(NH_4)_2SO_4$) solution. High recovery (over 97%) of BSA was also obtained at an appropriate ligand density. In addition, our results show that binding capacity tends to increase with the increase of the polymer chain length and chain density as well as the salt concentration at binding. Here we investigate the effects of salt type and salt concentration on dynamic/static binding capacity and recovery of the responsive membranes grafted with

106

PVCL ligands. Moreover, the effects of pH on binding capacity and recovery are also studied.

3.2 Materials

N-Vinylcaprolactam (98%), 2-Bromo-2-methylpropionyl bromide (BIB, 98%), 4-(dimethylamino) pyridine (DMAP, ≥99%), copper (I) chloride (≥99.995%), copper (II) chloride (≥99.995%) and N,N,N′,N″,N″-pentamethyldiethylenetriamine (PMDETA, 99%) were purchased from Sigma Aldrich (St. Louis, MO). Triethylamine (TEA, ≥99%) and aluminum sulfate (≥97%) were obtained from Alfa Aesar (Ward Hill, MA). Methanol (99.8%) ,acetonitrile (99.8%) and zinc sulfate heptahydrate (≥99.5%) were obtained from EMD Chemicals (Billerica, MA). Boric anhydride was purchased from Avantor Performance Materials (Center Valley, PA). Anhydrous acetonitrile was obtained by distilling acetonitrile with boric anhydride. Sodium chloride (≥99.5%), ammonium sulfate (≥99.0%) and sodium sulfate (≥99.0%) were bought from Macron™ Fine Chemicals (Center Valley, PA). Regenerated cellulose membranes (0.45 μm pore size, RC55, 47mm diameter) were purchased from Whatman Ltd. (Pittsburgh, PA). Bovine serum albumin (BSA) (>99 %, pI 4.7, 66 kDa) was obtained from Avantor Performance Materials (Center Valley, PA). Purified human IgG$_4$ monoclonal antibody (pI 7.1, 146 kDa) was provided by Eli Lilly (Indianapolis, IN).

3.3 Experiments

3.3.1 Membrane Surface Modification

Membranes were modified through surface-initiated ATRP as previously reported by our earlier studies[46, 66, 67, 68]. Basically, regenerated cellulose (RC) membranes were first immobilized with ATRP initiator 2-bromoisobutyryl bromide (80 mM) in acetonitrile for 3 hours. Then the monomer, copper (I) chloride, copper (II) chloride, ligand N, N,N′,N″,N″-

pentamethyldiethylenetriamine (PMDETA), and solvent, methanol/water mixture (1:1,v/v) were mixed together and degassed with argon for 15-20 min. The ratio among monomer: CuCl: CuCl$_2$: PMDETA is 200:1:0.2:2. Prior to polymerization reaction, flasks containing initiator immobilized membranes were de-oxygenated by vacuum and argon back-filling process three times. At last, the polymerization solution was transferred to the flask by a syringe. After 4 h ATRP, membranes were first rinsed with methanol and water mixture (1:1, v/v) three times and then washed with DI water for overnight. The schematic of the modification procedure is shown in Figure 3.1.
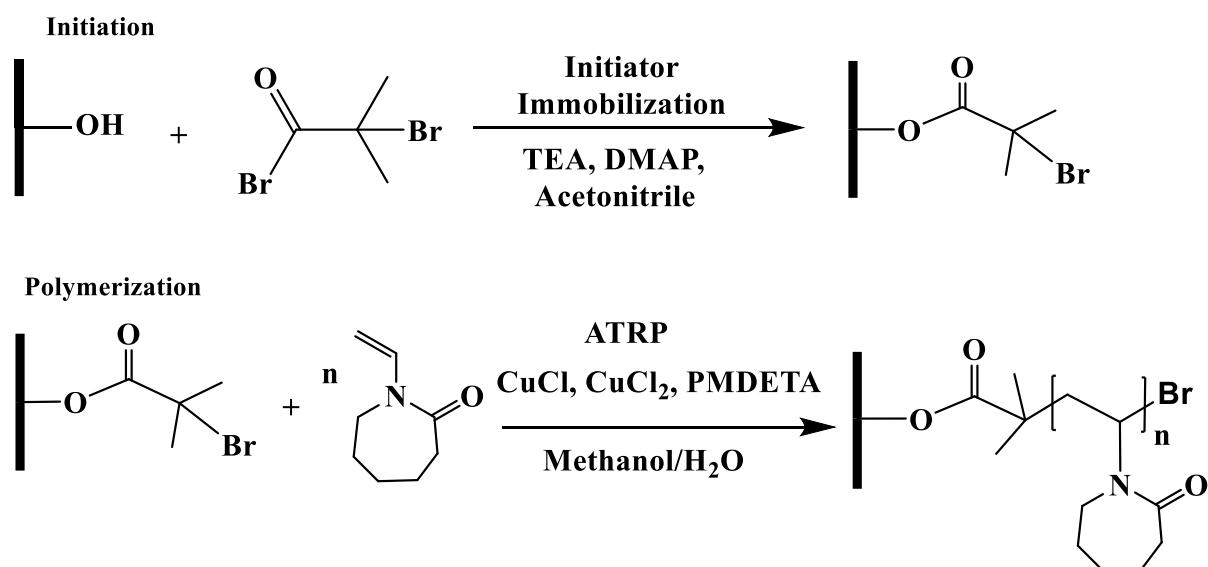
Figure 3.1 Reaction scheme of ATRP for surface modification of regenerated cellulose membranes.

3.3.2 Characterization

Turbidity Test The turbidity of solutions containing PVCL was determined using UV/Vis Spectrophotometer (Thermo Scientific™ GENESYS 10S) for measuring the transmittance at 515 nm. The previous protocol for determining the LCST of PVCL with turbidity change was used[69]. The change of solution turbidity indicates the LCST or the hydrophobic-to-hydrophilic transition of the PVCL polymers. The increase in turbidity indicates the polymers become hydrophobic and start to aggregate. All measurements were conducted at room temperature. The LCST transition is induced by the addition of various types and

concentrations of salt. The onset of the increased turbidity corresponds to the salt concentration for each salt type needed to decrease the LCST of PVCL to room temperature at which experiments were performed. The results further confirmed that LCST of PVCL depends strongly on salt type and salt concentration.

Contact Angle Measurement Measurements were conducted by the sessile drop method. The set up includes an optical angle meter (OCA 20, *Future Digital Scientific Corp.*, NY) and a dosing needle. Membranes were cut into small pieces and fixed on a flat glass chip with double side tape for measurements. The dosing volume is 2 μL. Each result was reported by averaging at least 5 measurements at random locations and the standard deviations were shown as error bars.

3.3.3 Protein Binding Experiments for HIC Membranes

Static BSA Binding Studies All membranes were first equilibrated with adsorption buffer A (contains various high concentrations of salt) for 1 hour. Then, certain concentrations of BSA solutions were prepared using buffer A. All equilibrated membranes were incubated with BSA solution for 5 hours at room temperature on a shaker. Also, five different concentrations of protein solutions prepared with BSA and buffer A were shaken at the same time. The equilibrium concentrations of protein solutions were first determined by UV absorbance at 280nm with the standard curves of protein solutions. For salt like $ZnSO_4$ and $Al_2(SO_4)_3$, no sodium phosphate was added in buffer due to precipitation. Binding capacity and recovery were calculated as follow:

$$\text{Binding capacity } \boldsymbol{q} = \frac{\text{Amount of protein bound to membrane (mg)}}{\text{membrane volume (mL)}}$$

$$\text{Recovery} = \frac{\text{Amount of protein Elute (mg)}}{\text{Amount of protein bound to membrane (mg)}}$$

Dynamic Binding Studies Bovine serum albumin (BSA) or human serum Immunoglobulin (IgG$_4$) stock solutions were prepared by dissolving 100 mg of proteins each into 10 mL 20 mM phosphate buffer solutions (pH 7, Buffer B), which contained no other salt. Then, the stock solutions of protein were added into buffers containing various amount of salt (Buffer A) to yield 0.1 mg/mL protein solutions. All the buffer and protein solutions were filtered with Whatman 0.22 μm PES membrane before the dynamics binding tests. A set of four membranes (total bed volume 0.08 mL) was loaded into a stainless steel flow cell (Mustang Coin ® module, Pall Corporation) with two flow distributers to ensure the uniform flow across all of the membranes. All runs were conducted by using ÄKTA FPLC from GE Healthcare Bio-Sciences Corp. The method was developed with the Unicorn software v. 5.31 to automate the BSA binding and elution experiments as previously published[66]. First, the membranes stack was wet with buffer B (elution buffer) in the reverse flow configuration over 5 minutes by increasing the flow rate from 0.2 mL/min to 1.0 mL/min in 0.2 mL/min increment. Next, the membrane stack was equilibrated in the forward flow configuration in the buffer A (adsorption buffer) at 1 mL/min for 10 minutes. Then 0.1 mg/mL protein solution was loaded onto the membrane stack at a flow rate of 1 mL/min for 10 minutes. Unbound protein was subsequently washed from the membranes using the buffer A (adsorption buffer) for 10 minutes at 1 mL/min, followed by a step change of running buffer B (elution buffer) through the membrane at 1 mL/min. The run ended when the UV absorbance at 280 nm becomes stable. The washing fraction (includes loading fraction) and elution fraction were collected and the volumes were determined accordingly. Protein concentrations in the sample solution, washing fraction, and elution fraction were calculated through UV absorbance at the wavelength of 280 nm.

3.4 Result and Discussion

3.4.1 Salt Effects on PVCL ligand

In order to study the effects of salt ions on the LCST of PVCL solutions, PVCL polymers are synthesized using free radical polymerization based on the protocol reported by Laukkanen et.al[70]. The successful polymerization was confirmed by H[1]NMR (Figure A2.1). The hydrodynamic diameters (D_h) of synthesized PVCL in aqueous solution at different temperatures were determined using dynamic light scattering (DLS) with a DelsaNano HC particle analyzer instrument (Beckman Coulter, Miami , FL) at a fixed scattering angle of 165 °. Results were processed by DelsaNano program (v.3.7) with CONTIN algorithm. Similar to the D_h results observed before[71], the increase in PVCL D_h is likely caused by the aggregation of PVCL when the temperature increases above LCST when it is hydrophobic. The LCST of our synthesized PVCL is around 37°C, shown by the DLS results (Figure A2.2). Previously reported PVCL synthesized by free radical polymerization has a LCST ranging from 30-50 °C, depending on the molecular weight[72].

Turbidity measurements were conducted to further investigate the effects of salt on the LCST of our synthesized PVCL in salt solutions. Similar to PNIPAM, earlier studies show that the presence of KCl decreases the LCST of PVCL[69]. Here, systematic studies were carried out to investigate the effects of salt type on the LCST of PVCL. Different sulfate salts were used for the investigation. Turbidity (transmittance) of PVCL solution was measured in monovalent (Na^+, NH_4^+), divalent (Zn^{2+}) and trivalent (Al^{3+}) sulfate salt solutions at room temperature of around 23°C. The impact of cations on the reduction of LCST was plotted as a function of the ionic strength (Figure 3.2a) and the activity (Figure 3.2b) of different salt solutions. Our results show that the impact of ions on the reduction of PVCL LCST follows: $Na^+ > NH_4^+ > Zn^{2+} > Al^{3+}$ based on nominal ionic strength or $Al^{3+} > Zn^{2+} > Na^+ > NH_4^+$ based on the ionic activity. Clearly the results based on activity should be more meaningful than the

ones based on nominal ionic strength since higher valence ions have a stronger tendency to associate with each other even though they have a higher degree of solvation. Moreover, it was observed earlier that Al^{3+} ion largely exists as $Al(OH)_4^-$ in aqueous solution forming a polymeric network[73, 74]. Based on the turbidity as a function of ionic activity as shown in Figure 3.2b, a reverse Hofmeister series is observed. This agrees with earlier studies on the effects of cations on the LCST of PNIPAM[75]. It is worthwhile to point out that PVCL/PNIPAM and proteins are quite different as proteins generally contain multiple charged residues whereas PVCL/PNIPAM do not have net charges. Our earlier studies[37, 38, 39] show that monovalent cations bind directly with the amide O on PNIPAM whereas anions interact indirectly with the hydrophobic residues on the polymer. The interaction strength is modulated by the competition between the favorable electrostatic interaction and the unfavorable dehydration force. Our earlier studies[37, 38, 39] further show that divalent ions actually do not bind directly or only bind weakly with the amide O. Clearly the unfavorable dehydration force is dominant for the higher valence ions as they typically have significant hydration free energy. Here the trivalent and to a great extent the divalent ions do not bind with the amide O directly. Instead, these ions lead to a higher surface tension due to the stronger solvation free energy which in turn stabilizes the hydrophobic conformation of the polymer leading to an enhanced reduction in LCST. The NH_4^+ and Na^+ ions, on the other hand, have relatively small hydration free energies. NH_4^+ ion has a similar radius to K^+. The hydration free energy is more negative for Na^+ than for NH_4^+. As a result, the increase in surface tension in Na_2SO_4 salt solution tends to be slightly higher than in the same concentration of $(NH_4)_2SO_4$ salt solution as shown in Figure A2.3 of the supplementary document.
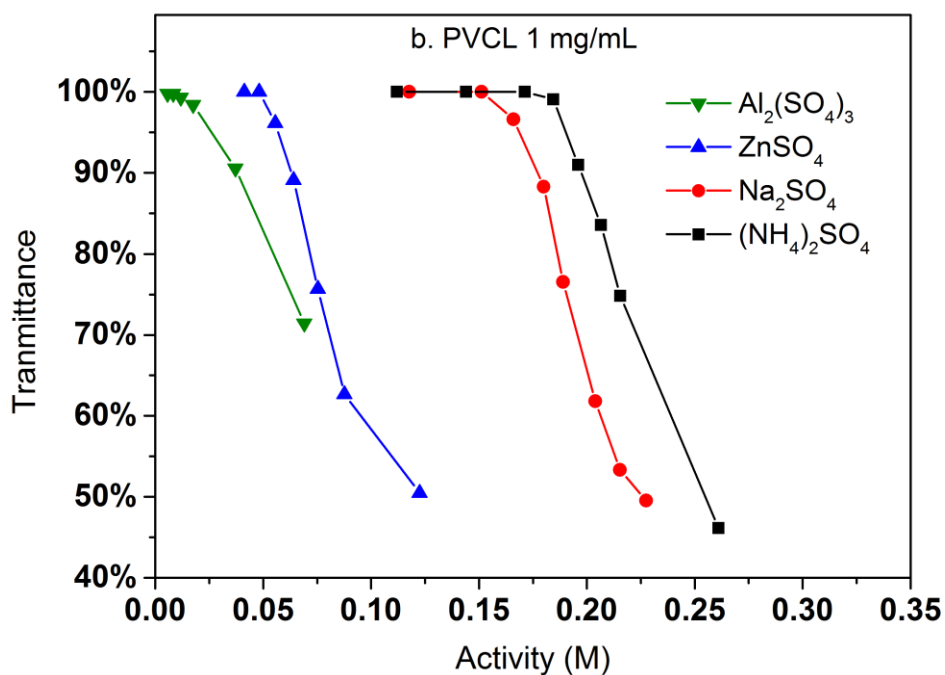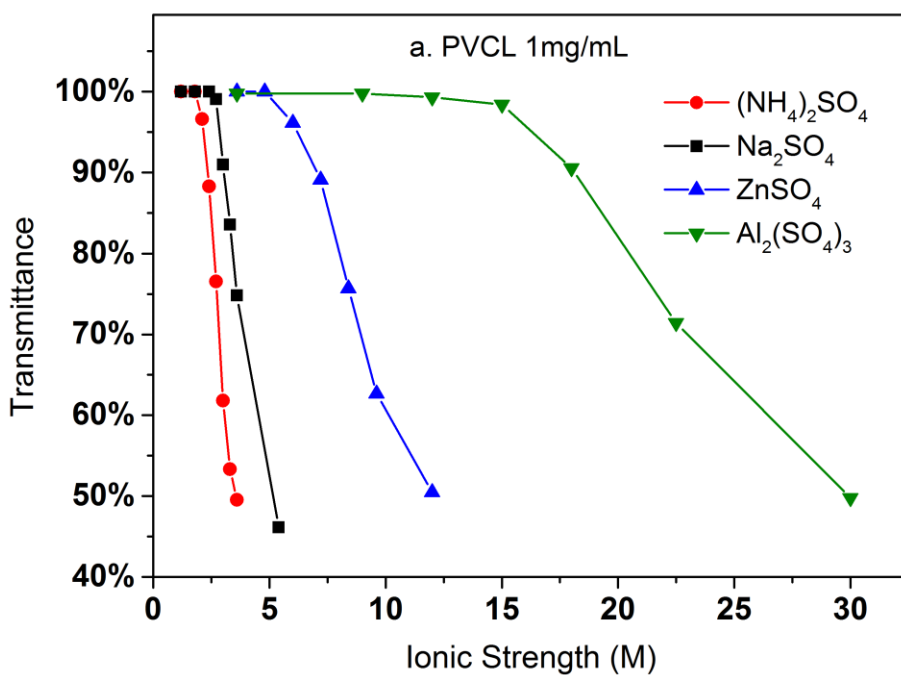
Figure 3.2 The variation of transmittance of the synthesized PVCL as a function of ionic strength (a) and ionic activity (b) in various sulfate salt solutions at room temperature during the turbidity test. Transmittance was measured at 515 nm at 1 mg/mL PVCL concentration. Activity coefficients were from literature [76, 77].

Compared to a non-responsive ligand where the hydrophobicity does not change with salt ion concentration and salt ion type, the hydrophobicity of the thermo-responsive ligand will be different for different solution conditions. This is expected to have a strong impact in the binding and elution of proteins on these ligands. As a result, the hydrophobicity change and reduction in LCST for the grafted PVCL polymers on membrane substrates in different salt solutions were investigated by contact angle measurement and previously discussed turbidity test. Firstly, the hydrophobicity change was investigated by measuring the static contact angle of salt drops on membrane surface. Here only Na_2SO_4 salt solutions were investigated as Na_2SO_4 salt demonstrates a stronger effect on the capacity for protein binding. Two non-responsive surfaces were also tested under the same conditions for comparison purposes. As shown in Figure 3.3, the contact angle increases from 60° to 100° when the Na_2SO_4 salt concentration increases from 0.2 to 1.2 M indicating that higher salt concentration results in an increase in hydrophobicity. Besides grafted PVCL ligands, surface morphology will also affect the hydrophobicity after surface modification. The morphologies of modified membranes under salt solutions as well as at temperatures above its LCST up to 45^oC were imaged using atomic force microscopy (AFM). Not obvious change in roughness and morphology has been observed at 500 nm and 1 μm scales (results not shown). Therefore, the increase in the hydrophobicity of PVCL grafted membrane is likely to due to the conformational changes occurring at the molecular level. Additionally, a sudden increase in the hydrophobicity of the membrane surface was observed when the salt concentration increases to 0.6 M. This corresponds exactly to the earlier PVCL ligand turbidity results which show that at least 0.6 M Na_2SO_4 is needed in order to reduce the LCST from 37^oC to room temperature. By comparison, no significant contact angle change was observed for the glass chip and parafilm under the same salt conditions. This indicates that higher surface tension from higher salt concentration does not increase the hydrophobicity of the substrate

surface. Enhanced binding between the protein and membrane substrate grafted with non-responsive ligand at higher salt concentration is likely due to the stronger hydrophobic force resulting from the higher salt concentration.
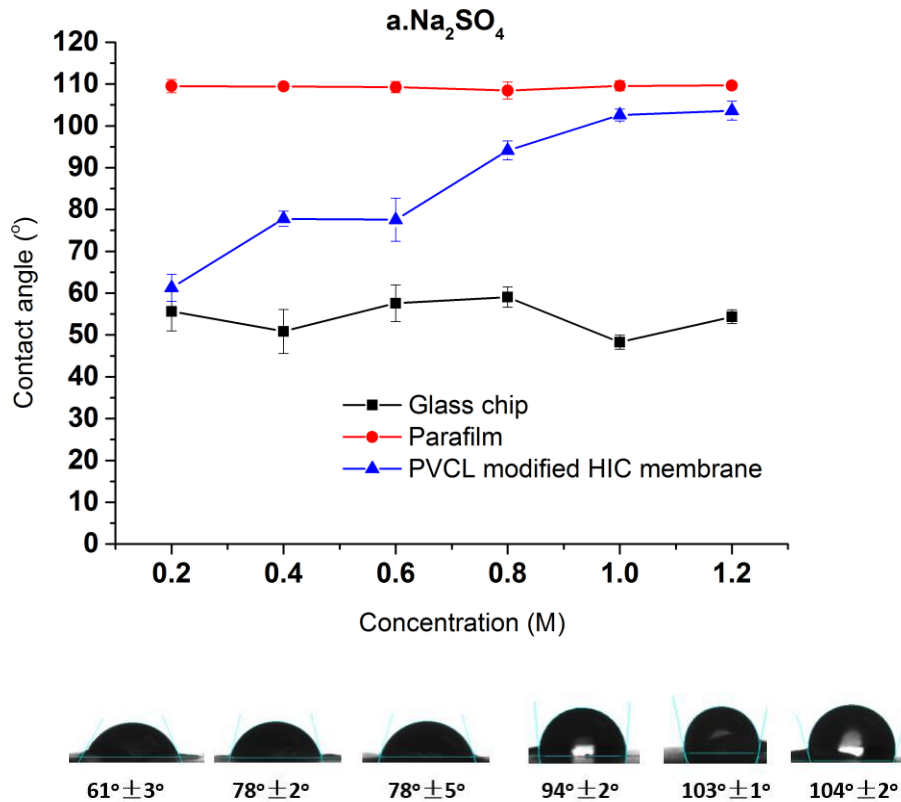
Figure 3.3 Salt concentration effects on contact angle of HIC membranes (Na_2SO_4 solutions were tested here for concentrations ranging from 0.2 M to 1.2 M). The average results of five different locations were reported here (Figure 3.3a).

3.4.2 Salt Effects on Protein Binding Studies

In order to elucidate the binding mechanism and binding energetics, BSA binding isotherms were determined by static binding in ionic strength of 3.6 M $(NH_4)_2SO_4$, Na_2SO_4, $Al_2(SO_4)_3$ and NaCl salt solutions. Figure 3.4 shows BSA isotherm curves fitted with Langmuir model based on equation (1), where q and q_{max} represent the binding capacity and maximum binding capacity, respectively. K is the equilibrium constant and c is the protein concentration at equilibrium. The linear regression equations and parameters are shown in Table 3.1. The order of static binding follows $Na_2SO_4 > (NH_4)_2SO_4 > NaCl > Al_2(SO_4)_3$ in

term of capacity, binding constant K and binding free energy ΔG at the same ionic strength of 3.6 M. These binding results agree with our earlier results on the effects of salt ion and salt concentration on the PVCL LCST transition in various sulfate salt solutions from the turbidity measurement. As discussed earlier, divalent sulfate salt solutions have a stronger effect on the transition temperature than the monovalent chloride salt solutions. This is due to the higher surface tension induced by sulfate ions than by the chloride ions at the same ionic strength as measured experimentally and shown in Figure A2.3 of the supplementary document. The reason that the binding capacity is lower in $Al_2(SO_4)_3$ solution at the same ionic strength of other salt solutions is due to the significantly reduced activity of the Al^{3+} ions resulting from its hydrolysis and subsequent polymerization.

In contrast to the case in Na_2SO_4 solution, there is no detectable binding between the PVCL ligand and BSA in 3.6 M ionic strength of $ZnSO_4$ solution even though $ZnSO_4$ and Na_2SO_4 have similar increases in surface tension[30]. This is probably due to the significantly reduced activity coefficient in the case of Zn^{2+} ion than the monovalent ions and that the solution at 3.6 M ionic strength does not reduce the LCST to room temperature as the experiments were performed. This can be seen from Figure 3.2b that the LCST transition occurs only when the ionic strength of the $ZnSO_4$ solution is larger than 5 M. As seen from Figure A2.4, binding was observed when the ionic strength increases to 6.8 M. However, binding in 3.6 M ionic strength of $Al_2(SO_4)_3$ salt solution has already been observed as shown in Figure 3.4 despite the fact the LCST transition occurs at much higher ionic strength in $Al_2(SO_4)_3$ salt solution as shown in Figure 3.2a. In order to reconcile the discrepancies observed in the two salt solutions, the nature of binding and the interaction of salt cations with BSA have to be taken into account. Besides a thermo- and ionic strength responsive ligand, PVCL is a somewhat hydrophobic ligand that can bind protein at higher salt conditions similar to conventional hydrophobic ligand. Thus at 3.6 M $Al_2(SO_4)_3$ when the

116

PVCL ligand has not gone through the hydrophilic to hydrophobic transition yet, relative low binding interaction has already occurred. This accounts for the observed binding shown in Figure 3.4. In the case of $ZnSO_4$, some binding at 3.6 M ionic strength should also be expected even though the ligand remains more hydrophilic. On the contrary, no binding was observed. This is due to the fact that BSA with a pI at 4.6 is negatively charged at the pH investigated. The divalent Zn^{2+} ion tends to have a stronger electrostatic interaction with the negatively charged BSA protein. This will lead to the reduction of hydrophobicity of the BSA protein as ions have strong hydration tendency. As the pH decreases below the pI of BSA, the protein becomes more positively charged leading to the electrostatic repulsion between the Zn^{2+} and the protein. As a result, the hydrophobicity of the BSA is not reduced leading to the binding interaction with the PVCL ligand as shown in Figure A2.4. The pH dependency of the BSA binding in $ZnSO_4$ is rather clear. On the other hand, due to the strong hydrolysis of the Al^{3+} ion to form $Al(OH)_4^-$, no direct cation interaction with the protein is present leading to conventional hydrophobic binding between the protein and ligand.

$$\frac{c}{q} = \frac{c}{q_{max}} + \frac{1}{K \cdot q_{max}} \qquad (1)$$
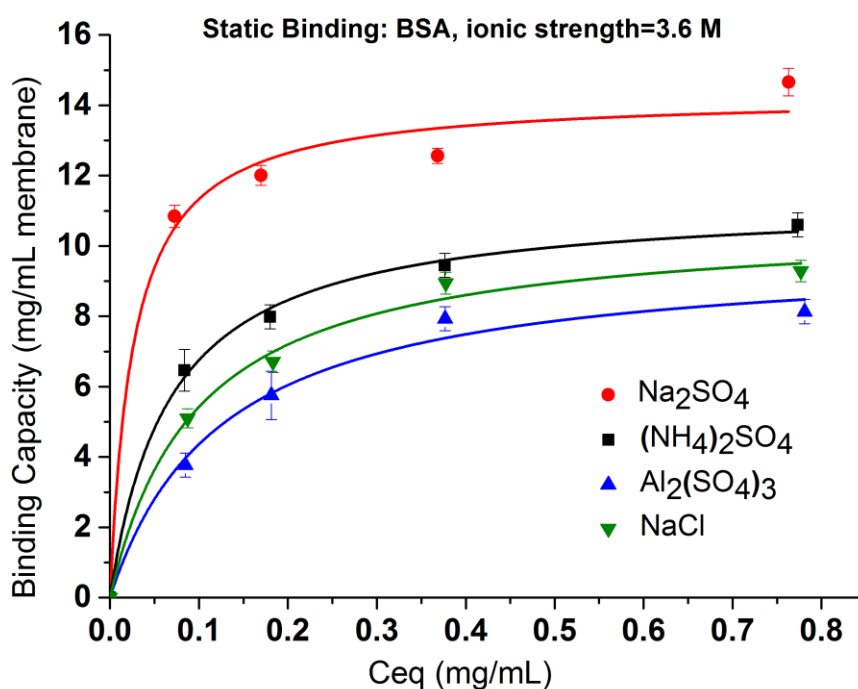
Figure 3.4 Salt type effect on BSA isotherm curves

Table 3.1 Langmuir fitting of BSA isotherm under different salt conditions

	Na$_2$SO$_4$	(NH$_4$)$_2$SO$_4$	NaCl	Al$_2$(SO$_4$)$_3$
Fitting Equation	c/q = 0.064c + 0.002	c/q = 0.080c + 0.005	c/q = 0.095c+ 0.007	c/q = 0.105c+ 0.011
Fitting Coefficient	R^2 = 0.994	R^2 = 0.996	R^2 = 0.997	R^2 = 0.992
q$_{max}$ (mg/mL)	15.63	12.20	10.53	9.52
Ionic Strength (M)	3.6	3.6	3.6	3.6
Activity (M)	0.23	0.22	2.80	0.006

Dynamic binding experiments were performed using BSA and IgG$_4$ as model proteins in a bind and elute mode. Binding conditions were varied with respect to the salt type, salt concentration and pH, whereas the protein feed concentration and elution conditions were kept the same. Chromatograms of protein loading (100% breakthrough), membrane washing and membrane eluting steps were shown in Figure 3.5. It can be seen that, for IgG$_4$, the higher the salt concentration is, the longer the time it takes for a breakthrough to start. This indicates that more IgG$_4$ are bound to the membranes at higher salt concentrations with

corresponding higher binding capacities. However, a different salt concentration effect was observed for the breakthrough curve of BSA. Comparing the dynamics binding and breakthrough curves under the highest and lowest Na_2SO_4 concentrations, the longest time delay for the start of BSA breakthrough is only 0.5 min whereas the corresponding time delay is about 9 min for IgG_4. This indicates that capacity for IgG binding is higher and that the effect of salt concentration on IgG_4 binding is stronger than the corresponding BSA. It also took significantly longer time for IgG_4 to reach 100% breakthrough than BSA due to the stronger binding interaction between the IgG_4 and the substrate and the subsequent higher binding capacity. It is known that IgG is more hydrophobic than BSA resulting in higher binding capacity for the IgG protein. Our results appear to indicate that salt concentration affects BSA binding kinetics after breakthrough occurred whereas salt concentration affects IgG_4 mainly on the time for the breakthrough to start. The change in slope in the BSA breakthrough curves suggests that probably different kinetics exist for BSA binding at different salt concentrations. Earlier results[78] show that BSA adsorption onto the hydrophobic ligand at relatively low salt concentrations is a two-stage process involving adsorption and the subsequently spreading. It is known that BSA is relatively soft with adiabatic compressibility of $1.05 \times 10^{-10}\, m^2/N$. The presence of salt ions and their concentrations will affect BSA conformations upon adsorption when the kinetics is relatively slow and binding interaction is relatively weak. IgG has a lower adiabatic compressibility around $6 \times 10^{-11}\, m^2/N$, which means it is more rigid than BSA[79, 80]. In the case of stronger binding interactions, more rigid proteins and faster kinetics as shown in the IgG4 chromatogram, the two-step adsorption and spreading process is less apparent thus similar breakthrough slopes are observed.
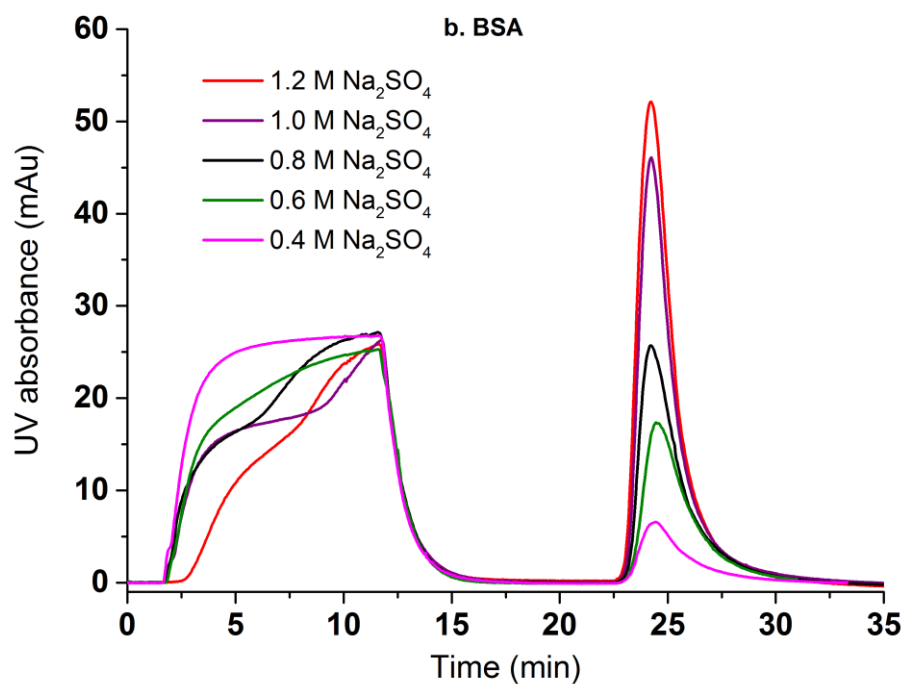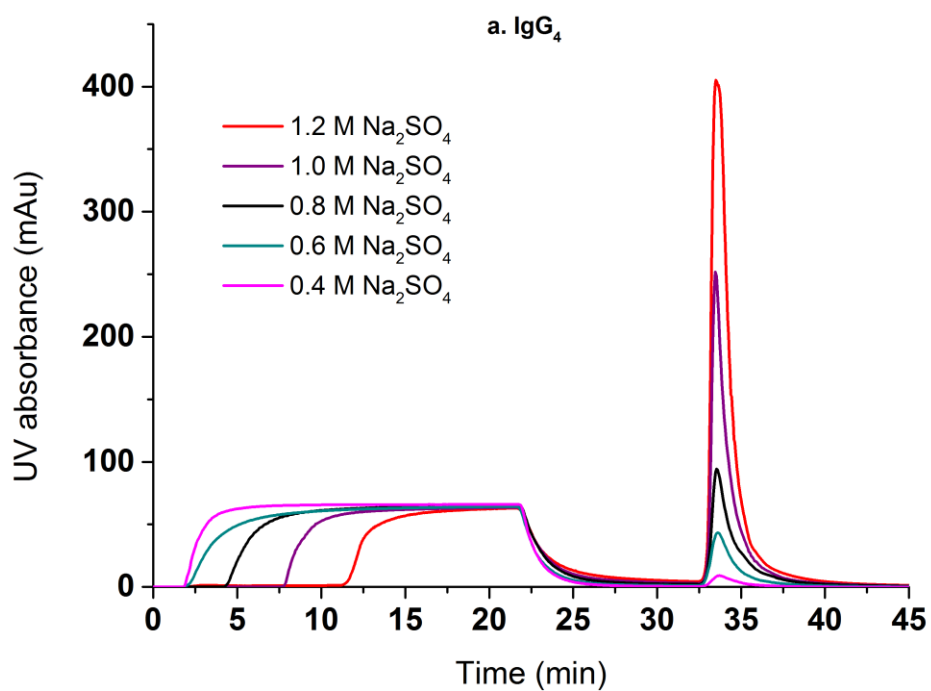
Figure 3.5 Salt concentration effects on breakthrough curves and elution curves with IgG₄ (a) and BSA (b).

Figure 3.6 compares the dynamic binding capacities and recoveries for IgG₄ and BSA

when the binding ionic strength of Na₂SO₄ varies from 0.6 to 3.6 M. For both proteins, the

binding capacity increases with the increase of the ionic strength. However, their behaviors are different suggesting that the effects of salt ions on the adsorption of the two proteins are different. Overall, the binding capacity for IgG_4 is higher than for BSA indicating that IgG_4 has a stronger hydrophobic interaction with PVCL as discussed earlier. In addition, the binding capacity for IgG_4 improves more rapidly as the salt ionic strength increases. On the contrary, the increase in BSA binding capacity becomes less obvious when the ionic strength reaches beyond 3 M. These results are consistent with the observed breakthrough curves for these two proteins. As IgG is more hydrophobic, the stronger interaction between the protein and ligand leads to fast adsorption kinetics. The more hydrophobic the protein is, the higher the salt concentration, the stronger the attractive hydrophobic force leading to rapid increase in binding capacities for more hydrophobic proteins. On the other hand, the increase in the ionic strength of the Na_2SO_4 solution will lead to the unfolding and denaturation of the more flexible BSA protein. As was discussed earlier, Na^+ ion has a stronger impact on protein denaturation than the NH_4^+ ion. The unfolded or denatured protein may prefer to aggregate rather than adsorb onto the membrane substrate depending on the magnitudes of the relative forces involved. As a result, the increase of the dynamic binding capacity slows down at higher ionic strength of the salt solution. Comparing the recoveries for the two proteins, it can be seen that the recovery of BSA is very high at lower ionic strength reaching over 90%. However, the recovery decreases to around 85% when the ionic strength increases to more than 2 M. It is known that hydrophobic force increases as the salt concentration increases leading to stronger binding of the protein to the membrane substrate. The stronger hydrophobic interaction leads to larger deformation or spreading of the protein after adsorption resulting in irreversible binding and the reduction in recovery. The recovery of IgG_4 remains more or less the same at around 80% but is always lower than the

corresponding BSA. As mentioned earlier, the stronger hydrophobic force in the IgG interaction with PVCL ligand leads to irreversible binding and subsequent reduced recovery.
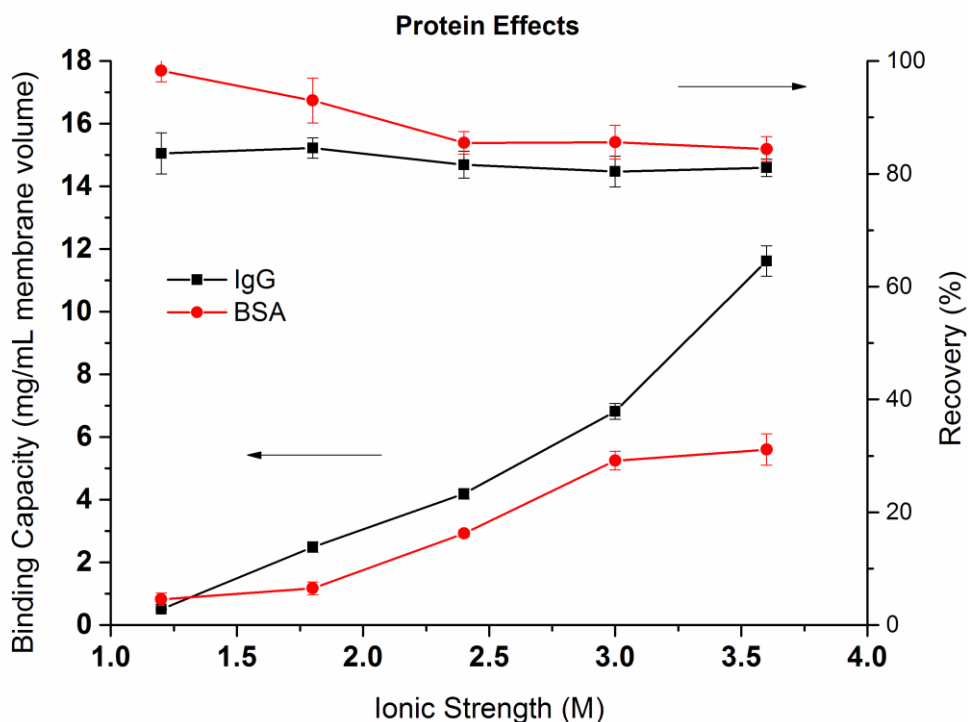
Figure 3.6 Binding capacity and recovery of IgG4 and BSA under various ionic strength of Na_2SO_4.

In order to investigate the effects of different salt and their concentrations on the dynamic binding capacity and recovery, BSA dynamic binding and recovery tests were conducted in monovalent NaCl, divalent $(NH_4)_2SO_4$, Na_2SO_4 salt solutions with ionic strength varying from 1 to 5.5 M. Since the solubility of K_2SO_4 salt, only two low salt ionic strengths were tested. As shown in Figure 3.7, in contrast to Na_2SO_4, BSA recovery remains high (>90%) in $(NH_4)_2SO_4$ and NaCl buffer conditions throughout the different ionic strengths. This is consistent with previous discussions that NaCl and $(NH_4)_2SO_4$ are weaker denaturants which lead to more reversible binding even at high ionic strengths. As expected, the binding capacity is strongly salt dependent. The higher the ionic strength, the higher the binding capacity due to the stronger hydrophobic interactions induced. The divalent $(NH_4)_2SO_4$ and Na_2SO_4 solutions have larger binding capacities than the corresponding NaCl

solution. The binding capacity follows the order: Na_2SO_4 > $(NH_4)_2SO_4$ > NaCl. The order is in agreement with our turbidity tests for PVCL as well as static binding results. However, protein binding is more complex as both ligand and protein are affected by the ionic strength and the specific salt ions present.
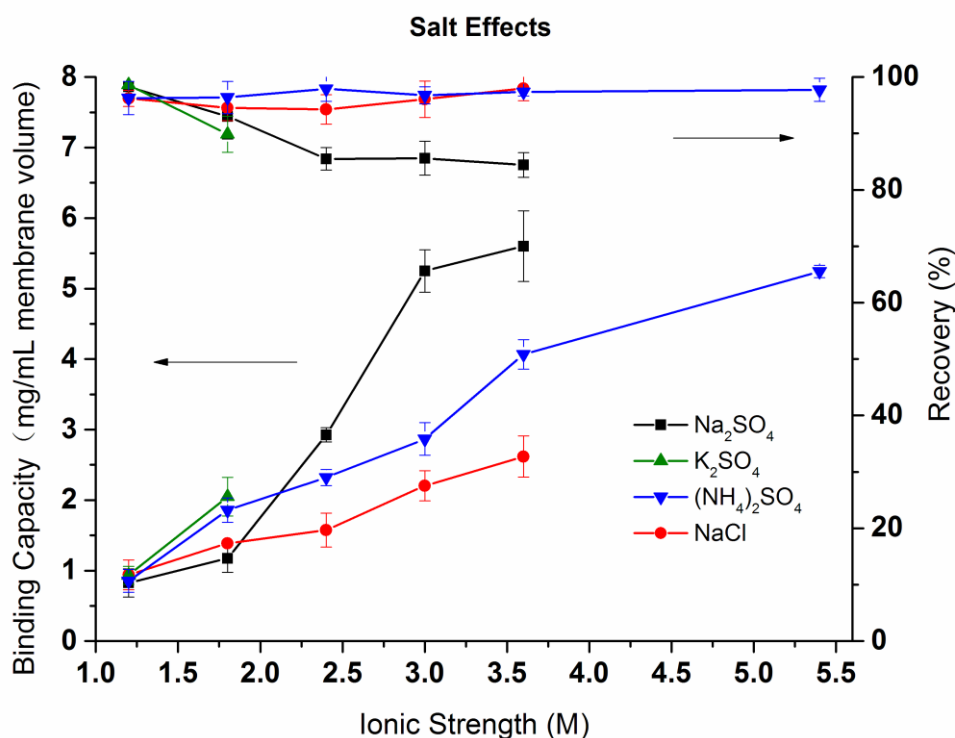
Figure 3.7 Salt type effect on the dynamic binding capacity and recovery of BSA. Since the solubility of K_2SO_4 in water is very low, it reached its solubility limitation on the second data point and so only two points were shown here.

3.4.3. pH Effect on Protein Binding Studies

The effects of pH on the dynamic binding capacity and recovery of BSA were also investigated. As the surface charge on protein is strongly pH dependent, binding of the protein to ligands will be affected as charge has a significant impact on the hydration and dehydration of proteins and polymers. A recent study shows that for conventional HIC resins, when the pH is close to the isoelectric point (pI) of lysozyme, the corresponding dynamic binding capacity had an increase of 25% compared to the capacity at neutral pH[56]. This is

relatively easy to understand since the protein surface charge is strongly dictated by the pH. As mentioned earlier, the degree of hydration and dehydration is closely related to the charge. At protein pI, the surface charge is almost zero which leads to a higher degree of dehydration thus higher probability for protein aggregation and adsorption as the nature of hydrophobic interaction is to remove structured water to bulk water. Therefore, BSA binding at its pI of 4.7 was conducted. The binding capacity results as shown in Figure 3.8a demonstrate that at low ionic strength of Na_2SO_4 (< 2.8 M), higher binding capacities were achieved at pH 4.7 than at pH 7. At pH 7, BSA is negatively charged. The monovalent Na^+ ions in the solution tend to bind to the negatively charged residues via electrostatic interaction leading to the stronger hydration of the BSA protein. However, for binding in $(NH_4)_2SO_4$ salt solutions as shown in Figure 3.8b, BSA binding capacities remain more or less the same at pH 4.7 as at pH 7.0. This is probably due to the fact that NH_4^+ is not a strong denaturant with relatively low hydration free energy. Moreover, NH_4^+ ion forms extensive hydrogen bonding network with water molecules and less likely to form strong electrostatic interactions with the charged residues. Under both salt solutions, the BSA recoveries are not affected by the binding pH indicating the denaturation of the BSA protein is not affected by the pH conditions. As discussed earlier, a strong pH dependent binding capacity for divalent salt $ZnSO_4$ at ionic strength of 6.8 M was observed as shown in Figure A2.4. Higher pH leads to a lower binding capacity. Again this is due to the electrostatic interaction between the Zn^{2+} ion and the negative charges on protein surface resulting in a stronger degree of protein hydration which subsequently leads to a lower binding capacity.
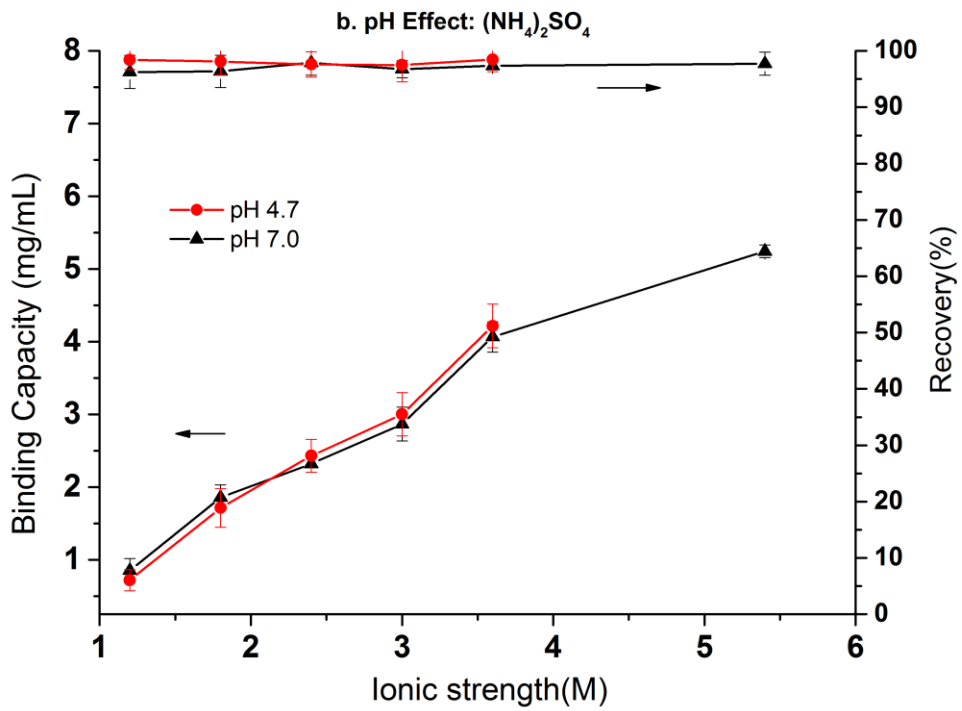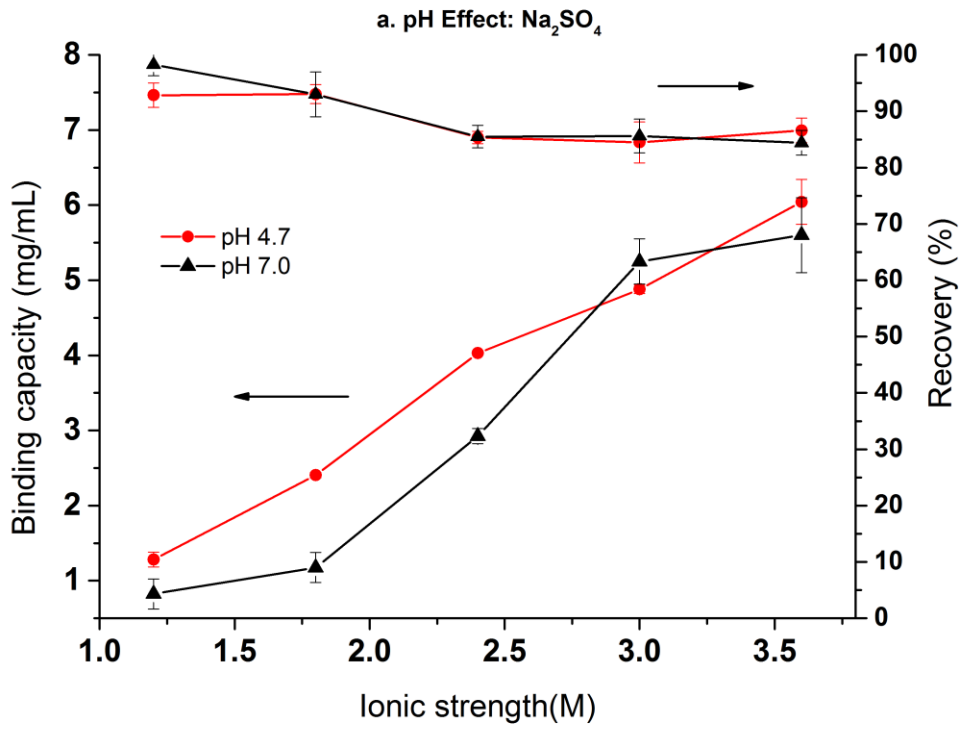
Figure 3.8 The pH effect on BSA binding capacity and recovery for Na_2SO_4 (3.8a) and $(NH_4)_2SO_4$ (3.8b).

3.5 Conclusion

The specificity of salt ions on binding capacity and recovery was investigated for the performance of responsive HIC membranes. Turbidity results show the effects of salt cations on the reduction of LCST for PVCL follows the order with $Na^+ > NH_4^+ > Zn^{2+} > Al^{3+}$ at the same ionic strength and with $Al^{3+} > Zn^{2+} > Na^+ > NH_4^+$ at the same activity. The contact angle of PVCL grafted membrane surface increases with Na_2SO_4 concentration indicating the corresponding increase in the hydrophobicity. Static binding and dynamic binding study show the capacity follows the order of $Na^+ > NH_4^+ > Al^{3+} > Zn^{2+}$ at the same ionic strength. The recovery is almost independent of the binding salt concentration for $(NH_4)_2SO_4$ and NaCl. However, for Na_2SO_4, the recovery decreases when Na_2SO_4 concentration is above 0.8 M. In addition, our results show that the binding capacity of IgG is higher than BSA. Some pH dependence on BSA binding for Na_2SO_4 salt solution was observed whereas no binding difference was observed for the $(NH_4)_2SO_4$ salt solution.

References

1.   Cramer, S. M.; Holstein, M. A. Downstream bioprocessing: recent advances and future promise. *Curr. Opin. Chem. Eng.* **2011,** *1* (1), 27-37.

2.   Guiochon, G.; Beaver, L. A. Separation science is the key to successful biopharmaceuticals. *J. Chromatogr. A* **2011,** *1218* (49), 8836-8858.

3.   Freitag, R. Chromatographic Techniques in the Downstream Processing of Proteins in Biotechnology. In *Animal Cell Biotechnology*, Pörtner, R., Ed.; Humana Press, 2014; Vol. 1104, pp 419-458.

4.   Roper, D. K.; Lightfoot, E. N. Separation of biomolecules using adsorptive membranes. *J. Chromatogr. A* **1995,** *702* (1–2), 3-26.

5.   Ghosh, R. Protein separation using membrane chromatography: opportunities and challenges. *J. Chromatogr. A* **2002,** *952* (1-2), 13-27.

6.   Weaver, J.; Husson, S. M.; Murphy, L.; Wickramasinghe, S. R. Anion exchange membrane adsorbers for flow-through polishing steps: Part II. Virus, host cell protein, DNA clearance, and antibody recovery. *Biotechnol. Bioeng.* **2013,** *110* (2), 500-510.

7.   Yoo, S. M.; Ghosh, R. Simultaneous removal of leached protein-A and aggregates from monoclonal antibody using hydrophobic interaction membrane chromatography. *J. Membr. Sci.* **2012,** *390*, 263-269.

8.   Weaver, J.; Husson, S. M.; Murphy, L.; Wickramasinghe, S. R. Anion exchange membrane adsorbers for flow-through polishing steps: Part I. clearance of minute virus of mice. *Biotechnol. Bioeng.* **2013,** *110* (2), 491-499.

9.   Phillips, M.; Cormier, J.; Ferrence, J.; Dowd, C.; Kiss, R.; Lutz, H.; Carter, J. Performance of a membrane adsorber for trace impurity removal in biotechnology manufacturing. *Journal of Chromatography A* **2005,** *1078* (1–2), 74-82.

10.   Bhut, B. V.; Weaver, J.; Carter, A. R.; Wickramasinghe, S. R.; Husson, S. M. The role of polymer nanolayer architecture on the separation performance of anion-exchange membrane adsorbers: Part II. DNA and virus separations. *Biotechnol. Bioeng.* **2011,** *108* (11), 2654-2660.

11.   Wei, Y.; Ma, J.; Wang, C. Preparation of high-capacity strong cation exchange membrane for protein adsorption via surface-initiated atom transfer radical polymerization. *J. Membr. Sci.* **2013,** *427* (0), 197-206.

12.   Singh, N.; Wang, J.; Ulbricht, M.; Wickramasinghe, S. R.; Husson, S. M. Surface-initiated atom transfer radical polymerization: A new method for preparation of polymeric membrane adsorbers. *J. Membr. Sci.* **2008,** *309* (1–2), 64-72.

13.   Schwark, S.; Ulbricht, M. Toward protein-selective membrane adsorbers: A novel surface-selective photo-grafting method. *Eur. Polym. J.* **2012,** *48* (11), 1914-1922.

14.   Jain, P.; Vyas, M. K.; Geiger, J. H.; Baker, G. L.; Bruening, M. L. Protein Purification with Polymeric Affinity Membranes Containing Functionalized Poly(acid) Brushes. *Biomacromolecules* **2010,** *11* (4), 1019-1026.

15.   He, D.; Sun, W.; Schrader, T.; Ulbricht, M. Protein adsorbers from surface-grafted copolymers with selective binding sites. *J. Mater. Chem.* **2009,** *19* (2), 253-260.

16.   Chenette, H. C. S.; Robinson, J. R.; Hobley, E.; Husson, S. M. Development of high-productivity, strong cation-exchange adsorbers for protein capture by graft polymerization from membranes with different pore sizes. *J. Membr. Sci.* **2012,** *423–424* (0), 43-52.

17.   Bhut, B. V.; Husson, S. M. Dramatic performance improvement of weak anion-exchange membranes for chromatographic bioseparations. *J. Membr. Sci.* **2009,** *337* (1–2), 215-223.

18.   Ghosh, R. Separation of proteins using hydrophobic interaction membrane chromatography. *J. Chromatogr. A* **2001,** *923* (1–2), 59-64.

19.   Lienqueo, M. E.; Mahn, A.; Salgado, J. C.; Asenjo, J. A. Current insights on protein behaviour in hydrophobic interaction chromatography. *J. Chromatogr. B* **2007,** *849* (1-2), 53-68.

20.   Chen, J.; Sun, Y. Modeling of the salt effects on hydrophobic adsorption equilibrium of protein. *J. Chromatogr. A* **2003,** *992* (1–2), 29-40.

21.   Chen, J.; Cramer, S. M. Protein adsorption isotherm behavior in hydrophobic interaction chromatography. *J. Chromatogr. A* **2007,** *1165* (1–2), 67-77.

22.   Xia, F.; Nagrath, D.; Cramer, S. M. Modeling of adsorption in hydrophobic interaction chromatography systems using a preferential interaction quadratic isotherm. *J. Chromatogr. A* **2003,** *989* (1), 47-54.

23.   Nagrath, D.; Xia, F.; Cramer, S. M. Characterization and modeling of nonlinear hydrophobic interaction chromatographic systems. *J. Chromatogr. A* **2011,** *1218* (9), 1219-1226.

24.   Nfor, B. K.; Hylkema, N. N.; Wiedhaup, K. R.; Verhaert, P. D. E. M.; van der Wielen, L. A. M.; Ottens, M. High-throughput protein precipitation and hydrophobic interaction chromatography: Salt effects and thermodynamic interrelation. *J. Chromatogr. A* **2011,** *1218* (49), 8958-8973.

25.   Hofmeister, F. Zur Lehre von der Wirkung der Salze. *Archiv für experimentelle Pathologie und Pharmakologie* **1888,** *24* (4-5), 247-260.

26.   Zhang, Y.; Cremer, P. S. Interactions between macromolecules and ions: the Hofmeister series. *Curr. Opin. Chem. Biol.* **2006,** *10* (6), 658-663.

27.   Schwierz, N.; Horinek, D.; Netz, R. R. Anionic and Cationic Hofmeister Effects on Hydrophobic and Hydrophilic Surfaces. *Langmuir* **2013,** *29* (8), 2602-2614.

28.   Naini, C. A.; Thomas, M.; Franzka, S.; Frost, S.; Ulbricht, M.; Hartmann, N. Hofmeister Effect of Sodium Halides on the Switching Energetics of Thermoresponsive Polymer Brushes. *Macromol. Rapid Commun.* **2013,** *34* (5), 417-422.

29.   Melander, W. R.; Corradini, D.; Horváth, C. Salt-mediated retention of proteins in hydrophobic-interaction chromatography : Application of solvophobic theory. *J. Chromatogr. A* **1984,** *317* (0), 67-85.

30.   Melander, W.; Horváth, C. Salt effects on hydrophobic interactions in precipitation and chromatography of proteins: An interpretation of the lyotropic series. *Arch. Biochem. Biophys.* **1977,** *183* (1), 200-215.

31.   Perkins, T. W.; Mak, D. S.; Root, T. W.; Lightfoot, E. N. Protein retention in hydrophobic interaction chromatography: modeling variation with buffer ionic strength and column hydrophobicity. *J. Chromatogr. A* **1997,** *766* (1–2), 1-14.

32.   Roettger, B. F.; Myers, J. A.; Ladisch, M. R.; Regnier, F. E. Adsorption Phenomena in Hydrophobic Interaction Chromatography. *Biotechnol. Progr.* **1989,** *5* (3), 79-88.

33.   Arakawa, T. Thermodynamic analysis of the effect of concentrated salts on protein interaction with hydrophobic and polysaccharide columns. *Arch. Biochem. Biophys.* **1986,** *248* (1), 101-105.

34.   Tsumoto, K.; Ejima, D.; Senczuk, A. M.; Kita, Y.; Arakawa, T. Effects of salts on protein–surface interactions: applications for column chromatography. *J. Pharm. Sci.* **2007,** *96* (7), 1677-1690.

35.   Müller, E.; Vajda, J.; Josic, D.; Schröder, T.; Dabre, R.; Frey, T. Mixed electrolytes in hydrophobic interaction chromatography†. *J. Sep. Sci.* **2013,** *36* (8), 1327-1334.

36.   Müller, E.; Faude, A. Investigation of salt properties with electro-acoustic measurements and their effect on dynamic binding capacity in hydrophobic interaction chromatography. *J. Chromatogr. A* **2008,** *1177* (2), 215-225.

37.   Du, H.; Wickramasinghe, R.; Qian, X. Effects of Salt on the Lower Critical Solution Temperature of Poly (N-Isopropylacrylamide). *J. Phys. Chem. B* **2010,** *114* (49), 16594-16604.

38.   Du, H.; Wickramasinghe, S. R.; Qian, X. Specificity in Cationic Interaction with Poly(N-isopropylacrylamide). *J. Phys. Chem. B* **2013,** *117* (17), 5090-5101.

39.   Du, H.; Qian, X. The Interactions between Salt Ions and Thermo-Responsive Poly (N-Isopropylacrylamide) from Molecular Dynamics Simulations. In *Responsive Membranes and Materials*; John Wiley & Sons, Ltd., 2012, pp 229-242.

40.   Kuczewski, M.; Fraud, N.; Faber, R.; Zarbis-Papastoitsis, G. Development of a polishing step using a hydrophobic interaction membrane adsorber with a PER.C6®-derived recombinant antibody. *Biotechnol. Bioeng.* **2010,** *105* (2), 296-305.

41.   Saufi, S. M.; Fee, C. J. Mixed matrix membrane chromatography based on hydrophobic interaction for whey protein fractionation. *J. Membr. Sci.* **2013,** *444* (0), 157-163.

42.   Puthirasigamany, M.; Wirges, M.; Zeiner, T. Membrane chromatography for the purification of laccase from the supernatant of Pleurotus sapidus. *Biochem. Eng. J.* **2013,** *70* (0), 180-187.

43.   Mah, K. Z.; Ghosh, R. Paper-based composite lyotropic salt-responsive membranes for chromatographic separation of proteins. *J. Membr. Sci.* **2010,** *360* (1-2), 149-154.

44.   Kosior, A.; Antošová, M.; Faber, R.; Villain, L.; Polakovič, M. Single-component adsorption of proteins on a cellulose membrane with the phenyl ligand for hydrophobic interaction chromatography. *J. Membr. Sci.* **2013,** *442* (0), 216-224.

45.   Wu, Q.; Wang, R.; Chen, X.; Ghosh, R. Temperature-responsive membrane for hydrophobic interaction based chromatographic separation of proteins in bind-and-elute mode. *J. Membr. Sci.* **2014,** *471* (0), 56-64.

46.   Liu, Z.; Du, H.; Wickramasinghe, S. R.; Qian, X. Membrane Surface Engineering for Protein Separations: Experiments and Simulations. *Langmuir* **2014,** *30* (35), 10651-10660.

47.   Yu, D. Q.; Shang, X. J.; Ghosh, R. Fractionation of different PEGylated forms of a protein by chromatography using environment-responsive membranes. *J. Chromatogr. A* **2010,** *1217* (35), 5595-5601.

48.   Wang, L.; Ghosh, R. Feasibility Study for the Fractionation of the Major Human Immunoglobulin G Subclasses Using Hydrophobic Interaction Membrane Chromatography. *Anal. Chem.* **2010,** *82* (1), 452-455.

49.   Ghosh, R. Fractionation of human plasma proteins by hydrophobic interaction membrane chromatography. *J. Membr. Sci.* **2005,** *260* (1-2), 112-118.

50.   Wang, L.; Ghosh, R. Fractionation of monoclonal antibody aggregates using membrane chromatography. *J. Membr. Sci.* **2008,** *318* (1-2), 311-316.

51.   Ghosh, R.; Wang, L. Purification of humanized monoclonal antibody by hydrophobic interaction membrane chromatography. *J. Chromatogr. A* **2006,** *1107* (1-2), 104-109.

52.   Zhang, R.; Yang, G.; Xin, P.; Qi, L.; Chen, Y. Preparation of poly(N-isopropylacrylamide)-grafted polymer monolith for hydrophobic interaction chromatography of proteins. *J. Chromatogr. A* **2009,** *1216* (12), 2404-2411.

53.   Yu, D.; Chen, X.; Pelton, R.; Ghosh, R. Paper-PEG-based membranes for hydrophobic interaction chromatography: Purification of monoclonal antibody. *Biotechnol. Bioeng.* **2008,** *99* (6), 1434-1442.

54.   Huang, R.; Mah, K. Z.; Malta, M.; Kostanski, L. K.; Filipe, C. D. M.; Ghosh, R. Chromatographic separation of proteins using hydrophobic membrane shielded with an environment-responsive hydrogel. *J. Membr. Sci.* **2009,** *345* (1-2), 177-182.

55.   Huang, R.; Kostanski, L. K.; Filipe, C. D. M.; Ghosh, R. Environment-responsive hydrogel-based ultrafiltration membranes for protein bioseparation. *J. Membr. Sci.* **2009,** *336* (1-2), 42-49.

56.   Baumann, P.; Baumgartner, K.; Hubbuch, J. Influence of binding pH and protein solubility on the dynamic binding capacity in hydrophobic interaction chromatography. *J. Chromatogr. A* **2015,** *1396*, 77-85.

57.   McCue, J. T. Chapter Five - Use and Application of Hydrophobic Interaction Chromatography for Protein Purification. In *Methods in Enzymology*, Jon, L., Ed.; Academic Press, 2014; Vol. Volume 541, pp 51-65.

58.   Boström, M.; Parsons, D. F.; Salis, A.; Ninham, B. W.; Monduzzi, M. Possible Origin of the Inverse and Direct Hofmeister Series for Lysozyme at Low and High Salt Concentrations. *Langmuir* **2011,** *27* (15), 9504-9511.

59.   Paterová, J.; Rembert, K. B.; Heyda, J.; Kurra, Y.; Okur, H. I.; Liu, W. R.; Hilty, C.; Cremer, P. S.; Jungwirth, P. Reversal of the Hofmeister Series: Specific Ion Effects on Peptides. *J. Phys. Chem. B* **2013,** *117* (27), 8150-8158.

60.   Schwierz, N.; Horinek, D.; Netz, R. R. Reversed Anionic Hofmeister Series: The Interplay of Surface Charge and Surface Polarity. *Langmuir* **2010,** *26* (10), 7370-7379.

61.   Xia, F.; Nagrath, D.; Garde, S.; Cramer, S. M. Evaluation of selectivity changes in HIC systems using a preferential interaction based analysis. *Biotechnol. Bioeng.* **2004,** *87* (3), 354-363.

62.   Ladiwala, A.; Xia, F.; Luo, Q.; Breneman, C. M.; Cramer, S. M. Investigation of protein retention and selectivity in HIC systems using quantitative structure retention relationship models. *Biotechnol. Bioeng.* **2006,** *93* (5), 836-850.

63.   Chen, J.; Yang, T.; Cramer, S. M. Prediction of protein retention times in gradient hydrophobic interaction chromatographic systems. *J. Chromatogr. A* **2008,** *1177* (2), 207-214.

64.   Xia, F.; Nagrath, D.; Cramer, S. M. Effect of pH changes on water release values in hydrophobic interaction chromatographic systems. *J. Chromatogr. A* **2005,** *1079* (1–2), 229-235.

65.   Patra, L.; Vidyasagar, A.; Toomey, R. The effect of the Hofmeister series on the deswelling isotherms of poly(N-isopropylacrylamide) and poly(N,N-diethylacrylamide). *Soft Matter* **2011,** *7* (13), 6061-6067.

66.   Himstedt, H. H.; Qian, X.; Weaver, J. R.; Wickramasinghe, S. R. Responsive membranes for hydrophobic interaction chromatography. *J. Membr. Sci.* **2013,** *447* (0), 335-344.

67.   Himstedt, H. H.; Yang, Q.; Dasi, L. P.; Qian, X.; Wickramasinghe, S. R.; Ulbricht, M. Magnetically Activated Micromixers for Separation Membranes. *Langmuir* **2011,** *27* (9), 5574-5581.

68.   Qian, X.; Lei, J.; Wickramasinghe, S. R. Novel polymeric solid acid catalysts for cellulose hydrolysis. *RSC Adv.* **2013,** *3* (46), 24280-24287.

69.   Maeda, Y.; Nakamura, T.; Ikeda, I. Hydration and Phase Behavior of Poly(N-vinylcaprolactam) and Poly(N-vinylpyrrolidone) in Water. *Macromolecules* **2001,** *35* (1), 217-222.

70.   Laukkanen, A.; Valtola, L.; Winnik, F. M.; Tenhu, H. Formation of Colloidally Stable Phase Separated Poly(N-vinylcaprolactam) in Water: A Study by Dynamic Light Scattering, Microcalorimetry, and Pressure Perturbation Calorimetry. *Macromolecules* **2004,** *37* (6), 2268-2274.

71.   Hou, L.; Wu, P. LCST transition of PNIPAM-b-PVCL in water: cooperative aggregation of two distinct thermally responsive segments. *Soft Matter* **2014,** *10* (20), 3578-3586.

72.   Meeussen, F.; Nies, E.; Berghmans, H.; Verbrugghe, S.; Goethals, E.; Du Prez, F. Phase behaviour of poly(N-vinyl caprolactam) in water. *Polymer* **2000,** *41* (24), 8597-8602.

73.   Moolenaar, R. J.; Evans, J. C.; McKeever, L. D. Structure of the aluminate ion in solutions at high pH. *J. Phys. Chem.* **1970,** *74* (20), 3629-3636.

74.   O'Reilly, D. E. NMR Chemical Shifts of Aluminum: Experimental Data and Variational Calculation. *J. Chem. Phys* **1960,** *32* (4).

75.   Fu, H.; Hong, X.; Wan, A.; Batteas, J. D.; Bergbreiter, D. E. Parallel Effects of Cations on PNIPAM Graft Wettability and PNIPAM Solubility. *ACS Appl. Mat. Interfaces* **2010,** *2* (2), 452-458.

76.   Guendouzi, M. E.; Mounir, A.; Dinane, A. Water activity, osmotic and activity coefficients of aqueous solutions of Li2SO4, Na2SO4, K2SO4, (NH4)2SO4, MgSO4, MnSO4, NiSO4, CuSO4, and ZnSO4 at T=298.15 K. *J. Chem. Thermodyn.* **2003,** *35* (2), 209-220.

77.   Lide, D. R. *Handbook of Chemistry and Physics*; 89th ed.; CRC Press: Boca Raton, FL, 2008.

78.   Haimer, E.; Tscheliessnig, A.; Hahn, R.; Jungbauer, A. Hydrophobic interaction chromatography of proteins IV: Kinetics of protein spreading. *J. Chromatogr. A* **2007,** *1139* (1), 84-94.

79.   Gavish, B.; Gratton, E.; Hardy, C. J. Adiabatic compressibility of globular proteins. *PNAS* **1983,** *80* (3), 750-754.

80.   Thakkar, S. V.; Joshi, S. B.; Jones, M. E.; Sathish, H. A.; Bishop, S. M.; Volkin, D. B.; Middaugh, C. R. Excipients differentially influence the conformational stability and pretransition dynamics of two IgG1 monoclonal antibodies. *J. Pharm. Sci.* **2012,** *101* (9), 3062-3077.

Chapter 4 The Effects of Polymer Architecture on Responsive Hydrophobic Interaction Membrane Chromatography

Abstract

In this paper, comb-like salt-responsive copolymers have been successfully grafted on regenerated cellulose (RC) membranes (pore size 0.45 μm) as ligands for membrane-based hydrophobic interaction chromatography (HIC). Poly (hydroxylethyl methacrylate) (poly (HEMA)) primary brushes were grafted directly on RC membrane substrate followed by the grafting of secondary responsive HIC ligands, poly (N-vinylcaprolactam) (PVCL). Atom-transfer radical polymerization (ATRP) was used to control the polymer chain length and chain density of both the primary and secondary polymer brushes. Our results show that both primary and secondary polymer chain length and chain length as well as the overall architecture have a significant impact on protein binding and recovery. Our results demonstrate that bovine serum albumin binding capacity and recovery are highest for membranes grafted with short primary poly (HEMA) chains. Long or high density primary poly (HEMA) chains exhibit a reduced binding capacity and recovery. BSA isotherm follows Freundlich model suggesting a multi-layer adsorption.

4.1 Introduction

Biopharmaceuticals represent a large and growing market in the pharmaceutical industry. The large demand for biopharmaceuticals heightens the need for a more efficient and consistent manufacturing process. In the past 20-30 years, the increasing product titer has shifted the bottleneck of manufacturing from upstream fermentation to downstream purification[1, 2, 3]. Depending on the processes, the downstream processing cost could contribute to up to 80% of the total manufacturing cost[4]. The efficiency of the downstream

processing largely depends on the chromatographic unit operations, which typically includes an initial capture step using affinity chromatography followed by 1-2 polishing steps with ion exchange, hydrophobic interaction or multi-modal chromatography. Packed bed column chromatography has become the workhorse of the chromatographic steps in industry for many years. However, resin-based packed bed column system suffers from low operating flow rate due to the slow pore diffusion, large buffer consumption and extra packing and validation costs. Therefore, significant efforts have been devoted to looking for alternatives to packed bed column chromatography.

Membrane adsorbers or adsorptive membranes are macroporous membranes functionalized with ligands on the surface. Membrane adsorbers have been developed to replace packed bed columns. In a packed bed column system, the slow pore diffusion, also known as channeling effect, is the major bottleneck for increasing the flow rate without losing the binding capacity. The macroporous structure of membranes eliminates the slow pore diffusion process during protein binding to ligands. Consequently, many studies have shown that the dynamic binding capacity of membranes is independent of a wide range of flow rate[5, 6, 7]. As a result, membrane adsorbers can be run at much high flow rates, which means higher productivity as well as lower possibility of fouling and product degradation. In addition, membranes have many other advantages over packed bed columns, including less buffer usage, no extra packing and validation cost, single-use and ease of scale-up. However, the main drawback of membrane adsorbers is the low capacity because of its lower surface area per volume compared to resins. Commercialized membrane adsorbers have been used mainly in a flow-through mode[8] after the protein A chromatographic purification step to remove low-level containments such as protein aggregates[9], viruses[10, 11] and DNAs[11, 12]. More recently, high capacity membrane adsorbers have been developed either by increasing the

surface area of base membrane matrices[13] or using polymeric ionic exchange or multi-modal ligands[14, 15].

Hydrophobic interaction chromatography (HIC) has been used extensively in the polishing step of downstream chromatographic processes. HIC is considered to be an orthogonal unit operation to protein A and ion-exchange chromatography. Protein binds to HIC ligands under high salt concentration buffer and elution is conducted under low salt concentration buffer. Additives, such as ethanol, detergents and chaotropic salts, are commonly used to promote protein elution or ligand regeneration[16]. Compared to protein A or ion-exchange chromatography, the capacity of HIC is generally 2-3 times lower ($DBC_{10\%}$ < 40 mg/mL)[17]. Thus, HIC is widely used for aggregates removal in a flow-through mode since aggregates are typically more hydrophobic than monomeric antibodies and the total impurity level is rather low after protein A affinity step. Previous studies on HIC mainly focused on its performance under different conditions, including salt, pH and temperatures[1, 18, 19, 20, 21]. There is very little study on HIC ligand effects, such as chain length and chain density since most HIC ligands are monomers or polymers grafted with uncontrollable free radical polymerization. In addition, most HIC studies were conducted under isocratic elution with limited bind-and-elute investigations on ligand effects.

Previously, we have developed responsive HIC membranes with poly (N-vinylcaprolactam) (PVCL) as salt responsive ligands[22]. PVCL is a thermo-responsive polymer which has a LCST ranging from 30-50°C depending on its molecular weight and concentration[23, 24]. Our previously developed responsive HIC membranes have demonstrated binding capacity and protein recovery specificity to salt ion type and salt ion concentration. However, the effects of polymer grafting chain length and chain density on protein binding and recovery have not been investigated and optimized. Although our previous work investigated the ligand density effect by varying the initiation reaction time, the grafting

degree and binding capacity show limited improvement[22]. In addition, the ligand density effect on protein binding and recovery was investigated for PVCL polymers grafted on membrane substrate directly. Earlier results suggest that the low binding capacity of HIC is due to the low ligand density grafted[25]. Therefore, there is a need to increase the ligand density controllably and systematically. To the best of our knowledge, this is the first work on investigating three-dimensional architecture of HIC polymeric ligand on protein binding and recovery.

In the past decades, atom transfer radical polymerization (ATRP) has been widely investigated to achieve high capacity[6, 26, 27], high selectivity[28] and high recovery[22] membrane adsorbers. ATRP is superior to other uncontrolled radical polymerization methods due to its better control on polymer chain length and chain density[29, 30]. In addition, block polymers with various specific structures were synthesized via ATRP. The polymer architecture synthesized includes star-shaped, comb-like, cyclic copolymers[29]. Comb-like polymer is one of the emerging polymeric ligands that has been synthesized as affinity ligands for lectin binding[31, 32], thermo-responsive polymers[33, 34, 35, 36, 37], ion-exchange ligands[38], colorimetric sensors[39] and polymers brushes for anti-fouling purposes[40]. Comb-like polymer architecture has been used to increase the number of binding sites leading to an improved capacity for protein binding. Ulbricht et.al has shown that dynamic binding capacity increased more than 3 times using the 3-D comb-like ligands for lectin binding[31]. Baker et.al incorporated comb-like copolymers in the multilayer polyelectrolyte films with 2-4 folds of enhancement in capacity for protein binding[38]. Comb-like PNIPAM has been successfully modified by ATRP on the macroporous polypropylene membrane[35], PTFE membrane[36] and beads[34]. Wang et.al developed a comb-like multimodal ligand grafted on regenerated cellulose membranes[15]. The measured ion-exchange capacity of grafted ligands increased 3-4 times compared to that of commercialized resin, particularly achieving very high IgG binding capacity. As shown in

Figure 4.1, we have also designed comb-like ligands involving both primary and secondary polymer chains to increase the ligand density in a more effective and controllable way via ATRP. The HIC PVCL ligands are grafted from the primary polymer chains. The polymer chain density of PVCL can be controlled by the grafting condition of the more easy to grow primary polymer. Recently, Macro et.al has developed dendritic butyl HIC ligands immobilized on resins with improved grafting density and capacity[25]. However, only two branching degrees of the dendritic ligands were investigated in their study. As far as we know, we are the first to use the comb-like polymers as HIC ligands for membrane adsorbers. We are also the first one to use a controlled polymerization method to investigate the effects of HIC polymeric ligands with a 3-D architecture on protein binding capacity and recovery.
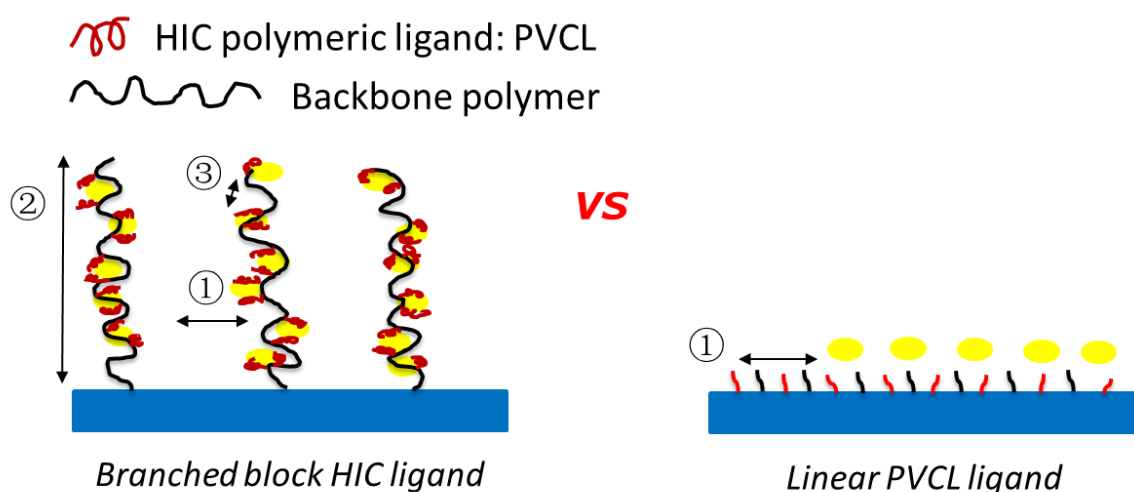

Figure 4.1 Scheme of comb-like PVCL ligand compared to old PVCL ligand. Backbone density (1) and length (2) are varied by HEMA initiator concentration and ATRP time of HEMA. The density of PVCL (3) on each backbone is varied by VCL initiator concentration.

The major variables in ATRP modification condition to synthesize these comb-like brushes include the concentrations of ATRP initiator BIB (Figure 4.2a), primary monomer HEMA (Figure 4.2b) and secondary HIC monomer VCL (Figure 4.2c) as well as various reaction time. 2-hydroxyethyl methacrylate (HEMA)[31, 32, 35] is used as a primary monomer here because it has a reactive hydroxyl group that can be used to initiate the grafting of the

137

secondary polymers. Moreover, grafting poly (HEMA) on membrane substrate has been well studied with well-controlled grafting degrees[41, 42, 43]. Figure 4.3 represents the reaction scheme for grafting comb-like ligands from RC membrane surface. The poly (HEMA) brush density and the 2nd PVCL brush density were varied by initiation reaction condition. The impacts of the ligand architecture on protein binding, which includes primary chain density and chain length of poly (HEMA) as well as the secondary chain density of PVCL, were investigated systematically by dynamic protein binding studies. AFM and contact angle measurements of modified membranes were used to correlate surface properties with the binding results. At last, bovine serum albumin isotherms were fitted with Freundlich model to provide some insights on the binding mechanism.
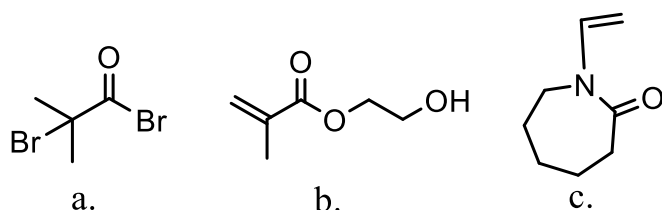

Figure 4.2 Structure of ATRP initiator, BIB (a), primary monomer, HEMA (b) and secondary HIC monomer, VCL (c).

4.2 Materials

N-Vinylcaprolactam (98%), 2-Hydroxyethyl methacrylate (98%), 2-Bromo-2-methylpropionyl bromide (BIB, 98%), 4-(dimethylamino) pyridine (DMAP, $\geq$99%), copper (I) chloride$\geq$99.995%), copper (II) chloride ($\geq$99.995%) and N,N,N′,N″,N″-pentamethyldiethylenetriamine (PMDETA, 99%) were purchased from Sigma Aldrich (St. Louis, MO). Triethylamine (TEA, $\geq$99%) was obtained from Alfa Aesar (Ward Hill, MA). Methanol (99.8%) and acetonitrile (99.8%) were obtained from EMD Chemicals (Billerica, MA). Boric anhydride was purchased from Avantor Performance Materials (Center Valley, PA). Anhydrous acetonitrile was obtained by distilling acetonitrile with boric anhydride.

Ammonium sulfate (≥99.0%) was bought from Macron™ Fine Chemicals (Center Valley,

PA). Regenerated cellulose membranes (0.45 μm pore size, RC55, 50 mm diameter) were

purchased from GE Healthcare (Pittsburgh, PA). Bovine serum albumin (BSA) (>99 %, pI

4.7, 66 kDa) was obtained from Avantor Performance Materials (Center Valley, PA).

4.3 Experimental

4.3.1 Membrane Surface Modification

Atom transfer radical polymerization (ATRP) Membranes were modified through surface-

initiated ATRP as previously reported by our earlier studies[22, 28, 41, 44]. Regenerated cellulose

(RC) membranes were first immobilized with ATRP initiator 2-bromoisobutyryl bromide

(BIB) in acetonitrile for 3 hours. The ATRP for the primary poly (HEMA) chains was

conducted in the methanol/water solvent mixture with HEMA (monomer, 0.5 M), copper (I)

chloride, copper (II) chloride, bipyridine (Bpy). The mole ratio among HEMA: CuCl: $CuCl_2$:

Bpy is 200:1:0.4:3.5. Methanol/water mixture (1:1, v/v) was used as the polymerization

solvent. ATRP solution was first degassed with argon for 15-20 min before CuCl and $CuCl_2$

were added. Flasks attached in Schlenk line containing initiator immobilized membranes

were de-oxygenated by vacuum and back-filled with argon three times. At last, the reaction

mixture was transferred to the flasks by a syringe. After the predetermined polymerization

time, membranes were first rinsed with methanol/water mixture (1:1, v/v) three times and

then washed with DI water overnight. After membranes were dried in vacuum, the second

initiation for grafting the secondary PVCL polymer was carried out with various

concentrations of BIB. At last, ATRP of N-vinylcaprolactam (VCL) monomer (1 M) solution

was conducted for 4 hours in methanol/water mixture (v/v 1:1). ATRP solution was

comprised of copper (I) chloride, copper (II) chloride, ligand N,N,N′,N″,N″-

pentamethyldiethylenetriamine (PMDETA). The mole ratio among VCL: CuCl: $CuCl_2$:

PMDETA is 200:1:0.2:2. The schematic of the modification procedure is shown in Figure 4.3.
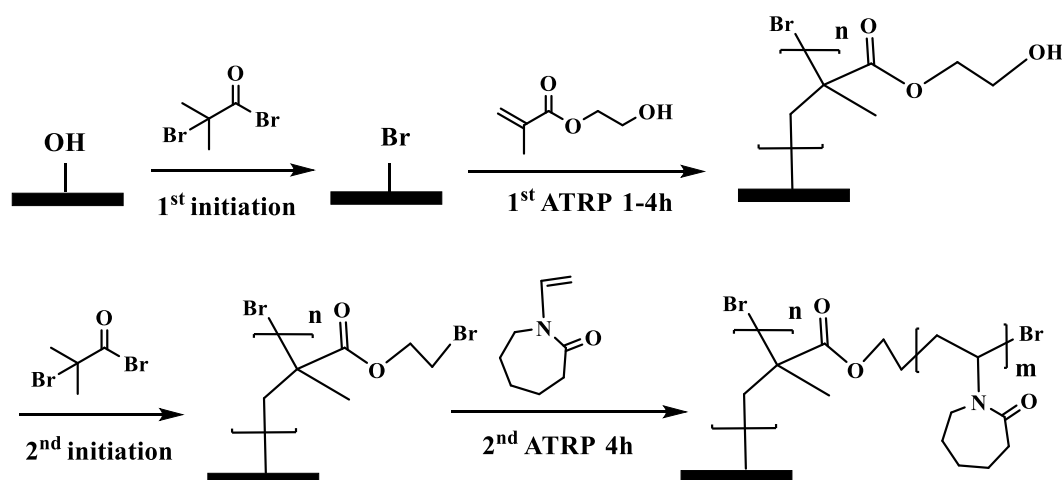

Figure 4.3 Modification scheme of comb-like PVCL through ATRP. Except for the 2nd ATRP for grafting PVCL, the initiation conditions as well as the 1st ATRP for grafting poly (HEMA) were varied accordingly to investigate PVCL chain density effect.

4.3.2 Membrane Surface Characterization

Attenuated total reflection- Fourier transform infrared spectroscopy (ATR-FTIR) ATR-FTIR provides a qualitative characterization of the functional groups on the grafted polymer. ATR-FTIR measurements were performed using IRAffinity (Shimadzu, MD) with a horizontal ZnSe accessary. Membranes were scanned in the 1000-2000 cm^{-1} wavenumber range for a total of 50 scans with a 8 cm^{-1} resolution. The data were processed by first subtracting the background and being normalized at the same 0-1 scale for comparisons.

Contact Angle Membrane surfaces were also characterized by contact angle measurements. The instrument has an optical angle meter (OCA 20, *Future Digital Scientific Corp.*, NY) and a dosing needle. Membranes were cut into small pieces and pasted on a glass chip with a double side tape. Sessile drop method was used for the characterization. A liquid drop was placed on the membrane surface and the image of the drop was recorded by camera for later analysis. The dosing volume of the solvent is 2 μL. The results for each membrane were averaged with at least 3 measurements at random locations.

Atomic Force Microscopy (AFM) Surface morphology and roughness of the modified

membranes were characterized by AFM (Dimension Icon, Bruker Corporation, MA) with Bruker's sharp nitride lever (SNL-10c) probes in liquid. ScanAsyst mode (in liquid) was used to image the morphology of membranes at room temperature in water. The scan rate is set at 1 Hz with a resolution of 256 samples per line. After scanning, the image is processed with a third order flatten command with Bruker's nanoscope analysis program. Roughness was then calculated by the nanoscope analysis program after the flatten command.

4.3.3 Protein Binding Studies

Dynamic Binding Studies   The method of dynamic binding studies was developed with the Unicorn software v. 5.31 to automate the BSA binding and elution experiments as previously discussed[22]. The 1 mg/mL bovine serum albumin (BSA) solutions were prepared for dynamic binding tests. All the buffer and protein solutions were filtered through 0.22 μm nylon membrane before the dynamics binding tests. A set of four membranes (total bed volume 0.08 mL) was loaded into a stainless steel flow cell (Mustang Coin ® module, Pall Corporation) with two flow distributers to ensure a uniform flow across all of the membranes. All runs were conducted by using ÄKTA FPLC from GE Healthcare Bio-Sciences Corp. More specifically, the membrane stack was first wetted with buffer B (elution buffer, 20 mM Na_2HPO_4) in the reverse flow configuration over 5 minutes by an increasing the flow rate from 0.2 mL/min to 1.0 mL/min in 0.2 mL/min increment. Next, the membrane stack was equilibrated in the forward flow configuration in the buffer A (adsorption buffer, 1.8 M $(NH_4)_2SO_4$) at 1 mL/min for 10 minutes. Then 1 mg/mL protein solution was loaded onto the membrane stack at a flow rate of 1 mL/min for 10 minutes. Unbound proteins were subsequently washed from the membranes using the buffer A (adsorption buffer, 1.8 M $(NH_4)_2SO_4$) for 10 minutes at 1 mL/min, followed by a step change of running buffer B (elution buffer, 20 mM Na_2HPO_4) through the membrane at 1 mL/min. The run ended when the UV absorbance at 280 nm becomes stable. The washing fraction (includes loading

fraction) and elution fraction were collected and their volumes were determined accordingly. Protein concentrations in the sample solution, washing fraction, and elution fraction were calculated through UV absorbance at the wavelength of 280 nm.

4.4 Results and Discussion

4.4.1 Comb-like PVCL

The primary polymer chain poly (HEMA) was first grafted on RC membranes by ATRP after initiator BIB immobilization on the membrane substrate. The initiator concentration and ATRP polymerization time were varied to control the initiator density and polymer chain length. The degree of grafting (DG, $\mu g/cm^2$) was calculated based on the following equation:

$$DG = \frac{W_1 - W_0}{W_0 \times Spec} \quad (1)$$

where W_0 and W_1 are the weight of the membrane before and after ATRP respectively. Spec represents the specific area of the membrane (6.3 m^2/g was used in this study based on the recommendation by the manufacturer). DG results for poly (HEMA) modified membranes are shown in Figure 4.4. HEMA polymerization rate is relatively fast in the first hour and then polymer grows at a slower but steady rate leading to a linear DG increase after 1 h. The rapid growth of poly (HEMA) at the first hour is probably due to the high monomer and Cu (I) concentrations relative to the available initiation sites at the beginning of the ATRP reaction. As reported before for ATRP, the polydispersity of the chain is usually higher at beginning[30]. Once the equilibrium between Cu (I) and Cu (II) is established and the concentration of monomer is reduced, the polymerization rate is more stable following a linear growth period. Overall, membranes modified under high initiator concentration (160

mM) have a higher and faster growth of DG than membranes modified under low initiator concentration (40 mM). It should be pointed out that the growth rate for high density poly (HEMA) is less than twice of that for low density chain even though there is 4 times increase in the corresponding initiator concentration. This indicates that the initiator immobilization is not 100% effective due to limited availability of initiation sites on membrane substrate and/or that there is significant chain termination at the beginning of the polymerization due to the proximity of chains at high density case. However, our results show that the primary poly (HEMA) chain density and chain length can be effectively controlled by varying the initiator concentration and polymerization time respectively.
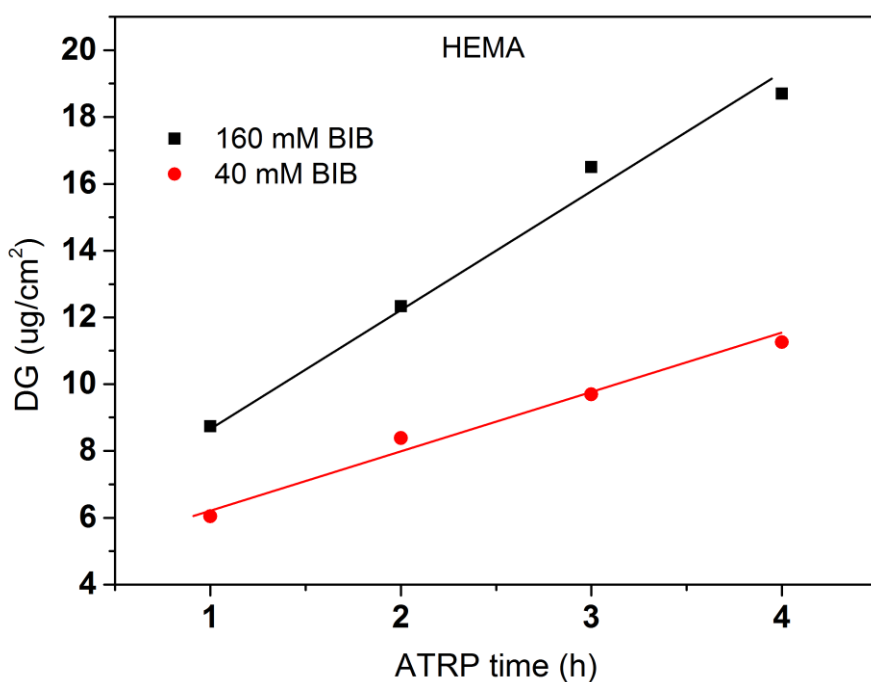

Figure 4.4 Grafting degree of poly (HEMA) under two initiator concentrations (40 mM and 160 mM) and four different polymerization times (1-4 h).

After the primary polymer chain poly (HEMA) was grafted on RC membranes, the 2nd initiation for ATRP was conducted using 160 mM BIB initiator concentration. Figure 4.5 shows the grafting density of immobilized the 2nd initiator under different poly (HEMA) chain length and density measured by the increase in weight after and before 2nd initiator

immobilization reaction. It can be seen that the 2nd initiator grafting density increases as the poly (HEMA) chain density increases even though the increase is somewhat small measured by the slope. This indicates that the 2nd initiators have successfully reacted with the hydroxyl groups on poly (HEMA). It also can be seen that membranes with longer poly (HEMA) chains (1 h ATRP) have a more steep increase of 2nd BIB grafting degree compared to the shorter poly (HEMA) chains (15 min ATRP). This is expected because longer poly (HEMA) chain has more hydroxyl groups to react. It is also interesting to note that with even higher poly (HEMA) density at 200 mM of the 1st initiator concentration (not shown), the 2nd BIB grafting density actually decreased to 2.3 and 5.6 $\mu g/cm^2$ for 15 min and 1 h ATRP of HEMA respectively from the corresponding values at 3.5 and 8 $\mu g/cm^2$ with 80 mM 1st BIB concentration. When poly (HEMA) chain density is too high, the stronger interaction and intertwining of the polymers make the initiator hard to reach due to steric hindrance and increased reaction barrier. The increase reaction barrier is caused by the formation of strong hydrogen bonds between the hydroxyl groups when the density of polymer chains becomes high.
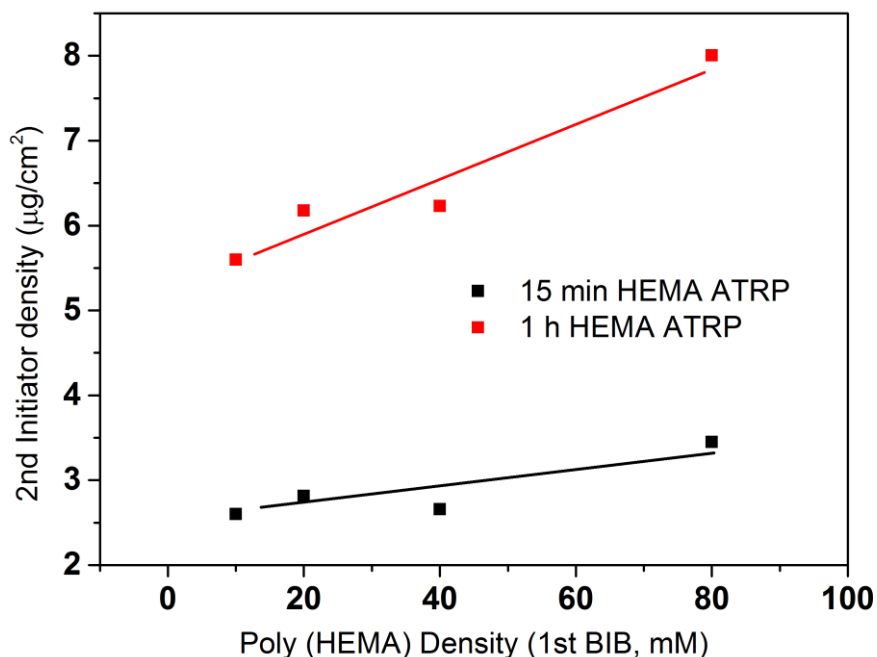
Figure 4.5 The effects of the primary polymer poly (HEMA) chain density and chain length on the grafting density of the 2nd initiation reaction

In order to further quantify the effectiveness of the modification process, conversion yields were determined. Conversion yields were calculated by the percentage of the number of second initiator immobilized with respect to the number of hydroxyl groups on the poly(HEMA) chain. It is plotted in Figure 4.6. The results indicate that the yield is strongly dependent on the 2nd initiator concentration. The conversion of the reaction shows a slight decrease as the density of the primary polymer poly (HEMA) increases. This is more evident in the 200 mM BIB condition for the second initiation process. As was discussed earlier, higher poly (HEMA) density actually hinders the initiation reaction due to increased reaction barrier and steric hindrance. In addition, as the number of hydroxyl group increases, it is also likely the initiation reaction is limited by the availability of initiator. Overall, the yields of the 2nd initiation reaction are approximately 15%, 45% and 80% at 10 mM, 160 mM and 200 mM of second BIB initiator concentrations respectively. The second initiator BIB concentration of

200 mM was used for the subsequent studies since it gives the highest yield of conversion. Again, these results demonstrate the feasibility of controlling the primary poly(HEMA) chain and secondary PVCL chain densities by varying the BIB concentration used in the reaction.
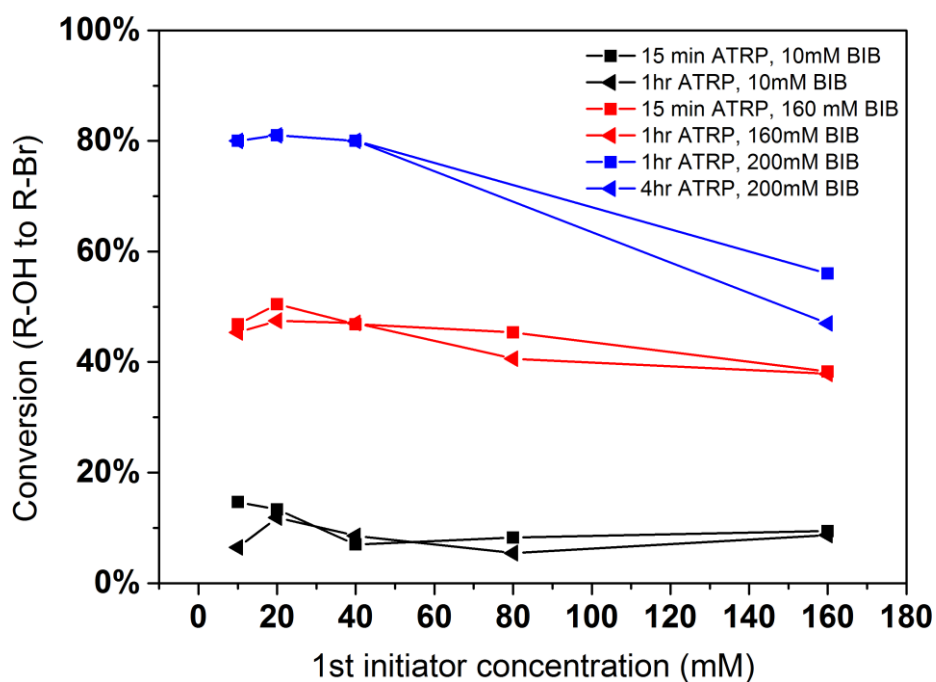

Figure 4. 6 Conversion of hydroxyl group to alkyl bromide in the 2nd initiation reaction. Black, red and blue represent 10 mM, 160 mM and 200 mM concentrations of BIB used for the secondary initiation reaction.

Once the second initiation was completed, ATRP was conducted for grafting PVCL on the primary poly (HEMA) ligands on the RC membranes. The ATRP time was kept at 4 h for all investigations here. As shown in Figure 4.7 (a), the DG of PVCL grafted on RC membranes increases with the increase of the DG of poly (HEMA) indicating the successful grafting of secondary polymer PVCL from the primary poly (HEMA) backbone. It can be seen that the low density (LD, 40 mM BIB) poly (HEMA) modified membranes have a more rapid PVCL DG growth during 1-4 h of ATRP than that of the high density (HD, 160 mM BIB) ones during the same ATRP time. PVCL grafted on the LD primary poly(HEMA) polymer chains follows an exponential growth mode indicating a first order reaction with

146

regard to the chain density of poly(HEMA) ($\sim$ k1[poly(HEMA)]^2+k2[poly(HEMA)]). On the other hand, PVCL chains grown on HD poly(HEMA) follow a logarithmic growth mode indicating a second order reaction with regard to the density of primary poly(HEMA) polymer chains ($\sim$ k_1[poly(HEMA)] + k_2[poly(HEMA)]$^{-1}$). One of the possible explanations for the polymer growth behavior is that chain termination reaction for PVCL is more likely to happen when the primary poly (HEMA) chain density is higher. As discussed earlier, high primary chain density can lead to steric hindrance for initiator immobilization and an increased reaction barrier for the initiation reaction as the strong hydrogen bonding interaction between the –OH groups could occur. These results suggest that the density of primary poly (HEMA) chains can have a significant impact on the polymerization of the secondary PVCL chains.

The effects of BIB concentration for the second initiation reaction on PVCL polymerization were also investigated on a chosen grafted primary poly(HEMA) chains as shown in Figure 4.7 (b). ATRP time for all the initiator concentrations was kept constant at 4 h. The results show the DG of PVCL increases with initiator concentration until it reaches a plateau corresponding to possibly a maximum density of PVCL on the chosen primary polymer chains. The results indicate again that a higher chain density, the possibility for chain termination leads to a slow-down in the polymerization reaction. Again, the results indicate the grafting density can be effectively controlled by varying the concentration of BIB initiator.
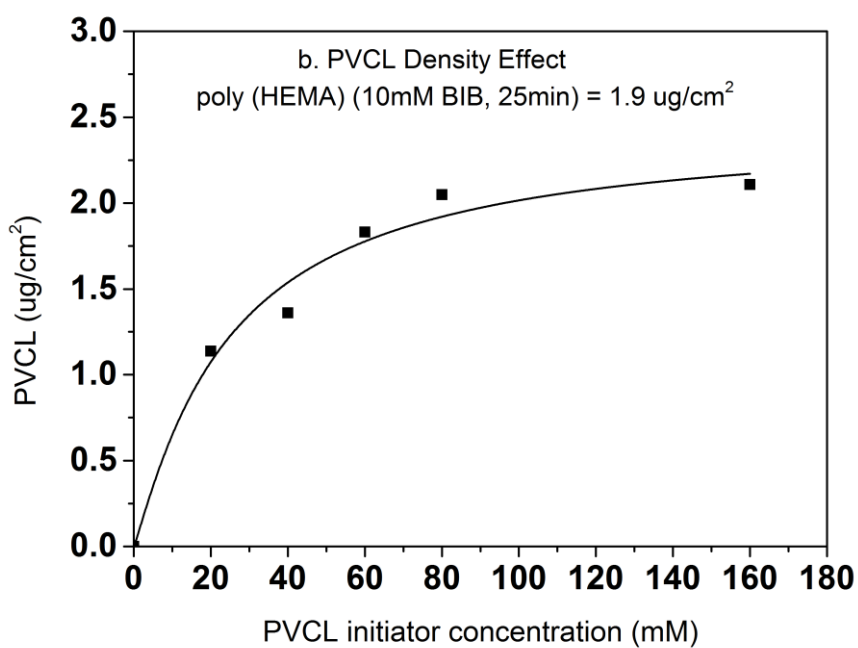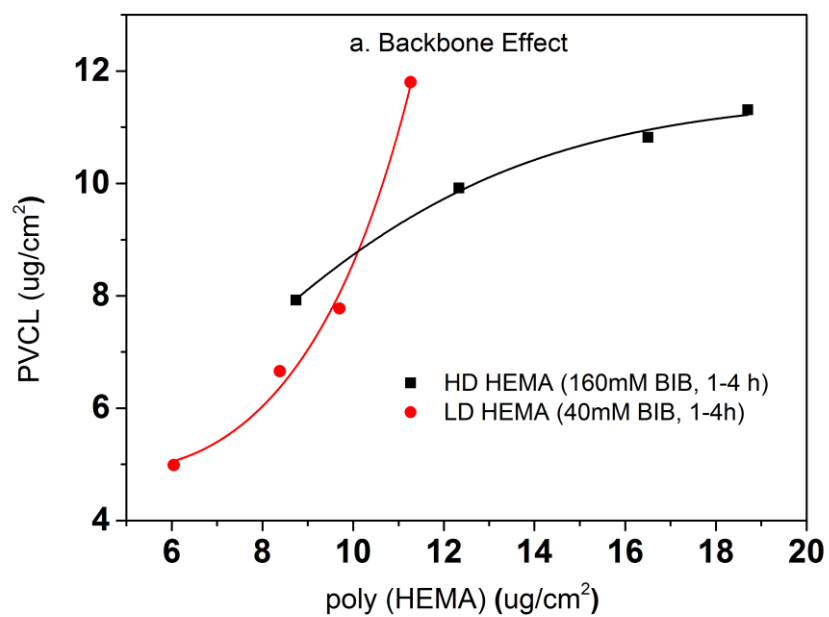
Figure 4.7 Degree of grafting for PVCL as a function of backbone length and density (a) and 2nd BIB concentration (b)

Figure 4.8 shows ATR-FTIR of unmodified, poly (HEMA) modified and comb-like

PVCL modified membranes. Compared to unmodified membrane, the poly (HEMA)

modified membrane exhibits a peak at around 1724 cm^{-1}, which is from the C=O stretch of

the ester bond from the grafted poly (HEMA). The presence of this ester peak indicates the successful modification of the primary poly (HEMA) polymer on membrane substrate. For comb-like PVCL modified membrane, the presence of the amide C=O stretch peak at 1630 cm^{-1} indicates the successful grafting of the secondary PVCL polymer on the primary chains. In addition, the disappearance of the hydroxyl group at 3000 cm^{-1} also confirms the grafting of PVCL. Overall, our ATR-FTIR spectra further demonstrate our two-step comb-like modification is successful.
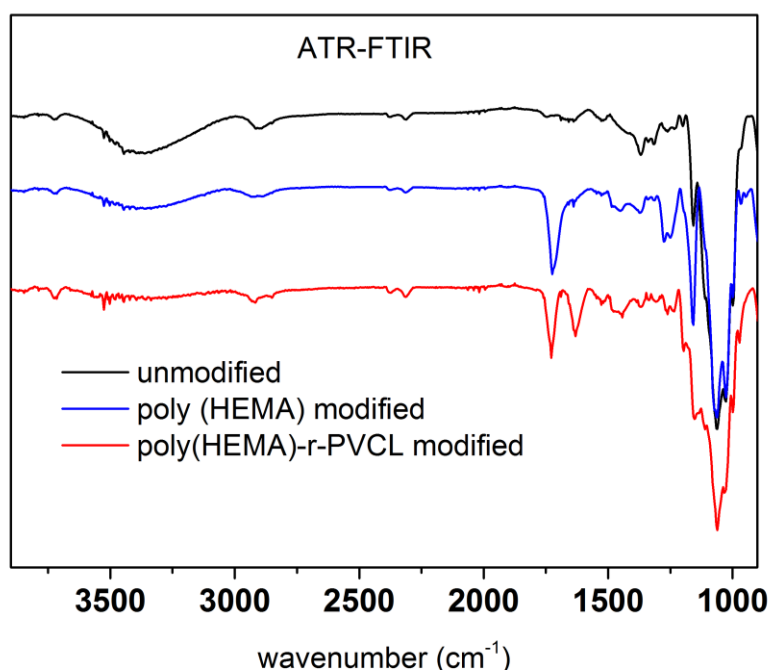
Figure 4.8 ATR-FTIR spectrum of unmodified RC membrane, poly (HEMA) and poly (HEMA)-r-PVCL modified membranes.

Table 4.1 summarizes the dynamic binding capacity and recovery under different primary poly(HEMA) modification conditions. For all the studies shown in the table, PVCL polymerization time is kept at 4 h with the same initiator immobilization condition (200 mM 2nd BIB). Binding capacity and recovery are plotted in Figure 4.9 as a function of PVCL chain grafting density. It can be seen that DG has been improved 10-50 times compared to

the DG value when PVCL chains are directly grafted on membrane substrate. However, the improvement for dynamic binding capacity is generally less than 2 times. Instead, a slight decrease in DBC has been observed with the increase of DG for membranes grafted with comb-like polymer architecture. The results show that unlike polymeric ion-exchange ligand[45], the relationship between DG of PVCL chains and DBC is not simply linear. Moreover, as it can be seen from Figure 4.9b that recovery has clearly shown a decrease when DG increases. As schematically shown in Figure 4.10, four different scenarios were proposed to illustrate the effects of grafted polymer architecture on DBC. Short poly (HEMA) chains (case I, III) give better improvement of capacity at around 12 mg/mL while maintaining the recovery close to 80%. On the other hand, long and high density poly (HEMA) chains (case IV) have a lower capacity of about 9 mg/mL while protein recovery is only at 60-70%. The capacity for low density and long chains (case II) remains at 11-12 mg/mL whereas recovery reduces to about 70%. Our previous results show that grafting degree of PVCL is generally less than 1% when grafted directly on RC membrane substrate. Moreover, our earlier data indicate that higher grafting degree results in higher dynamic binding capacities. The best performance for DBC is around 7 mg/mL and for recovery is over 96% when PVCL DG is about 0.2 $\mu g/cm^2$. In the case of grating these comb-like block copolymers on RC membrane substrates, it is possible to increase the PVCL grafting degree to over 10%. BSA binding capacity reaches 12 mg/mL when the grafting degree is around 2 $\mu g/cm^2$ with a reduced recovery of about 80%. Further increase in DG results in a significant reduction in capacity and further reduction in recovery. These results suggest that significant steric hindrance could occur for long primary poly(HEMA) polymer chains. Steric hindrance not only affects the binding capacity, but also recovery particularly during dynamic binding test when kinetics plays a critical role. In conclusion our results suggest that short and

relatively dense primary polymer chains give the best capacity and recovery for dynamic

binding test of BSA for these comb-like PVCL ligands.

Table 4.1 Backbone density and length effects on dynamic binding capacity and recovery

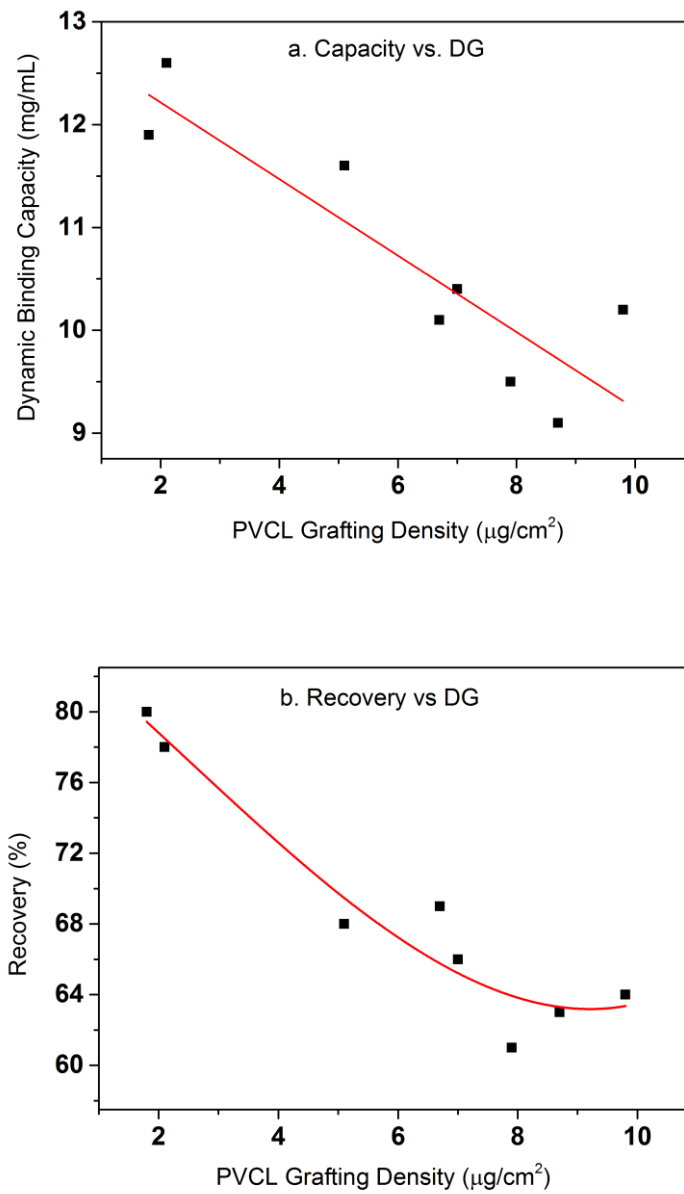| HEMA Initiator (mM)	HEMA Polymerization Time (h)	PVCL (µg/cm^2)	DBC (mg/mL)	Recovery (%)
10	0.25	1.8	11.9±0.4	80±3
10	1	5.1	11.6±0.6	68±4
10	4	8.7	9.1±0.9	63±4
20	1	6.7	10.1±0.7	69±4
20	4	9.8	10.2±0.5	64±4
40	1	7.0	10.4±0.6	66±3
80	0.25	2.1	12.6±0.3	78±3
80	1	7.9	9.5±0.4	61±3
Linear PVCL		0.2	6.9±0.3	96±3

Figure 4.9 Dynamic binding capacity (a) and recovery (b) as a function of PVCL grafting density.
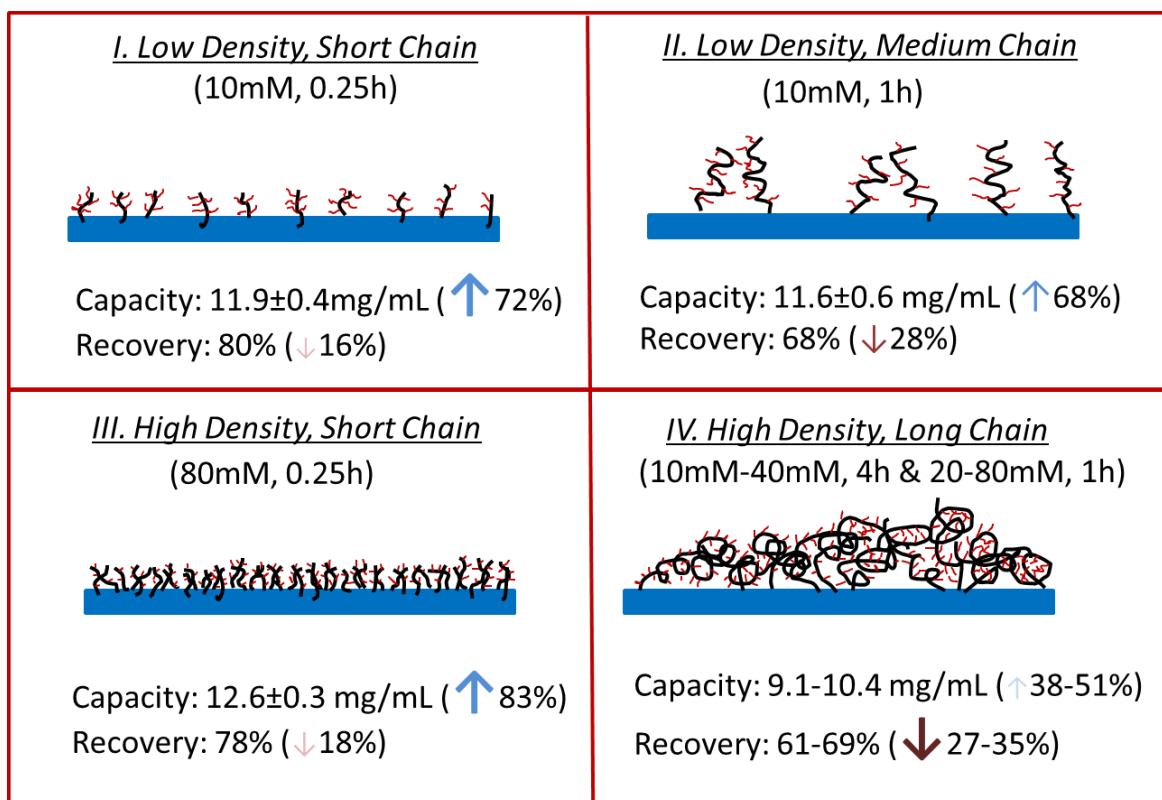
Figure 4.10 Backbone density/length effect on capacity and recovery.

We have characterized primary poly (HEMA) modified membrane surfaces in water with AFM at room temperature (Figure 4.11). Compared to the unmodified regenerated cellulose membrane, high density (160 mM BIB) or long chain (4 h ATRP) modified membranes show much less pore structure. The membrane pores are likely to be covered with grafted polymers as shown in Figure 4.11 a-d. The roughness for the membrane surfaces (10 μm $\times 10$ μm) also shows an evident change of the surface morphology after modification (Figure 4.12). The longer the ATRP time of poly(HEMA), the higher the roughness values are. The blockage of the pore structure can cause reduced protein binding as well as decreased recovery because of the difficulty for protein to reach the bind sites and to elute out once they are bound.
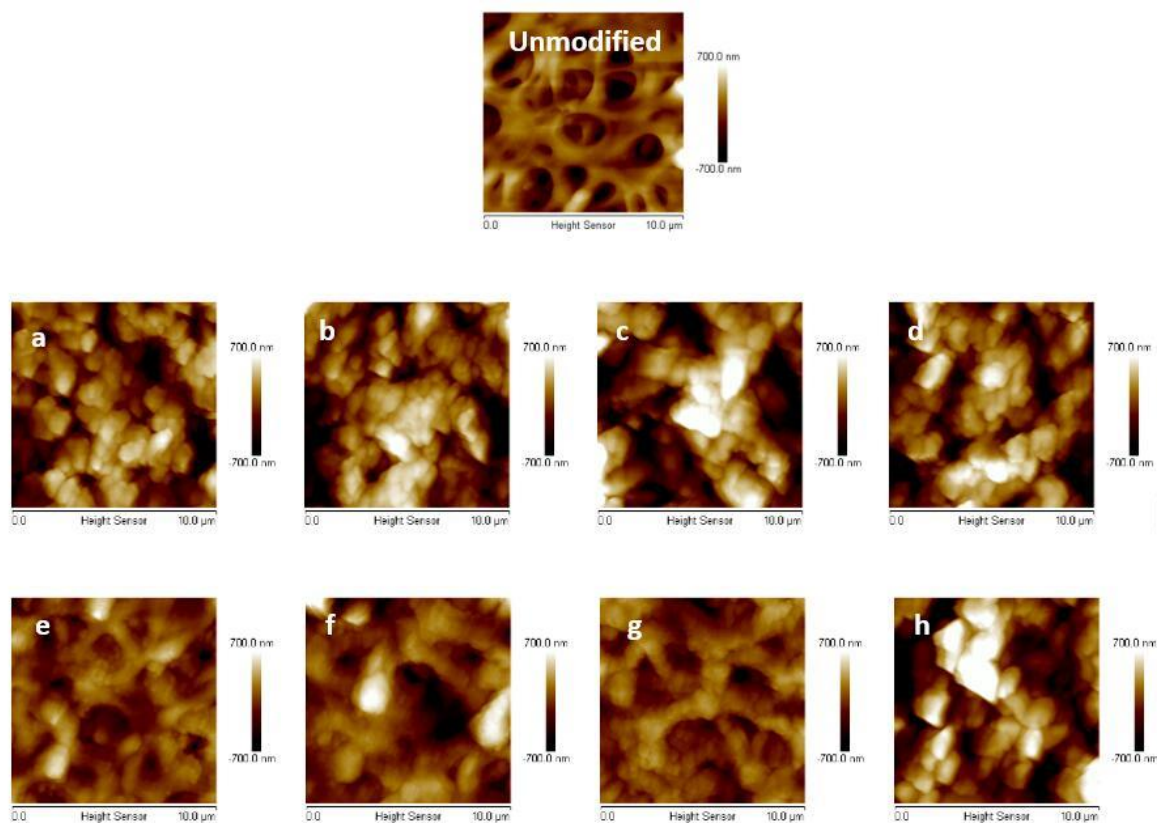
Figure 4.11 AFM results of unmodified membrane and comb-like PVCL modified membranes (a-d, 160mM BIB and 1,2,3 and 4h ATRP of HEMA; e-h, 40 mM BIB and 1,2,3,4 h ATRP of HEMA).
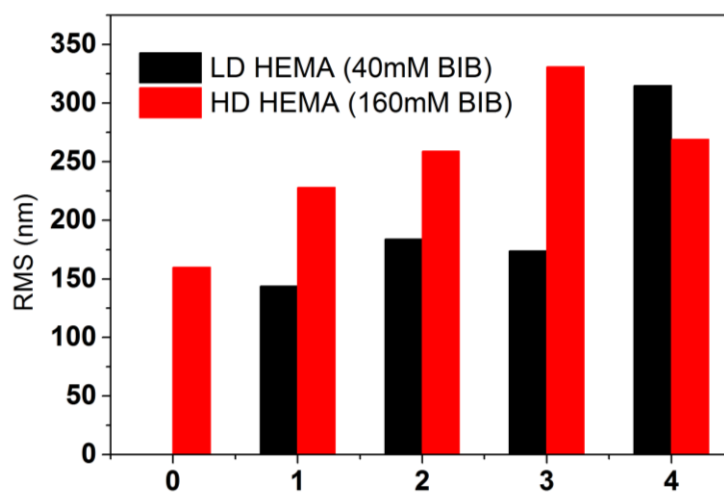

Figure 4.12 Root mean square roughness (Rq) analysis of the comb-like modified membranes.

Besides investigating the effects of the chain density and chain length of grafted

primary poly(HEMA) chains, the effects of membrane pore size on protein binding and

recovery were also studies. RC membranes with 1 μm and 0.45 μm pore sizes were modified with 15 min ATRP time of HEMA in order to prevent any possible blockage of pores after modification. Overall, the DG of poly (HEMA) and PVCL for 1 μm pore size membrane is about half of the DG for 0.45 μm pore size at the same initiator immobilization and polymerization conditions as shown in Table 4.2. This is probably due to the fact that the total surface area of 1 μm membrane is less than 0.45 μm membrane. To our surprise, the recovery for 1 μm pore size RC membrane is even lower than that for the 0.45 μm pore size membrane. The contact angle of water for these two membranes further confirmed that 1 μm pore size membrane is more hydrophobic, which explains the low recovery results. The responsiveness of 1 μm pore size membrane to the presence of salt ions, measured by the contact angle differences between DI water and 1.8 M $(NH_4)_2SO_4$ salt solution, is found to be less ($< 2^o$) than that ($\sim 6^o$) of the 0.45 um pore size membrane at the same conditions. Moreover, the contact angles in both DI water and salt solution for the 1 μm modified RC membrane are much higher than the corresponding ones for the 0.45 μm modified RC membrane. As is known, that the LCST of PVCL is strongly dependent on the molecular weight of the polymer chains[23]. Higher molecular weight chains tend to have a reduced LCST. Since it is easier for molecules to diffuse through larger pores and that there is less crowding effect in larger pores, it is likely that the molecular weight of the PVCL chains grafted on 1 μm RC membrane is higher than the corresponding 0.45 μm one even though the grafting degree is lower. As a result, the PVCL chains are more hydrophobic when grafted on the 1 μm pore size membrane.

Table 4.2 Membrane pore size effects on binding capacity and recovery. Grafting degrees are normalized by the weight of unmodified membranes.

Pore size	HEMA ATRP	[HEMA BIB]	DG HEMA (g/g)	DG BIB (g/g)	DG PVCL (g/g)	DBC (mg/mL)	Recovery (%)	Contact Angle	
								Water	1.8M $(NH_4)_2SO_4$
1 μm	15 min	10 mM	6.6	6.6	10.8	7.4	27%	109.0°	110.4°
		80 mM	7.5	8.1	13.6	7.5	13%	114.3°	116.2°
0.45 μm	15 min	10 mM	11.3	11.6	19.6	11.9	80%	98.2°	104.6°
		80 mM	13.2	13.5	23.7	12.6	78%	96.2°	102.2°

In addition, the effects of grafted secondary PVCL chain density on protein binding and recovery were also investigated. As shown in Table 4.3, the 2nd initiator concentration for grafting PVCL varies from 10 mM to 160 mM while the primary polymer chain grafting conditions (10 mM BIB and 0.25 h ATRP for grafting poly (HEMA)) were kept the same. The corresponding DG value of grafted PVCL increases from 1.14 to 2.21 $\mu m/cm^2$. Dynamic binding capacity also increases as the DG of PVCL increases, while the recovery shows a slight decline from 96% to 80%. From the contact angle measurement results under 1.8 M $(NH_4)_2SO_4$ solution, it shows that the higher the density of PVCL, the higher the contact angle indicating the surface is more hydrophobic at higher density leading to a higher binding capacity. This study shows that there is likely a trade-off between the dynamic capacity and recovery. Similar results have also been observed in our previous work for linear PVCL grafted RC membranes[22]. It is likely that when PVCL density is high, steric hindrance limits the mobility of the proteins leading to a lower recovery during dynamic binding tests. Based on our results, the initiator concentration for grafting PVCL needs to be kept below 80 mM if the required recovery is above 90%.

Table 4.3 PVCL polymer chain density effect on binding capacity and recovery at the same the grafting conditions (10 mM BIB and 0.25 h ATRP for grafting poly (HEMA)) for the primary poly(HEMA) chains on 0.45 μm pore size RC membranes

VCL initiator (mM)	DG PVCL ($\mu g/cm^2$)	DBC (mg/mL)	Recovery (%)	Contact Angle (1.8 M $(NH_4)_2SO_4$)
10	1.14	8.4	96	101.6 ± 1.0
20	1.37	8.8	96	104.0 ± 0.6
40	1.83	9.0	93	104.4 ± 1.7
80	2.05	9.1	84	105.5 ± 0.8
160	2.11	11.7	80	108.0 ± 0.3

In order to further explore the binding mechanism of our comb-like responsive PVCL ligands, the BSA binding isotherms were determined based on static protein adsorption studies. The results were fitted with the Freundlich adsorption model (Eq 2), where qe is the binding capacity at the protein equilibrium concentration Ce. K_F and 1/n are fitting parameters for a given adsorbant.

$$\log qe = \log K_F + 1/n \log Ce \qquad (2)$$

Unlike the linear PVCL which fits well with the Langmuir model, Freundlich model fits much better here for the comb-like PVCL ligands binding isotherm. Freundlich model has been widely applied to the highly interactive species adsorbed on the activated carbon or molecular sieves[46, 47, 48]. It is also known as an empirical model applied to the multi-layer adsorption with a heterogeneous surface[46], whereas Langmuir model assumes monolayer adsorption. Therefore, the multi-layer adsorption is very likely to happen for our comb-like ligands, although not all the sites are available for BSA binding. As shown in Table 4.4, the slope of the fitting line (1/n) indicates the heterogeneity of the binding sites probably due to the steric hindrance effect. The PVCL ligands located on the out-layer of the poly(HEMA) chains are more accessible to protein. The denser the backbone is, the harder it becomes for protein to reach to the inner binding sites. As the results shown in Figure 4.13, the slope is

lower in a high-density poly(HEMA) condition, which means the binding sites are more
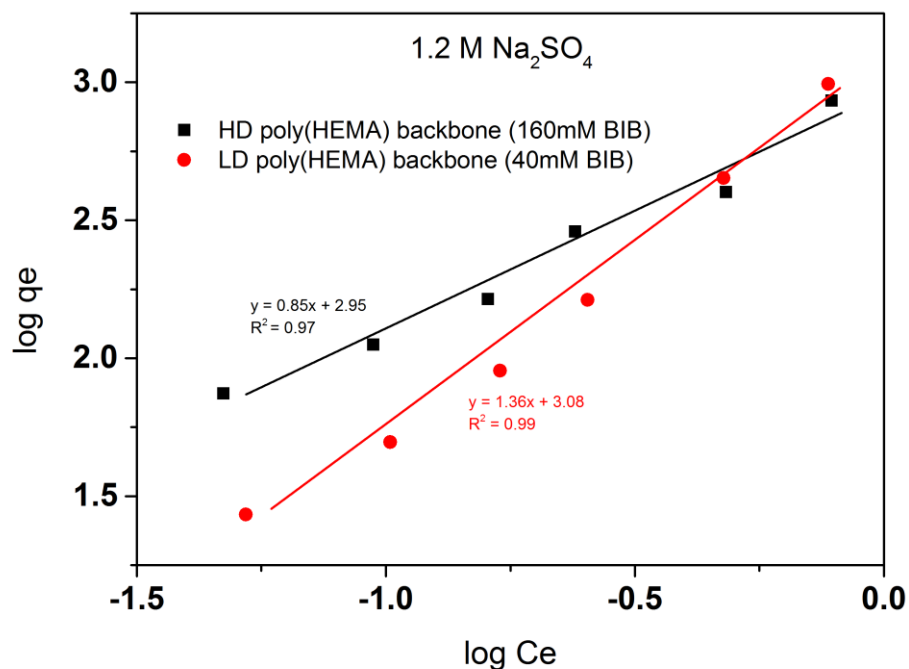
heterogeneous when backbone chains become denser.

Figure 4.13 Freundlich linear fitting of BSA isotherm for comb-like HIC membranes. Two backbone densities were tested here with 40 mM and 160 mM BIB used in the first initiation step.

Table 4.4 Fitting parameters of Freundlich model for comb-like PVCL modified membranes with a high/low density of poly (HEMA) backbones.

	Fitting Equation	1/n	K_F
HD poly (HEMA) backbone	y=0.85x+2.95	0.85	891.25
LD poly (HEMA) backbone	y=1.36x+3.08	1.36	1202.26

4.5 Conclusions

We have successfully increased the grafting degree of PVCL on RC membranes by

10-40 times by introducing a primary poly (HEMA) brushes as backbones to grow the

secondary PVCL brushes forming comb-like ligands. The effects of both primary and

secondary polymer chain length and chain density on protein binding and recovery were systematically studied by varying the ATRP initiation and polymerization conditions. Based on the results of BSA capacity and recovery, the optimal DG of PVCL has been found to be 1-2 μg/cm^2, where the capacity has improved from 7 to 12 mg/mL, for the linear PVCL homopolymer brushes grafted directly on the membrane substrate while the recovery is maintained above 80%. Our results show that introducing long primary poly (HEMA) chains decreases the protein recovery dramatically with a limited improvement in binding capacity. Further increase in primary poly (HEMA) chain length decreases the BSA binding capacity. AFM measurements show that the pore could be blocked at high DG of PVCL. This can partly explain the low recovery results at long primary polymer chains. The self-interaction of collapsed brushes, which buried most of the binding ligands and made proteins difficult to approach to the ligands, is likely the reason for the limited improvement in binding capacity. Larger 1 μm pore size RC membranes showed a worse binding capacity and recovery than the 0.45 μm pore size membranes. The effects of PVCL chain density on protein binding and recovery demonstrate a trade-off between the two. The higher the PVCL DG value, the higher the contact angle of the membrane surface, and the higher the binding capacity. In contrast, the recovery decreases at higher PVCL DG value. Finally, BSA isotherm shows that it is likely to be a multi-layer adsorption model for the comb-like ligands grafted rather than the mono-layer adsorption model for the linear PVCL ligands. Based on the parameters obtained from Freundlich model, it was found that the heterogeneity of the binding sites increases as the primary poly (HEMA) chain density increases.

Reference

1.   Cramer, S. M.; Holstein, M. A. Downstream bioprocessing: recent advances and future promise. *Curr. Opin. Chem. Eng.* **2011,** *1* (1), 27-37.

2.   Guiochon, G.; Beaver, L. A. Separation science is the key to successful biopharmaceuticals. *J. Chromatogr. A* **2011,** *1218* (49), 8836-8858.

3.   Freitag, R. Chromatographic Techniques in the Downstream Processing of Proteins in Biotechnology. In *Animal Cell Biotechnology*, Pörtner, R., Ed.; Humana Press, 2014; Vol. 1104, pp 419-458.

4.   Gottschalk, U. Downstream Processing of Monoclonal Antibodies: from High Dilution to High Purity. *Biopharm. Int.* **2005,** *18*, 42-58.

5.   Bhut, B. V.; Husson, S. M. Dramatic performance improvement of weak anion-exchange membranes for chromatographic bioseparations. *J. Membr. Sci.* **2009,** *337* (1–2), 215-223.

6.   Chenette, H. C. S.; Robinson, J. R.; Hobley, E.; Husson, S. M. Development of high-productivity, strong cation-exchange adsorbers for protein capture by graft polymerization from membranes with different pore sizes. *J. Membr. Sci.* **2012,** *423–424* (0), 43-52.

7.   Ghosh, R. Separation of proteins using hydrophobic interaction membrane chromatography. *J. Chromatogr. A* **2001,** *923* (1–2), 59-64.

8.   Weaver, J.; Husson, S. M.; Murphy, L.; Wickramasinghe, S. R. Anion exchange membrane adsorbers for flow-through polishing steps: Part II. Virus, host cell protein, DNA clearance, and antibody recovery. *Biotechnol. Bioeng.* **2013,** *110* (2), 500-510.

9.   Yoo, S. M.; Ghosh, R. Simultaneous removal of leached protein-A and aggregates from monoclonal antibody using hydrophobic interaction membrane chromatography. *J. Membr. Sci.* **2012,** *390*, 263-269.

10.   Weaver, J.; Husson, S. M.; Murphy, L.; Wickramasinghe, S. R. Anion exchange membrane adsorbers for flow-through polishing steps: Part I. clearance of minute virus of mice. *Biotechnol. Bioeng.* **2013,** *110* (2), 491-499.

11.   Phillips, M.; Cormier, J.; Ferrence, J.; Dowd, C.; Kiss, R.; Lutz, H.; Carter, J. Performance of a membrane adsorber for trace impurity removal in biotechnology manufacturing. *J. Chromatogr. A* **2005,** *1078* (1–2), 74-82.

12.   Bhut, B. V.; Weaver, J.; Carter, A. R.; Wickramasinghe, S. R.; Husson, S. M. The role of polymer nanolayer architecture on the separation performance of anion-exchange membrane adsorbers: Part II. DNA and virus separations. *Biotechnol. Bioeng.* **2011,** *108* (11), 2654-2660.

13.   Dods, S. R.; Hardick, O.; Stevens, B.; Bracewell, D. G. Fabricating electrospun cellulose nanofibre adsorbents for ion-exchange chromatography. *J. Chromatogr. A* **2015,** *1376*, 74-83.

14.   Bhut, B. V.; Wickramasinghe, S. R.; Husson, S. M. Preparation of high-capacity, weak anion-exchange membranes for protein separations using surface-initiated atom transfer radical polymerization. *J. Membr. Sci.* **2008,** *325* (1), 176-183.

15.   Wang, J.; Sproul, R. T.; Anderson, L. S.; Husson, S. M. Development of multimodal membrane adsorbers for antibody purification using atom transfer radical polymerization. *Polymer* **2014,** *55* (6), 1404-1411.

16.   Queiroz, J. A.; Tomaz, C. T.; Cabral, J. M. S. Hydrophobic interaction chromatography of proteins. *J. Biotechnol.* **2001,** *87* (2), 143-159.

17. Ghose, S.; Tao, Y.; Conley, L.; Cecchini, D. Purification of monoclonal antibodies by hydrophobic interaction chromatography under no-salt conditions. *mAbs* **2013,** *5* (5), 795-800.

18. To, B. C. S.; Lenhoff, A. M. Hydrophobic interaction chromatography of proteins: I. The effects of protein and adsorbent properties on retention and recovery. *J. Chromatogr. A* **2007,** *1141* (2), 191-205.

19. To, B. C. S.; Lenhoff, A. M. Hydrophobic interaction chromatography of proteins: III. Transport and kinetic parameters in isocratic elution. *J. Chromatogr. A* **2008,** *1205* (1–2), 46-59.

20. To, B. C. S.; Lenhoff, A. M. Hydrophobic interaction chromatography of proteins: II. Solution thermodynamic properties as a determinant of retention. *J. Chromatogr. A* **2007,** *1141* (2), 235-243.

21. Haimer, E.; Tscheliessnig, A.; Hahn, R.; Jungbauer, A. Hydrophobic interaction chromatography of proteins IV: Kinetics of protein spreading. *J. Chromatogr. A* **2007,** *1139* (1), 84-94.

22. Himstedt, H. H.; Qian, X.; Weaver, J. R.; Wickramasinghe, S. R. Responsive membranes for hydrophobic interaction chromatography. *J. Membr. Sci.* **2013,** *447* (0), 335-344.

23. Meeussen, F.; Nies, E.; Berghmans, H.; Verbrugghe, S.; Goethals, E.; Du Prez, F. Phase behaviour of poly(N-vinyl caprolactam) in water. *Polymer* **2000,** *41* (24), 8597-8602.

24. N.A. Yanul, O. Y. Z., K.K. Kalninsh, Yu. E. Kirsh. *Zurnal Fiziceskoj Chimii* **1998,** *72*, 1037

25. Mata-Gómez, M. A.; Yaman, S.; Valencia-Gallegos, J. A.; Tari, C.; Rito-Palomares, M.; González-Valdez, J. Synthesis of adsorbents with dendronic structures for protein hydrophobic interaction chromatography. *J. Chromatogr. A* **2016,** *1443*, 191-200.

26. Wang, J.; Jenkins, E. W.; Robinson, J. R.; Wilson, A.; Husson, S. M. A new multimodal membrane adsorber for monoclonal antibody purifications. *J. Membr. Sci.* **2015,** *492*, 137-146.

27. Singh, N.; Wang, J.; Ulbricht, M.; Wickramasinghe, S. R.; Husson, S. M. Surface-initiated atom transfer radical polymerization: A new method for preparation of polymeric membrane adsorbers. *J. Membr. Sci.* **2008,** *309* (1-2), 64-72.

28. Liu, Z.; Du, H.; Wickramasinghe, S. R.; Qian, X. Membrane Surface Engineering for Protein Separations: Experiments and Simulations. *Langmuir* **2014,** *30* (35), 10651-10660.

29. Matyjaszewski, K. Atom Transfer Radical Polymerization (ATRP): Current Status and Future Perspectives. *Macromolecules* **2012,** *45* (10), 4015-4039.

30. Matyjaszewski, K.; Xia, J. Atom Transfer Radical Polymerization. *Chem. Rev.* **2001,** *101* (9), 2921-2990.

31. Yang, Q.; Ulbricht, M. Cylindrical Membrane Pores with Well-Defined Grafted Linear and Comblike Glycopolymer Layers for Lectin Binding. *Macromolecules* **2011,** *44* (6), 1303-1310.

32.   Yang, Q.; Tian, J.; Hu, M.-X.; Xu, Z.-K. Construction of a Comb-like Glycosylated Membrane Surface by a Combination of UV-Induced Graft Polymerization and Surface-Initiated ATRP. *Langmuir* **2007,** *23* (12), 6684-6690.

33.   Wu, G.; Chen, S.-C.; Zhan, Q.; Wang, Y.-Z. Well-Defined Amphiphilic Biodegradable Comb-Like Graft Copolymers: Their Unique Architecture-Determined LCST and UCST Thermoresponsivity. *Macromolecules* **2011,** *44* (4), 999-1008.

34.   Annaka, M.; Matsuura, T.; Kasai, M.; Nakahira, T.; Hara, Y.; Okano, T. Preparation of Comb-Type N-Isopropylacrylamide Hydrogel Beads and Their Application for Size-Selective Separation Media. *Biomacromolecules* **2003,** *4* (2), 395-403.

35.   Wan, L.-S.; Yang, Y.-F.; Tian, J.; Hu, M.-X.; Xu, Z.-K. Construction of comb-like poly(N-isopropylacrylamide) layers on microporous polypropylene membrane by surface-initiated atom transfer radical polymerization. *J. Membr. Sci.* **2009,** *327* (1–2), 174-181.

36.   Han, C.-C.; Wei, T.-C.; Wu, C.-S.; Liu, Y.-L. Temperature-responsive poly(tetrafluoroethylene) membranes grafted with branched poly(N-isopropylacrylamide) chains. *J. Membr. Sci.* **2010,** *358* (1–2), 60-66.

37.   Wever, D. A. Z.; Riemsma, E.; Picchioni, F.; Broekhuis, A. A. Comb-like thermoresponsive polymeric materials: Synthesis and effect of macromolecular structure on solution properties. *Polymer* **2013,** *54* (21), 5456-5466.

38.   Ma, Y.; Dong, J.; Bhattacharjee, S.; Wijeratne, S.; Bruening, M. L.; Baker, G. L. Increased Protein Sorption in Poly(acrylic acid)-Containing Films through Incorporation of Comb-Like Polymers and Film Adsorption at Low pH and High Ionic Strength. *Langmuir* **2013,** *29* (9), 2946-2954.

39.   Liu, L.; Li, W.; Liu, K.; Yan, J.; Hu, G.; Zhang, A. Comblike Thermoresponsive Polymers with Sharp Transitions: Synthesis, Characterization, and Their Use as Sensitive Colorimetric Sensors. *Macromolecules* **2011,** *44* (21), 8614-8621.

40.   Krishnan, S.; Ayothi, R.; Hexemer, A.; Finlay, J. A.; Sohn, K. E.; Perry, R.; Ober, C. K.; Kramer, E. J.; Callow, M. E.; Callow, J. A.; Fischer, D. A. Anti-Biofouling Properties of Comblike Block Copolymers with Amphiphilic Side Chains. *Langmuir* **2006,** *22* (11), 5075-5086.

41.   Himstedt, H. H.; Yang, Q.; Dasi, L. P.; Qian, X.; Wickramasinghe, S. R.; Ulbricht, M. Magnetically Activated Micromixers for Separation Membranes. *Langmuir* **2011,** *27* (9), 5574-5581.

42.   Yang, Q.; Himstedt, H. H.; Ulbricht, M.; Qian, X.; Ranil Wickramasinghe, S. Designing magnetic field responsive nanofiltration membranes. *J. Membr. Sci.* **2013,** *430*, 70-78.

43.   Himstedt, H. H.; Yang, Q.; Qian, X.; Ranil Wickramasinghe, S.; Ulbricht, M. Toward remote-controlled valve functions via magnetically responsive capillary pore membranes. *J. Membr. Sci.* **2012,** *423–424*, 257-266.

44.   Qian, X.; Lei, J.; Wickramasinghe, S. R. Novel polymeric solid acid catalysts for cellulose hydrolysis. *RSC Adv.* **2013,** *3* (46), 24280-24287.

45.   Bhut, B. V.; Conrad, K. A.; Husson, S. M. Preparation of high-performance membrane adsorbers by surface-initiated AGET ATRP in the presence of dissolved oxygen and low catalyst concentration. *J. Membr. Sci.* **2012,** *390–391*, 43-47.

46.   Foo, K. Y.; Hameed, B. H. Insights into the modeling of adsorption isotherm systems. *Chem. Eng. J.* **2010,** *156* (1), 2-10.

47.   Haghseresht, F.; Lu, G. Q. Adsorption Characteristics of Phenolic Compounds onto Coal-Reject-Derived Adsorbents. *Energy & Fuels* **1998,** *12* (6), 1100-1107.

48.   Ahmaruzzaman, M. Adsorption of phenolic compounds on low-cost adsorbents: A review. *Adv. Colloid Interface Sci.* **2008,** *143* (1–2), 48-67.

Chapter 5 The Effects of Copolymerization on Responsive Hydrophobic Interaction Membrane Chromatography

Abstract

In this chapter, the focus is on developing copolymeric responsive HIC ligands for protein separations. Vinyl caprolactam (VCL) monomer was copolymerized with various monomers with varying hydrophobicity. Copolymeric ligands were mainly grafted from PES membrane substrates via UV initiated polymerization. The effects of copolymer composition on binding capacity and recovery were investigated. It was found that protein binding capacity decreases with the increase of hydrophilic monomers incorporated. Additionally, a pH-responsive monomer (4-vinyl pyridine, 4-VP) was successfully copolymerized with VCL, which renders a pH/salt responsive membrane adsorber. The percentage of 4-VP incorporated affects binding capacity as well as recovery due to the change in copolymer hydrophobicity. In addition, the copolymer is sensitive to pH due to its effects on the net charge of 4-VP and subsequently the electrostatic interactions with BSA. Overall, this chapter provides some preliminary studies on the copolymeric responsive HIC ligands. The pH effect was studied by static and dynamic binding tests using BSA and lysozyme as model proteins. The pH/salt responsive HIC membranes are promising as a next generation smart chromatographic materials with a facile elution advantage.

5.1 Introduction

Over the years, monomers of the thermo-responsive polymers, such as N-isopropylacrylamide (NIPAM), have been copolymerized with various other functional monomers for cell separations[1], hydrophilic analyte separations[2] and biomolecular separations[3, 4, 5, 6]. Both hydrophilic and hydrophobic monomers have been incorporated to form copolymers of PNIPAM. As shown in Figure 5.1, monomers such as butyl methacrylate (BMA)[1, 2, 5, 7, 8] and butyl acrylate (BA)[6, 9] have been widely copolymerized with NIPAM. In general, incorporating hydrophilic monomers tend to increase the LCST of the copolymer whereas incorporating hydrophobic monomers tend to decrease the LCST. Hydrophilic charged monomers such as 2-(dimethylamino)ethylmethacrylate[3], 2-acrylamido-2-methylpropanesulfonate[10] and acrylic acid[4] have also been copolymerized with NIPAM via ATRP for bioseparations. Based on the results[1, 2], BMA and NIPAM seem to have very similar ATRP polymerization rates. Copolymerizing 5% BMA into PNIPAM, the LCST has decreased to 16-19 $^{\circ}$C from 32°C in water[1, 2]. However, other PNIPAM-co-BMA copolymer with free radical polymerization exhibits a LCST at 25-26 $^{\circ}$C [7, 8] when 5% BMA was incorporated. When NIPAM was copolymerized with (dimethylamino) ethylmethacrylate, the LCST increases to 60 $^{\circ}$C[3]. Kenichi Nagase et.al copolymerized three monomer acrylic acid, PNIPAM and butylacrylamide in solution. Their results show that by incorporating the hydrophobic monomer butylacrylamide and with an appropriate mole fraction of acrylic acid (3-11%), it is possible to control the LCST to reach somewhere between 26-35 $^{\circ}$C[4]. Wu et. al copolymerized VCL with NIPAM to form block copolymers by reversible addition−fragmentation chain-transfer polymerization (RAFT)[11]. Their results show that only one LCST transition can be observed for the copolymer. The transition temperature shifts between the LCST of PNIPAM (32 $^{\circ}$C) and PVCL (42 $^{\circ}$C) based on the mole ratio between these two. Interestingly, the differential scanning calorimetry (DSC) curve shows that the

block copolymer combines the sharp change of PNIPAM as well as the gradual change of PVCL.

For HIC studies, Qu et.al developed a HIC giga-porous polystyrene (PS) microspheres with PNIPAM-co-PBMA as the responsive ligand[5]. The binding kinetics show improvement and three model proteins (Trypsin, BSA and acid phosphatase) have been fractionated by temperature gradient elution. Binding capacity is around 25 mg BSA/g dry microsphere, which is close to the highest binding capacity of our PVCL-ATRP (4 h) membrane (21 mg BSA/ dry membrane) under 1.2 M Na_2SO_4. Also, the polystyrene substrate may have impacts on BSA binding since the unmodified microsphere showed the highest binding capacity (close to 90 mg BSA/g unmodified microsphere). In addition, there is no recovery data of the microsphere for the BSA binding test. Ghosh et.al designed a comb-like HIC ligand grafted on RC membrane by UV-initiated polymerization[6]. The comb-like ligand contains a PNIPAM backbone and branches of PNIPAM-co-poly (butyl acrylate) (PBA) copolymer. This ligand showed a two-step phase transition behavior due to the backbone PNIPAM LCST (32 °C) and branches of PNIPAM-co-PBA LCST (21°C). Monoclonal antibody hIgG1-CD4 was purified from simulated CHO cell culture supernatant. However, the binding capacity is still low. Moreover, run-to-run differences were observed since the experimental temperature control is not precise enough.

Poly 4-vinylpyridine (P4VP) has been widely used to form pH-responsive polymers for biomedical and environmental applications[12]. Di-block copolymer P4VP (quaternized)-co-poly (acrylic acid) has been synthesized by Aryers et.al. Its pH-responsive behavior is found to be dependent on the copolymer composition[13]. pH-responsive membranes or films were also synthesized with P4VP or its derivatives [14, 15, 16, 17]. Protein separations were achieved with PS-co-P4VP membranes based on the charge-based mechanism under different pH conditions[18, 19]. Here, our main goal is to control the LCST of PNIPAM-co-P4VP by

varying the pH of the solution. At low pH, the pyridine group is protonated and therefore the LCST increases dramatically, which promotes the elution. On the other hand, when pH is high, the pyridine group is almost neutral and LCST should be unaffected. This could provide some advantages for multi-modal chromatography (MMC) to be used in a bind-and-elute mode because the elution is always complicated for MMC. Based on the property of the product (pI, hydrophobicity etc.), the operation window for binding and elution should be easier to determine with the pH responsive MMC. In this chapter, we still focus on HIC and provide some proofs that protein's binding and elution are affected by pH.
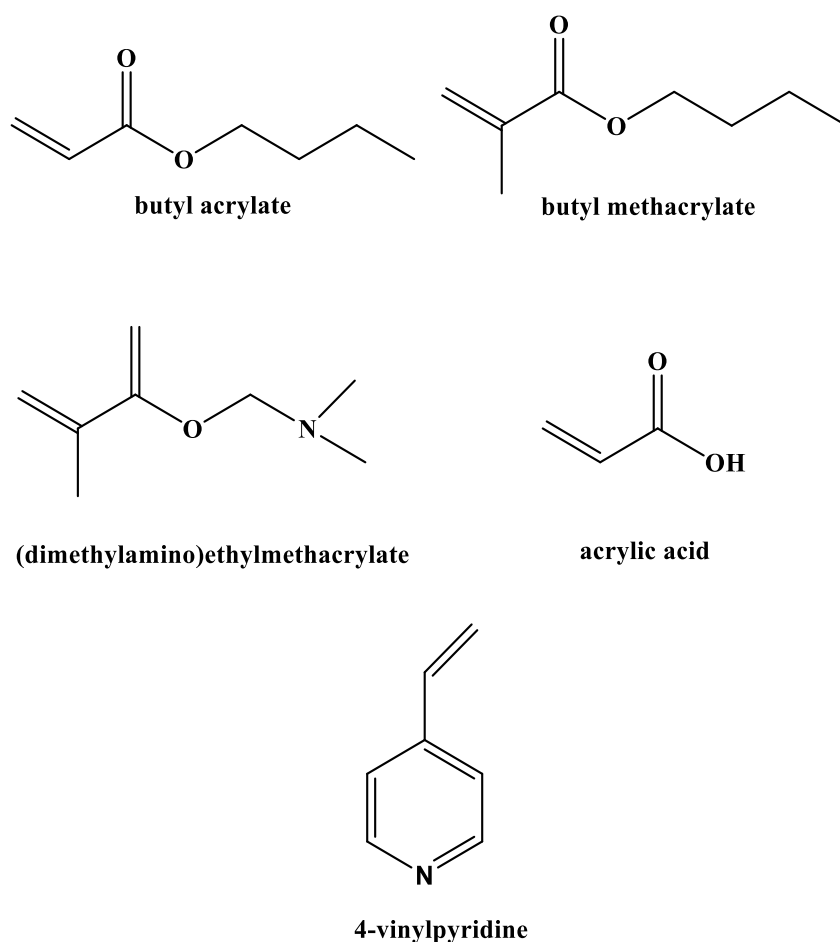
Figure 5.1 Reported monomers incorporated with NIPAM and pH responsive monomer 4-vinyl pyridine (4-VP).

Compared to the more expensive and tedious ATRP reaction, UV-induced polymerization has many advantages, although it has less control on the polydispersity of the grafted

polymers. First, the polymerization rate is much faster than ATRP. Here, we use polyethersulfone (PES) membranes as the substrate. Initiation is not necessary for PES membranes since the backbone of the membrane is UV sensitive (Figure 5.2). Unlike ATRP, it is a cleaner process since there is no copper catalyst used in the monomer solution. The mechanism of the initiation mechanism of PES membrane is shown in Figure 5.2 as reported earlier[20]. The C-S bond at the sulfone linkage is cleaved under the UV-irradiation. Two radical sites were generated and polymerization can happen at either site. In this chapter, UV-induced polymerization is conducted to investigate the effect of copolymerization. Different monomers were copolymerized with VCL and the dynamic binding capacity as well as recovery were tested.
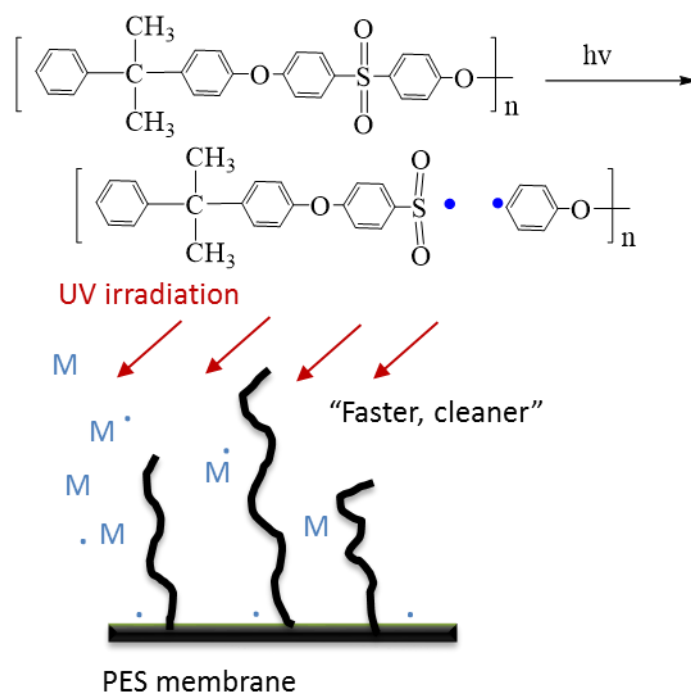
Figure 5.2 UV-induced polymerization for PES membranes: UV initiation mechanism and polymerization process.

5.2 Materials

N-Vinylcaprolactam (98%), 2-Hydroxyethyl methacrylate (98%), 2-Bromo-2-methylpropionyl bromide (BIB, 98%), 4-(dimethylamino) pyridine (≥99%), copper (I)

168

chloride ⩾99.995%), copper (II) chloride (⩾99.995%) and N,N,N′,N′′,N′′-

pentamethyldiethylenetriamine (PMDETA, 99%) were purchased from Sigma Aldrich (St.

Louis, MO). Triethylamine (TEA, ⩾99%), 4-Vinylpyridine (96%) and aluminum sulfate (⩾

97%) were obtained from Alfa Aesar (Ward Hill, MA). Methanol (99.8%) and acetonitrile

(99.8%) were obtained from EMD Chemicals (Billerica, MA). Boric anhydride was

purchased from Avantor Performance Materials (Center Valley, PA). Anhydrous acetonitrile

was obtained by distilling acetonitrile with boric anhydride. Ammonium sulfate (⩾99.0%)

was bought from Macron™ Fine Chemicals (Center Valley, PA). Regenerated cellulose

membranes (0.45 μm pore size, RC55, 47 mm diameter) were purchased from GE Healthcare

(Pittsburgh, PA). Bovine serum albumin (BSA) (>99 %, pI 4.7, 66 kDa) was obtained from

Avantor Performance Materials (Center Valley, PA). N-(2-hydroxypropyl) methacrylamide

(HPMA) was purchased from Polysciences, Inc (Warrington, PA).

5.3 Experimental

5.3.1 Membrane Surface Modification

UV-induced Polymerization PES membranes were first washed with methanol for 10 min.

Then, membranes were dried in a vacuum oven. Monomer solutions were prepared with

different ratios between VCL and other monomers. The total monomer concentration is kept

at 1 M with methanol/water (v/v=1:1) mixture as solvent. UV-induced polymerization was

followed by procedures published before[21]. PES membranes were immersed into the

monomer solution in a petri dish. Then, a glass cover was put on the top of the membrane.

UV-irradiation was conducted in a UV reactor (HONLE UV AMERICA, Inc) with standard

operational procedures. UV irradiation time was also varied.

5.3.2 Membrane Surface Characterization

ATR-FTIR ATR-FTIR provides a qualitative characterization for the membrane surface modification. The spectrum is taken by IRAffinity (Shimadzu, MD) with a horizontal ZnSe accessary. A piece of membrane was loaded on the crystal and scanned from 1000-2000 cm^{-1} wavenumber with a 8 cm^{-1} resolution. The results were processed with a baseline correction and normalized into the same scale (0-1) for comparison.

Contact Angle Membrane surface property is characterized by contact angle measurements. The instrument has an optical angle meter (OCA 20, *Future Digital Scientific Corp.*, NY) and a dosing needle. Membranes were cut into small pieces and pasted on a glass chip with double side tape. Sessile drop method was used for characterization. A liquid drop was placed on the membrane surface and the imagine is recorded by a camera for later analysis. The dosing volume of the solvent is 2 μL. The results for each membrane were averaged with at least 3 measurements at random locations.

AFM Surface morphology and roughness of the modified membranes were characterized by AFM (Dimension Icon, Bruker Corporation, MA) with Bruker's sharp nitride lever (SNL-10c) probes. ScanAsyst mode (in liquid) was used to image the morphology of membranes at room temperature in water. The scan rate is set at 1 Hz with a resolution of 256 samples per line. After scanning, the image is first processed with a third order flatten with Bruker's nanoscope analysis program. Roughness is calculated by the nanoscope analysis program after flatten.

5.3.3 Protein Binding Studies

Dynamic Binding Studies   All the buffer and protein solutions were filtered with 0.22 μm nylon membrane before the dynamics binding tests. 0.1 mg/mL bovine serum albumin (BSA) solutions were used for dynamic binding. Four layers of membranes (total bed volume 0.08 mL) were loaded into a stainless steel flow cell (Mustang Coin ® module, Pall Corporation)

Membrane stack was placed between two flow distributers to ensure a uniform flow distribution. Dynamic binding is conducted with ÄKTA FPLC from GE Healthcare. Running method was using Unicorn software v. 5.31 to automate the BSA binding and elution experiments as published before[22]. Briefly, the membrane stack was wet with buffer B (elution buffer, 20 mM Na_2HPO_4) over 5 minutes by gradient flow rate from 0.2 mL/min to 1 mL/min with a 0.2 mL/min increment. Next, buffer A (adsorption buffer, 1.8 M $(NH_4)_2SO_4$) was used for equilibrium at 1 mL/min for 10 minutes. Then 0.1 mg/mL protein solution was loaded onto the membrane holder at a flow rate of 1 mL/min for 10 minutes. Unbound protein was subsequently washed from the membranes using the buffer A (adsorption buffer, 1.8 M $(NH_4)_2SO_4$) for 10 minutes at 1 mL/min, followed by a step change of running buffer B at 1 mL/min for elution. The run ended when UV absorbance 280 nm and conductivity reached baseline. The washing fraction (includes loading fraction) and elution fraction were collected respectively. The total protein amount of these two fractions were determined by volumes and UV absorbance at 280 nm. The overall mass balance is over 90%.

Static Binding Studies After extensive washing of modified membranes with water, membranes were first immersed in high-salt concentration buffer for equilibrium. Then, membranes were taken out and wiped with the filter paper to remove the buffer on the surface. Membranes were soaked in the protein solution for 20 h. The concentration of protein was determined by UV absorbance at 280 nm with standard curves.

5.4 Results and Discussion

5.4.1 UV-induced polymerization

UV-induced polymerization was first optimized by varying the VCL concentration and UV irradiation time. Figure 5.3 shows that DG of PVCL increases exponentially at 1M and 0.25 M. It also shows that the polymerization rate is independent of concentration when

UV-irradiation time is less than 15 min. This result indicates that the monomer concentration is not a limiting factor here within the first 20 min for grafting PVCL. DG of PVCL reaches a plateau at 25 min under 2 M VCL condition. Interestingly, we have repeated the polymerization twice sequentially for 20 min and membrane with a very high DG was obtained. The results suggest that for longer UV irradiation time, not only PVCL has a longer chain, but also the grafting density is likely to be higher. Yamagishi et.al [20] studied the irradiation time effect on the grafting depth of PES membrane. It was found that the modification depth of PES membrane increases with the UV time.
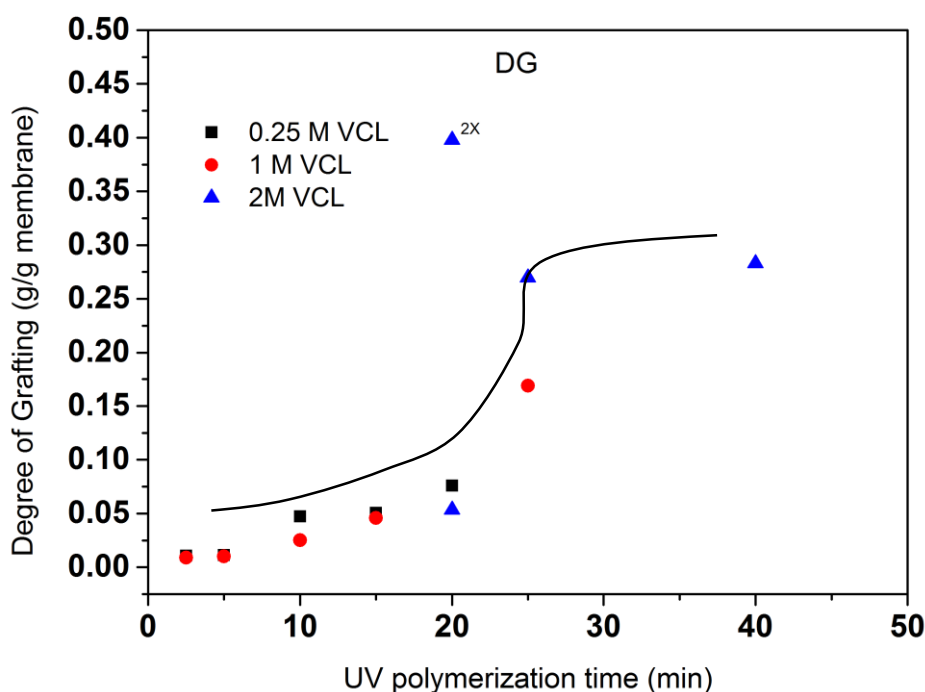
Figure 5.3 DG of PVCL under different UV polymerization time.

Figure 5.4 shows the ATR-FTIR spectra of PVCL modified PES membranes under different UV irradiation times. The peak at 1700 cm^{-1} corresponds to the amide group (C=O vibration). All the spectra have been normalized to the same scale for comparison. It can be seen that the intensity of the peak increases with UV time, suggesting that a higher grafting degree of PVCL can be obtained as UV irradiation time increases.
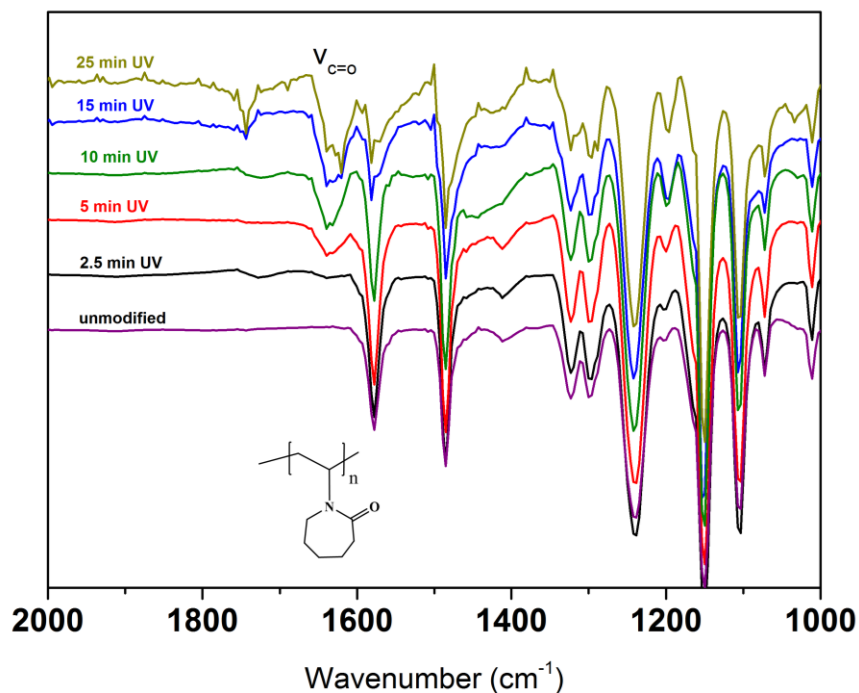
Figure 5.4 ATR-FTIR of PVCL modified PES membranes under different UV irradiation time.

Figure 5.5 shows the effect of UV polymerization time on the contact angle of modified membrane in 1.8 M $(NH_4)_2SO_4$ salt solution. The contact angle increases with UV polymerization time indicating that the membrane surface becomes more hydrophobic at longer UV irradiation time. These results correlate well with the dynamic binding results as shown in Figure 5.6. The higher the DG of PVCL is, the larger contact angle results, the higher the binding capacity will be. As discussed earlier, higher grafting degree with longer UV time results in a more hydrophobic surface. Besides the grafting density effect, it is also possible that the grafted PVCL chain is longer under longer UV irradiation time. The longer chains of PVCL are likely to have a lower LCST and a larger binding area for protein interaction. The density effect and chain length effect are hard to de-couple due to the well-known disadvantage of non-controllable UV-initiated radical polymerization.
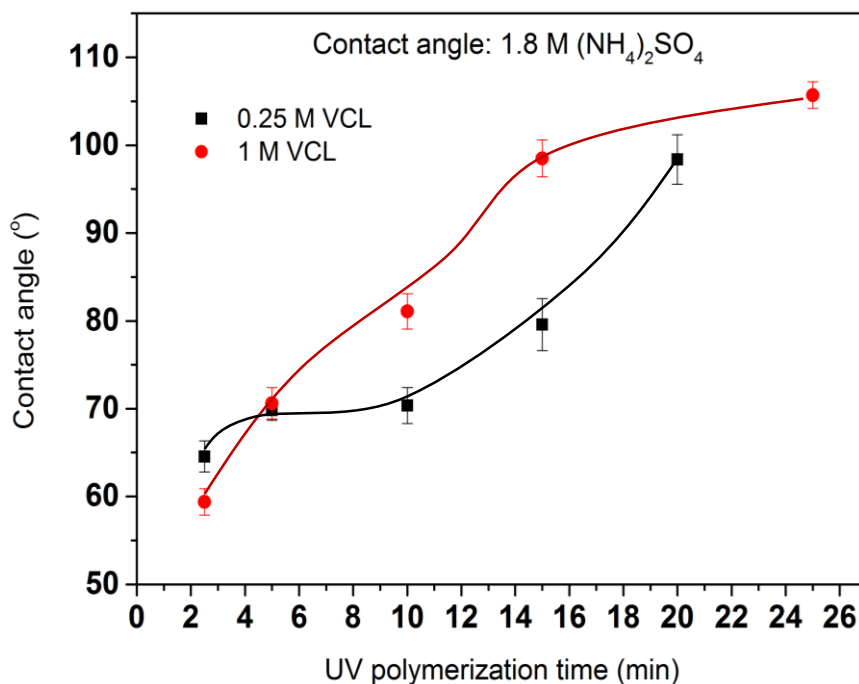
Figure 5.5 Contact angle of 1.8 M $(NH_4)_2SO_4$ for PVCL modified PES membranes with different DG.

Figure 5.6 (a) shows the effect of UV time on the dynamic binding capacity and recovery. The capacity shows a linear increase with UV time. The monomer concentration seems to have a minor effect on the binding capacity. The recovery is very high for all the conditions. As Figure 5.6 (b) shown, the breakthrough curves have a lower UV absorbance for longer UV time modified membranes. The elution peak area also increases accordingly with UV polymerization time. Overall, the binding capacity reaches about 4 mg/mL, which is close to what we obtained before for regenerated cellulose membrane with ATRP. The difference is likely due to the different total surface area for these two membrane substrates. Regenerated cellulose membranes are likely to have a higher total surface area because it has a smaller average pore size (0.45 μm) compared to PES membranes (0.65 μm).
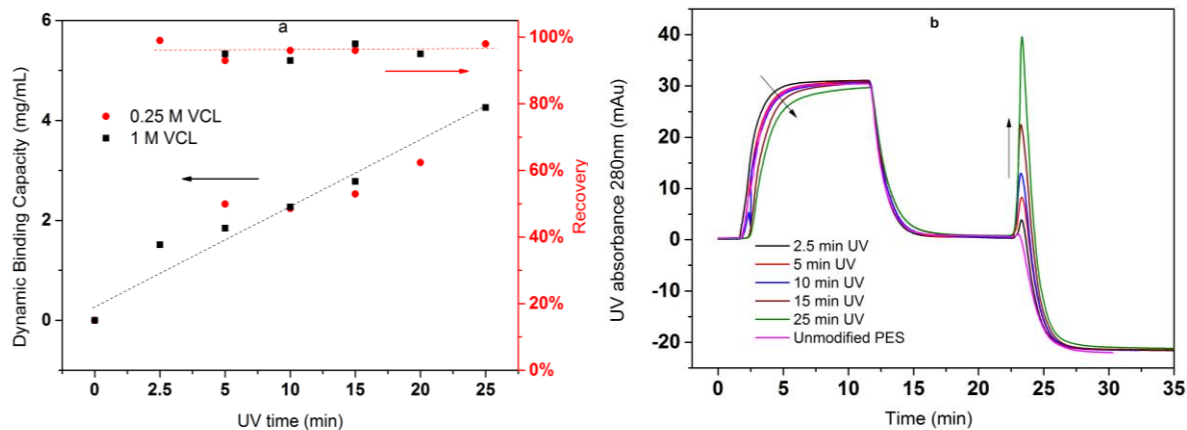
Figure 5.6 Dynamic binding capacity (a) and chromatogram (b) of PVCL modified PES membranes under different UV irradiation time and different monomer concentrations (0.25 M and 1 M VCL).

5.4.2 Linear copolymerization

In order to further understand the LCST effect of PVCL on protein binding, we have copolymerized VCL with monomers with different properties. Based on the optimized UV condition that has the highest binding capacity, all the UV irradiation time was kept for 20 min and the total monomer concentration is kept at 1 M. As shown in Figure 5.7, monomer *a* and *b* are hydrophilic. Monomer *c* and *d* are relatively more hydrophobic, and after polymerization, *c* and *d* form thermo-responsive and pH responsive polymers, respectively.

N-(2-Hydroxypropyl) methacrylamide
a.HPMA

N-Hydroxyethyl acrylamide
b.HEA

N-Isopropylacrylamide
c.NIPMA

4-vinylpyridine
d.4-VP
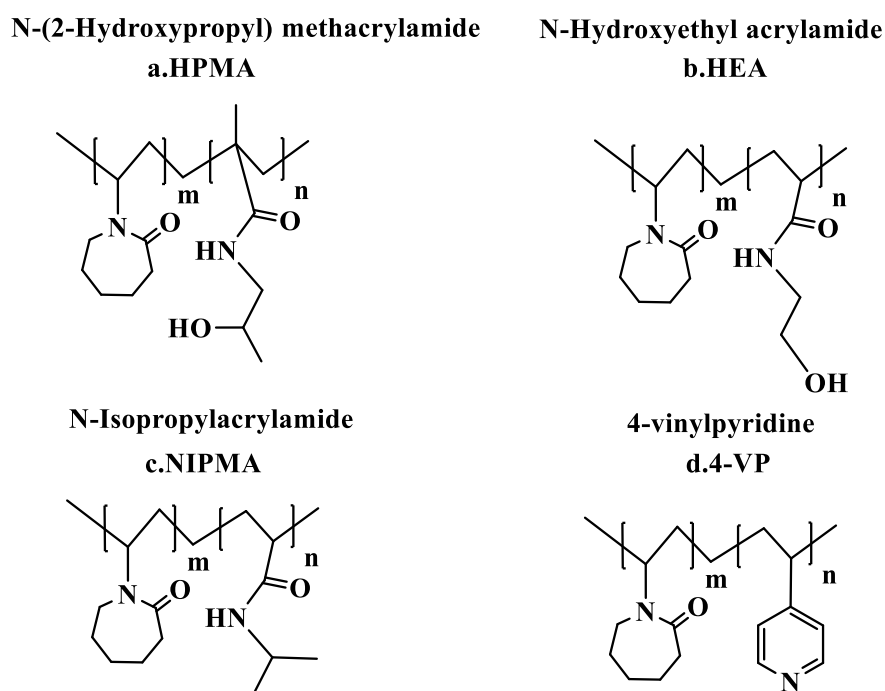
Figure 5.7 Copolymers with VCL by ATRP or UV-initiated polymerization.

Based on the binding results, copolymerization of the first three monomers (a-c) renders the static binding capacity 2-3 times less than the corresponding homopolymer PVCL. This is likely due to the fact that the copolymers become more hydrophilic after copolymerizing with hydrophilic monomers. In other words, the LCST increases after copolymerizing with a hydrophilic monomer. It is also interesting to note that PNIPMA has a relatively low binding capacity compared to PVCL, even though its DG is much higher. 4-vinyl pyridine (4-VP) is a pH responsive monomer. Its conjugated acid form has a pKa at around 5. When the solution pH is 5 and above, the deprotonated form of 4-VP is more stable. The protonated 4-VP becomes more stable when pH is below 5. The distribution of the neutral and protonated form of 4-VP is simulated by Marvinsketch 16.2 as shown in Figure 5.8. We have varied the monomer ratio between VCL and 4-VP for UV-induced copolymerization. Figure 5.9 shows the DG values for VCL and 4-VP individually under different UV irradiation times. It can be seen that 4-VP seems to have a more linear DG growth over time. We used 25 min UV irradiation time for all the subsequent

copolymerization studies. The total monomer concentration was kept at 1 M with varying the mole ratio between 4-VP and VCL. Dynamic binding studies with 0.1 mg/mL BSA were conducted under 1.8 M $(NH_4)_2SO_4$ for binding and 20 mM NaOAc buffer for elution. The pH of the binding buffer was varied from 6.0 to 8.5 and the elution pH was tested under 4.0 and 7.0.
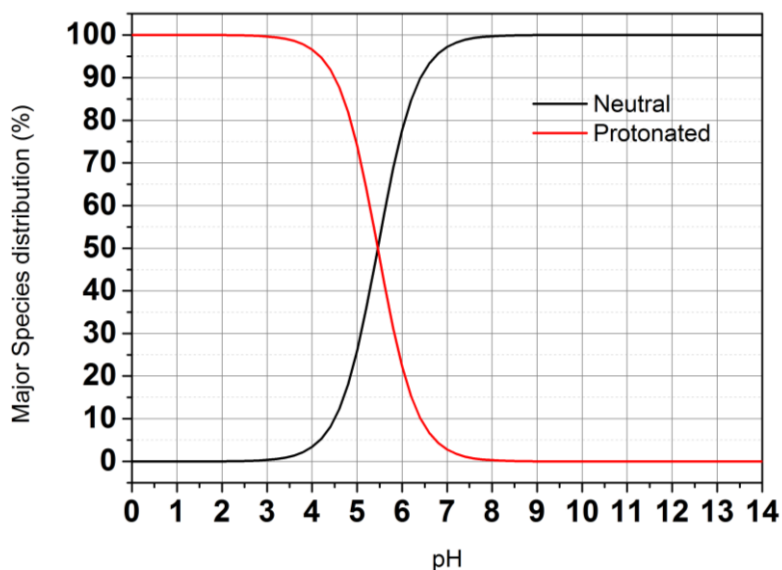

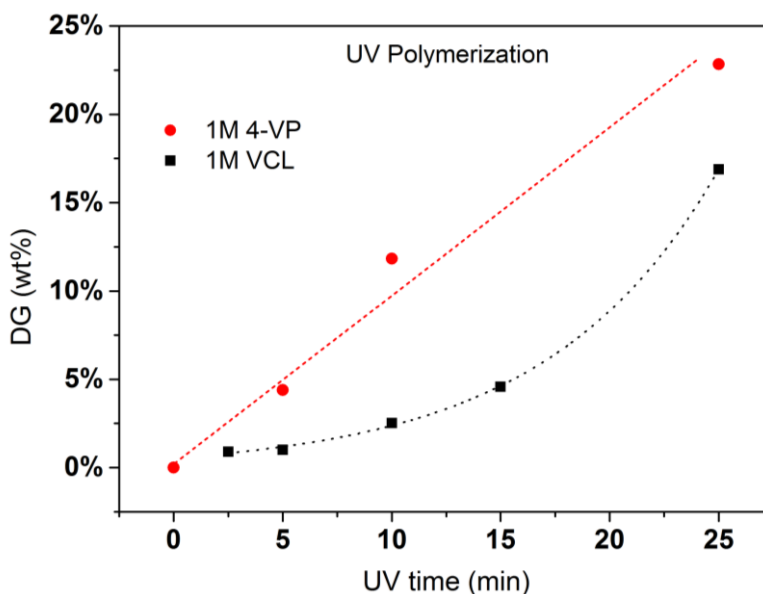**Figure 5.8** Simulated 4-VP species distribution curve under various pHs.

Figure 5.9 DG of 4-VP and VCL under different UV irradiation time.

Figure 5.10 shows the contact angles of modified PES membranes as a function of the pH of the aqueous buffer solution. The contact angles of both poly(4-VP) and poly (4-VP)-co-PVCL modified membranes exhibit a sudden decrease between pH value 4 and 6, which is close to the pKa of monomeric protonated 4-VP at 5. Our earlier studies[23, 24, 25] show that the pKa of polymeric acid or conjugate base could be different from its monomer value. Typically, the pKa of polymeric acid will shift to a higher value due to the different dielectric and electrostatic environment between the monomer and polymer. When 4-pyridine is protonated, membrane surface becomes very hydrophilic due to the strong hydration of the cationic residues leading to a decrease in contact angle. It is important to note that with a 1:1 ratio of VCL:4-VP in the monomer solution, the poly(4-VP)-co-PVCL modified membrane still retains some pH responsiveness.
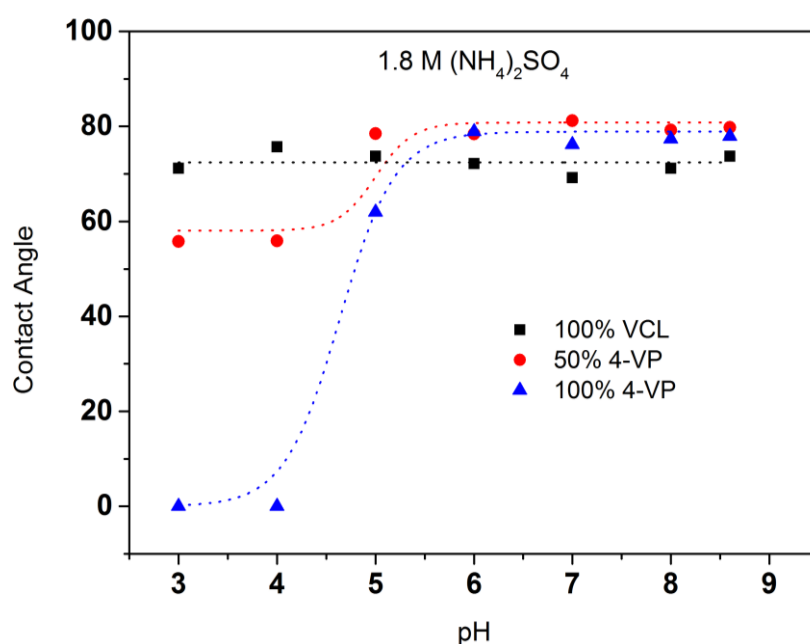
Figure 5.10 Contact angle under different pHs for PVCL modified membranes (100% VCL in monomer solution), poly(4-VP)-co-PVCL modified membranes (VCL:4-VP=1:1 in monomer solution) and poly(4-VP) modified membranes.

Figure 5.11 shows the dynamic binding capacity and recovery at various modification conditions and at different binding and elution pH values. Overall, the binding capacity decreases at the ratio of 4-VP/VCL increases at neutral pH 7. However, the binding capacity

is highest when there is about 5% 4-VP in the monomer composition at other pH conditions

at 6, 8 and 8.5. Further increase in monomer ratio of 4-VP to VCL appears to decrease the

binding capacity. This is probably due to the increase of LCST for the copolymer when more

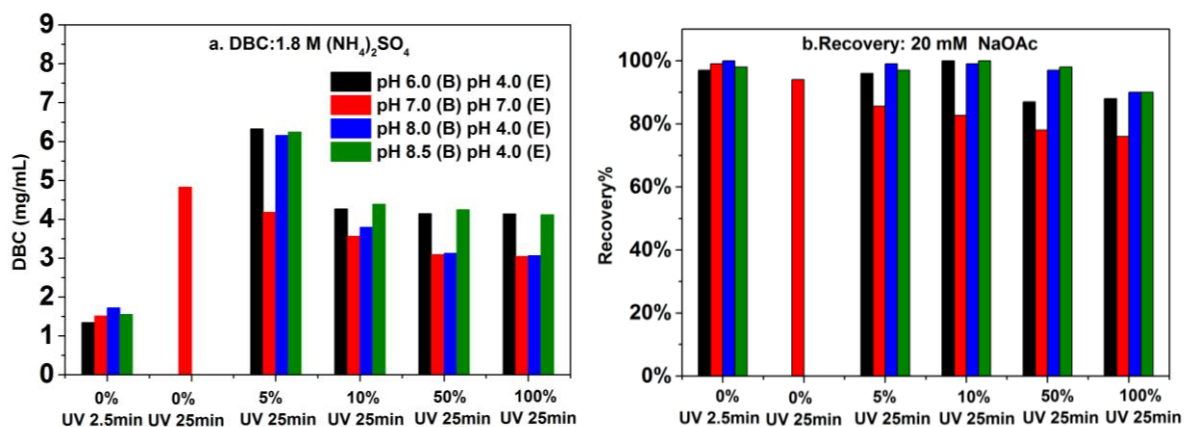4-VP is incorporated. An increase in LCST will lead to the reduction in the binding capacity.

Figure 5.11 Dynamic binding capacity (a) and recovery (b) of poly(4-VP)-co-PVCL
modified membranes.

Our dynamic binding tests using 20 mM NaOAc adsorption buffer at pH 7 further

confirmed the existence of electrostatic interactions between 4-VP and BSA at the neutral pH

as shown in Figure 5.12. Binding capacity is higher at pH 8.0 and 8.5 compared to pH 7.0 for

the copolymer modified membranes. When pH is at 6.0, binding capacity is also higher

because BSA tends to aggregate. At pH 6.0 and 5.0, the elution peaks exhibit a shoulder

indicating the formation of aggregates (results not shown). These binding results indicate that

pH condition not only affects the hydrophobicity of the copolymer ligand but also affects the

charge and conformational state of the protein. For recovery, Figure 5.11 (b) shows that

recovery at pH 7 is generally lower than at pH 4. At pH 4, both protein and ligand are

positively charged leading to the electrostatic repulsion and strong hydration of the charges

residues. This eventually leads to an enhanced recovery for proteins. On the other hand, the

lower recovery at pH 7 for the elution condition is likely due to the attractive electrostatic

interaction between the positively charged 4-VP and the negatively charged BSA. The

gradual decrease of the recovery over the 4-VP/VCL ratio is also in agreement with the

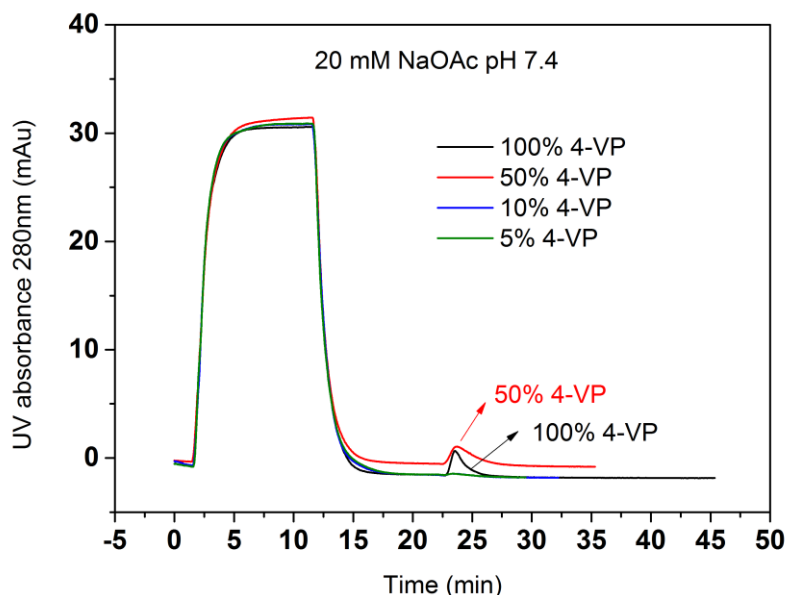electrostatic interaction between 4-VP and BSA.

Figure 5.12 Bind and elute chromatogram of poly(4-VP)-co-PVCL modified membranes
under 20mM NaOAc condition for binding at pH 7 and elution at pH 4.

We have also conducted static binding studies at different pH with lysozyme. Unlike

BSA with a pI at 4.7, lysozyme has a pI at 11.35, which is far away from the pka of 4-VP at

around 5. The results show that at pH 3, the capacity decreases as the percentage of 4-VP

monomer in solution increases as shown in Figure 5.13. At pH 3, both lysozyme and 4VP are

positively charged so that the electrostatic repulsion leads to a reduction in binding capacity

when more 4-VP monomers are incorporated into the ligand. It also can be seen at pH 11

which is close to the pI of lysozyme, the binding capacity increases due to the resulting

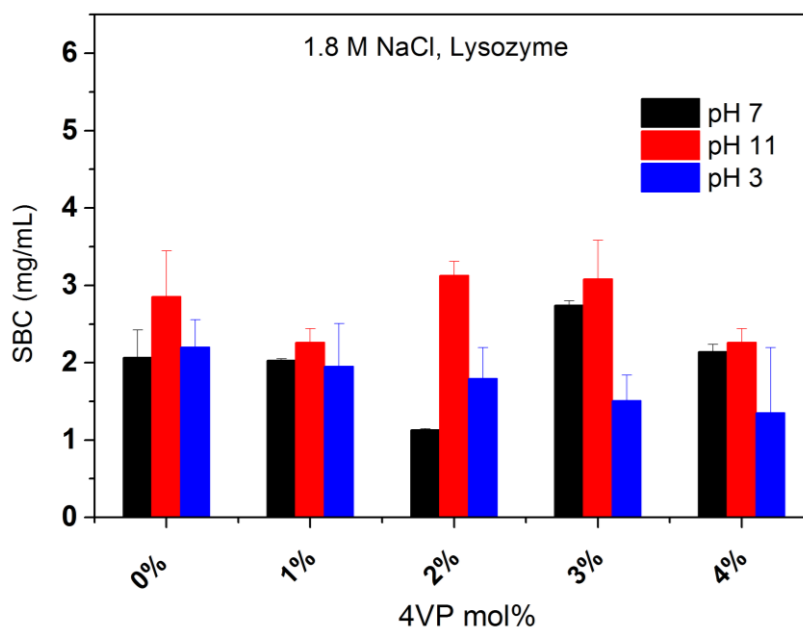weaker electrostatic interaction and stronger hydrophobic interaction.

Figure 5.13 Static binding studies of P4VP-co-PVCL modified membranes under different pHs. The binding is conducted at 1.8 M NaCl using lysozyme as the model protein.

5.5 Conclusions

In this chapter, we have developed a quick, simple and clean UV-induced polymerization process for grafting PVCL on PES membrane. The modification condition is optimized by varying the VCL concentration and polymerization time. Higher VCL condition only shows higher DG when UV time is longer than 20 min. High binding capacity (4-5 mg/mL) is achieved with longer UV irradiation time, which is comparable to what we obtained with PVCL modified RC membranes with ATRP. Dynamic binding capacity increases with DG of PVCL and contact angle. Recovery is high (> 90%) for all the PVCL modified PES membranes.

Various monomers were copolymerized with VCL. Very hydrophilic monomer like HPMA, HEA and NIPAM cause the decrease of binding capacity. 4-VP was copolymerized with VCL to introduce pH responsiveness. Our preliminary results show the hydrophobicity

changes around pH 5.0 for poly(4-VP) modified membranes. Poly(4-VP)-co-PVCL modified

membrane has retained the pH responsiveness at pH 5.0. Binding results show capacity is

higher at pH 8.0 and 8.5 compared to pH 7.0. At pH 7.0, there are likely to have some

electrostatic interactions between protonated 4-vinylpyridine and BSA, rendering a low

recovery. The recovery is evidently higher at pH 4.0 due to the repulsion between protonated

4-vinylpyridine and BSA. In sum, this copolymer ligand shows promising results for

developing salt-and-pH dual responsive HIC membranes for bioseparations.

Reference

1.   Nagase, K.; Hatakeyama, Y.; Shimizu, T.; Matsuura, K.; Yamato, M.; Takeda, N.; Okano, T. Hydrophobized Thermoresponsive Copolymer Brushes for Cell Separation by Multistep Temperature Change. *Biomacromolecules* **2013,** *14* (10), 3423-3433.

2.   Nagase, K.; Kumazaki, M.; Kanazawa, H.; Kobayashi, J.; Kikuci, A.; Akiyama, Y.; Annaka, M.; Okano, T. Thermoresponsive Polymer Brush Surfaces with Hydrophobic Groups for All-Aqueous Chromatography. *ACS Appl. Mat. Interfaces* **2010,** *2* (4), 1247-1253.

3.   Nagase, K.; Kobayashi, J.; Kikuchi, A.; Akiyama, Y.; Kanazawa, H.; Okano, T. Preparation of Thermoresponsive Cationic Copolymer Brush Surfaces and Application of the Surface to Separation of Biomolecules. *Biomacromolecules* **2008,** *9* (4), 1340-1347.

4.   Nagase, K.; Kobayashi, J.; Kikuchi, A.; Akiyama, Y.; Kanazawa, H.; Annaka, M.; Okano, T. Preparation of Thermoresponsive Anionic Copolymer Brush Surfaces for Separating Basic Biomolecules. *Biomacromolecules* **2010,** *11* (1), 215-223.

5.   Qu, J.-B.; Chen, Y.-L.; Huan, G.-S.; Zhou, W.-Q.; Liu, J.-G.; Zhu, H.; Zhang, X.-Y. Preparation and characterization of a thermoresponsive gigaporous medium for high-speed protein chromatography. *Anal. Chim. Acta* **2015,** *853* (0), 617-624.

6.   Wu, Q.; Wang, R.; Chen, X.; Ghosh, R. Temperature-responsive membrane for hydrophobic interaction based chromatographic separation of proteins in bind-and-elute mode. *J. Membr. Sci.* **2014,** *471* (0), 56-64.

7.   Kanazawa, H.; Kashiwase, Y.; Yamamoto, K.; Matsushima, Y.; Kikuchi, A.; Sakurai, Y.; Okano, T. Temperature-Responsive Liquid Chromatography. 2. Effects of Hydrophobic Groups in N-Isopropylacrylamide Copolymer-Modified Silica. *Anal. Chem.* **1997,** *69* (5), 823-830.

8.   Takei, Y. G.; Aoki, T.; Sanui, K.; Ogata, N.; Okano, T.; Sakurai, Y. Temperature-responsive bioconjugates. 2. Molecular design for temperature-modulated bioseparations. *Bioconjugate Chem.* **1993,** *4* (5), 341-346.

9.   Škvarla, J.; Zedník, J.; Šlouf, M.; Pispas, S.; Štěpánek, M. Poly(N-isopropyl acrylamide)-block-poly(n-butyl acrylate) thermoresponsive amphiphilic copolymers:

Synthesis, characterization and self-assembly behavior in aqueous solutions. *Eur. Polym. J.* **2014,** *61* (0), 124-132.

10.   Ye, Y.; Shangguan, Y.; Song, Y.; Zheng, Q. Influence of charge density on rheological properties and dehydration dynamics of weakly charged poly(N-isopropylacrylamide) during phase transition. *Polymer* **2014,** *55* (10), 2445-2454.

11.   Hou, L.; Wu, P. LCST transition of PNIPAM-b-PVCL in water: cooperative aggregation of two distinct thermally responsive segments. *Soft Matter* **2014,** *10* (20), 3578-3586.

12.   Sahiner, N.; Ozay, O. Responsive tunable colloidal soft materials based on p(4-VP) for potential biomedical and environmental applications. *Colloids Surf., A* **2011,** *378* (1–3), 50-59.

13.   Ayres, N.; Cyrus, C. D.; Brittain, W. J. Stimuli-Responsive Surfaces Using Polyampholyte Polymer Brushes Prepared via Atom Transfer Radical Polymerization. *Langmuir* **2007,** *23* (7), 3744-3749.

14.   Burillo, G.; Bucio, E.; Arenas, E.; Lopez, G. P. Temperature and pH-Sensitive Swelling Behavior of Binary DMAEMA/4VP Grafts on Poly(propylene) Films. *Macromol. Mater. Eng.* **2007,** *292* (2), 214-219.

15.   Liu, R.; Liao, P.; Liu, J.; Feng, P. Responsive Polymer-Coated Mesoporous Silica as a pH-Sensitive Nanocarrier for Controlled Release. *Langmuir* **2011,** *27* (6), 3095-3099.

16.   Shevate, R.; Karunakaran, M.; Kumar, M.; Peinemann, K.-V. Polyanionic pH-responsive polystyrene-b-poly(4-vinyl pyridine-N-oxide) isoporous membranes. *J. Membr. Sci.* **2016,** *501*, 161-168.

17.   Wang, R.; Xiang, T.; Yue, W.; Li, H.; Liang, S.; Sun, S.; Zhao, C. Preparation and characterization of pH-sensitive polyethersulfone hollow fiber membranes modified by poly(methyl methylacrylate-co-4-vinyl pyridine) copolymer. *J. Membr. Sci.* **2012,** *423–424*, 275-283.

18.   Nunes, S. P.; Behzad, A. R.; Hooghan, B.; Sougrat, R.; Karunakaran, M.; Pradeep, N.; Vainio, U.; Peinemann, K.-V. Switchable pH-Responsive Polymeric Membranes Prepared via Block Copolymer Micelle Assembly. *ACS Nano* **2011,** *5* (5), 3516-3522.

19.   Qiu, X.; Yu, H.; Karunakaran, M.; Pradeep, N.; Nunes, S. P.; Peinemann, K.-V. Selective Separation of Similarly Sized Proteins with Tunable Nanoporous Block Copolymer Membranes. *ACS Nano* **2013,** *7* (1), 768-776.

20.   Yamagishi, H.; Crivello, J. V.; Belfort, G. Development of a novel photochemical technique for modifying poly (arylsulfone) ultrafiltration membranes. *J. Membr. Sci.* **1995,** *105* (3), 237-247.

21.   Qian, X.; Lei, J.; Wickramasinghe, S. R. Novel polymeric solid acid catalysts for cellulose hydrolysis. *RSC Adv.* **2013,** *3* (46), 24280-24287.

22.   Himstedt, H. H.; Qian, X.; Weaver, J. R.; Wickramasinghe, S. R. Responsive membranes for hydrophobic interaction chromatography. *J. Membr. Sci.* **2013,** *447* (0), 335-344.

23. Dong, H.; Du, H.; Qian, X. Theoretical Prediction of pKa Values for Methacrylic Acid Oligomers Using Combined Quantum Mechanical and Continuum Solvation Methods. *The Journal of Physical Chemistry A* **2008,** *112* (49), 12687-12694.

24. Dong, H.; Du, H.; Qian, X. Prediction of pKa Values for Oligo-methacrylic Acids Using Combined Classical and Quantum Approaches. *J. Phys. Chem. B* **2009,** *113* (39), 12857-12859.

25. Dong, H.; Du, H.; Wickramasinghe, S. R.; Qian, X. The Effects of Chemical Substitution and Polymerization on the pKa Values of Sulfonic Acids. *J. Phys. Chem. B* **2009,** *113* (43), 14094-14101.

Chapter 6: Conclusions and Future Direction

6.1 Conclusions

Overall, we have shown that ATRP is an effective method for developing membrane chromatography with different polymeric ligand architectures. Our work further shows that copolymeric ligands have many potentials for achieving high performance bioseparations, which includes being developed as high affinity ligands and stimuli-responsive ligands. Major conclusions for developing affinity membranes work and responsive HIC membranes are summarized below.

Our work shows how the composition of the copolymer affects the protein binding capacity and recovery. The property of copolymer changes with different copolymerization condition, either by varying the copolymerization time or the ratio between two monomers. For the affinity membrane work, we have shown that with longer ATRP copolymerization time, more affinity monomers were incorporated into the copolymer, which provides more binding sites and leads to higher binding capacity. As for the HIC membrane work, we found that the hydrophobicity of the incorporated monomer plays an important role in binding capacity. With hydrophilic monomers copolymerized with VCL, the binding capacity decreases with more hydrophilic monomer incorporated. The copolymerization with pH responsive monomer (4-VP) also shows that with higher pH (8 and 8.5) when 4-VP is less protonated, binding capacity is higher compared to the condition at pH 7. Our result also shows that at pH 7, the protonated 4-VP interacts strongly with the negative charges on BSA and leading to decrease of recovery. The decrease of recovery is more evident when more 4-VP monomers were incorporated in the copolymer chains. Static binding results with lysozyme as the model protein also show the repulsion between positively charged ligand and lysozyme reduces the binding capacity.

Our work also shows how the structure of copolymer has an impact on the protein binding capacity and recovery. For the affinity membrane work, our work highlights the importance of incorporating the hydrophilic spacer monomers. The spacer monomer is likely to increase the flexibility of the copolymer as the affinity monomer has a rigid and bulky structure. Our simulation results also show the spacer monomer actively interacts with lysozyme through hydrogen bonding interaction. Another copolymer structure effect we have investigated is the HIC membrane work. The comb-like branched copolymer HIC ligand has been designed to improve the grafting degree of PVCL. PVCL has been modified from the backbones of the polymers grafted from the membrane surface with ATRP. The backbone density and length as well as the PVCL density on each backbone have been successfully varied by adjusting initiator concentration and polymerization time. Overall, the binding studies show that long and high density of backbone structure is not preferred for HIC due to the low recovery and its limited improvement in capacity. Unlike other ion exchange polymeric ligands, the binding capacity does not simply increase with grafting degree of HIC ligands linearly. The 3D structure of the ligand has a large impact on the protein recovery.

In addition to the studies on property and structure of copolymer ligands, we have also investigated how the responsive PVCL ligands perform under different salt, pH and protein conditions. Sulfate salts were studied and the binding capacity follows: $Na^+>NH_4^+>Al^{3+}>Zn^{2+}$ (compared in the same ionic strength). Our turbidity studies on the reduction of LCST PVCL ligands also show the same order for Na^+ and NH_4^+ at the same ionic strength. Moreover, we have shown the contact angle of PVCL grafted membrane increases with the increase of Na_2SO_4 concentration, indicating an evident change of ligand hydrophobicity under different salt concentrations. Overall, our results may suggest that ligand hydrophobicity can be modulated by the salt ion concentration and salt type and that it plays a critical role in the binding capacity.

6.2 Future Direction and Suggestion

6.2.1 Ligand Characterization

It is important to analyze the molecular weight and grafting density of the grafted ligands. Traditionally, the characterization for thickness is usually estimated by grafting ligands on a different surface, such as silicon wafer or gold. The polymerization kinetics could be quite different between a small flat surface and a porous membrane. Other methods like performing solution ATRP under the same condition may also suffer from the uncertainty of polymerization kinetics for brushes. Therefore, it would be useful to develop a method to analyze the polymer ligands grafted on the membranes directly. Appendix III shows a promising case study of cleaving PNIPAM from the regenerated cellulose membrane after ATRP. The cleavage condition and yield were investigated and the cleaved PNIPAM is confirmed by turbidity tests, H^1NMR and GPC. Future work is to look at the yield of the whole cleavage process and compare with results measured with other techniques.

6.2.2 Controlled Polymerization of PVCL

PVCL chain length effect with our current ATRP condition is still unknown due to the low grafting degree (DG) of PVCL and the interference of moisture on the weight of RC membranes. It would be interesting to look at how the ATRP time would affect the DG of PVCL in the comb-like studies since the overall DG has been increased 10-40 times. It might be also helpful to use another ATRP ligand (CuBr/Me$_6$(Cyclam)[1]) for higher polymerization rate. Recent polymerization progress has also shown that reversible addition–fragmentation chain transfer (RAFT) with xanthates as chain transfer agents allow for well-controlled polymerization of non-conjugated N-vinyl monomers[2].

6.2.3 Decouple LCST Effect on Protein Binding

Due to the complexity of protein binding and elution process, it is still difficult to decouple the ligand LCST effect from the protein effect under different salt conditions. It might be helpful if a model compound (such as polystyrene) that has a small hydrophobicity change can be used for isocratic tests under different salt conditions. In addition, a non-responsive polymer with similar structure of PVCL can be studied as a control for proving the hypothesis that elution is enhanced by the hydrophilic state of PVCL.

6.2.4 Developing High Capacity Responsive Ligand with a Facile Elution Advantage

Our current binding capacity ($DBC_{10\%}$) of PVCL modified membrane is about 3 times less than commercialized HIC membranes (Sartobind Phenyl HIC). Appendix IV shows the comparison studies between our HIC PVCL and HIC phenyl membranes. It is important to note that our membrane holder is not designed very effectively compared to the one for Sartobind phenyl membranes. As earlier studies suggest, traditional membrane holder has a larger radial diameter than the axial diameter, rendering a possible early breakthrough and low capacity[3, 4]. Besides that, the ligand density maybe another reason why our capacity is lower. High binding capacity may be achieved through the improvement of specific area of the membranes. High capacity ion-exchange membranes with electrospun fibers or hydrogels have been commercialized. As far as we know, so far there is no report on high capacity HIC membranes with improved membrane matrix.

In addition to the capacity, the large usage of salt is another drawback for HIC process. Therefore, increasing the hydrophobicity of ligand would lower the required salt concentration for binding. It has been shown that for flow-through HIC studies, no-salt condition has similar performance as conventional HIC with high salt conditions[5]. For our copolymerization work with VCL monomer, it would be worthwhile to incorporate hydrophobic monomers for lowering the LCST.

In recent years, multi-modal chromatography has shown high binding capacity and salt-tolerance. However, the problem with multi-modal chromatograpy to be used in the bind-and-elute study is the expected low recovery due to the conflicted mechanisms between the hydrophobic interaction and electrostatic interaction. The operation window is normally determined by Design of Experiments (DoE). With the pH responsive monomer work we have shown in chapter 5, it is promising to provide a facile elution strategy for the multi-modal chromatography, which can shorten the process development time and cost.

Reference

1.   Jiang, X.; Li, Y.; Lu, G.; Huang, X. A novel poly(N-vinylcaprolactam)-based well-defined amphiphilic graft copolymer synthesized by successive RAFT and ATRP. *Polymer Chemistry* **2013,** *4* (5), 1402-1411.

2.   Nakabayashi, K.; Mori, H. Recent progress in controlled radical polymerization of N-vinyl monomers. *Eur. Polym. J.* **2013,** *49* (10), 2808-2838.

3.   Ghosh, R.; Wong, T. Effect of module design on the efficiency of membrane chromatographic separation processes. *J. Membr. Sci.* **2006,** *281* (1-2), 532-540.

4.   von Lieres, E.; Wang, J.; Ulbricht, M. Model Based Quantification of Internal Flow Distributions from Breakthrough Curves of Flat Sheet Membrane Chromatography Modules. *Chemical Engineering & Technology* **2010,** *33* (6), 960-968.

5.   Ghose, S.; Tao, Y.; Conley, L.; Cecchini, D. Purification of monoclonal antibodies by hydrophobic interaction chromatography under no-salt conditions. *mAbs* **2013,** *5* (5), 795-800.

DEVELOPMENT OF HIGH PERFORMANCE AFFINITY MEMBRANE

ADSORBERS GRAFTING SYNTHETIC COPOLYMERIC LIGAND*

* This section is adapted from a published paper by Liu, Z.; Du, H.; Wickramasinghe, S. R.; Qian, X. Membrane Surface Engineering for Protein Separations: Experiments and Simulations. Langmuir 2014, 30 (35), 10651-10660.

1. **Synthesis of ATRP monomer 5-(methacryloylamino)-m-xylyenebisphosphonic acid tetramethylester (Bis-P)**

Materials   Carbon tetrachloride (≥99.9%), 2,2′-azobis (2-methylpropionitrile) (98%) and 4-(dimethylamino) pyridine (≥99%) were obtained from Sigma Aldrich (St. Louis, MO). 5-Nitro-m-xylene (99%), N-bromosuuccinimide (99%), trimethylphosphite (99%), palladium on carbon (wet, 10%), filter aid, Celite Hyflo Super-cel®, methacryloylchloride (97%), and triethylamine (TEA, ≥99%) were obtained from Alfa Aesar (Ward Hill, MA). Chloroform-d (99.9 atom %D) was obtained from Acros Organics (Pittsburgh, PA). Silica gel 60 (high purity) was obtained from VWR (West Chester, PA). Dicholormethane (99.8%) was obtained from EMD Chemicals (Billerica, MA).

5-Nitro-xylylene bisphosphonic acid tetramethylester The procedure for the synthesis was shown in Figure A1.1. 5-Nitro-m-xylene (9.52 g, 63 mmol, 1.0 eq) was added to tetrachloromethane (CCl_4, 150 mL, solvent) to form a yellow solution. N-bromosuuccinimide (NBS, 33.84 g, 189 mmol, 3 eq) and azobisisobutyronitrile (AIBN, 0.2 g) were mixed together and grounded to ensure complete mixing before they were added in CCl_4. The mixture was refluxed for 13 hours at 76 °C. After filtering off the insoluble succinimide, the solvent was evaporated and the remaining oil was dissolved in excessive amount of trimethylphosphite (9.99 g, 80.5 mmol). The trimethylphosphite solution was heated with stirring for 5 hours at 100 °C. Subsequently, the volatile components were removed by the

Evaporator and the final product was purified using column chromatography by silica gel 60.

A total of 3 g yellowish solid was obtained corresponding to a yield of 13% over 2 steps.

Some modification on the original monomer synthesis procedure[1, 2] was made. We found that

the NBS bromination reaction was not complete under the condition provided in the

literature. Thus, we increased the mole amount of NBS to 3 eq. Moreover, we found that it

was difficult to recrystallize 3,5-bis (bromomethyl) nitrobenzene after NBS bromination. As

suggested by the authors who first reported this monomer[1], the oily product from reaction (1)

was used directly without recrystallization. The mixture products in reaction (2) were purified

with silica gel eluting with dichloromethane/methanol (gradient v/v 25:1, 18:1, 15:1,

R_f=0.33). ^{1}H-NMR (CDCl$_3$; 400 MHz; **Figure A1.2**): δ (ppm) = 3.26 (d, 2 JH, P=22.0 Hz, 4

H); 3.74 (d, 3 JH, P=11.0 Hz, 12 H); 7.61 (s, 1 H); 8.06 (s, 2 H).
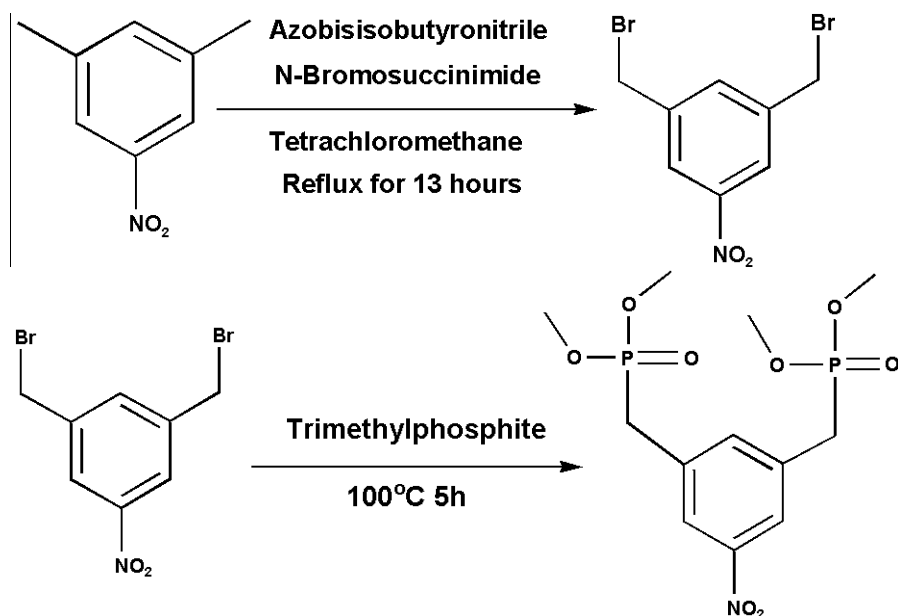
Figure A1.1 Two-step synthesis of 5-nitro-xylylene bisphosphonic acid tetramethylester.
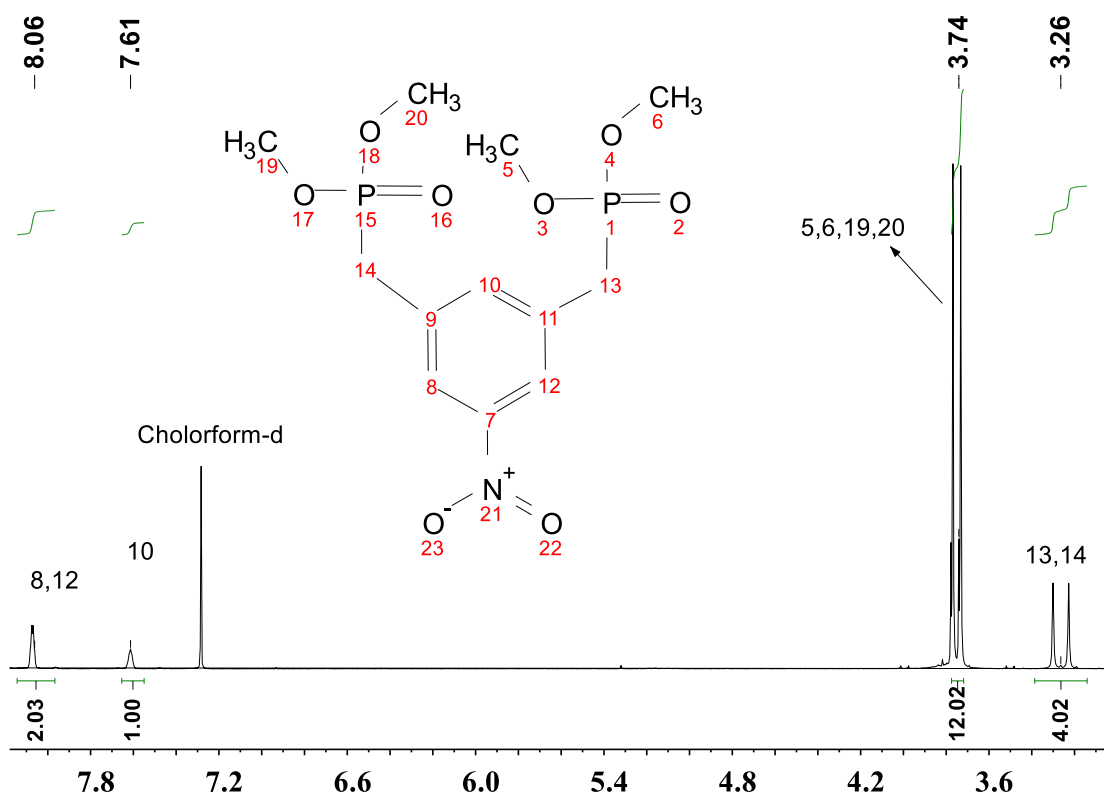
Figure A1.2 ^{1}H NMR (CDCl3; 400Hz) of the product 5-nitro-xylylene bisphosphonic acid tetramethylester.

5-Amino-m-xylene bisphosphonic acid tetramethylester 5-Nitro-m-xylylene

bisphosphonic acid tetramethylester (3 g) was dissolved in methanol. The reaction mixture

was first degassed with nitrogen for 15 min. Palladium on carbon (0.7g, 10% Pd) was added

to the solution. The reaction was conducted under a hydrogen atmosphere for 24 h. The

product was concentrated by evaporation after removing the catalyst by filtration over celite.

A yield of 85% with a total of 2.3 g slightly yellow solid was obtained. ^{1}H-NMR (CDCl$_3$; 400

MHz; **Figure A1.3**): δ (ppm) = 3.06 (d, 2 JH, P = 20.4 Hz, 4 H); 3.66 (d, 3 JH, P = 10.9 Hz,

12 H); 6.63 (s, 1 H); 6.55 (s, 2 H).
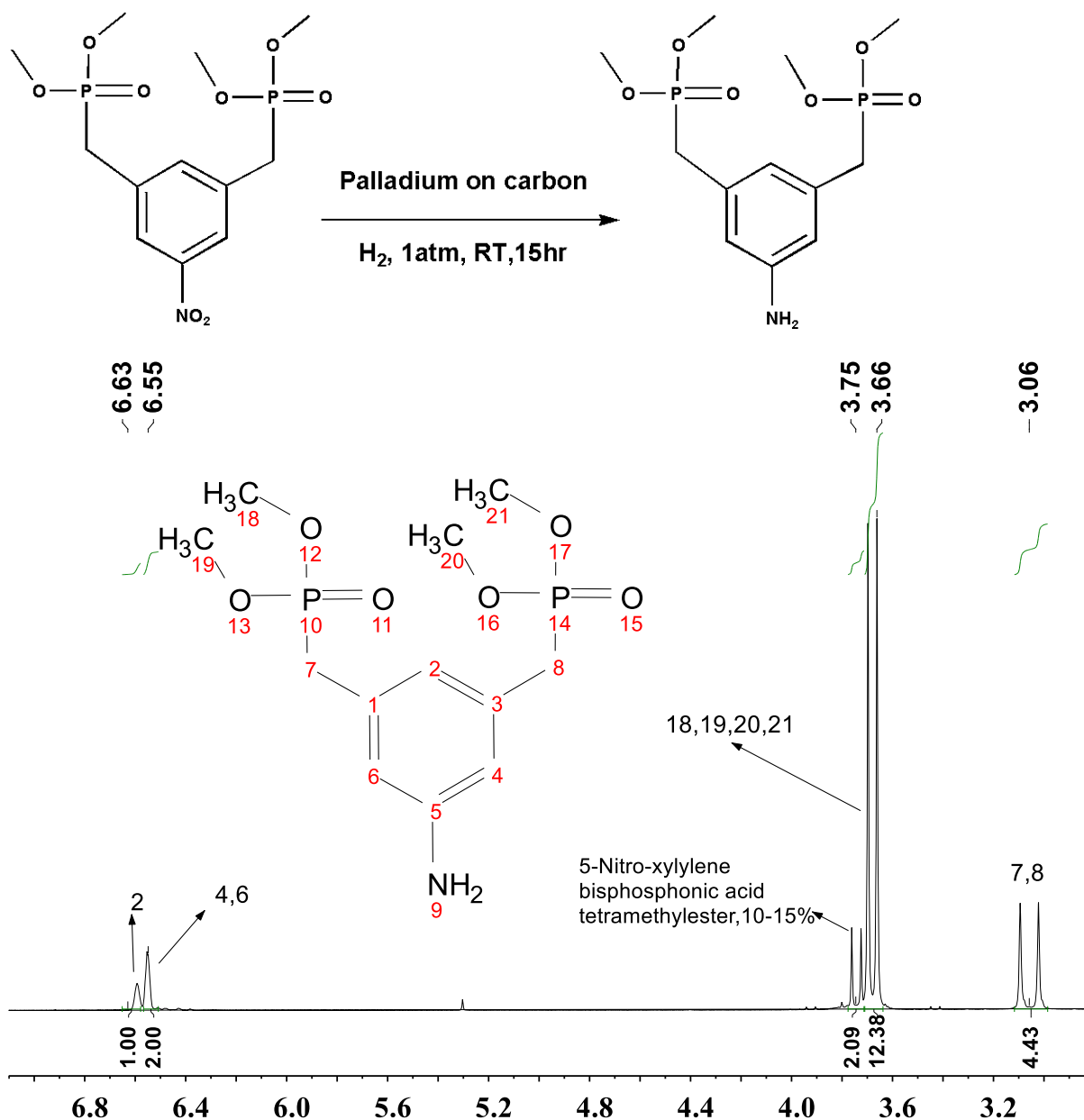
Figure A1.3 ^{1}H NMR (CDCl3; 400Hz) of the product 5-amino-m-xylene bisphosphonic acid tetramethylester.

5-(Methacryloylamino)-m-xylylenebisphosphonic acid tetramethylester

5-Amino-m-xylene bisphosphonic acid tetramethylester (1.36 g) was first dissolved in 44.8

mL dicholormethane. Triethylamine (0.66 mL) and catalytic amount of 4-(N,N-

dimethylamino)-pyridine were added into the solution. Methacryloyl chloride (0.59 mL)

dissolved in 12 mL dicholormethane was added drop-wise at 0 ℃ within 1 hour. Reaction

solution was kept stirring for 5 h at room temperature. The reaction was conducted under the

protection of nitrogen all the time. The crude product was washed with sodium hydroxide

(100 mL, 0.6 N) twice. The final product was purified with silica gel chromatography

(dichloromethane/methanol, 14:1 v/v) to remove triethylamine and reactant. A yield of 74%

and a total of 1.2 g purified final product were obtained. ^{1}H-NMR (CDCl$_3$; 400 MHz; **Figure

A1.4**): δ (ppm) = 2.06 (dd, 3 H); 3.15 (d, 2 JH, P= 22.0 Hz, 4 H); 3.70 (d, 3 JH, P= 10.8 Hz,

12 H); 5.48 (qd, 1 H); 5.80 (qd, 1 H); 7.00 (s, 1 H); 7.43-7.47 (d, 2 H); 7.58 (sb, 1 H).
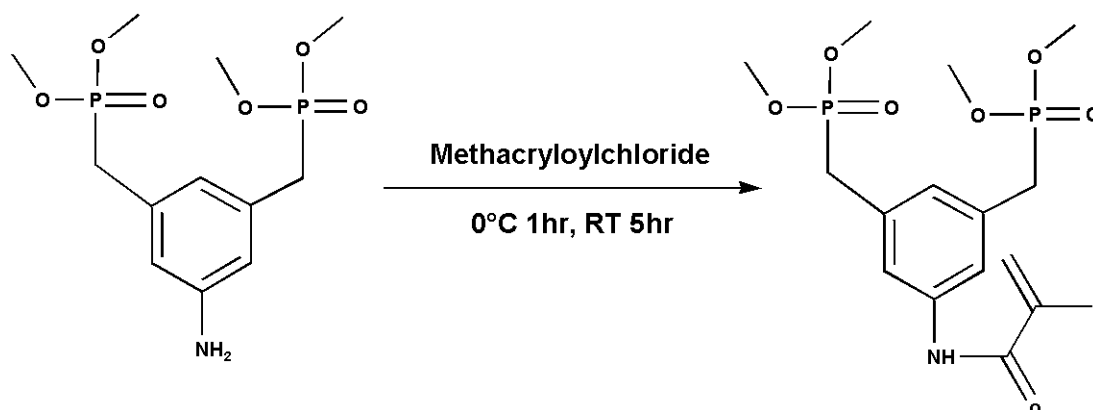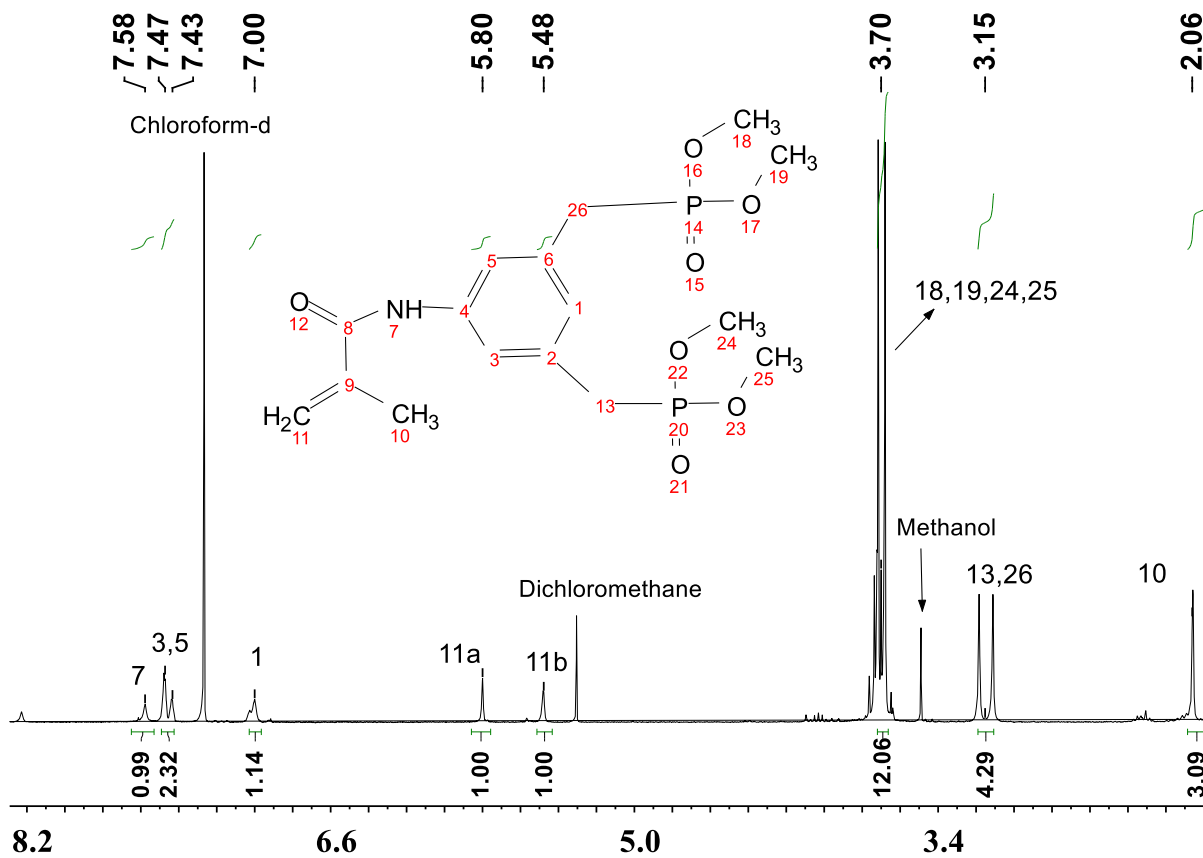
Figure A1.4 ^{1}H NMR (CDCl3; 400Hz) of the final product 5-(methacryloylamino)-m-xylylenebisphosphonic acid tetramethylester.

2. MD Simulations
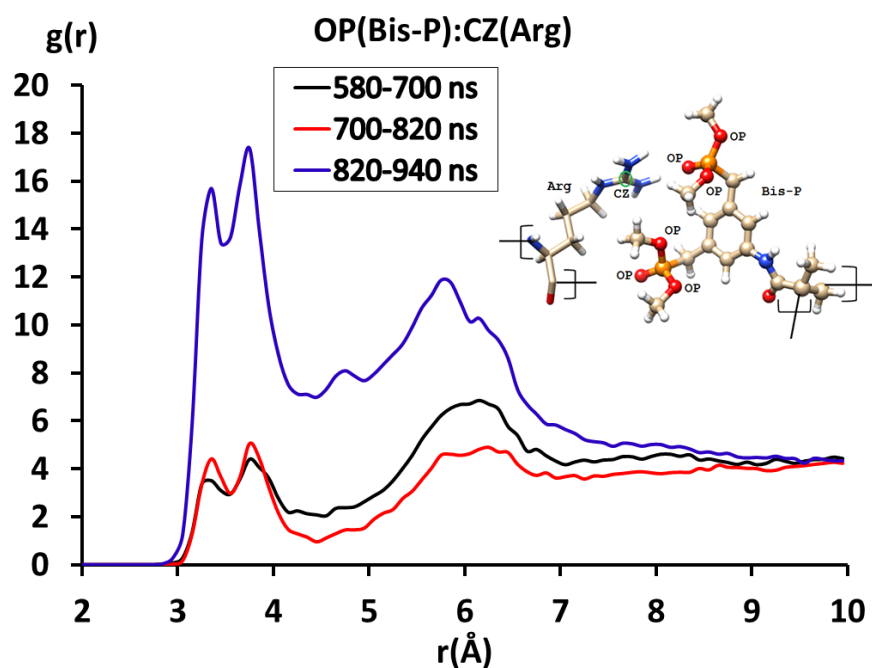
Figure A1.5 The pair correlation function between the oxygen atoms (OP) in the phosphate groups of Bis-P and the carbon atoms (CZ) in the Arg residues of lysozyme during three simulation periods at 580-700, 700-820 and 820-940 ns.

References

1.   Renner, C.; Piehler, J.; Schrader, T. Arginine- and lysine-specific polymers for protein recognition and immobilization. *J. Am. Chem. Soc.* **2005,** *128* (2), 620-628.

2.   He, D.; Sun, W.; Schrader, T.; Ulbricht, M. Protein adsorbers from surface-grafted copolymers with selective binding sites. *J. Mater. Chem.* **2009,** *19* (2), 253-260.

DEVELOPMENT OF NOVEL RESPONSIVE MEMBRANES FOR HYDROPHOBIC

INTERACTION CHROMATOGRAPHY PART I. SALT EFFECTS STUDY
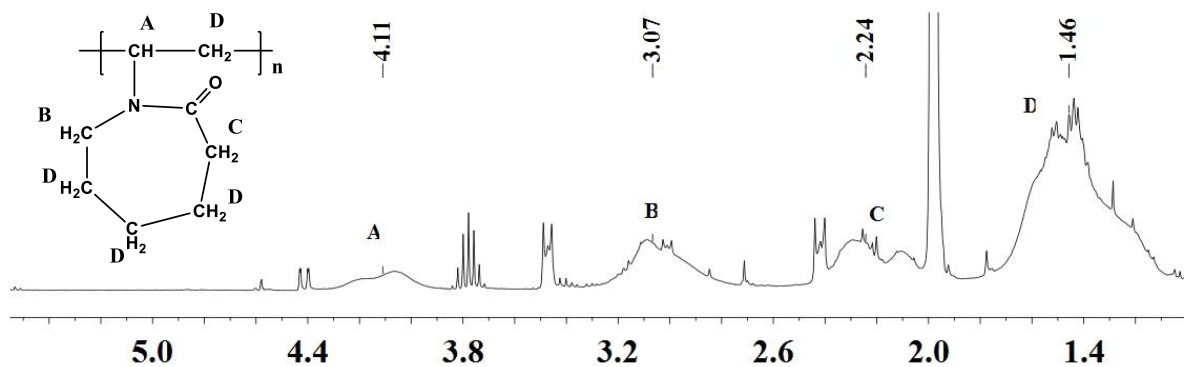
Figure A2.1 ^{1}HNMR of synthesized poly (vinylcaprolactam) (PVCL) by solution free radical polymerization.
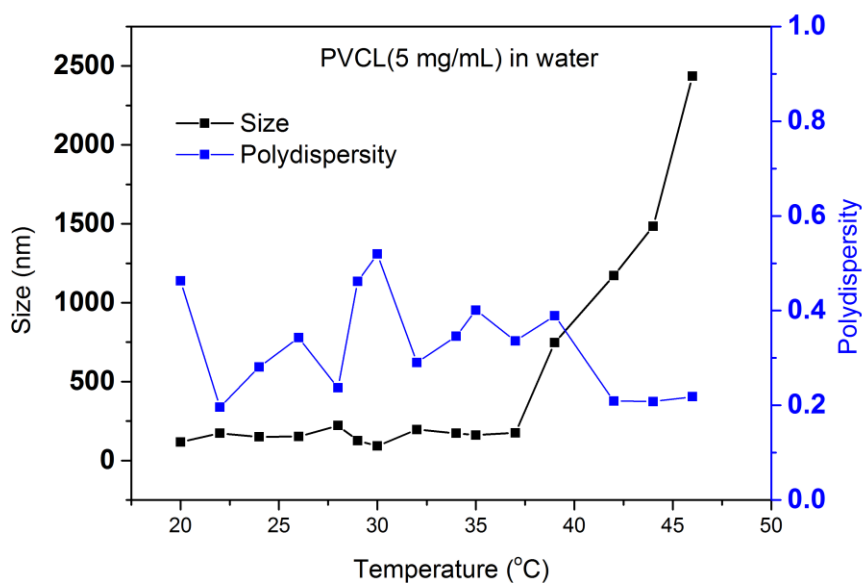
Figure A2.2 Size measurement of synthesized PVCL under different temperature by dynamic light scattering.
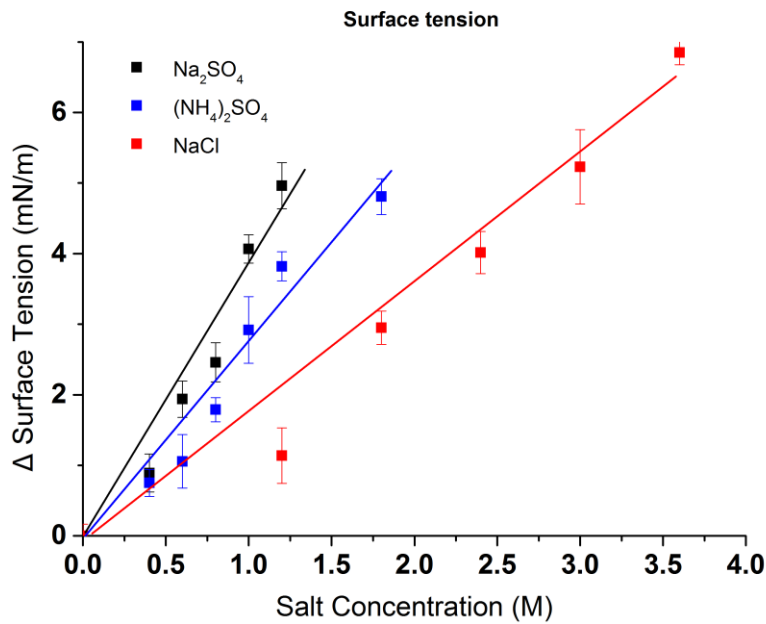
Figure A2.3 Excess surface tension of $(NH_4)_2SO_4$, Na_2SO_4 and NaCl at various concentrations (water surface tension is 73.54 ± 0.16 mN/m). All data were averaged by five measurements.
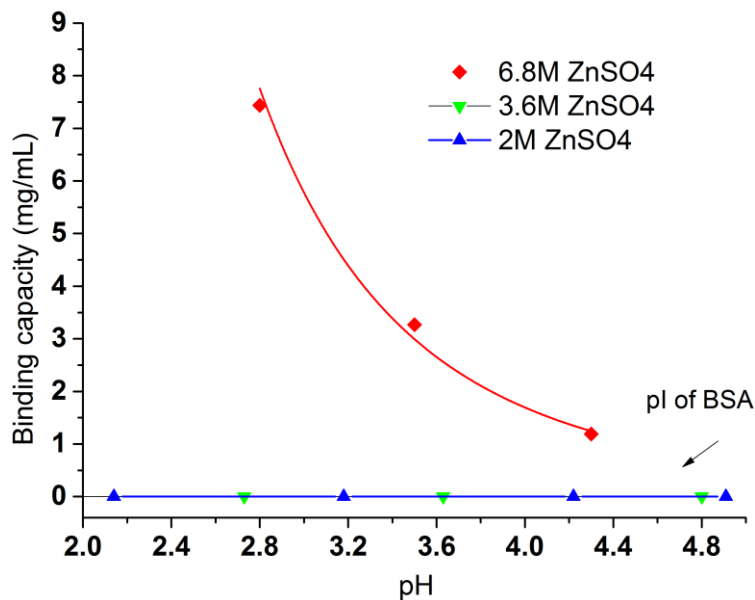
Figure A2.4 The pH effects of BSA binding under various ionic strength of ZnSO4. All results are averaged by two membranes' results conducted under the same binding condition. Initial BSA concentration was kept at 0.09 mg/mL.

Appendix III

CLEAVAGE STUDIES FOR PNIPAM GRAFTED RC MEMBRANES

1. PNIPAM Cleavage Protocol

    a. 4-5 mg membranes were cut and immersed (grafted 1-3 mg PNIPAM, DG 40%-80%) in 0.5-1 mL NaOH or ethylenediamine solution for a predetermined time.

    b. After hydrolysis, the solution contained cleaved polymer was filtrated through a nanofiltration process (NF 270 membrane). Then, 1-2 mL DI-water was used for filtration again to wash the remaining NaOH. Here, a dead-end nanofiltration process was used to reject the cleaved polymer.

    c. NF 270 Membrane that has rejected polymers on the surface was first dried in oven and then dissolve in solvent for NMR or GPC.
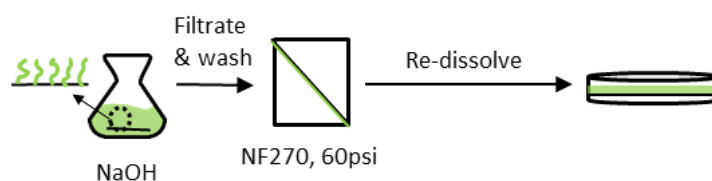
Figure A3.1 A general cleavage procedure for grafted PNIPAM ligands, including hydrolysis, filtration, drying and re-dissolving 4 steps.

2. GPC Protocol

Table A3.1 GPC column information

Column	Supplier	Column Material	Particle size (um)	Column size (I.D.*length)	Separation range
Shodex SB-806M HQ	Shodex	Polymethyacrlate	13 (1.5 um pore size)	8mm×300mm	10^2-10^7 Da

2.1 Start the run (water as eluent)

1. Load method "Zizhao Start up": RID 35ºC or set flow rate to 0.2 mL/min

2. Connect small tubing on the column out flow side to remove the sodium azide (column storage solution)

3. Connect guard column inlet slowly with the flow on (0.2 ml/min) to exclude any air bubble (before connecting, make sure both column ends are off)

4. Secure the column with the two metal plates and check if there is any leaking

5. Start collect sodium azide in a beaker

6. Set gradient flow rate:0.2-0.5 mL/min in 15min to wash out sodium azide (0.5 ml/min) for 50 ml.

7. Connect the column outlet to the system and make RID detector ready by equilibrium for 3-4 hrs

8. Double check shut down method (solvent and speed)!!!!!!

9. Name the sample and start the run

2.2 Removing the column

1. Change the flow rate to 0.2 ml/min

2. Disconnect column outlet from the system

3. Connect small tubing on the column out flow side to collect the sodium azide

4. Put the tubing for pump A in 0.2% sodium azide solution

5. Set gradient flow rate :0.2-0.5 mL/min in 10 min and run for 30 min to load sodium azide (0.5 ml/min) in the column

6. Set minimum pressure to 10 bar (to stop the flow when column disconnected)

7. Disconnect the guard column+ column and cap both ends.

8. Change the flow rate to 0.2 ml/min and restart the pump

9. Add HPLC water to a centrifuge tube and put the pump A tubing in that tube

10. Set gradient flow rate :0.2-0.5 mL/min in 5 min and run for 15 min

11. Change the flow rate to 0.2 ml/min

12. Change the water in centrifuge tube again and set gradient flow rate :0.2-0.5 mL/min in 5 min and run for 5 min

13. Change the flow rate to 0.2 ml/min

14. Change the water in centrifuge tube the 3rd time and set gradient flow rate :0.2-0.5 mL/min in 5 min and run for 5 min

15. Change the flow rate to 0.2 ml/min

16. Put the pump A tubing to the bottle and connect the capillary tube

3. Investigation on Cleavage Conditions (temperature & time effect):
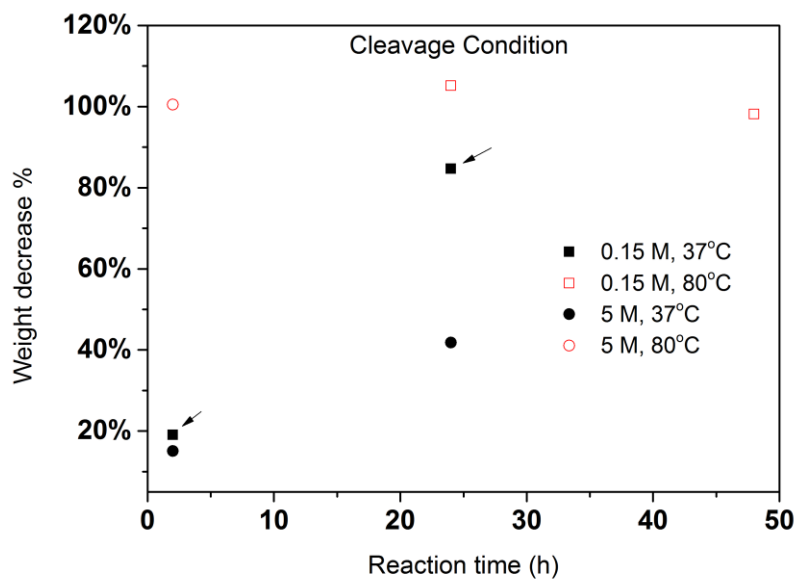
Figure A3.2 Cleavage temperature and time effect on the cleavage yield (measured by weight decrease of membrane). Weight decrease $\% = (w_0 - w_1)/w_{\text{grafted PNIPAM}}$

4. Characterization of Cleaved PNIPAM
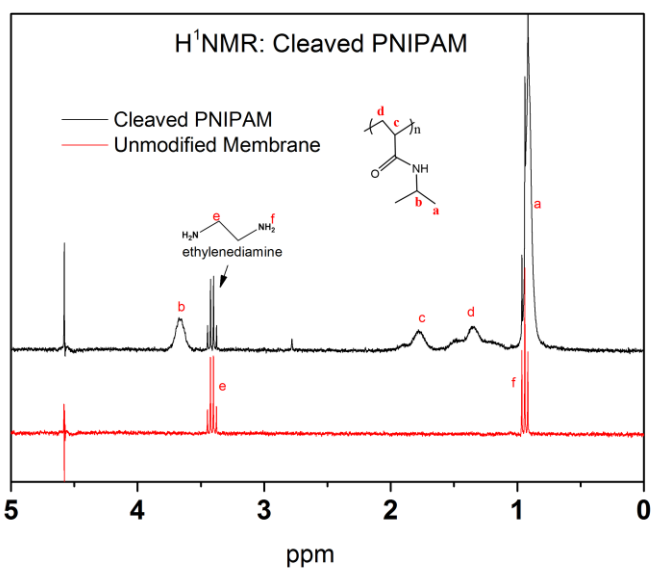
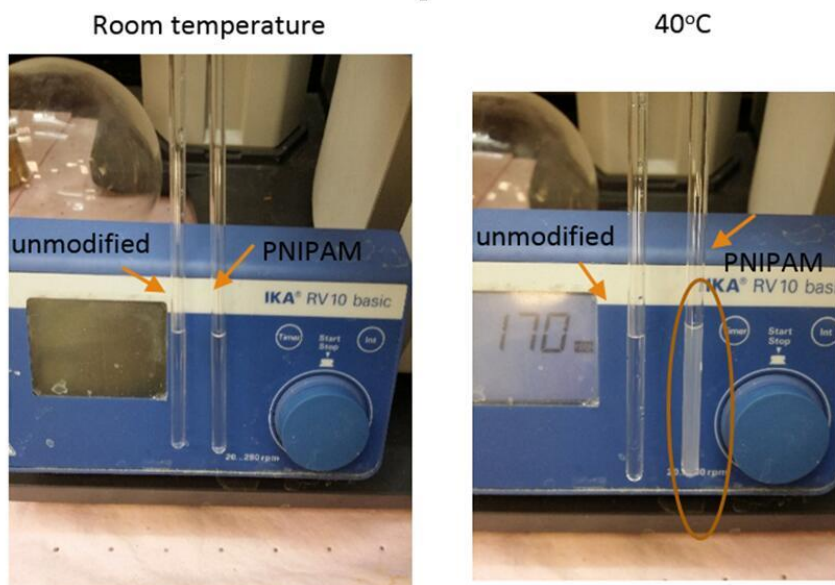**Figure A3.3** ^{1}HNMR for cleaved PNIPAM (hydrolyzed in ethylenediamine).

Figure A3.4 Turbidity change of cleaved PNIPAM re-dissolved in D_2O. Solution (left) obtained from unmodified membrane was used as a control from the same cleavage condition.

5. GPC (0.5 mL/min, water, 40°C)
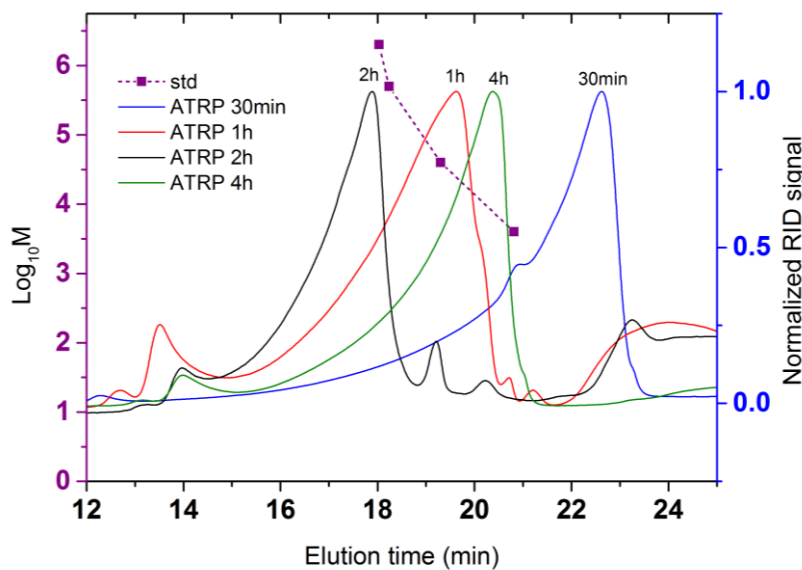
Figure A3.5 GPC chromatogram of cleaved PNIPMA polymers dissolved in water.
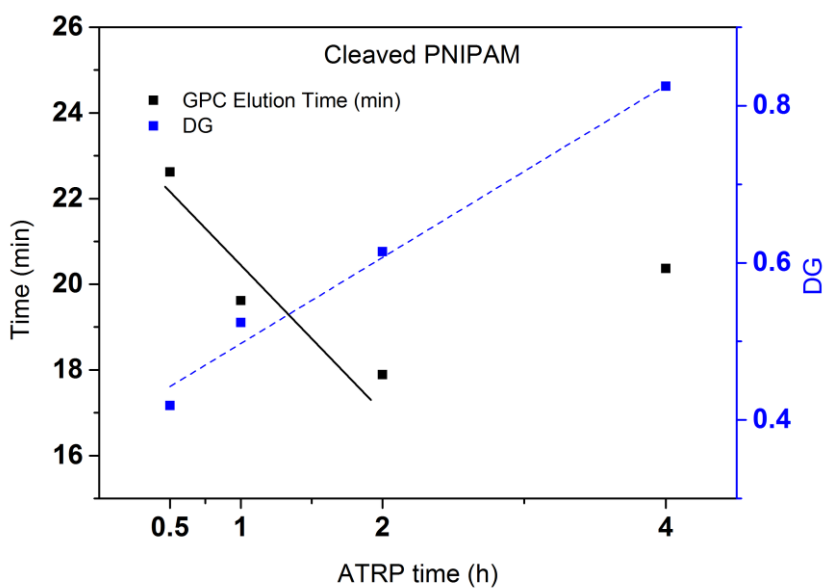
Figure A3.6 Relation between GPC elution times of cleaved PNIPAM and DG/ATRP time

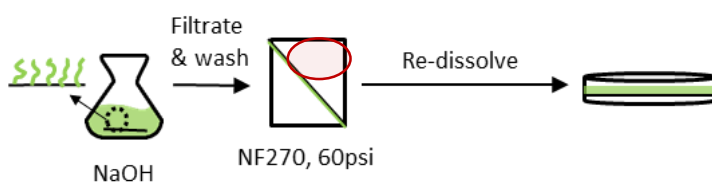## 5. Investigation on GPC Characterization of Synthesized PVCL

Figure A3.7 Procedure of the investigation of wash effect in the cleavage process
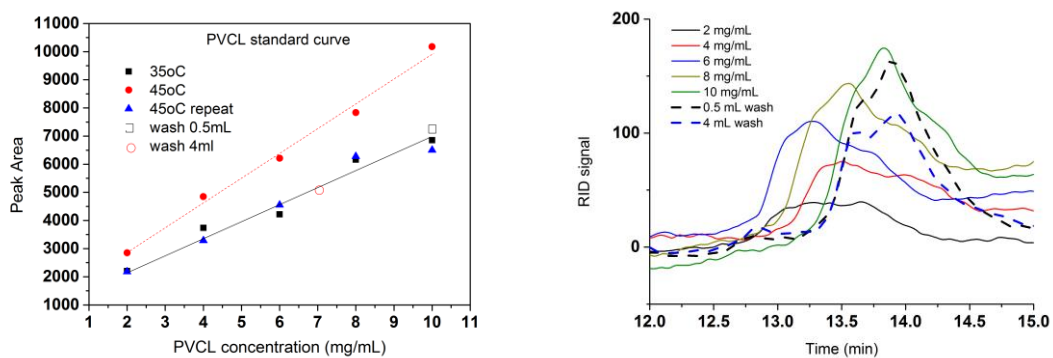
Figure A3.8 Standard curve of PVCL and wash effect on the total yield of the process

Appendix IV

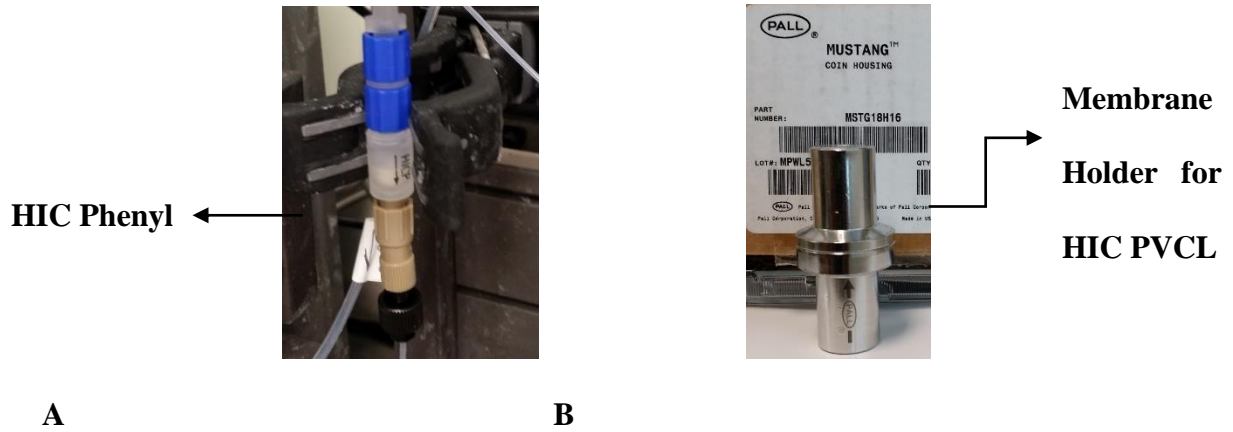**Comparison Study: HIC Phenyl pico and HIC PVCL membranes**

1. FPLC Set-up

HIC Phenyl

Membrane Holder for HIC PVCL

A   B

Figure A4.1 FPLC set-up and testing protocols for HIC Phenyl membranes (A) and HIC PVCL membranes (B, Mustang Coin ® Membrane Holder (Pall Corporation)).
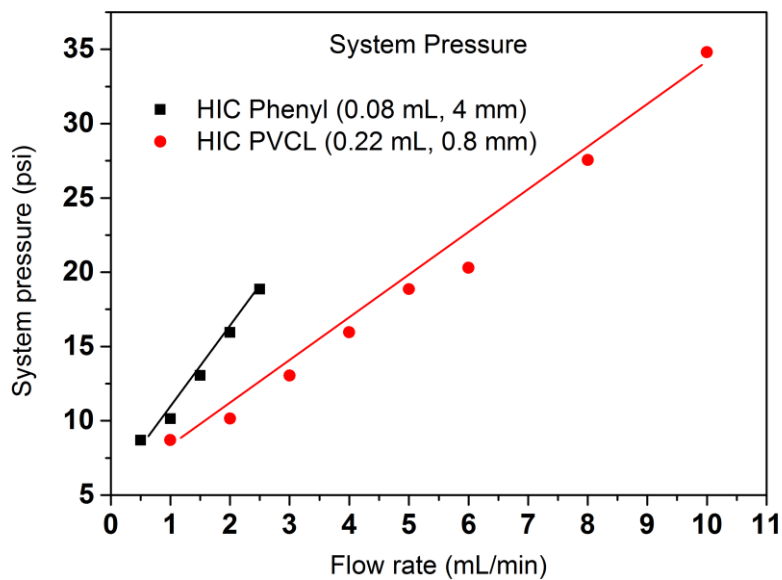
2. Operating Pressure and Flow Rate

Figure A4.2 Operating pressure and flow rate relationship for HIC phenyl and HIC PVCL. Tests were conducted in 20 mM sodium phosphate buffer at room temperature.
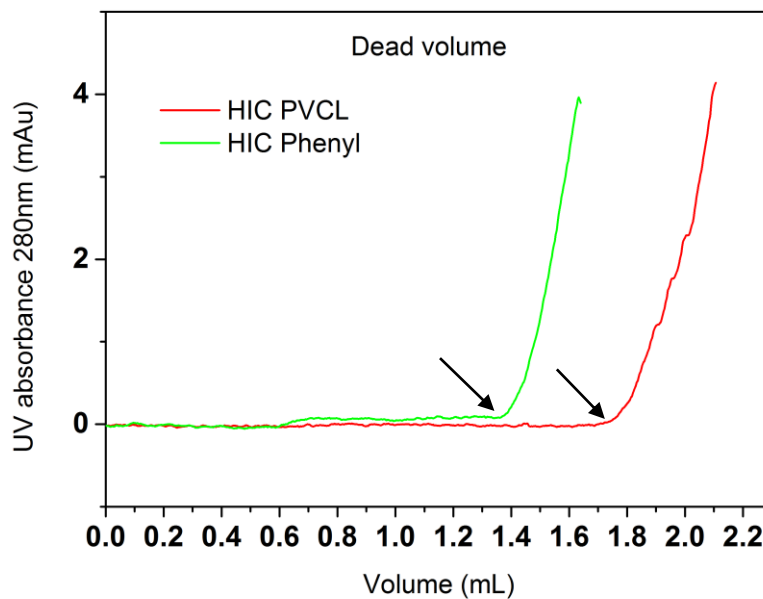
3. Dead Volume Measurement

Figure A4.3 FPLC dead volume measurement for HIC PVCL and HIC Phenyl under 1mL/min. Measurements were conducted with BSA dissolved in the 20 mM sodium phosphate buffer with membranes in the module or holder.

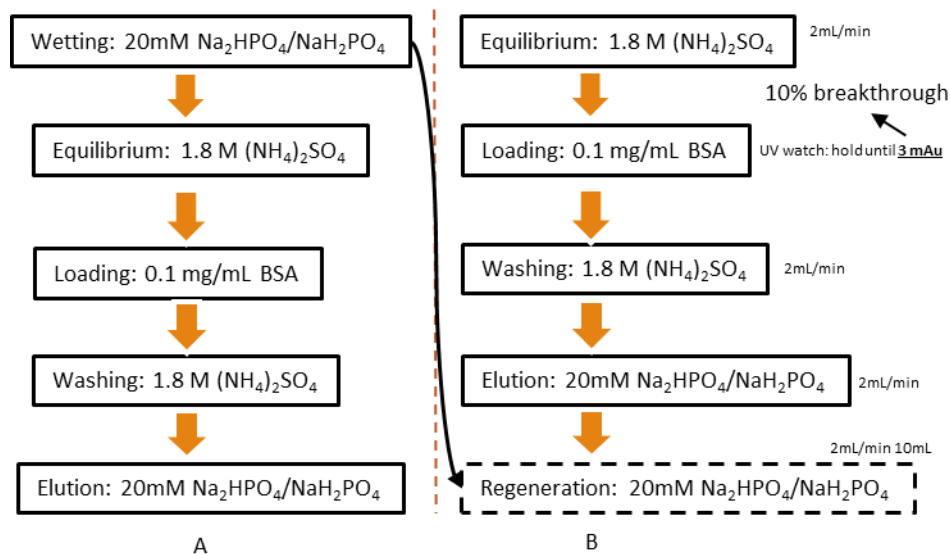## 4. Dynamic Binding Test (BSA)

4.1 DBC Measurement Protocol

Figure A4.4 DBC measurement protocols for old HIC binding test (A) and new test protocol (B) with a shorter running cycle time (reduced from 1h to 30min).

Table A4.1 Dynamic binding capacity (DBC) comparison between HIC Phenyl pico and HIC PVCL.

	Bed volume (mL)	Bed height (mm)	DBC 10% (mg/mL)	Recovery (%)
HIC PVCL run1 (old)	0.22	0.8	2.4	95
HIC PVCL (old)	0.08	0.3	2.4	96
HIC PVCL (new) run1	0.08	0.3	3.4	90
HIC PVCL (new) run10	0.08	0.3	2.7	95
HIC Phenyl run1	0.08	4	8.1	100
HIC Phenyl run10	0.08	4	7.9	103

* The $DBC_{10\%}$ is calculated according to $DBC_{10\%} = (V_{10\%} - V_0) \times C_0 / V_m$. $V_{10\%}$ and V_0 are the volume for 10% breakthrough and system dead volume, respectively. C_0 is the initial loading BSA concentration. V_m is the volume of membrane stacks. Recovery is calculated based on the 10% breakthrough.
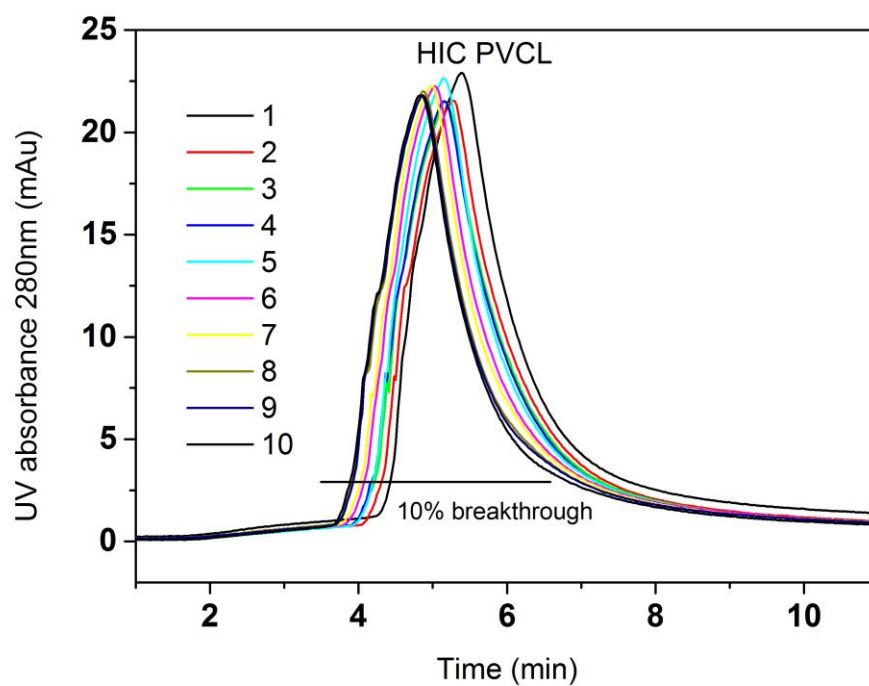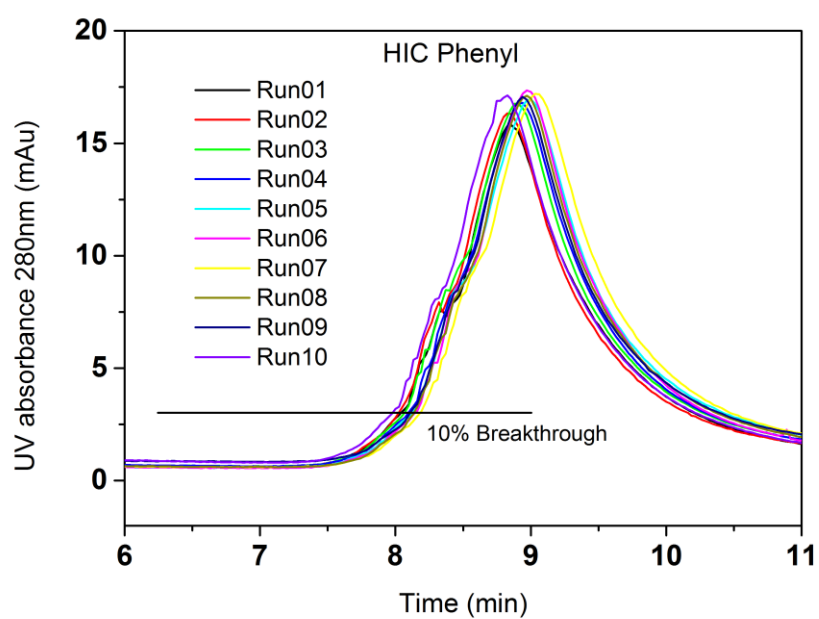
Figure A4.5 Breakthrough curves of 10 consecutive runs at 1.8 M $(NH_4)_2SO_4$ for 0.1 mg/mL BSA. Loading volume is determined by the program that it stops when 10% breakthrough (3 mAu in this case) reaches.
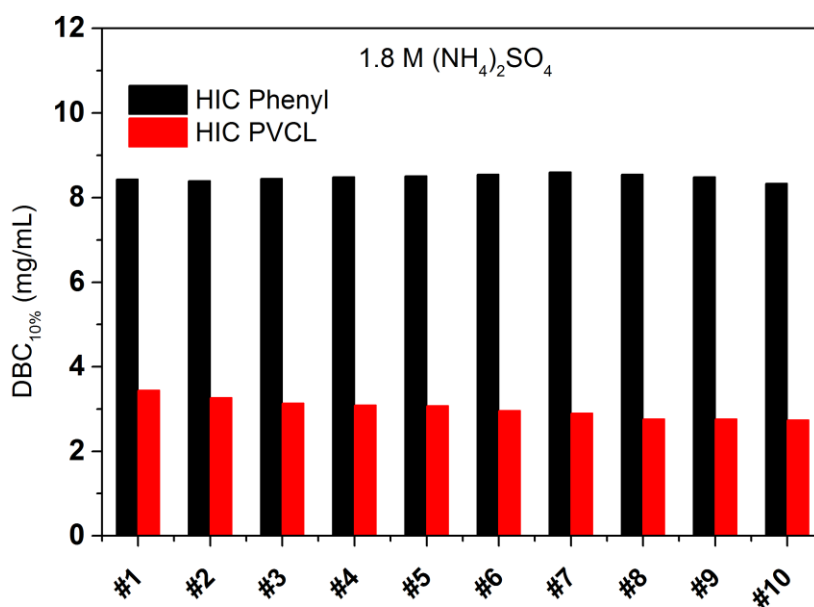
Figure A4.6 Dynamic binding capacity ($DBC_{10\%}$) of HIC phenyl and PVCL membranes in 10 consecutive runs.
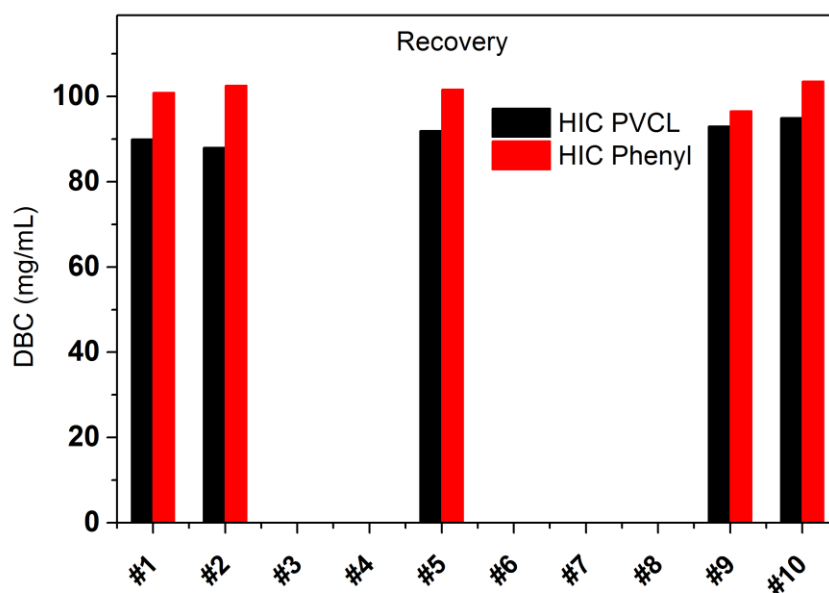

Figure A4.7 Recovery of $DBC_{10\%}$ of HIC phenyl membranes in 10 consecutive runs. The results are based on the mass balance.
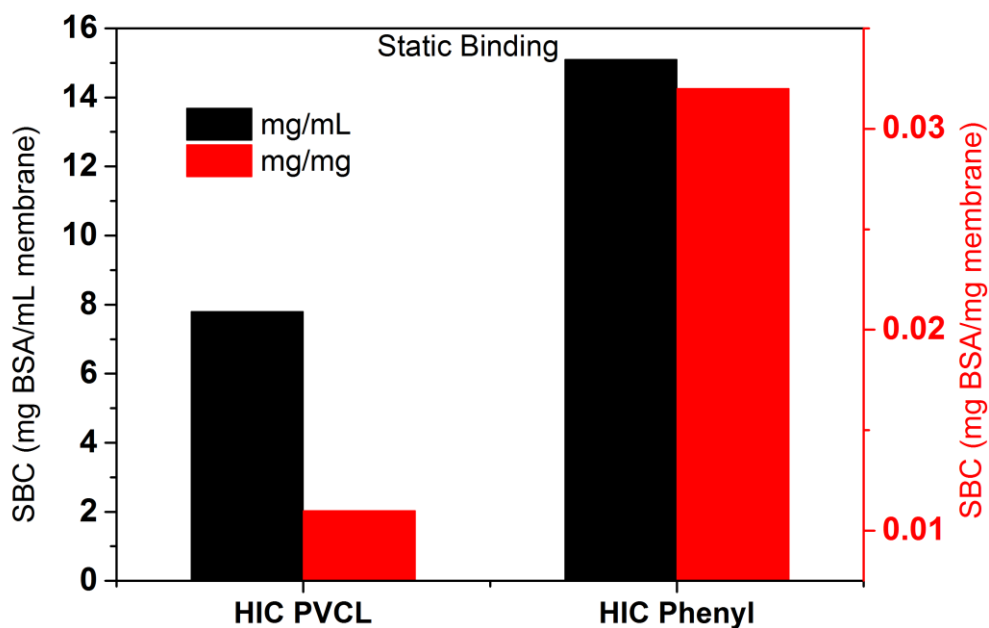
Figure A4.8 Static binding results of HIC PVCL and HIC Phenyl membranes. Binding tests were conducted at 1.8 M $(NH_4)_2SO_4$, 0.1 mg/mL BSA.

5. FPLC Method code:

5.1 Dead Volume Measurement:

```
  Main method:
  ▪  (Main)
   0.00  Base
  Volume
   0.00  BufferValveA  A1
   0.00  Gradient  100 (% B) 0.00 {base}
   0.00  Flow  0.2 {ml/min}
  ▪  0.00  Block  Equilibration
     (Equilibration)
     0.00  Base  Volume
     0.00  Valve7  1
     0.00  Set_Mark  "Equil"
     0.00  Gradient  100 (% B)  0.00 {base}
     0.00  Flow  1 {ml/min}
     0.00  ColumnPosition  Position2
     5.00
  AutozeroUV
     6.00
  End_Block
```

- 0.00 Block
  Load
  (Load)
  0.00 Base
Time
  0.00 Flow 0.00 {ml/min}
  0.00 InjectionValve Inject
  0.00 OutletValve F2
  0.01 SampleFlow_960 1 {ml/min}
  0.01 Set_Mark "Load"
  0.01 Hold_Until UV Greater_Than 3.0000 {mAU} INFINITE {base}
  0.02 SampleFlow_960 0.0 {ml/min}
  0.02
End_Block

5.2 Old HIC protocol and new protocol based on DBC$_{10\%}$

Old HIC Protocol (based on 10mL loading)

Main method:
- (Main)
 0.00 Base Volume
- 0.00 Block
  Sample_Pump
  (Sample_Pump)
  0.00 Base Time
  0.00 SampleFlow_960 1 {ml/min}
  0.2 SampleFlow_960 0.0 {ml/min}
  0.20 End_Block
 0.00 BufferValveA A1
 0.00 Gradient 0 (% B) 0.00 {base}
 0.00 Flow 0.2 {ml/min}
- 0.00 Block Wetting
  (Wetting)
  0.00 Base Volume
  0.00 ColumnPosition (Position2)#Column_Position
  0.00 Valve7 2
  0.00 OutletValve F1
  0.00 Alarm_Pressure Enabled 3 {MPa} 0.000 {MPa}
  0.00 Gradient 0 (% B) 0.00 {base}
  0.01 Flow 0.2 {ml/min}
  0.21 Flow 0.4 {ml/min}
  0.61 Flow 0.6 {ml/min}
  1.21 Flow 0.8 {ml/min}
  2.51 Flow 1.0 {ml/min}
  5.00 End_Block
- 0.00 Block
  Equilibration

(Equilibration)
0.00 Base Volume
0.00 Valve7 1
0.00 Set_Mark "Equil"
0.00 Gradient 100 (% B) 0.00
{base}
0.00 Flow 1 {ml/min}
8.00 AutozeroUV
10.00 End_Block
- 0.00 Block
  Load
  (Load)
  0.00 Base Time
  0.00 Flow 0.00 {ml/min}
  0.00 InjectionValve
Inject
  0.00 OutletValve F2
  0.01 SampleFlow_960 1 {ml/min}
  0.01 Set_Mark "Load"
  (10.00)#Load_Volume SampleFlow_960 0 {ml/min}
  10.10 InjectionValve
Load
  10.10 End_Block
- 0.00 Block
  Wash
  (Wash)
  0.00 Base Volume
  0.00 InjectionValve
Load
  0.00 Gradient 100 (% B) 0.00
{base}
  0.00 Set_Mark "Wash to Base"
  0.00 Flow 1 {ml/min}
  25.00 End_Block
- 0.00 Block Elution
  (Elution)
  0.00 Base Volume
  0.00 Set_Mark "Elution"
  0.00 Gradient 0 (% B) 0 {base}
  0.00 Flow 1 {ml/min}
  0.01 Hold_Until UV Greater_Than 1.5 {mAU} 10
{base}
  0.05 OutletValve F3
  0.15 Hold_Until Cond Less_Than 1 {mS/cm} 15
{base}
  0.20 End_Block

New HIC Protocol (based on DBC$_{10\%}$)

Main method:

- (Main)
  0.00 Base Volume
  0.00 BufferValveA A1
  0.00 Gradient 0 (% B) 0.00 {base}
  0.00 Flow 0.2 {ml/min}
- 0.00 Block Equilibration
  (Equilibration)
  0.00 Base Volume
  0.00 Valve7 1
  0.00 Set_Mark "Equil"
  0.00 Gradient 100 (% B) 0.00 {base}
  0.00 Flow 2 {ml/min}
  0.00 ColumnPosition Position2
  4.00 AutozeroUV
  5.00 End_Block
- 0.00 Block Load
  (Load)
  0.00 Base Time
  0.00 Flow 0.00 {ml/min}
  0.00 InjectionValve Inject
  0.00 OutletValve F2
  0.01 SampleFlow_960 1 {ml/min}
  0.01 Set_Mark "Load"
  0.01 Hold_Until UV Greater_Than 3.0000 {mAU} INFINITE {base}
  0.02 SampleFlow_960 0.0 {ml/min}
  0.02 End_Block
- 0.00 Block Wash
  (Wash)
  0.00 Base Volume
  0.00 InjectionValve Load
  0.00 Gradient 100 (% B) 0.00 {base}
  0.00 Set_Mark "Wash to Base"
  0.00 Flow 2 {ml/min}
  0.01 Hold_Until UV Less_Than 1 {mAU} 15.00 {base}
  0.02 End_Block
- 0.00 Block Elution
  (Elution)
  0.00 Base Volume
  0.00 Set_Mark "Elution"
  0.00 Gradient 0 (% B) 0 {base}
  0.00 Flow 2 {ml/min}
  0.01 Hold_Until UV Greater_Than 1.5 {mAU} 10 {base}
  0.05 OutletValve F3
  0.15 Hold_Until Cond Less_Than 3.4 {mS/cm} 15 {base}
  0.20 End_Block
- 0.00 Block Regen
  (Regen)

0.00 Base Volume
0.00 OutletValve F3
0.00 Set_Mark "Regeneration"
0.00 Gradient 0 (% B) 0.00 {base}
0.00 Flow 2.0 {ml/min}
10.00 End_Block